The role and regulation of 11β-hydroxysteroid dehydrogenase in lung inflammation

Fu Yang

Doctor of Philosophy

University of Edinburgh

2010

Abstract

Glucocorticoids are steroid hormones that have potent anti-inflammatory actions. Endogenous glucocorticoid action is modulated by 11β-hydroxysteroid dehydrogenase (11β-HSD) which catalyses the interconversion of active glucocorticoids (cortisol, corticosterone) and intrinsically inert forms (cortisone, 11-dehydrocorticosterone). There are 2 isozymes; 11β-HSD type 1 regenerates active glucocorticoids *in vivo* whereas 11β-HSD type 2 inactivates glucocorticoids. Although 11β-HSD1 is highly expressed in the lung, its role there has been little explored. In this study, the expression and localization of 11β-HSD1 mRNA in lung was confirmed by *in situ* hybridization. Immunohistochemical staining of mouse lung localized 11β-HSD1 to the cytoplasm of fusiform cells in alveolar walls, in a multivesicular pattern characteristic of interstitial fibroblasts. A lung fibrosis model of inflammation was used to test the role and regulation of 11β-HSD1. The results suggest that levels of 11β-HSD1 mRNA and enzyme were not changed during bleomycin-induced lung inflammation. However, 11β-HSD1-deficient mice showed a more severe inflammatory response than congenic wild-type controls, with greater inflammatory cell infiltration into the lung, and increased levels of HO-1 and iNOS mRNA 14 days following bleomycin installation into lung. Picrosirius red staining of lung sections suggested more collagen deposition in 11β-HSD1-deficient mice than in wild-type controls during the course of the lung inflammatory response. Moreover, whereas naïve 11β-HSD1-deficient mice had significantly lower collagen content in lung (84% of WT levels, $p<0.05$). 28d after bleomycin there was no significant difference between genotypes (KO having 94% of WT levels, $p=0.42$) confirming more collagen production in 11β-HSD1-deficient mice following bleomycin.

Fibroblasts are critical in the regulation of inflammatory responses and are essential in the model of bleomycin-induced lung injury. Lung fibroblasts may have a different transcriptional regulation of 11β-HSD1 compared to other tissues. In the majority of tissues, 11β-HSD1 can be transcribed from 2 promoters; the P1 promoter is the main promoter used in lung, with other tissues mainly using the P2 promoter. To address the relevance of the P1 promoter in lung and to identify the cell type using the P1 promoter, mouse lungs were collagenase-digested to isolate primary fibroblast and epithelial cells. Isolated lung fibroblasts highly expressed 11β-HSD1, predominantly from the P1 promoter. During passage, primary lung fibroblasts switched promoter usage from P1 to P2. In fibroblast primary culture, treatment with TGF-β for 72h markedly decreased 11β-HSD1 expression to 38% of untreated levels, an effect which was reversed by SB431542, a TGF-β receptor antagonist. Whilst TGF-β reduced levels of mRNA initiating at the P2 promoter, initiation from the P1 promoter was completely repressed. Treatment with TGF-β receptor antagonist increased levels of P1-initiated 11β-HSD1 mRNA by 6.6-fold compared to untreated cells. These data suggest that the switch in 11β-HSD1 promoter usage may be regulated by TGF-β during an inflammatory response. Furthermore, as the P1 and P2 promoters are differentially regulated (e.g. by C/EBPβ, a cytokine-responsive transcription factor), the promoter switch may place 11β-HSD1 under a different transcriptional regulation during inflammation. Taken together, these results suggest that 11β-HSD1 deficiency worsens lung inflammation and results in greater lung fibrosis. Therefore, amplification of intracellular glucocorticoids levels, by 11β-HSD1, may represent an important mechanism to limit the inflammatory response and shape fibroblast function, limiting subsequent collagen production and fibrosis.

Dedication

To my wife Winnie, who has inspired me to attempt more than I believed myself capable of.

Acknowledgement

In writing this thesis, I have benefited enormously from the support and advice of many people. First and foremost, I must thank Professor Karen Chapman, my principal supervisor, who has made my studies in the University of Edinburgh possible. I am exceedingly grateful to her continual inspiration and guidance since the beginning of this research project. She has patiently guided me through all the experiments and writings. Her unswerving support and encouragement have kept me motivated over the years. I am deeply indebted to her and can never fully repay her kindness.

Likewise, I would also like to thank Professor Jonathan Seckl and Professor John Savill, for giving me unfailing support and insightful comments. Their astonishing expertise in endocrinology and immunology has helped me greatly in this project. Dr. Roger Duffin and Dr. Agnes Coutinho should also be included in this section. Roger has been helping me set up bleomycin animal model. Agnes, both a colleague and a mentor, has unfailingly given me support on my project and life.

Special thanks must also be given to all the colleagues who have been a constant source of encouragement. Mrs Val Kelly has skillfully taught me very useful laboratory techniques. Dr Tiina Kipari and Dr Hongwei Wang give tremendous help with flow cytometry. Miss Janet Man has been extremely helpful in lab experience. I also wish to give heartfelt thanks to Professor Sarah Howie and Micheal Gibsson for their enormous effort in assisting me in lung histology analysis. Thanks also to all of the staff of the Endocrinology Unit and the CIR.

Finally, I would like to thank to my family. My mother, Qiuping and my father, Huijiang have been always supportive and believing that I can achieve anything I set myself to. Above all and everything, I want to express additional gratitude to my wife, Winnie, who has been giving me endless amount of love and care. I thank her for constantly standing by me, enlightening me and cheering for me, without which I could not have moved forward to the next stage of life. Last but not least, a special thank you to my baby girl whose coming has greatly encouraged me towards the end of this work.

Declaration

I, Fu Yang, declare that this thesis and the data presented in it are the result of my own efforts with technical help from following individuals; Dr Rodger Duffin who performed the intra-trachea instillation of bleomycin; Dr Hongwei Wang and Dr Tiina Kipari who set up flow cytometric analysis; Dr Agnes Coutinho who took tail blood and set up immunoradio assay. This work has not been submitted for any other professional qualification or degree, except as specified.

_____

Fu Yang

Edinburgh, 2010

Table of Contents

Index of Figures

Index of Tables

List of Abbreviations

11β-HSD	11 beta-Hydroxysteroid dehydrogenase
11-DHC	11-Dehydrocorticosterone
ACTH	Adrenocorticotrophic hormone
ANOVA	Analysis of variance
AP-1	Activator protein-1
BMD	Bone marrow derived
bp	Base pairs
BSA	Bovine serum albumin
CBG	Corticosterone binding globulin
CD	Cluster of differentiation
CNS	Central nervous system
CRH	Corticotrophin releasing hormone
DAB	Diaminobenzidine
DC	Dendritic cell
DEPC	Diethylpyrocardbonate
DMEM	Dulbeco's modified Eagle's medium
DNA	Deoxyribo-nucleic acid
DTT	Dithiothriotol
EDTA	Ethylene diamine tetraacetic acid
FCS	Foetal calf serum
FITC	Fluorescein isothiocyanate
GC	Glucocorticoid
GM-CSF	Granulocyte/Mϕ colony stimulating factor
GR	Glucocorticoid receptor
GRE	Glucocorticoid response element
H6PDH	Hexose-6-phosphate dehydrogenase
HPA-axis	Hypothalamic-pituitary gland-adrenal gland-axis
HPLC	High pressure liquid chromatography
hps	Heat shock protein
HRP	Horse radish peroxidase
Ig	Immunoglobulin
IL	Interleukin
LPS	Lipopolysachharide
MCP-1	Monocyte chemoattractant protein l
MR	Mineralocorticoid receptor
mRNA	Messenger RNA
NAD	Nicotinamide adenine dinucleotide
NADP	Nicotinamide adenine dinucleotide phosphate
NFκB	Nuclear factor-kappa B
PBS	Phosphate buffered saline
PCR	Polymerase chain reaction

PE	Phycoerythrin
RNA	Ribo-nucleic acid
RT	Reverse transcription
SP	Surfactant protein
TGF-β	Transforming growth factor beta
TNF-α	Tumor necrosis factor alpha

1 Chapter One: Introduction

1.1 Glucocorticoids

1.1.1 The discovery and application of glucocorticoids

Glucocorticoids (GC) were first discovered in the 1940s and in the years that followed, synthetic glucocortcoids soon became one of the most effective medicines to treat inflammation (Hench, Slocumb et al. 1949). As well as their function in immunomodulation, endogenous GC, produced in the adrenal gland, also regulate stress, metabolism, homeostasis and behavior. Endogenous GC are necessary for survival at birth (Cole, Blendy et al. 1995) and are also essential in adults following certain inflammatory or infectious stimuli (Webster and Sternberg 2004). Adrenalectomized mice died following treatment with LPS, TNF-α or IL-1, but pretreatment with the synthetic GC, dexamethasone, rescued the mice (Bertini, Bianchi et al. 1988).

1.1.2 GC synthesis

All steroid hormones are derived from cholesterol, the basic structure of which is maintained throughout the steroid biosynthetic pathways. Cholesterol contains a cyclopentane ring and 3 cyclohexane rings (Figure 1.1). Each steroid is synthesized by sequential enzymatic action – predominantly by hydroxylases located in either the smooth endoplasmic reticulum or in mitochondria. GC are produced by the adrenal cortex but the adrenals do not store GC, which are synthesized and secreted by the adrenal cortex into the circulation when required (De Kloet, Rosenfeld et al. 1988).

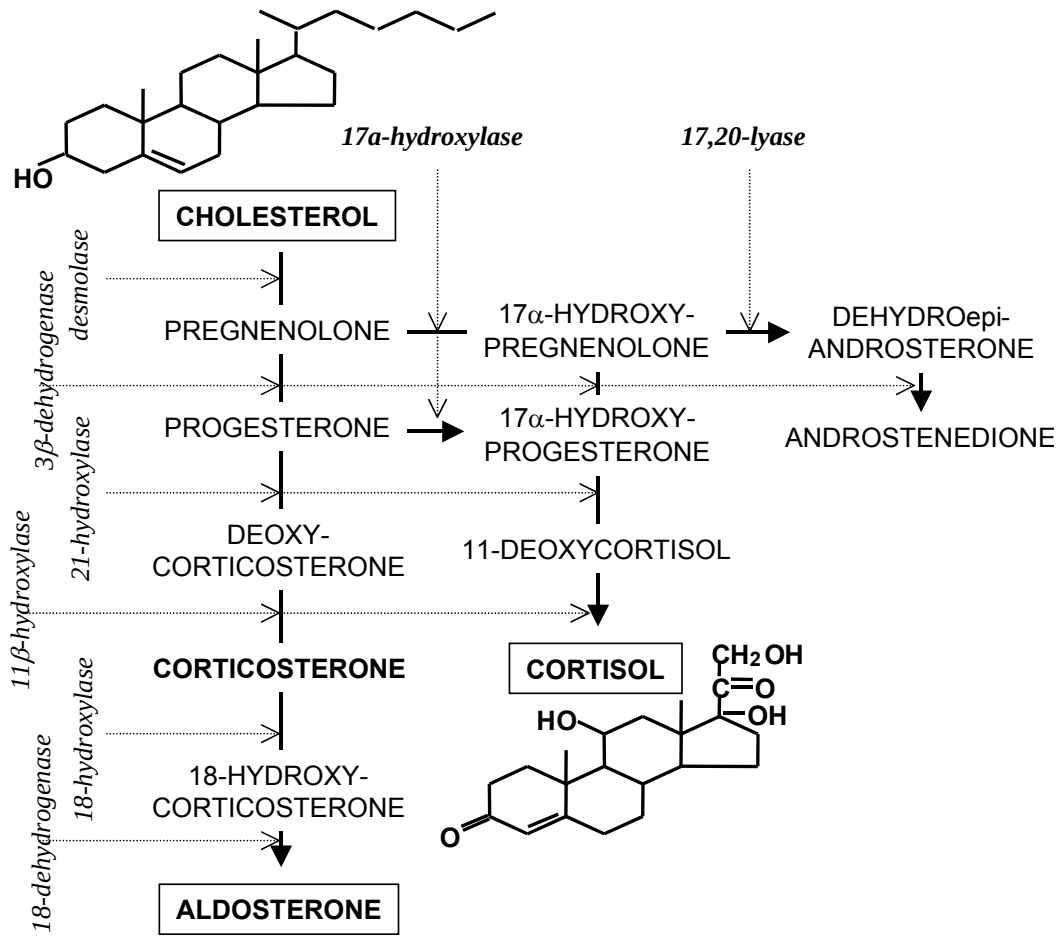

Figure 1.1 Summary of corticosteroid bio-synthetic pathways.
Cortisol and corticosterone are synthesized from cholesterol in the adrenal cortex. The above pathways are all present in human adrenal gland. Rodents lack 17α-hydroxylase in the adrenal gland and so cannot produce cortisol. Hence, in rodents, only corticosterone is made whereas humans (and most other vertebrate species) produce mainly cortisol. Diagram adapted from (O'Riordan JLH 1982)

1.1.3 Regulation of GC secretion

The hypothalamic-pituitary-adrenal (HPA) axis regulates GC secretion. GCs are secreted with a circadian rhythm and also in response to stress. Upon appropriate stimulus (e.g. stress, such as pain, trauma or emotional stress), the cells of the paraventricular nucleus of the hypothalamus express corticotropin-releasing hormone (CRH) which is released into the hypophyseal blood. CRH then stimulates the anterior pituitary gland to release adrenocorticotropin hormone (ACTH) into the bloodstream. Then, ACTH stimulates the synthesis and secretion of GCs from the adrenal cortex into the circulation (Axelrod and Reisine 1984). After HPA axis activation, GCs suppress their own synthesis via a negative feedback loop in which circulating GC inhibits the production of CRH and ACTH (Figure 1.2).

Most circulating glucocorticoids are bound to plasma proteins; mainly corticosteroid binding globulin (CBG). Approximately 90% plasma cortisol and 80% plasma corticosterone is found associated with CBG, with much of the remaining GCs normally associated with albumin (Dunn, Nisula et al. 1981). New evidence suggests CBG is more than just a GC carrier; it is actively involved in influencing the GC response to stress (Richard, Helbling et al. 2010). Because GCs are lipophilic, they can easily cross cell membranes, binding to intracellular glucocorticoid receptors which then change their conformation and translocate to the nucleus where they bind to DNA, regulating gene expression (Tronche, Kellendonk et al. 1998) (Figure 1.2).

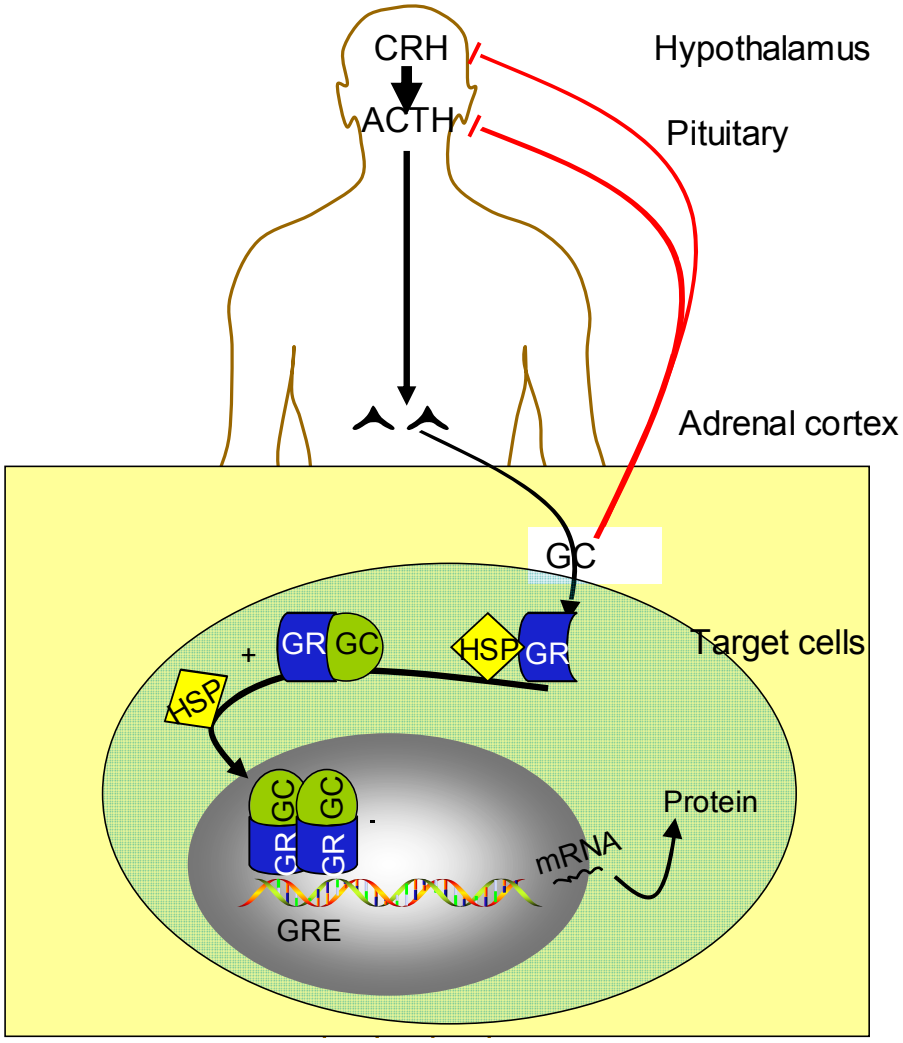

Figure 1.2 The HPA axis regulates GC secretion and GC regulate gene expression in target cells

The hypothalamus expresses CRH which stimulates the anterior pituitary gland to release ACTH into the blood stream to stimulate the synthesis and secretion of GCs from the adrenal cortex into the circulation. GCs suppress their own synthesis via a negative feedback loop to inhibit the production of CRH and ACTH (indicated by red colour). In target cells, before hormone binding, GR in the cytoplasm is complexed with HSP. After binding to GCs, GR dissociates from the complex, and translocates to the nucleus where it binds to DNA to regulate target gene transcription.

Arrows indicate the positive effect whereas bars indicate inhibitory effects. CRH, corticotropin-releasing hormone; ACTH, adrenocorticotropin hormone; GC, glucocorticoid; GR, glucocorticoid receptor; HSP, heart shock protein; GRE, glucocorticoid response element. Adapted from (Axelrod and Reisine 1984; Grad and Picard 2007).

There are 2 types of glucocorticoid receptor; the type I (or mineralocorticoid) receptor (MR) and the main receptor, the type II (or glucocorticoid) receptor (GR).

1.1.4 Glucocorticoid receptor (GR) and its mechanism of action

25 years ago, the cloning of GR opened up a new aspect to the research of GC function (Hollenberg, Weinberger et al. 1985). GR was the 2nd member of the nuclear hormone receptor family to be cloned, a family which includes receptors for other steroid hormones (Beato 1989). GR is a DNA binding protein that regulates transcription initiation (Yamamoto 1985). Before hormone binding, GR in the cytoplasm is complexed with chaperone proteins, that include heat shock proteins (Hsp) 90, 70 and 23, and the immunophilins; FKBP51, FKBP52, Cyp44, DP5 (reviewed in (Pratt, Galigniana et al. 2004)) (Figure 1.2).

After binding to GCs, GR dissociates from the complex and undergoes a conformational change, which exposes a nuclear localization sequence (Picard and Yamamoto 1987). GR then translocates into the nucleus to form a complex with regulatory cofactors, influencing target gene transcription (reviewed in (Beato 1989; Grad and Picard 2007)).

GR both activates and suppresses target gene transcription. Genes positively regulated by GCs contain glucocorticoid response elements (GRE) within the promoter region (reviewed in (Beato 1989; Reichardt and Schutz 1998)). GR binds to

these elements, normally as a dimer (Wrange, Eriksson et al. 1989; Reichardt and Schutz 1998), although other configurations may be possible (Adams, Meijer et al. 2003; Meijsing, Pufall et al. 2009) and recruits coactivator proteins to remodel chromatin and facilitate transcription (reviewed in (Rhen and Cidlowski 2005; Liberman, Druker et al. 2007)). The mechanism(s) by which GR repress transcription are less clear, although it has been proposed that monomers of GR can bind to pro-inflammatory transcription factors such as AP-1 and nuclear factor-κB (NF-κB), preventing their binding to cognate DNA binding sites and thus preventing pro-inflammatory gene transcription (reviewed in (McKay and Cidlowski 1999; Liberman, Druker et al. 2007)).

1.1.5 Physiological effects of GC

GCs affect many physiological processes, some of which are reviewed below. GC have critical effects on inflammation and inflammatory processes. There are reviewed in Section 1.4 (below). It is important to distinguish between the normal physiological effects of GCs and effects produced by supra-physiological levels (Munck and Naray-Fejes-Toth 1992). High levels of GC or long term pharmacological GC treatment causes Cushing's syndrome (Dorn, Burgess et al. 1995). Patients with Cushing's syndrome show deleterious symptoms, including hypertension, insulin resistance, increased cardiovascular disease risk and atypical depression (Dorn, Burgess et al. 1995; Souverein, Berard et al. 2004). GC deficiency, for example seen in Addison's disease, cause weight loss, increased insulin

sensitivity, fatigue and hypotension (Chrousos 2004).

1.1.5.1 GC effects on lipid and glucose homeostasis

GCs play an important role in the regulation of daily energy flow (Munck, Guyre et al. 1984). GCs promote hepatic glucose output, increasing gluconeogenesis, mobilizing stored glycogen and decreasing glucose uptake into peripheral tissues (eg. muscle). They also promote lipolysis of stored triglycerides from adipose tissue (Gaillard, Wabitsch et al. 1991).

1.1.5.2 GC effects on development

GCs are essential for tissue maturation in preparation for birth (Fowden, Li et al. 1998). In particular, GCs are essential for lung maturation in both humans and mice (reviewed in (Garbrecht, Klein et al. 2006)). GCs are used clinically in premature infants with respiratory distress syndrome (Liggins and Howie 1972). In human fetal lung, GCs increase lung cell proliferation, promote the differentiation of type 2 alveolar epithelial cells and cause thinning of alveolar walls (reviewed in (Garbrecht, Klein et al. 2006)). Surfactant is produced and secreted by type 2 alveolar epithelial cells, and functions to reduce surface tension at the alveolar air-liquid interface, thereby preventing alveoli from collapsing at the end of expiration. Pulmonary surfactant contains four surfactant proteins (SPs): SP-A, SP-B, SP-C and SP-D (reviewed in (Mason 2006)). GCs promote the expression and mRNA stability of SP-B, SP-C, and SP-D (Liley, White et al. 1989; Dulkerian, Gonzales et al. 1996). In

rats, GCs stimulate fetal lung fibroblasts to secrete fibroblast-pneumonocyte factor, which increases surfactant synthesis by type 2 alveolar epithelial cells *in vitro* and accelerates lung maturation *in vivo* (Floros, Post et al. 1985; Torday and Kourembanas 1990).

Results from GR-deficient mice are consistent with these GC functions in lung. GR knockout mice die within a few hours after birth because of respiratory failure and lung structural immaturity (Cole, Blendy et al. 1995; Nemati, Atmodjo et al. 2008). The lungs at birth are severely atelectatic, and development is impaired from day 15.5 of pregnancy (Cole, Blendy et al. 1995). The differentiation of type I epithelial cells is decreased by about 50% and the mRNA levels of SP-A and SP-C are also reduced by approximately 50% in GR knockout mice at day 18.5 of pregnancy (Cole, Solomon et al. 2004). Mice with tissue specific GR KO in lung airway epithelial cell using a Cre-LoxP system with Cre controlled by the SP-C promoter show 50% decreased viability shortly after birth, and their lungs have an immature appearance with increased lung cellularity and increased pools of glycogen in the epithelium (Manwani, Gagnon et al. 2009). These mice also showed reduced epithelial cell differentiation and reduced mRNA expression of all 4 surfactant proteins (Manwani, Gagnon et al. 2009). Another line of transgenic mice which expresses GR exclusively in the distal airway epithelium (KO for GR, with a transgene expressing GR from the human SP-C promoter), show a more mature histological appearance

than GR KO mice, with a reduction in cellularity to normal values (Gagnon, Atmodjo et al. 2006). However, those mice also develop respiratory insufficiency at birth and there is no difference in viability compared to GR KO mice (Gagnon, Atmodjo et al. 2006). Those results suggest GC signaling through a fully functional GR is important for the maturation of the lung and restoration of GR expression only in airway epithelial cells is not enough to rescue GR KO mice. Therefore, GC must target other lung cells in addition to epithelial cells to mature the fetal lung.

1.2 Inflammation

Before considering the effects of GC on inflammation, it is necessary first to briefly review the processes affected. Inflammation is initiated at the site of injury. Resident macrophages play a key role in initiating the inflammatory response by secreting proinflammatory cytokines, including IL-1, IL-6, TNF-α and chemokines such as monocyte chemotactic protein (MCP)-1 (Topley, Mackenzie et al. 1993; Borish and Steinke 2003). These pro-inflammatory mediators recruit leukocytes to the site of injury along the chemotactic gradient, resulting in the pain, redness and swelling of inflammation (Kolaczkowska, Shahzidi et al. 2002; Borish and Steinke 2003). Activated granulocytes are quickly attracted to the injured site, followed by monocyte emigration from blood vessels and maturation into macrophages (reviewed in (Serhan and Savill 2005)). Then phagocytes (neutrophils and macrophages) start to ingest microbial pathogens and cellular debris from necrotic cells as well as apoptotic cells (Greenberg and Grinstein 2002). Following recruitment, neutrophils

undergo constitutive apoptosis, which leads to macrophage ingestion of the intact apoptotic neutrophils to prevent release of further proinflammatory mediators (Haslett, Lee et al. 1991). Usually, acute inflammation resolves quickly. However, it can become persistent and lead to a chronic inflammatory state that can progress to irreversible organ damage (reviewed in (Haslett, Savill et al. 1994; Heasman, Giles et al. 2003)).

1.3 Fibrosis

Lung fibrosis is a common final pathway of many interstitial lung diseases and is characterized by accumulation of excess collagen and other extracellular matrix (ECM) components, resulting in the destruction of normal tissue architecture and function (reviewed in (Shukla, Meisler et al. 1999)). The normal alveolar basement membrane is lined with alveolar epithelial cells. After epithelial damage, neutrophils/monocytes are accumulating in the injured area (Selman and Pardo 2002). Then epithelial cells can undergo transition to a mesenchymal phenotype giving rise to fibroblasts and myofibroblasts (Willis and Borok 2007) and fibroblasts/myofibroblasts generate extracellular matrix (ECM), which serves as the foundation for re-establishment of tissue integrity and provides tissue support (Gomperts and Strieter 2007). During the repair phase, myofibroblasts undergo apoptosis and disappear, and ECM is degraded and epithelial cells migrate denuded area to reepithelialize (Selman and Pardo 2002). Matrix proteins in the lung

including collagen are continually synthesized and degraded (Laurent 1987). Imbalances in this process lead to either more fibrosis or loss of connective tissue (Mays, McAnulty et al. 1989).

1.3.1 Fibroblasts

Fibroblasts are the most abundant cell type in stromal tissue and participate in repair and regenerative processes in almost every tissue and organ (reviewed in (White, Lazar et al. 2003)). They are traditionally identified by their spindle shape morphology and their ability to adhere to plastic *in vitro* (Tarin and Croft 1969). A few proteins have been used to identify fibroblasts, such as CD 90, vimentin, fibroblast-specific protein, fibroblast activation protein and CD248 (Franke, Schmid et al. 1978; Rettig, Garin-Chesa et al. 1993; Strutz, Okada et al. 1995; MacFadyen, Haworth et al. 2005). However, to date, there is no single marker to identify fibroblasts. Fibroblasts are not just passive structural cells, which form a scaffold to support the surrounding tissue, but are actively involved in immune regulation by producing growth factors, chemokines and extracellular matrix (reviewed in (Kalluri and Zeisberg 2006)). Fibroblasts are able to regulate tissue-infiltrating leukocytes, governing their accumulation, survival and differentiation (reviewed in (Parsonage, Filer et al. 2005)). Following injury to the lung, fibroblasts migrate to the damaged area and are stimulated to secrete collagen and other ECM (Kuhn and McDonald 1991). They also release various proteases that can degrade and remodel these matrix

proteins (Parsonage, Falciani et al. 2003). They contribute to the tissue-specificity of inflammatory reactions and play an active role in the persistence of chronic inflammatory reactions (Parsonage, Falciani et al. 2003). Dysregulation of this process can result in fibroblast foci, followed by abnormal remodeling of the ECM and subsequent destruction of the lung architecture (Basset, Ferrans et al. 1986; Kuhn, Boldt et al. 1989).

1.3.2 Myofibroblasts

Myofibroblasts are unique mesenchymal cells with properties inherent to both smooth muscle and fibroblasts. They are widely distributed in embryos, are essential for the formation of functional adult tissue, and are intimately involved in tissue homeostasis and wound healing (reviewed in (Walker, Guerrero et al. 2001)). Cytoskeletal protein expression and contractile properties distinguish them from fibroblasts (reviewed in (Walker, Guerrero et al. 2001)). Myofibroblasts are the primary source of type I collagen gene expression in active fibrotic sites in animal models (reviewed in (Phan 2002)). In pulmonary fibrosis, myofibroblasts were shown to be derived from peribronchial and perivascular adventitial fibroblasts (Zhang, Rekhter et al. 1994), however, it is still controversial, some authors think they have hematopoietic origin (Ogawa, LaRue et al. 2006). A common marker for myofibroblast differentiation is the expression of α-smooth muscle actin (α-SMA) (Gabbiani, Hirschel et al. 1972). Primary cultured lung fibroblasts can be induced to

differentiate into myofibroblasts by treatment with cytokines such as transforming growth factor TGF-β (Hu, Wu et al. 2003).

1.3.3 TGF-β

TGF-β is member of a family of growth and differentiation factors with multiple functions in a variety of different organ systems. TGF-β is notable for its capacity to modulate a variety of cellular behaviors, including cell proliferation, differentiation, and apoptosis (reviewed in (Bartram and Speer 2004)). Its receptors and effects are found in all cells at injured or repaired tissue. There are 3 forms of TGF-β expressed by mammalian cells, TGF-β_{1-3}, all of which are potential stimulators of ECM production, promoting synthesis of fibronectin, tenascin and collagen by fibroblasts (Ignotz and Massague 1986; Fine and Goldstein 1987; Shukla, Meisler et al. 1999). Of the TGF-βs, TGF-β_1 is the isoform predominantly expressed during the pathogenesis of experimental pulmonary fibrosis (Coker, Laurent et al. 1997). It can stimulate fibroblast differentiation to the myofibroblast phenotype and suppress myofibroblast apoptosis (Zhang and Phan 1999). TGF-β intracellular signaling is mediated by the family of Smad transcription factors. Binding of TGF-β to its receptor leads to phosphorylation of Smad2 and Smad3, which then form a heteromeric complex with Smad4 (reviewed in (Bartram and Speer 2004)). Then, the Smad complex translocates to the nucleus and activates target genes by binding to specific promoter elements (reviewed in (Bartram and Speer 2004)).

Both GCs and TGF-β control collagen synthesis, but in opposite directions. GCs can decrease collagen production through a depressant effect on the synthesis of soluble collagen and decreased prolyl hydroxylase activity which hydroxylates proline to hydroxyproline, a major component of collagen, in rat lung (Cutroneo and Counts 1975). In a bleomycin model of lung fibrosis (see section 1.8.2), rats treated with bleomycin showed higher prolyl hydroxylase activity and hydroxyproline content compared to untreated control rats (Sterling, DiPetrillo et al. 1982). However, when rats were treated with both bleomycin and GC, they showed normal prolyl hydroxylase activity and hydroxyproline content, similar to control rats without any treatment (Sterling, DiPetrillo et al. 1982). Dexamethasone (dex), a synthetic GC, caused a decrease in TGF-β_1 mRNA in rat lung fibroblasts *in vitro*; the treatment also resulted in decreased TGF-β activity (Shull, Meisler et al. 1995). There is a putative GRE in the promoter region of TGF-β_1 (Parrelli, Meisler et al. 1998) but this has not been investigated further. The gene encoding Proα1(I) collagen has a TGF-β response element in the promoter region (Meisler, Chiu et al. 1999). When rat skin fibroblasts were treated with Dex, less TGF-β nuclear activator protein was bound to the TGF-β response element in the promoter region of proα1(I) collagen which led to a decrease in proα1(I) collagen gene promoter activity (Meisler, Shull et al. 1995). These data indicate that GC may regulate collagen synthesis both by decreasing TGF-β levels and thus activity and also by interfering with TGF-β signaling within the nucleus of lung fibroblasts.

1.4 GC effects on inflammation

Clinically, GCs have been widely used for their immunosuppressive and anti-inflammatory function since their discovery in the 1940s. Synthetic GCs are commonly used to treat a variety of inflammatory diseases, including asthma and rheumatoid arthritis. More recent evidence suggests GC are not exclusively anti-inflammatory, they modulate the immune response as well (Sapolsky, Romero et al. 2000). GC exhibit immunosuppressive functions at higher doses, but show immunomodulatory function at physiological levels (Yeager, Guyre et al. 2004).

One of the most intriguing effects of GC on immune cells (Figure 1.3) is the ability to induce apoptosis in immature thymocytes. Adrenalectomized mice showed increased thymus size and GC decreased thymus size (Jaffe 1924). GC-induced T cell death is believed to be one of the mechanisms by which T cell selection occurs in the thymus (Cohen, Fschbach et al. 1970). Also, GC decrease circulating lymphocytes in blood (Keller, Weiss et al. 1981), by reducing the availability of chemoattractants and suppressing adhesion molecules (Schneider, Bruckmann et al. 1997). GC inhibit immunoglobulin synthesis on T cells and B cells, thus altering T cell function and B cell proliferation (Cupps, Gerrard et al. 1985).

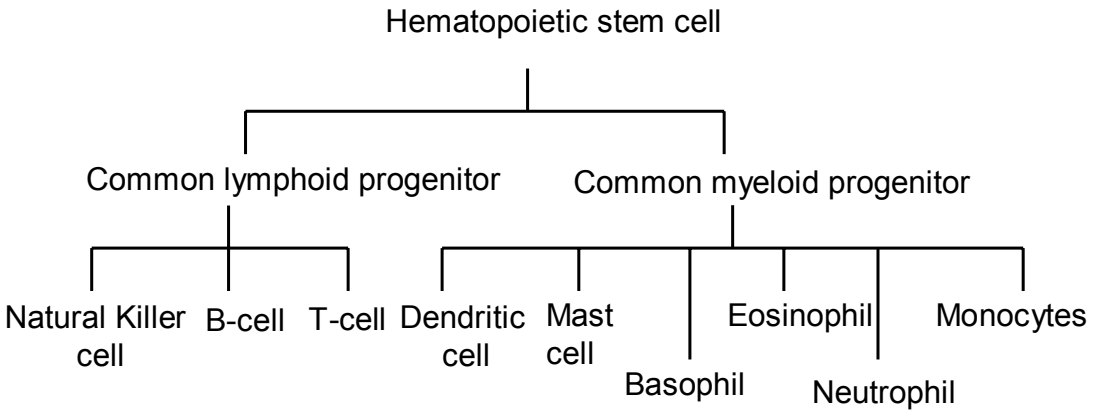

Figure 1.3 A scheme showing development of immune cells from lineage-restricted progenitor populations

Common lymphoid and myeloid progenitor cells develop from hematopoietic stem cells. Common lymphoid progenitor cells develop into natural killer cells, B-cells and T-cells. Common myeloid progenitor cells develop into dendritic cells, mast cells, basophils, eosinophils, neutrophils and monocytes. Adapted from (Iwasaki, Mizuno et al. 2006). GC reduce lymphocyte numbers in blood, promote T cell apoptosis and T cell polarization, inhibit DC cell maturation, influence monocyte/macrophage function and accelerate eosinophil apoptosis whilst delaying neutrophil apoptosis and promoting neutrophilia (see text for details).

GC also modulate myeloid immune cells (Figure 1.3). GC increase neutrophil numbers in blood (Nakagawa, Terashima et al. 1998), possibly due to a delay in apoptosis (Meagher, Cousin et al. 1996; Zhang, Moilanen et al. 2001) as well as increased release from bone marrow (McEwen, Biron et al. 1997). Dendritic cells (DC) are specialized in antigen capture, processing and presentation to T cells. Mature DC can efficiently induce the development of T effector cells, whereas immature DC are involved in antigen-specific T cell tolerance, which is critical for the prevention of autoimmunity (reviewed in (Mahnke, Schmitt et al. 2002)). GCs potently regulate DC maturation and activation, decreasing the expression of cytokine and antigen presentation molecules (Piemonti, Monti et al. 1999; Matyszak, Citterio et al. 2000) and inhibiting the migration of DC towards lymph nodes (Cumberbatch, Dearman et al. 1999). GC-treated DC maintain an immature state and produce preferentially the immunomodulatory cytokine IL-10, rather than the proinflammatory cytokines, IL-6 and IL-12 (Luther, Adamopoulou et al. 2009). Moreover, GC-treated DC induce hyporesponsive $CD4^+$ T cells, which suppress autologous $CD4^+$ T cell proliferation to prevent autoimmunity (Luther, Adamopoulou et al. 2009). Therefore GCs are important in regulating the maturation and condition of DC, which may relate to the clinical effects of GCs.

Macrophages play an important role in resolving inflammation by recognition and phagocytosis of dying cells (reviewed in (Savill, Dransfield et al. 2002)). GCs induce

human monocytes to become highly phagocytic, highly motile anti-inflammatory macrophages (Giles, Ross et al. 2001; Heasman, Giles et al. 2003). GC-stimulated macrophages show down-regulation of adhesion-related proteins and reduced ability to adhere to plastic surfaces (Ehrchen, Steinmuller et al. 2007) consistent with increased migratory properties. GCs can also cause macrophages to ingest more apoptotic leucocytes (Liu, Cousin et al. 1999), a process that depends on the Mer tyrosine kinase-dependent apoptotic cell clearance pathway (McColl, Bournazos et al. 2009). GCs suppress expression of a number of cytokines in macrophages, to alter immune responses (Reichardt, Tuckermann et al. 2001). Importantly, in mouse monocytes, GCs induced a phenotype with low adhesiveness, high migratory capacity and markers suggestive of a tumor-associated macrophage phenotype (Varga, Ehrchen et al. 2008).

Traditionally, gene activation by GR was believed to occur exclusively through homodimers of GR binding to a consensus GR binding site, comprising two 6bp "half sites" arranged in an inverted repeat (palindrome) separated by a 3bp spacer (reviewed in (Beato 1989; Karin 1998)). The dimerization of the DNA binding domain of GR is dependent on a short 5 amino acid segment and the mutation of these residues strongly impaired binding of GR as a dimer to a palindromic GRE (Dahlman-Wright, Wright et al. 1991). Mice with a mutation in this region of GR (known as GR^{dim}), unable to transactivate via GR binding to palindromic GREs but

still able to repress NF-κB and AP-1, maintain anti-inflammatory activity *in vivo* (Reichardt, Kaestner et al. 1998). This has supported the hypothesis that the anti-inflammatory actions of GR are mediated by dimerization-independent interactions with other transcription factors, especially NF-κB and AP-1, impairing their ability to activate pro-inflammatory gene expression.

Dual specificity phosphatase (DUSP)-1, also known as MKP-1 (mitogen activated protein kinase [MAPK] phosphatase 1) is a crucial anti-inflammatory factor (Hammer, Mages et al. 2006). It dephosphorylates and inactivates members of the MAPK family which regulate inflammatory gene expression at both transcriptional and post-transcriptional levels (reviewed in (Dean, Sully et al. 2004)). Typically, the expression of DUSP1 is rapidly increased after GC stimulation (reviewed in (Clark 2007)). The induction of DUSP1 by dex is unimpaired in GR^{dim} mouse macrophages and GCs fail to suppress zymosan-induced inflammation in $DUSP1^{-/-}$ mice, whereas inflammation was suppressed in control mice (Abraham, Lawrence et al. 2006), implying that GR dimerization is unnecessary to activate DUSP1 expression and demonstrating that DUSP1 induction is an important mechanism in the anti-inflammatory effects of GC. More recently, GREs containing GR binding sites have been identified in both the human and mouse *DUSP1* loci (Tchen, Martins et al. 2010), supporting direct regulation of DUSP1 by GR in a dimerization-independent manner. How many of the anti-inflammatory effects of GC are attributable to DUSP1

induction remain unclear.

Although GCs are universally considered to be anti-inflammatory, there is some evidence suggesting that GCs contribute to pro-inflammatory responses as well. If GCs are administered prior to Lipopolysaccharides (LPS) challenge, they potentiate both the peripheral and central pro-inflammatory response; however, if GCs are administered after LPS challenge, GCs suppress the pro-inflammatory response to LPS (Frank, Miguel et al. 2010). Experiments on macrophages show different concentrations of GC have different effects (Lim, Muller et al. 2007). Low levels of GCs enhance NO production as well as pro-inflammatory cytokine and chemokine production, whereas high GC concentrations repress macrophage function (Lim, Muller et al. 2007). It is also important to note that most experiments to test the effects of GC on cells are carried out with high doses of synthetic GC (e.g. dex), and lower doses or endogenous GC (which are metabolized more readily, bind less avidly to receptors and which activate both MR and GR (Rousseau, Baxter et al. 1972)) may have different effects.

1.5 11β-HSD and pre-receptor GC metabolism

Physiological GC action depends on the intracellular concentration of GC. In intact cells, 11β-HSDs regulate intracellular GC levels (reviewed in (Seckl 2004)). There are two 11β-HSD isozymes, 11β-HSD1 and 11β-HSD2, which both belong to the

short-chain dehydrogenase reductase (SDR) family (Baker 1994). They interconvert active GC (cortisol in humans and corticosterone in rodents) and inactive GC (cortisone in humans and 11-dehydrocorticosterone in rodents) using nicotinamide cofactors to transfer hydride (Figure 1.4) (reviewed in (Agarwal and Auchus 2005)).

1.5.1 11β-HSD1 and 11β-HSD2; biochemistry

11β-HSD1 cDNA was first purified and cloned from rat liver (Lakshmi and Monder 1988; Agarwal, Monder et al. 1989) and it encodes an NADP(H)-dependent enzyme. Although bidirectional in homogenates (Lakshmi and Monder 1988) and some transfected cells (Agarwal, Monder et al. 1989; Bujalska, Shimojo et al. 1997; Odermatt, Arnold et al. 1999; Atanasov, Nashev et al. 2004), in intact cells and *in vivo*, 11β-HSD1 mainly shows reductase activity e.g. (Low, Chapman et al. 1994; Jamieson, Chapman et al. 1995; Kotelevtsev, Holmes et al. 1997; Jamieson, Walker et al. 2000). 11β-HSD1 is localized to the endoplasmic reticulum (ER) lumen with its N-terminus anchored to the ER membrane and the C-terminus inside the ER lumen (Ozols 1998; Mziaut, Korza et al. 1999; Odermatt, Arnold et al. 1999).

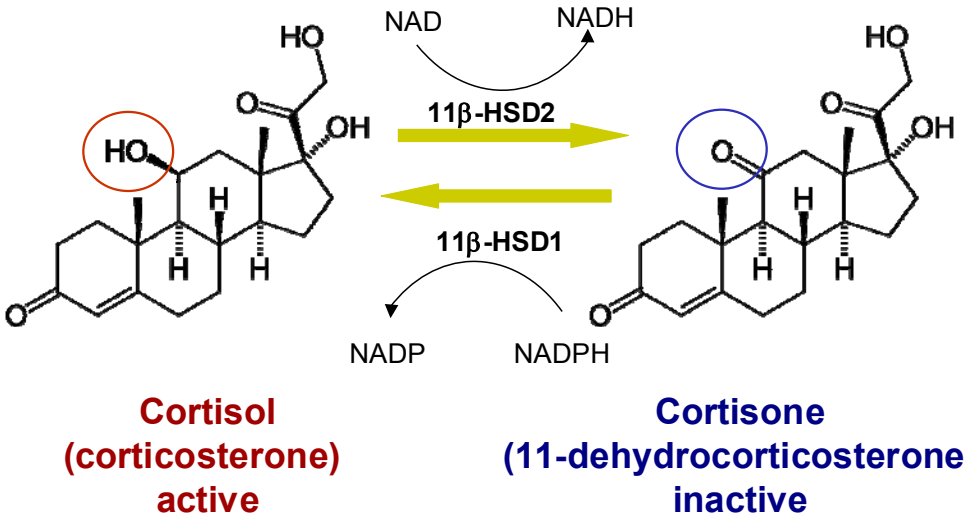

Figure 1.4 The reaction catalyzed by 11β-hydroxysteroid dehydrogenase (11β-HSD)

11β-HSD1 and 11β-HSD2 use nicotinamide cofactors to transfer hydride to interconvert active GC (cortisol in humans and corticosterone in rodents), able to bind to receptors, and inactive GC (cortisone in humans and 11-dehydrocorticosterone in rodents), which show negligible binding to receptors. A circle indicates the hydroxyl/keto group at the 11 position of cortisol/cortisone, respectively. In intact cells, 11β-HSD1 is predominately a reductase, converting cortisone (or 11-dehydrocorticosterone) to cortisol (or corticosterone), whereas 11β-HSD2 is a dehydrogenase, inactivating GC (adapted from (Seckl, Morton et al. 2004)).

11β-HSD1 utilizes the cofactor NADP(H) within the lumen of the ER (Odermatt, Atanasov et al. 2006). Hexose-6-phosphate dehydrogenase (H6PDH) which is adjacent to 11β-HSD1 in the ER lumen (Atanasov, Nashev et al. 2004), generates NADPH by catalyzing the first two steps of the pentose-phosphate pathway (Mason, Stevens et al. 1999), thereby stimulating oxoreductase activity of 11β-HSD1 (Atanasov, Nashev et al. 2004). H6PDH KO mice lose 11β-HSD1 reductase activity but gain dehydrogenase activity through changes in NADPH cofactor provision (Lavery, Walker et al. 2006). Although research on cortisone reductase deficiency (CRD) patients originally implicated a combination of mutations or gene variants in 11β-HSD1 and H6PDH which interacted to cause CRD (manifest in a reduction in 11β-HSD1 expression and impaired conversion of cortisone to cortisol) (Draper, Walker et al. 2003), more recent analysis has shown those patients only have *H6PD* gene mutations which suggests that CRD is caused by inactivating mutations in the *H6PD* gene and not in the 11β-HSD1 gene as originally thought (Lavery, Walker et al. 2008).

11β-HSD2 is an NAD(H)–dependent enzyme that oxidizes active GCs to their inactive 11-keto forms (Albiston, Obeyesekere et al. 1994; Brown, Chapman et al. 1996). It is also localized to the ER but with the opposite orientation to 11β-HSD1, facing the cytoplasm (Odermatt, Arnold et al. 1999). 11β-HSD2 dictates the specificity for the mineralocorticoid receptor (MR) by converting active GCs into

inert GCs, leaving aldosterone to occupy the MR (Edwards, Stewart et al. 1988; Funder, Pearce et al. 1988). Congenital deficiency of 11β-HSD2 results in the syndrome of apparent mineralocorticoid excess (AME); in these patients cortisol acts as a potent mineralocorticoid causing high blood pressure (Edwards, Walker et al. 1993). Whilst 11β-HSD1 is widely expressed, 11β-HSD2 shows a more restricted distribution, being mainly expressed in mineralocorticoid-target tissues, such as kidney and colon (reviewed in (Stewart and Krozowski 1999)). However, it is becoming clear that it is expressed in other tissues as well, e.g. the vasculature and the placenta (Li, Smith et al. 1996; Christy, Hadoke et al. 2003).

1.5.2 Tissue-specific distribution of 11β-HSD1

11β-HSD1 shows a broad tissue distribution in humans and rodents, with predominant expression in liver, brain, lung, kidney and adipose tissue (Moisan, Seckl et al. 1990; Tannin, Agarwal et al. 1991; Whorwood, Franklyn et al. 1992; Ricketts, Verhaeg et al. 1998; Brereton, van Driel et al. 2001). 11β-HSD1 is not always, however, uniformly expressed in the whole organ. For example, in kidney 11β-HSD1 is expressed in all renal tubular epithelia but is not detected in medullary interstitial cells (Yau, Van Haarst et al. 1991). During mouse development, 11β-HSD1 mRNA expression is first observed at E15 in lung and liver, and rises strongly later (Speirs, Seckl et al. 2004). 11β-HSD1 is also highly expressed in rat brain subregions in the early postnatal period (Moisan, Edwards et al. 1992).

1.5.3 The role of 11β-HSD1

11β-HSD1 plays an important role in regulating GC activity. The *in vivo* role of 11β-HSD1 has been elucidated largely by the generation of mice homozygous for a targeted disruption of the 11β-HSD1 gene (Kotelevtsev, Holmes et al. 1997). Experiments on 11β-HSD1-deficient mice confirm that 11β-HSD1 is the only 11β-reductase in mice, as they are unable to convert 11-dehydrocorticosterone to corticosterone (Kotelevtsev, Holmes et al. 1997). 11β-HSD1-deficient mice show compensatory increased adrenal secretion of corticosterone as well as adrenal hypertrophy and they have elevated basal plasma corticosterone levels (Kotelevtsev, Holmes et al. 1997). They also showed reduced sensitivity to glucocorticoid negative feedback upon the HPA axis and elevated responses to acute restraint stress (Harris, Kotelevtsev et al. 2001). However, transgenic re-expression of 11β-HSD1 selectively in liver of 11β-HSD1-deficient mice restored the HPA-axis phenotype (Paterson, Holmes et al. 2007) demonstrating that hepatic GC metabolism influences the function of the HPA axis. After back-crossing to the C57BL/6J genetic back-ground (from the original mixed 129/MF1 background), 11β-HSD1-deficient mice showed normal blood glucocorticoid levels (Yau, McNair et al. 2007; Carter, Paterson et al. 2009), but compensatory changes in GR expression in areas of the brain involved in GC negative feedback (Carter, Paterson et al. 2009). Therefore the different strains of mice have different mechanisms of regulating HPA activity and the genetic

background of mice influences the HPA phenotype of 11β-HSD1-deficient mice. Compared to wild-type mice, 11β-HSD1-deficient mice showed an enhanced angiogenesis *in vitro* and *in vivo* within sponges, wounds, and infarcted myocardium (Small, Hadoke et al. 2005). 11β-HSD1-deficient mice are also resistant to diet-induced metabolic disease, and have increased hepatic and adipocytic insulin sensitivity (Morton, Holmes et al. 2001; Morton, Paterson et al. 2004). They are also resistant to cognitive decline in old age (Yau, Noble et al. 2001; Yau, McNair et al. 2007). Mice deficient in 11β-HSD1 also reportedly lack bone marrow adipocytes (Justesen, Mosekilde et al. 2004) although this has not been confirmed in recent experiments (Agnes Coutinho, personal communication).

Based on the protective effects of 11β-HSD1-deficiency in metabolic disease and age-related cognitive decline (reviewed in (Seckl 2004)), 11β-HSD1 enzyme inhibition has been investigated as a treatment for type II diabetes, insulin resistance, cardiovascular disease and cognitive dysfunction (reviewed in (Seckl 2004)). Treatment with the non-selective 11β-HSD1 inhibitor, carbenoxolone, improved verbal fluency in healthy men and verbal memory in type 2 diabetes patients (Sandeep, Yau et al. 2004). In a murine model of atherosclerosis, inhibition of 11β-HSD1 slowed plaque progression in apolipoprotein E-deficient *Apoe*$^{-/-}$ mice, and the mice showed less accumulation of total cholesterol in aorta, as well as lower serum cholesterol (Hermanowski-Vosatka, Balkovec et al. 2005). Now clinical trials

have been reported by several pharmaceutical companies (Boyle and Kowalski 2009). Selective 11β-HSD1 inhibitors decreased blood glucose in diabetes by reducing glucose production in both rodents and humans (Alberts, Engblom et al. 2002; Barf, Vallgarda et al. 2002; Andrews, Rooyackers et al. 2003; Tiwari 2010).

1.6 11β-HSD1 and inflammation

1.6.1 Expression of 11β-HSD1 in leukocytes

It has recently been shown that 11β-HSD1 is expressed in immune cells and regulates both innate and adaptive immune responses (reviewed in (Chapman, Coutinho et al. 2009; Cooper and Stewart 2009)). 11β-HSD1 is induced in human monocytes upon differentiation to macrophages (Thieringer, Le Grand et al. 2001). It is also induced upon differentiation of monocytes into dendritic cells where it acts as an autocrine-negative regulator of dendritic cell differentiation from monocyte precursors (Freeman, Hewison et al. 2005). 11β-HSD1 expression has been detected in human neutrophils at both the mRNA and protein levels (Kardon, Senesi et al. 2008). With respect to the adaptive immune response, Zhang et al. showed that 11β-HSD1 mRNA, protein, and enzyme activity are expressed in murine $CD4^+$, $CD8^+$ and $B220^+$ lymphocytes (Zhang, Ding et al. 2005).

1.6.2 Inflammatory responses of 11β-HSD1-deficient mice

Most data show that during an acute inflammatory response, mice deficient in 11β-HSD1 show an exaggerated inflammatory response and altered resolution.

In vivo, in sterile peritonitis, more peritoneal cells are recruited to the peritoneum in 11β-HSD1-deficient mice than in control mice (Gilmour 2002), and following LPS administration, 11β-HSD1-deficient mice exhibited higher serum levels of TNF-α, IL-6 and IL-12p40 compared to WT controls (Zhang and Daynes 2007). Importantly, preliminary data in a mouse model of pleurisy suggested a greater influx of inflammatory cells in the pleural cavity of 11β-HSD1-deficient mice than in control mice following intrapleural injection of carrageenan (Coutinho 2009). *In vivo*, during sterile peritonitis, macrophages from 11β-HSD1-deficient mice showed delayed acquisition of phagocytic competence compared to WT mice, with more free apoptotic neutrophils 2 days following injection with thioglycollate (Gilmour, Coutinho et al. 2006) suggesting 11β-HSD1 may potentially contribute to the reduction of inflammation, although both genotypes resolved the peritoneal inflammation at the same time (Gilmour, Coutinho et al. 2006). *Ex vivo,* macrophages lavaged from the peritoneum of 11β-HSD1-deficient mice following thioglycollate showed a greater cytokine response to LPS stimulation (Gilmour, Coutinho et al. 2006; Zhang and Daynes 2007), probably due to TGF-β mediated up-regulation of SHIP1, a phosphatase that negatively regulates the activation of immune cells primarily via the phosphoinositide 3-kinase (PI3K) pathway (Zhang and Daynes 2007). In a model of self-resolving experimental arthritis, 11β-HSD1-deficient mice developed clinical signs of inflammation a day earlier than

control mice and were slower to resolve the inflammatory response (Coutinho 2009). Collectively, these data suggest that endogenous GC regulated by 11β-HSD1 play an important role in affecting the differentiation or activation of macrophages and that 11β-HSD1 activity may suppress acute inflammation and contribute to its successful resolution.

1.6.3 Regulation of 11β-HSD1 in inflammation

Several recent reports have shown that 11β-HSD1 expression is increased by pro-inflammatory stimuli or at sites of inflammation (reviewed in (Chapman, Coutinho et al. 2009)).

In human and animal colitis, colonic 11β-HSD1 activity and mRNA expression were strongly increased (Vagnerova, Kverka et al. 2006; Zbankova, Bryndova et al. 2007). In rheumatoid arthritis, within the joint, synovial inflammation was positively correlated with cortisone reactivation, suggesting increased synovial 11β-HSD1 activity (Schmidt, Weidler et al. 2005) and in rat adjuvant arthritis, which is similar to human rheumatoid arthritis, synovial 11β-HSD1 mRNA and reductase activity was increased (Ergang, Leden et al. 2010). This is consistent with increased 11β-HSD1 activity and mRNA levels in synovial tissues of patients with rheumatoid arthritis (Hardy, Rabbitt et al. 2008) and synovial fibroblasts highly express 11β-HSD1 following treatment with IL-1β or TNF-α (Hardy, Filer et al. 2006). In

sterile peritonitis, 11β-HSD1 expression was markedly increased in peritoneal cells (mainly immune cells) following *in vivo* injection of thioglycollate (Gilmour, Coutinho et al. 2006). IL-1β and TNF-α are potent stimulators of 11β-HSD1 expression in various cells. They induce mRNA and activity of 11β-HSD1 in human aortic smooth muscle cells, glomerular mesangial cells, ovarian surface epithelial cells and preadipocytes (Escher, Galli et al. 1997; Handoko, Yang et al. 2000; Cai, Wong et al. 2001; Tomlinson, Moore et al. 2001; Yong, Harlow et al. 2002), as well as all types of fibroblasts examined to date (Sun and Myatt 2003; Hardy, Rabbitt et al. 2008).

1.7 Regulation of 11β-HSD1

1.7.1 Promoters of 11β-HSD1

The 11β-HSD1 gene is transcribed from 3 promoters; P1, P2 and P3 (Moisan, Edwards et al. 1992; Bruley, Lyons et al. 2006). Lung mainly uses an upstream promoter, P1, which in mice, is located approximately 23 kb 5' to exon 2, whereas most other tissues (liver, brain, adipose tissue) use the downstream promoter, P2 (Bruley, Lyons et al. 2006) (Figure 1.5). P3, described in rat kidney, is located within the intron between exon 2 and 3 (Moisan, Edwards et al. 1992). It encodes a truncated protein, which doesn't show 11β-HSD1 enzyme activity (Mercer, Obeyesekere et al. 1993).

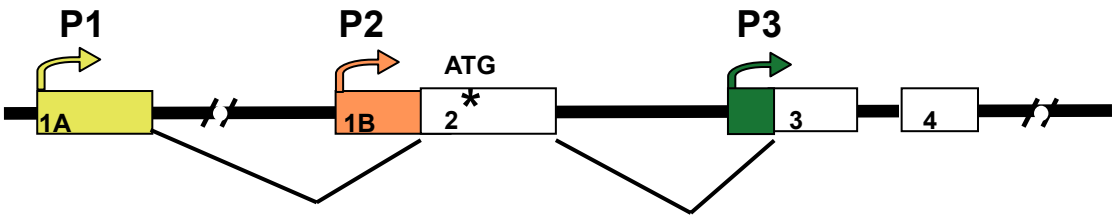

Figure 1.5 Schematic representation of the 11β-HSD1 promoter region
11β-HSD1 can be transcribed from the P1 promoter (transcribing exon 1A), from the P2 promoter (exon 1B), or from the P3 promoter in the intron between exons 2 and 3 (Moisan, Edwards et al. 1992; Bruley, Lyons et al. 2006). Transcription starts associated with each promoter are shown by curved arrows. Rectangular boxes indicate exons (numbers in boxes indicate the exon). An asterisk indicates the normal translation start of 11β-HSD1. Adapted from (Bruley, Lyons et al. 2006).

The regulation of the P1 and P3 promoters has not been characterized, although expression of 11β-HSD1 in lung (mainly from the P1 promoter) is C/EBPα–independent and the P1 promoter is not regulated by C/EBPα in transfected cells (Bruley, Lyons et al. 2006). The P2 promoter has been shown to be regulated by the CCAAT/enhancer binding protein (C/EBP) family of transcription factors. C/EBPs are major regulators of cell proliferation and terminal differentiation (reviewed in (McKnight 2001)). There are 6 members of the family; C/EBPα, β, γ, δ, ε and C/EBPζ (also known as CHOP) (Lekstrom-Himes and Xanthopoulos 1998). C/EBPα and C/EBPβ have both been implicated in the regulation of 11β-HSD1 transcription (reviewed in (Chapman, Coutinho et al. 2009)). C/EBPα plays a major role in energy metabolism (McKnight, Lane et al. 1989) and haematopoietic lineage determination (Iwasaki, Mizuno et al. 2006). C/EBPβ regulates inflammatory and native immunity functions (reviewed in (Poli 1998)). *In vivo*, C/EBPα is a major regulator of 11β-HSD1 P2 promoter activity in liver and brown adipose tissue (Williams, Lyons et al. 2000; Bruley, Lyons et al. 2006) as well as mature adipocytes (Dr Cristina Esteves, personal communication). C/EBPβ is also important for 11β-HSD1 expression in white adipose tissue (Payne, Au et al. 2007) and adipocytes (Dr Cristina Esteves, personal communication). *In vitro*, in 3T3-L1 preadipocytes, C/EBPβ is implicated in the basal level expression of 11β-HSD1 and its induction in response to cAMP, as 3T3-L1 preadipocytes are differentiated into adipocytes (Gout, Tirard et al. 2006). Similarly, when 3T3-L1 preadipocytes were

treated with ceramide or the AMPK activator, AICAR, 11β-HSD1 expression and enzyme activity was increased, and was dependent upon C/EBPβ binding to the P2 promoter (Arai, Masuzaki et al. 2007). In A549 lung epithelial cells, dex increased 11β-HSD1 expression, and it was dependent on C/EBPβ and associated with C/EBPβ binding to the P2 promoter of 11β-HSD1 (Sai, Esteves et al. 2008). Dex has also been shown to increase 11β-HSD1 activity in human skin fibroblasts (Hammami and Siiteri 1991) an effect which might also depend on C/EBPβ, which is regulated by GC (Berg, Didon et al. 2005; Yang, Mammen et al. 2005).

The P2 promoter is also regulated by cytokines. TNF-α increased 11β-HSD1 expression by inducing the binding of C/EBPβ to the P2 promoter of 11β-HSD1 in HepG2 (hepatoma) cells (Ignatova, Kostadinova et al. 2009). Similarly, the dramatic induction of 11β-HSD1 expression by IL-1 in human fetal lung fibroblasts required C/EBPβ binding to the P2 promoter of 11β-HSD1 (Yang, Zhu et al. 2009).

1.7.2 Expression of 11β-HSD1 in lung

11β-HSD1 is expressed in lung of all species examined to date, including rat, mouse, rabbit and human (Torday, Olson et al. 1976; Monder and Lakshmi 1990; Soldan, Nagel et al. 1999; Speirs, Seckl et al. 2004).

In rat lung, 11β-HSD enzyme activity is mainly reductase (Nicholas and Lugg 1982)

and the presence of the protein in lung has been confirmed by western blots after producing an antibody against rat liver 11β-HSD1 (Monder and Lakshmi 1990). In humans, expression of 11β-HSD1 varies widely between individuals, with an almost 20-fold range in 11β-HSD1 mRNA levels between different subjects (Soldan, Nagel et al. 1999) which suggests large inter-individual differences. Within lung, expression of 11β-HSD1 has been identified by IHC in fibroblasts and type II alveolar cells (Brereton, van Driel et al. 2001; Suzuki, Tsubochi et al. 2003). The IHC result is consistent with activity assays in isolated lung fibroblasts. Both human and rat lung fibroblasts *in vitro* show 11β-HSD reductase activity (Abramovitz, Branchaud et al. 1982; Torday, Post et al. 1985).

Very little 11β-HSD1 is expressed in rodents prior to birth (Speirs, Seckl et al. 2004). However, studies in the mouse, rat and rabbit have demonstrated a rise in conversion of 11-dehydrocorticosterone to corticosterone by the fetal lung in late pregnancy (Torday, Olson et al. 1976; Hundertmark, Ragosch et al. 1994; Suzuki, Tsubochi et al. 2003). In mouse lung, 11β-HSD1 mRNA expression is observed at E15 and increases strongly later in development (Speirs, Seckl et al. 2004).

Given the effects of GC on fetal lung maturation, these studies suggested that 11β-HSD1 may be important in the fetal development of lung. Consistent with such a role, 11β-HSD1 deficient mice exhibited delayed fetal lung development, with lower

surfactant protein (SP)-A levels and significant depletion of lung surfactant (Hundertmark, Dill et al. 2002). Chemical inhibition of fetal 11β-HSD1 activity also reduced the gestation-dependent accumulation of SP-A and decreased lamellar body content in alveolar type II cells in lung (Hundertmark, Dill et al. 2002). These data suggest 11β-HSD1 plays an important role in regulating GC levels in fetal lung to enhance lung maturation.

1.8 Lung inflammation and fibrosis

1.8.1 Lung structure

Lung is the main organ for air exchange, extracting oxygen from the air into the blood circulation and releasing CO_2. Lung can be divided into two components, airways and alveoli (Figure 1.6A). The airways comprise the upper airway (trachea) and lower airways (bronchi). At the end of the bronchi are the alveoli, which are surrounded by capillaries and are the site of gas exchange. There are 4 main kinds of cells in and around alveoli. Type I alveolar cells comprise ~95% of the alveolar surface area and are the major cell type in alveoli. They are thin, squamous epithelial cells that cover the pulmonary capillaries, and are required for effective gas exchange. Type II alveolar cells cover only about 5% of the alveolar surface area and their main function is to produce and secret surfactant to reduce surface tension of the alveolar wall. Fibroblast cells are present in the connective tissue of the alveoli to form the structure and alveolar macrophages are located inside the alveolar spaces to clear dust or bacteria (Figure 1.6B).

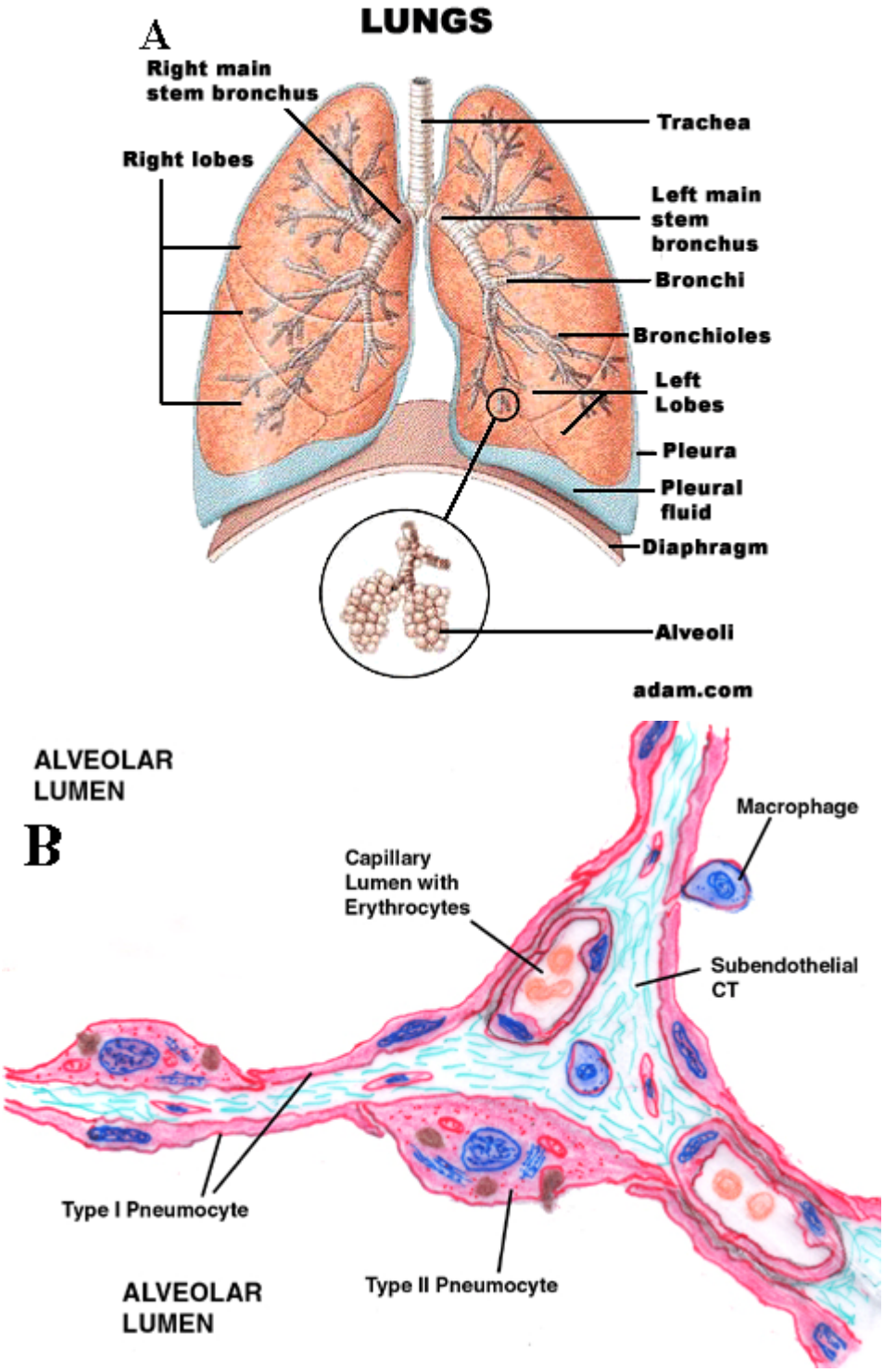

Figure 1.6 Lung structure

(A), basic structures of lung from trachea to alveoli, and the basic structure of alveoli (enlarged circle). (B), the detailed structure of alveolar sacs. CT represents connective tissue.

[Taken from http://education.vetmed.vt.edu/Curriculum/VM8054/Labs/Lab25/lab25.htm]

Lung is one of the few tissues or organs which are exposed to air directly. Due to the moist environment, it is an ideal place for bacteria to grow. Alveolar macrophages comprise about 85% of free cells in the alveoli and they are a distinctive cell type in a unique environment where they function to phagocytose and neutralize the large daily burden of foreign organisms and particles that reach the distal airways (Brody 1998). Clearance of these particles must be achieved without excessive inflammation that could compromise gas exchange, suggesting that alveolar macrophages are specialized phagocytes (Hu, Sonstein et al. 2000). It is well established that resting alveolar macrophages help to create an immunosuppressive environment in which the initiation of immune responses and the activation of antigen-specific T cells in the lung are limited (Strickland, Kees et al. 1996).

Minor lung injury is usually resolved by cycles of the normal physiological response of inflammation and repair. However, when injury is repetitive or larger in magnitude, the repair process is exaggerated and usually widespread and frequently results in scarring or fibrosis (Martinet, Menard et al. 1996).

1.8.2 Bleomycin-induced lung injury and fibrosis

Bleomycin belongs to a family of glycopeptides isolated from *Streptomyces verticillus* and is used clinically as a cancer chemotherapeutic agent for the treatment of several types of tumors, notably squamous cell carcinomas and malignant

lymphomas (Blum, Carter et al. 1973), probably because of its ability to mediate dioxygen activation and affect the degradation of DNA substrates (Hamamichi, Natrajan et al. 1992). It binds to DNA and iron which induces free radical formation, resulting in death of cells (Kane, Natrajan et al. 1994). Bleomycin has also been shown to mediate the oxidative degradation of all major classes of cellular RNA (reviewed in (Hecht 2000)). The main side effect of treatment with bleomycin is dose-dependent pulmonary toxicity and pulmonary fibrosis (reviewed in (Cooper, Zitnik et al. 1988)). Bleomycin increases total lung collagen content possibly resulting from an inflammatory response to lung injury (Sikic, Young et al. 1978). The symptoms following bleomycin treatment in animal models resemble human idiopathic pulmonary fibrosis (Giri, Nakashima et al. 1985). The bleomycin model includes four phases; an initial injury phase, an inflammatory phase, a proliferative phase involving connective tissue cells and other cells and a remodeling-repair phase. Typically, intratracheal instillation of bleomycin causes necrosis of type I alveolar cells up to one day post instillation, followed by acute alveolitis on day two or three, then an intense interstitial inflammation (Piguet, Collart et al. 1989). And the lung starts to express chemokines, such as CXCL-12 and CCL-18 to recruit inflammatory cells (Phillips, Burdick et al. 2004; Pochetuhen, Luzina et al. 2007). Overexpression of those chemokines worsens the severity of lung inflammation and fibrosis (Phillips, Burdick et al. 2004; Pochetuhen, Luzina et al. 2007). During the inflammation phase, fibroblasts start to proliferate and differentiate into myofibroblasts in an attempt to

repair the damaged alveolus, resulting in ECM accumulation. The collagen content can be elevated by 2-fold after three weeks of treatment (Bowden 1984). Fibrosis is seen within the interstitium and the alveolar spaces, and finally leads to extensive diffuse pulmonary fibrosis (Swaisgood, French et al. 2000). In normal wound healing, the number of myofibroblasts gradually declines as the healing process is successfully completed and it has been suggested that myofibroblast disappearance occurs via apoptosis (Gabbiani, Hirschel et al. 1972; Desmouliere, Redard et al. 1995).

TGF-β1 is one of the most important factors in inducing fibrosis in lung (Shukla, Meisler et al. 1999) and production of this cytokine has been widely demonstrated in bleomycin-induced pulmonary fibrosis (Zhang, Flanders et al. 1995). Bleomycin treatment increases the transcription of TGF-β mRNA, total cellular TGF-β mRNA, and total cellular type I procollagen mRNAs in rat lung fibroblasts (Cutroneo, Breen et al. 1991). C/EBP-β also plays a significant role in the development of pulmonary fibrosis (Hu, Ullenbruch et al. 2007) and it stimulates the expression of α-SMA during myofibroblast differentiation (Hu, Wu et al. 2004). C/EBP-$\beta^{-/-}$ mice were resistant to bleomycin induced fibrosis (Hu, Ullenbruch et al. 2007), demonstrating a key role for this transcription factor in the process.

1.9 Hypothesis and Aims of this study

Hypothesis:

Amplification of endogenous intracellular GC levels by 11β-HSD1 represents an important mechanism to limit the inflammatory response and the progression of fibrosis.

Aims:

This thesis aimed to test the above hypothesis, by determining the contribution of 11β-HSD1 to an inflammatory response, using 11β-HSD1-deficient mice subjected to experimental models of lung inflammation and fibrosis. Furthermore, to provide new insights into its role in the inflammatory response, the regulation of 11β-HSD1 was investigated in wild-type (WT) control mice. In particular the specific aims were:

- Firstly, to characterize the expression of 11β-HSD1 in lung and identify the cell types that express 11β-HSD1.
- Secondly, to identify the 11β-HSD1 gene promoter used in lung fibroblasts and determine if 11β-HSD1 is regulated by cytokines in these cells.
- Thirdly, to investigate whether there is a difference in lung inflammation and fibrosis in 11β-HSD1-deficient mice compared to WT mice in the bleomycin model.

2 Chapter Two: Materials and methods

2.1 Materials

2.1.1 Animals

Male Mice (~16-18 weeks of age) homozygous for a targeted disruption of the *Hsd11b1* gene encoding 11β-HSD1 (backcrossed >8 generations on a C57BL/6 background) (Kotelevtsev, Holmes et al. 1997) (Morton, Paterson et al. 2004) and age-matched C57BL/6 control mice (*Hsd11b1*$^{+/+}$) were used. Mice were bred on-site and were housed in groups of 2-6 per cage under controlled conditions (12h light/dark cycles, at 21ºC) with unlimited access to water and standard rodent chow. All experiments on animals were approved by the local ethics committee and were performed in accordance with the U.K. Home Office Animals (Scientific Procedures) Act of 1986.

2.1.2 Tissue culture materials

Attachment medium	500ml RPMI-1640 supplemented with 10 ml penicillin/streptomycin (5000U/ml) and 3.3 ml gentamycin (10mg/ml).
DC Medium	500ml RPMI-1640 supplemented with 10ml penicillin/streptomycin (5000U/ml), 0.5ml 50 mM 2-mercaptoethanol, 50ml FBS
Dissociation solution	12.5mg DNase I in 50ml of Phosphate buffered saline (PBS) (without calcium and magnesium),

	containing 500μg gentamycin and 800μg tylosine, filter sterilized, kept at room temperature and used fresh each time.
Fibroblast culture medium	500ml DMEM supplemented with 5ml penicillin/streptomycin (5000U/ml) and 50ml NBFS
GM-CSF solution	Reconstitute to 10μg/ml and store at –20°C in 40μl aliquots (for 10μg lots, dissolve in 100 μl sterile water, then add 900 μl sterile PBS)
Conditioned L929 media	Gift of Dr Jeremy Hughes lab
Macrophage medium	DMEM/F12 Glutmax (Invitrogen) supplemented with 50ml FBS, 5ml penicillin/streptomycin (5000U/ml) and 10% conditioned L929 medium
Trypsin solution	65mg Trypsin type I into 26ml PBS with calcium and magnesium. The solution dissolved slowly. After dissolve, solution was filter sterilized and used fresh at 37°C.

2.1.3 Tissue culture media and reagents

Cell strainer	BD Biosciences, The Danby Building, Edmund

	Halley Road, Oxford Science Park, OX4 4DQ Oxford, UK
Collagenase from Clostridium histolyticum, Type IA-S	Sigma-Aldrich Company Ltd. The Old Brickyard, New Road, Gillingham, Dorset, SP8 4XT
Dimethyl Sulphoxide (DMSO) D2650	Sigma-Aldrich (see above)
DMEM/F12 Glutmax medium	Invitrogen Ltd, 3 Fountain Drive, Inchinnan Business Park, Paisley, PA4 9RF
Dulbecco's Modified Eagle's Medium (DMEM)	Lonza Group Ltd, Muenchensteinerstrasse 38 CH-4002 Basel, Switzerland
F-12K Nutrient Mixture, Kaighn's Modification (1X), liquid	Invitrogen (see above)
Fetal bovine serum (FBS)	Lonza (see above)
Gentamicin solution (10mg/ml)	Sigma-Aldrich (see above)
Granulocyte-Macrophage Colony Stimulating Factor (GM-CSF) REC MS (BioSource™)	Invitrogen (see above)
L-Glutamine (200mM)	Lonza (see above)
2-mercaptoethanol	Sigma-Aldrich (see above)

NucleoCassette	ChemoMetec, Gydevang 43, DK-3450 Allerod, Denmark
NucleoCounter	ChemoMetec (see above)
Penicillin and streptomycin solution (5000U/ml)	Lonza (see above)
Petri dish	Barloworld ScientificBeacon Road, Stone, Staffordshire, ST15 0SA, UK
Phosphate buffered saline (PBS) (without calcium and magnesium)	Sigma-Aldrich (see above)
Phosphate buffered saline (PBS) (with calcium and magnesium)	Sigma-Aldrich (see above)
RPMI 1640 medium with L-glutamine	Lonza (see above)
Tissue culture flasks (25cm^2 and 75cm^2)	Corning Limited, The Guildway, Old Portsmouth Road, Artington, Surrey GU3 1LR, United Kingdom
Trypsin/ EDTA (trypsin 500mg/L, EDTA 200mg/L)	Lonza (see above)
Trypsin type I, from Bovine pancreas	Sigma-Aldrich (see above)
Tylosin solution (8mg/mL in	Sigma-Aldrich (see above)

0.9% NaCl)	
6,12 well plates	Corning (see above)

2.1.4 General reagents

All general reagents were purchased from Sigma-Aldrich, or were purchased as detailed below:

Acetone（99.5%）	Sigma-Aldrich (see above)
Aqueous picric acid solution	Sigma-Aldrich (see above)
LE Agarose	Lonza (see above)
Antibody diluent	Dako UK Ltd. Denmark House, Angel Drove, Ely, Cambridgeshire CB7 4ET
Avidin/biotin blocking kit	Vector Laboratories, Ltd., 3 Accent Park, Bakewell Road, Orton Southgate, Peterborough, PE2 6XS, England
Chloroform	Fisher Scientific UK Ltd, Bishop Meadow Road, Loughborough, Leicestershire, LE11 5RG
Diethyl Phyocarbonate (DEPC)	Sigma-Aldrich (see above)
Direct red 80	Sigma-Aldrich (see above)
Deionised formamide	Sigma-Aldrich (see above)
Dexamethasone	Sigma-Aldrich (see above)
Deoxyribonuclease I from bovine	Sigma-Aldrich (see above)

pancreas	
Diff-quick red staining solution	Dade Behring, Inc. Corporate Headquarters, 1717 Deerfield Road, Deerfield, Illinois
Diff-quick blue staining solution	Oy Reagena Ltd, Takojantie 18, FIN-70900 Toivala, Finland
Ethanol	Fisher Scientific (see above)
Fast green	Sigma-Aldrich (see above)
Formalin solution, 4%	Sigma-Aldrich (see above)
Hydrogen peroxide	VWR International Ltd, Hunter Boulevard, Magna Park, Lutterworth, Leicestershire, LE17 4XN
Harris' hematoxylin	Thermo, anatomical pathology international, 93-96 Chadwick Road, Astmoor, Runcorn, Cheshire, WA7 1PR, UK
Isopropyl alcohol	Fisher Scientific (see above)
Kodak MS-1 autoradiographic film	Sigma-Aldrich (see above)
Liquid Diaminobenzidine (DAB) + substrate chromogen system	Dako (see above)
Lipopolysaccharide (LPS)	Sigma-Aldrich (see above)
Methanol	Fisher Scientific (see above)

Mowiol 4-88 Reagent	MERCK CHEMICALS LTD, Padge Road, Beeston, Nottingham NG9 2JR, UK
NICK columns	Amersham Pharmacia Biotech UK Ltd
Pepsin from porcine gastric mucosa	Sigma-Aldrich (see above)
Phosphate buffered saline (PBS) tablets	Oxoid Ltd, Wade Road, Basingstoke, Hampshire, RG24 8PW, UK
Protein assay dye reagent concentrate	Bio-Rad Laboratories Ltd, Bio-Rad House, Maxted Road, Hemel Hempstead, Hertfordshire, HP2 7DX, UK
Protein assay reagent A	Bio-RAD (see above)
Protein assay reagent B	Bio-RAD (see above)
Protein block	Dako (see above)
Proteinase K	Promega UK Ltd, Delta House, Enterprise Road, Chilworth Research Centre, Southampton SO16 7NS
R.T.U. vectorstain kit (ABC reagent)	Vector (see above)
Sircol Dye Reagent	Biocolor Ltd, 8 Meadowbank Road, Carrickfergus, County Antrim, BT38 8YF, United Kingdom

20xSSC	Sigma-Aldrich (see above)
Xylene	Fisher Scientific (see above)

2.1.5 Antibodies

1) Primary antibodies:	
Anti-mouse F4/80 antigen, rat, 1:50 dilution	AbD Serotec, Endeavour House, Langford Business Park, Langford Lane, Kidlington, Oxford, OX5 1GE, UK
11β-HSD 1 polyclonal antibody, rabbit, 1:100 dilution	Cayman Chemical, 1180 E.Ellsworth Road, Ann Arbor, Michigan, 48108, USA
11β-HSD 1 polyclonal antibody, sheep, 1:1000 dilution	A gift from Dr Scott Webster, Endocrinology Unit, Queen's Medical Research Institute, 47 Little France Crescent, Edinburgh, EH16 4TJ.
Anti-Mouse CD11c, Hamster (Biotin-labeled), 1:50 dilution	Invitrogen (see above)
Ms X β-tubulin, 1:1000 dilution	CHEMICON, 290 Concord Road, Billerica, MA 01821, USA
GR polyclonal antibody (M20), rabbit, 1:100 dilution	Santa Cruz Biotechnology, Inc, Bergheimer Str. 89-2, 69115 Heidelberg, Germany
2) Secondary antibodies:	

Goat anti-Rabbit IgG, Biotin-labeled, 1:50 dilution	Dako (see above)
Rabbit anti-Rat IgG, Biotin-labeled, 1:200 dilution	AbD Serotec (see above)
Rabbit anti-Sheep IgG, HRP conjugate, 1:400 dilution	Millipore (U.K.) Limited, Units 3&5 The Courtyards, Hatters Lane, Watford, WD18 8YH, England
IRDye 800 conjugated Anti-mouse IgG, 1:1000 dilution	Rockland Immunochemicals, Gilbertsville, PA 19525, USA
Alexa 680 conjugated Anti-sheep IgG, 1:1000 dilution	Invitrogen (see above)

2.1.6 Molecular biology general reagents

Denhardt's solution	Sigma-Aldrich (see above)
Deoxynucleotide Triphophates (dNTPs)	Promega (see above)
DNA size markers (1000 base-pair ladder)	Invitrogen (see above)
Dnase I	Promega (see above)
GoTaq DNA polymerase	Promega (see above)
Kpn I restriction enzyme	Promega (see above)

Lightcycler 480 Probes Master Mix	Roche Diagnostics Ltd, Charles Avenue, Burgess Hill, RH15 9RY, United Kingdom
Not I restriction enzyme	Promega (see above)
Nuclease-free water	Promega (see above)
RNase OUT	Invitrogen (see above)
Random Primers (oligodeoxyribonucleotides, mostly hexamers)	Promega (see above)
RNaseOUT	Invitrogen (see above)
RNaseZAP	Ambion, Applied Biosystems, Lingley House 120 Birchwood Boulevard, Warrington WA3 7QH, UK
^{35}S-dUTP	GE healthcare, Pollards Wood, Nightingales Lane, Chalfont St Giles, BUCKS, HP8 4SP
SP6 RNA polymerase	Promega (see above)
SuperScript™ III Reverse Transcriptase	Invitrogen (see above)
T7 RNA polymerase	Promega (see above)
TRIzol Reagent	Invitrogen (see above)

2.1.7 Primers used for PCR

Primer name	Sequence	Comment
P868	5'-AGGATCCARAGCAAACTTGCTTGCA-3'	Primers used to amplify total 11β-HSD1, 470bp product. (Rajan, Chapman et al. 1995)
P869	5'-AAAGCTTGTCACWGGGGCCAGCAAA-3'	
Maser 1.4L	5'- GGAGCCGCACTTATCTGAA -3'	Primer used to amplify from mouse promoter 1 with P868; 627bp product.
Down stream Ex1 specific	5'- GGAGGTTGTAGAAAGCTCTG -3'	Primer used to amplify from mouse promoter 2 with P868; 646bp product.
P31 intron	5'- GTATGGAAAGCAAGACAAGG -3'	Primer used to amplify from mouse promoter 3 with P868; 543bp product.
Upstream exon1	5'-GAAGTCAGATTTGTTCGAAATCTTG-3'	Primer used to amplify from human promoter 1 with reverse primer exon 3; 272bp product
Downstream exon1-specifi	5'-GGAGGTTGTAGAAAGCTCTG-3'	Primer used to amplify from human promoter 2

c		with reverse primer exon 3; 285bp product
Common region	5’-TTCTGCAAACGAGGAATTCAG-3’	Primers used to amplify human total 11β-HSD1; 152bp product
Reverse primer exon 3	5’-GTAGAGTTTCTTTTGACCTCG-3’	Human reverse primer

2.1.8 Equipment

Wallac 1450 MicroBeta TriLux Liquid Scintillation Counter	Perkin Elmer, 940 Winter Street, Waltham, Massachusetts 02451, USA
Chamber Slide™ NUNC™ Lab-Tek™ II	VWR International Ltd, Hunter Boulevard, Magna Park, Lutterworth, Leicestershire, LE17 4XN
Cover slips	VWR (see above)
Cover plate	Thermo (see above)
Cytocentrifuge cytospin 3	Thermo (see above)
Cytoclip	Thermo (see above)
Eppendorf centrifuge	Eppendorf UK Limited, Endurance House, Vision Park, Chivers Way, Histon,

	Cambridge, CB4 9ZR
Filter card	Thermo (see above)
Fuji Film FLA-2000 phosphorimager and Fuji BAS phosphorimager tritium screen	Raytek Scientific Ltd, Sheffield, UK. Fuji photofilm Company Ltd, Tokyo, Japan.
Gene Quant RNA/DNA calculator	GE healthcare (see above)
Light cycler 480	Roche (see above)
OPTI max microplate reader	Molecular Devices Corporation, 1311 Orleans Drive, Sunnyvale, CA 94089-1136, U.S.A.
Sequenza staining Racks	Thermo (see above)
Superfrost plus microscope slides	VWR (see above)

2.1.9 Preparation of buffers and solution

Borate Buffer	8.25g Boric acid, 2.7g NaOH, and 3.5ml HCl (33M) was made up to 1L with H_2O (pH 7.4), then 0.5% BSA (0.5g/100ml) was added and stored at -20°C
Citrate Buffer, pH 6.0	1.92g Citric acid (anhydrous) made up to 1L with dH_2O and pH to 6.0, then 0.5 ml of Tween 20 added and solution autoclaved.
Deionised Formamide	150ml formamide mixed with 15g mixed bed

	ion-exchange resin for >1hr, filtered twice and stored protected from light
DEPC-treated H_2O	100ml dH_2O with 1 drop diethylpryocarbonate, left O/N before autoclaving
DNA ladder in loading buffer	30µl 1kb DNA ladder, 60µl TE and 30µl loading buffer.
10X MOPS buffer	200mM 3-(N-morpholino) propanesulfonic acid, 50mM sodium acetate, 10mM EDTA, pH to 7 then autoclaved.
Methyl-Carnoy fixative	60:30:10 (v/v) of methanol, chloroform and glacial acetic acid, respectively
RNase buffer	1ml 5M NaCl, 100µl 1M Tris and 40µl 250mM EDTA, made up to 10ml with Dep H_2O
PBST	0.5ml Tween 20 dissolved in 1000ml PBS
2X prehybridization solution	5.88ml Dep H_2O, 2.4ml 5M NaCl, 200µl 1M Tris (pH 7.5), 400µl 50x Denhardt's solution, 80µl 250mM EDTA, 1ml 10mg/ml sonicated salmon sperm DNA and 40µl 50mg/ml yeast tRNA
Prehybridization solution	6.68ml Dep H_2O, 2.4ml 5M NaCl, 200µl 1M Tris (pH 7.5), 400µl 50x Denhardt's solution, 80µl 250mM EDTA, 200µl 10mg/ml sonicated salmon sperm

	DNA, 40µl 50mg/ml yeast tRNA and 2.0g dextran sulphate
Peroxidase blocking solution	1ml 30% H_2O_2 added to 9ml 1X PBS, mix well and store at 4ºC, stable for 3 months.
Scott's Tap Water Substitute (STWS)	100g magnesium sulphate and 17.5g sodium bicarbonate, made to 5L in H_2O
10X TBE buffer	108.9g Trizma base, 55.7g boric acid, 4.7g EDTA, made to 1L in DEPC H_2O and autoclaved.
TE buffer	10mM Tris-HCl pH8, 1mM EDTA, made to 1L with dH_2O, then autoclaved.

2.1.10 Steroids and radiolabeled steroids

Dexamethasone (DEX)	(FW=392g) was dissolved in 100% ethanol to a stock concentration of 10mM and stored at –20°C
Corticosterone (B)	(FW=346.5g) was dissolved in 100% ethanol to a stock concentration of 10mM and stored at –20°C
11-Dehydrocorticosterone (A)	(FW=344.4g) was dissolved in 100% ethanol to a stock concentration of 10mM and stored at –20°C
[^{3}H]-Corticosterone	Commercial stock solutions of [^{3}H4]-Corticosterone (specific activity ~37 Ci/mmol; Amersham Pharmacia Biotech, Buckingham, UK) in ethanol (with

	concentrations of 13.7nmol/ml) were stored at -20°C
[^{3}H]-11-Dehydrocorticosterone	[^{3}H4]-11-Dehydrocorticosterone was synthesized in-house (preparation described in detail in Section 2.2.23.1), re-suspended in ethanol (for final concentrations of ~10-15nmol/ml) and stored at -20°C

2.1.11 Software

Gel electrophoresis (UVI pro)	UVItec Limited, Avebury House, 36a Union Lane, Cambridge CB4 1QB, United Kingdom
Phosphorimage analysis (Aida)	Raytek Scientific Ltd (see above)
Statistical analysis (Excel)	Microsoft Corporation
GraphPad Prism 4.00	GraphPad Software

2.2 Methods

2.2.1 Cell culture

2.2.1.1 Cell lines; maintenance of HFL-1 and A549 cells in culture

A549 cells were derived from a human lung adenocarcinoma cell line and resemble type 2 alveolar cells (Lieber M, Smith B et al. 1976). HFL-1 cells were derived from human fetal lung fibroblast cells (Breul, Bradley et al. 1980). HFL-1 and A549 cells were brought up from liquid nitrogen from one of the original passages then these cells were passaged, split and stored in liquid nitrogen to ensure that cells maintain

the original character and were not excessively passaged. If cells were passaged more than 15 times, the cells took on the appearance of quiescent cells and did not proliferate.

A549 cells were maintained in 75cm^2 corning flasks in DMEM containing 50U/ml penicillin/streptomycin and 10% FBS. HFL-1 cells were maintained in 75cm^2 corning flasks in F-12K Nutrient Mixture containing 50U/ml penicillin/streptomycin, 1.5mg/ml sodium bicarbonate and 10% FBS. Cells were passaged every week. Medium was aspirated and cells were washed with DMEM medium supplemented with 50U/ml penicillin/streptomycin to remove traces of serum. Cells were immersed in 2ml trypsin/EDTA for 5min in an incubator at 37°C, 5%CO_2. The flask was gently shaken to assist cell detachment from the surface of flask. Trypsin was neutralized by 8ml medium containing 10% FBS. Approximately 2.5ml cells were left for further culture, the rest were aspirated. 10ml fresh medium was added into the flask. Cells were incubated at 37°C and 5%CO_2 until the next passage. Two 75 cm^2 corning flasks were maintained and required for each experiment.

2.2.1.2 Primary cells; generation of murine bone marrow derived macrophages (BMDM)

Male mice were killed by cervical dislocation and immersed in 75% ethanol. A lateral incision was made in the skin midway down the abdomen and skin removed

from the lower abdomen and legs. The tissue surrounding the hip point and muscle on the femur was dissected using autoclaved surgical instruments. The femurs were removed by cutting through the knee joint and the hip joint (flexing the limb helped to pinpoint the spot to cut). The femurs were placed into PBS on ice and transported to a tissue culture hood. The tissues surrounding the femur were removed with a sterile scalpel. Any remaining connective tissue was removed with disinfectant wipes. The femurs were rinsed in 70% ethanol and placed in a small Petri dish with some medium. The proximal and distal ends of each femur were cut just below each joint. A 25G green needle was inserted into the bone cavity. The bone marrow were flushed out in 5ml medium and collected into a 30ml sterile container. This was repeated once from the opposite end of the bone. The cells were resuspended 3 times through a wider bore needle then transferred into 60ml Teflon pots and cultured in 30ml L929 medium in an incubator at 37°C, 5%CO_2. Half of the medium was replenished every other day. Macrophages were harvested for experiment at day 7. Usually the macrophage yield was about 1-2X10^7 per femur and purity, assessed by F4/80 staining of cytospin, was generally more than 90%.

2.2.1.3 Primary cells; generation of bone marrow derived dendritic cells

Bone marrow cells were isolated as above session 2.2.1.2, counted by haemocytometer and viability assessed by trypan blue exclusion. Dendritic cells (DC) were differentiated from bone marrow according to described methods (Lutz,

Kukutsch et al. 1999). On day 0, cells were seeded on bacteriological petri dishes at $2X10^5$/ml in 10ml DC medium containing 20ng/ml GM-CSF. Cells (200μl) were added dropwise to the centre of each petri dish containing medium. On day 3, 10ml of DC medium containing 20ng/ml GM-CSF was added to the petri dish. On day 6 and 8, the procedure was the same as day 3. On day 10, floating cells were harvested by gentle pipetting, counted and centrifuged at 300g for 5 min at room temperature. Cells were resuspended at $2X10^6$/ml in DC medium containing 5ng/ml GM-CSF to mature DC. On day 11, cells were harvested for experiment. The maturation of DCs was assessed by CD11c staining.

2.2.2 Cytocentrifugation

Cells were adhered onto Superfrost Plus microscope slides by cytocentrifugation in a cytoclip centrifuge (Thermo). Approximately $2X10^5$ cells in 120-140μl PBS containing 10% FBS were loaded into a cytospin chamber and the cells were adhered onto a glass slide by centrifugation at 300 rpm for 3min. Slides were then air dried and fixed in methanol for 2min. Diff-quick staining was performed by immersion into diff-quick red for 1min followed by diff-quick blue for 1min. For immunocytochemistry, slides were fixed in a combination of 9:1 (v/v) acetone: methanol and preserved at -80°C before use.

2.2.3 Bleomycin model

Bleomycin was administered by intra-tracheal (i.t.) instillation of 50µl of 0.025U bleomycin solution. This was carried out by Dr Rodger Duffin (CIR, QMRI). Mice were killed at various time points; 0d (untreated mice), 2d, 7d, 14d and 28d following bleomycin instillation. In same experiments, prior to termination, blood samples were collected by tail nick (section 2.2.16) for measurement of plasma corticosterone level and blood cell phenotype.

Mice were then anaesthetised by i.p injection of 150µl pentobarbital. The body was sprayed with 75% ethanol and the skin was removed by blunt dissection. BALF was collected as described in section 2.2.4. The lung and heart were isolated from the main body as described (section 2.2.4), preserved in formalin or in dry ice. Further, lungs were homogenated for RNA or protein extraction (section 2.2.8 and 2.2.23.2) or used to measure collagen content by Sircol assay (section 2.2.20). Formalin fixed lung were subjected to histology analysis (section 2.2.17). Adrenal glands were collected for weighing into 0.5ml tube with 0.2ml formalin. Subsequently adrenal glands were dissected to remove surrounding tissues and weighed.

2.2.4 Bronchial alveolar lavage + collection of cells + perfusion + preparation of lung

Bronchial alveolar lavage fluid (BALF) was collected according to described

methods (Oreffo, Morgan et al. 1990; Fitch 2005). Mice were anesthetized using a lethal intraperitoneal injection of 0.5ml pentabarbitone (Sagatal) (Merial Animal Health, UK). Fur was washed with 70% ethanol and then deflected from the skin, from the abdomen to the throat, on the ventral surface. The abdominal cavity was opened and the liver and other abdominal organs were removed without puncturing the diaphragm. The diaphragm was lifted up with forceps and carefully punctured to deflate the lungs. The rib cage over the lungs and heart were removed. The peritoneal cavity and neck were then exposed and a set of watchman scissors used to expose, stretch and lift the trachea, which was then incised at its top using a fresh scalpel. A blue 23G needle covered in a 1inch stretch of flexible tubing was then inserted into the trachea for approx 2cm, and tied off mid-cartilage ring via a fine suture.

0.8ml of PBS was then inserted into the lungs and withdrawn. Another 3 lavages, each 0.8ml, were used to maximize recovery of alveolar cells. Isolated cells were pooled and kept on ice at all times to reduce cellular activity and macrophages loss through adherence to the 50ml falcon tube. The purity of alveolar macrophages was assessed by F4/80 staining. The right ventricle of the heart was then cut, and cannulation tubing inserted. Saline was perfused through the lungs via the right ventricle under gravitational pressure. The lungs and heart were then carefully removed from the body. For immunohistochemistry, lungs were inflated with formalin via the tracheal tube and immersed in formalin. For cell culture, lungs were

inflated with PBS and preserved in PBS on ice before transporting to the lab.

2.2.5 Isolation of fibroblast and epithelial cells from mouse lung

The isolated lung was suspended in PBS at 37°C and expanded with 0.8ml trypsin solution which was rapidly withdrawn. The lungs were then filled completely with 5ml trypsin solution and left for 15min. During this time, the trypsin solution was topped up continuously. After 15min, the heart was removed and the lung transferred to a petri dish and chopped into 1-2mm cubes using a scalpel and scissors in 1ml FBS (Figure 2.1). The pieces were then transferred using a sterile transfer pipette to a 15ml tube with 4ml dissociation solution. After swirling for 4min, the solution was filtered through the cell strainer and a final volume of 4mls were centrifuged at 32G for 6 min at 10°C. The supernatant was removed to another tube and the pellet was resuspended in dissociation solution and recentrifuged. The pellet was then resuspended in 3ml attachment medium and placed in a petri dish at 37°C, 5% CO_2 for 1.5h. During this time, macrophages and fibroblasts attached to the bottom of the petri dish. The epithelial cells, consisting mainly of Clara cells could be isolated as clumped balls of cells by gently rocking the dish. Epithelial cells were counted and incubated in PBS with 10% FBS for cytocentrifugation or used for RNA extraction with TRIzol.

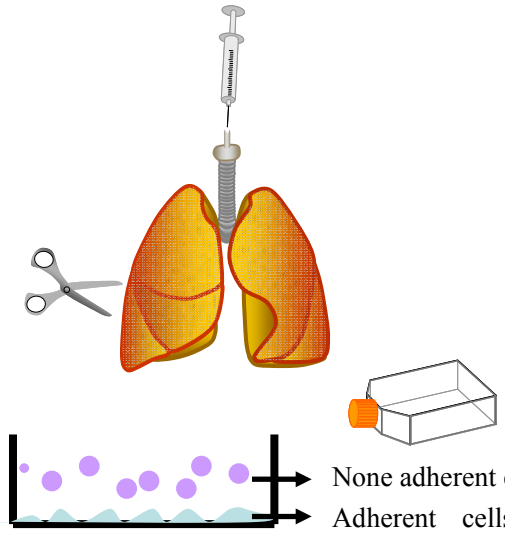

Figure 2.1 Diagram of lung cells isolation

Lung was chopped into cubes after trypsin digestion and then was filtered through the cell strainer. The cells were plated on a Petri dish. Purple color indicate floating cells, which is mainly epithelial cells, blue color indicate adherent cells, which are mainly fibroblast and interstitial macrophage.

2.2.6 Fibroblast culture and passage

Following isolation of epithelial cells, the remaining pieces on the cell strainer were plated into a 50ml tube with 20ml Collagenase Type IA-S and FBS solution (50mg Collagenase Type IA-S with 11ml FBS in 89ml PBS). The tubes were rotated for 10min at 37°C and the media was passed through pipette several times to dissociate cells. Then the tubes were rotated for another 10min and then the media was centrifuged at 300G for 5min at 4°C. Further the pellet was resuspended with DMEM with 10% FBS and was cultured at flask. Medium was replaced 24h after plating. After one week, fibroblasts were washed with PBS and trypsinized with 10% trypsin/EDTA diluted in PBS without calcium or magnesium at 37°C, 5% CO_2 for 30min. Trypsin was neutralized using DMEM containing 10% FBS and the cells were plated in a new flask. Fibroblasts were then cultured in DMEM with 10% NBFS and passaged every week.

2.2.7 TGF-β treatment on fibroblast cells

For TGF-β treatment, fibroblast cells were trypsinized and resuspended in medium. Cell density was determined using a haemocytometer and adjusted to $1X10^5$ cells/ml. Cell viability was determined by adding 100µl cells to 100µl 0.4% (w/v) Trypan blue and counting the number of cells taking up dye (dead cells) and those not. Viability was typically 90-95%. 2ml of suspended cells were plated per well in 6 well plates at $2X10^5$/well and placed in an incubator at 37°C with 5% CO_2, where they were

maintained for the entire culture period. 1d after plating, the medium was aspirated from the cells and 4ml starving medium containing 2% NBFS was added. 1d after starving, cells were treated with 2ng/ml TGF-β for 72h. Control groups were treated with appropriate concentration of DMSO.

2.2.8 RNA extraction and analysis

All instruments used for RNA extraction were autoclaved or treated with RNaseZap before use. All solutions were made with DEPC H_2O. Lung tissues were put into aluminum foil, placed on dry ice and broken into small pieces using a hammer. Tissues were weighed before homogenization. About 50mg of tissue or $5X10^6$ cells were added into 1ml TRIzol for RNA extraction. RNA was extracted following homogenization in TRIzol, according to the manufacture's instructions. Samples were incubated for 5min at room temperature to permit the complete dissociation of nucleoprotein complexes. 0.2ml chloroform per 1ml of TRIzol was added to the sample. Samples were vortexed vigorously for 15s, incubated at room temperature for 3min and then centrifuged at 12,000g at 4°C for 15min. The upper (aqueous) phase was transferred to a fresh tube and RNA precipitated by mixing with 0.5ml of isopropyl alcohol per 1ml of TRIzol. Samples were incubated at room temperature for 10min and then centrifuged at 12,000g at 4°C for 10min. The supernatant was removed and the RNA pellet was washed with 1ml ice cold 75% ethanol and centrifuged at 7,500g at 4°C for 5min. The pellet was air dried on ice and dissolved

in 30µl DEPC H_2O by pipetting up and down. Samples were stored at -80°C until required.

A GeneQuant RNA/DNA calculator was used to measure the optical density of RNA samples to quantify RNA concentration. 1µl RNA sample was diluted in 99µl DEPC H_2O and quantified by UV absorbance at 260nM. The ratio of A_{260}: A_{280} was also measured as an indicator of RNA purity. Generally, the ratio was between 1.6-1.8. RNA integrity was checked by denaturing gel electrophoresis. An aliquot of total RNA was electrophoresed in a 100ml 1.2% agarose/ formaldehyde denaturing gel. 1.2g of agarose was dissolved in 88ml DEPC water in a microwave oven. The mixture was allowed to cool slightly and then, in a fume hood, 2ml formaldehyde, 10ml 10X MOPS buffer and 2-5µl of 10mg/ml ethidium bromide were added. RNaseZAP was sprayed on combs, gel tray and electrophoresis tank. The molten gel was poured into a sealed tray with combs in place and allowed to set. The solidified gel was presoaked in an electrophoresis tank filled with 1X MOPS buffer. 2µg RNA sample was adjusted to 10µl with DEPC H_2O and 2.5µl formaldehyde, 2.5µl 10X MOPS and 10µl deionised formamide added in a fume hood. Samples were mixed, briefly centrifuged then incubated at 65°C for 15min. After denaturing, 2µl loading buffer was added to each sample. Then samples were loaded on the gel and electrophoresed at 100V for about 1-2h, until the leading dye was about 2/3 of the way along the gel. Ethidium bromide-stained RNA was visualized under UV at

260nm and integrity judged from relative intensities of 28S RNA and 18S RNA.

2.2.9 RT-PCR to detect specific mRNAs

Reverse transcriptase synthesizes single-stranded cDNA from total RNA, and the cDNA can be used directly in a PCR reaction. Invitrogen's SuperScript™ III Reverse Transcriptase system was used for generation of cDNA. Reactions (20µl) contained 1µg total RNA, 0.5µl 0.5µg/µl random hexamers, 1µl 10mM dNTPs and RNase free water. Reactions were heated at 65°C for 5min then incubated on ice for 2min. Tubes were briefly centrifuged and the following added: 4µl 5X First-Strand Buffer (supplied with SuperScript™ III RT), 1µl 0.1M DTT (supplied with SuperScript™ III RT), 1µl RNaseOUT and 1µl of SuperScript™ III RT. Samples were incubated at 25°C for 5min, then 50°C for 60min and 70°C for 15min. Negative controls containing RNase free water instead of either reverse transcriptase (no RT) or total RNA (no RNA) were used in parallel. Reverse transcription reactions were used directly as a template for amplification in PCR.

Promega GoTaq DNA polymerase was used for PCR amplification. 50µl reactions contained 4µl RT reaction, 0.4µl 5U/µl GoTaq, 10µl 5X Green GoTaq Reaction buffer (supplied with the polymerase), 1µl 2.5µM upstream primer, 1µl 2.5µM downstream primer, 1µl 10mM dNTPs and 32.6µl H_2O. Negative controls containing H_2O instead of RT reactions were used in parallel.

Initial denaturation was at 95°C for 5min. The cycle conditions were 95°C for 30s, 60°C for 30s, 72°C for 90s. Normally a total of 30 cycles were carried out followed by a 7min final extension at 72°C, before holding at 4°C.

RT-PCR products were normally separated on a 1.5% Agarose/0.5X TBE gel and visualized with ethidium bromide. The weight of agarose is 1.5g per 100ml of gel. Agarose was dissolved in 0.5X TBE solutions by boiling in a microwave oven. 1μl ethidium bromide per 50ml gel was added to detect DNA. The molten gel was then poured into a sealed tray with the appropriate comb, and allowed to solidify. The solidified gel was submerged in a gel electrophoresis tank containing 0.5X TBE solutions and the comb was removed to create loading wells for the DNA samples. 9μl PCR reaction products were loaded onto the gel directly after amplification. 4μl 1kb DNA ladder was used in order to confirm sizes of amplified products. Electrophoresis was carried out in 0.5X TBE at 120V for 50min, then the gel was viewed under UV light (wavelength 260nm) and imaged using an UVI Tec imager and printed on Mitsubishi video printer paper. DNA fragment size was estimated by comparison to 1kb ladder.

2.2.10 Real-time PCR

For all quantitative PCR (qPCR) experiments, real time-PCR was carried out using a LightCycler 480 (Roche). Primer-probe sets used to measure transcripts are listed in Table 2-1 and Table 2-2.

Table 2-1 Commercially available primer-probe sets.

Catalogue	Amplification gene
Mm00433832_m1	Glucocorticoid receptor, nuclear receptor subfamily 3, group C, member 1
Mm01241596_m1	Mineralocorticoid receptor, nuclear receptor subfamily 3, group C, member 2
Mm00516005_m1	heme oxygenase 1
Mm01204962_gH	actin, alpha 2, smooth muscle
Mm00476182_m1	hydroxysteroid 11-beta dehydrogenase 1
Mm00786711_s1	CCAAT/enhancer binding protein (C/EBP), delta
Mm00492541_g1	hydroxysteroid 11-beta dehydrogenase 2
Mm99999064_m1	interleukin 6
Mm01165187_m1	collagen, type I, alpha 2 Collagen Type I α 2 (COL1A2)
Mm00441726_m1	transforming growth factor, beta 1
Mm00446971_m1	TATA box binding protein
Mm00468869_m1	hypoxia inducible factor 1, alpha subunit
Mm00475988_m1	arginase
Mm01309902_m1	nitric oxide synthase 2, inducible
Mm00443258_m1	tumor necrosis factor
Mm00843434_s1	CCAAT/enhancer binding protein (C/EBP), beta

All primer-probe sets were purchased from Applied Biosystems.

Table 2-2 In-house designed primers and probe for 11β-HSD1 promoter detection

Gene	Forward primer (5’ to 3’)	Common reverse primer (5’ to 3’)	Common probe (5’ to 3’) MGB label
11β-HSD1	5'-TGGTGCTCTTCCTGGCCTACT-3'	5'-CCCAGTGACAATCACTTTCTTTCC-3'	5'-AGACCAGAAATGCTCC-3'
Promoter 1	5'-CCGCACTTATCTGAAGCCTCAA-3'		
Promoter 2	5'-CAGGTTTTCTTCGTGTGTCCTACA-3'		

The primers and probe are for mouse 11β-HSD1 and were designed by Dr Julie Nixon (Endocrinology Unit). They were ordered from Applied Biosystems.

For all the amplification of transcripts a commercial 20xassay primer-probe set (Applied Biosystems) and a LightCycler 480 Probes Master mix was used (Roche). Each real-time PCR reaction consisted of 0.5µl 20x primer/probe mixes, 5µl LightCycler 480 Probes Master mix, 2.5µl dH_2O and 2µl cDNA. Each sample was measured in triplicate. The Lightcycler 480 PCR programme was as follows: pre-incubation at 95^{o}C, 5min, amplification for 50 cycles of (95^{o}C, 10s; 60 ^{o}C, 30s; 72^{o}C, 1s) and cooling, 40 ^{o}C, 30s. Data were calculated by the 2nd derivative maximum method. According to manufacture's software application, this method determined the Cp of a sample as the point where the sample's fluorescence curve turns sharply upward. This turning point indicates the maximum of the second derivative of the amplification curve and the value were calculated by the LightCycler ® 480 Software automatically. The ratio of tested gene divided by the housekeeping gene (TBP) concentrations was determined for each sample.

The internal control used to correct for equal RNA concentrations between samples in the animal experiments (chapters 4 and 5) was TBP. 2 internal controls, TBP and 18S were tested. TBP showed good linear relationship with gene of interest and 18S did not have good linear relationship with gene of interest as TBP, so finally, TBP was used as an internal control for all experiments. Table 2-3 list the correlation of coefficient of TBP and GR or 18S and GR, tested on RNA isolated from bleomycin treated lung.

Table 2-3 Correlation of coefficient of TBP and GR or 18S and GR

	GR/18S	GR/TBP
WT 0D	0.91	0.92
WT 2D	-0.12	0.85
WT 7D	-0.45	0.96
WT 14D	0.03	0.92
WT 28D	-0.92	0.09
KO 0D	-0.21	0.92
KO 2D	0.74	0.64
KO 7D	0.46	0.89
KO 14D	0.01	0.97
KO 28D	0.01	0.46

2.2.11 *In situ* mRNA hybridization

Fresh frozen tissue was prepared by injecting 2ml of OCT embedding medium diluted in PBS (1:1, v/v) into lung through the trachea, then placing the lungs in a small container containing OCT on dry ice. 50% OCT/ 50% PBS was continually injected into the lung until the OCT solidified. The tissue was preserved at -80°C before processing. 10µm lung sections were cut using a cryostat and thaw-mounted onto poly-L-lysine slides. Sections were then stored at -80°C until use.

In situ 11β-HSD1 mRNA hybridization was performed according to a standard protocol used in the lab (Seckl et al., 1990). Tissue sections were fixed in cold paraformaldehyde for 10min followed by 2 washes for 5min each in PBS made up in DEPC H_2O. Sections were then incubated in 0.1M triethanolamine for 10min and dehydrated in serial ethanol solutions, from 50% to 100%. Both fixation and washing treatments were carried out in sterilized glassware.

Sufficient pre-hybridization mix was made to apply 200µl to each slide. The pre-hybridization mix consisted of 50% deionised formamide and 50% 2X pre-hybridization solution. Tissue sections were dried around, the edges with lens tissue before adding 200µl pre-hybridization mix to each slide and ensuring each tissue section was covered. Sections were placed flat in plastic boxes containing 3M paper (Whatman) soaked with box buffer consisting of 20% 20xSSC, 20% DEPC

H_2O and 50% deionised formamide (Sigma), for 3h at 50°C.

The 11β-HSD1 probe was transcribed *in vitro* from a PVL105 plasmid encoding a 470bp 11β-HSD1 mouse cDNA. For anti-sense probe, the plasmid was linearized with Not Ⅰ and cRNA was transcribed with SP6 RNA polymerase, in a 10μl reaction containing 1.1μg linearized plasmid and 4μl 37MB/μl [^{35}S]-UTP. For sense probe, the plasmid was linearized with Kpn Ⅰ and cRNA was transcribed with T7 RNA polymerase, in a 10μl reaction containing 1.1μg linearized plasmid and 4μl 37MB/μl [^{35}S]-UTP. Both anti-sense and sense probe were digested with Dnase Ⅰ and purified through Nick column. Then 1μl probe was added into 1ml scintillation fluid and counted in Microbeta liquid scintillation counter.

Sufficient hybridization mix was made up to apply 200μl to each slide. The hybridization mix consisted of 50% deionised formamide, 10M counts/ml of radioactive cRNA probe, made up to a final volume with 2x hybridization solution. This hybridization mix was denatured at 70°C for 10min, cooled on ice and 10μl/ml of 1M DTT added. Tissue sections were dried around the edges with lens tissue before adding 200μl hybridization mix to each slide and ensuring each tissue section was covered. Sections were placed flat in plastic boxes containing 3M paper soaked with box buffer. These boxes were then sealed with autoclave tape and incubated at 50°C overnight. Following hybridization, slides were rinsed twice in 2x SSC for

10min at room temperature prior to RNase digestion with 200µl of RNase buffer at 37°C for 1h. Slides were then washed in 2x SSC at room temperature for 1h followed by a more stringent wash of 0.1x SSC at 60°C for 1h. After dehydration in 50%, 70% and 90% ethanol in 0.3M ammonium acetate for 2min each, slides were air dried overnight in a fume hood before being exposed to autoradiographic film for 2 weeks, then dipped in photographic emulsion and stored at 4°C for 2 weeks. Films were developed in D19 developer (Kodak) for 2min and fixed in a 1:5 dilution of Amfix fixative (Kodak)**,** for 2min. For microscopic localization, slides were dipped in photographic emulsion (NTB2, Kodak), exposed in a light-tight box for 3 weeks. Then the slides were developed for 3min in D19 developer, rinsed in dH_2O, fixed in Amfix fixative for 3min and washed 5times in dH_2O for 5min each. In order to visualize silver grains clearly, slides were also counterstained with hematoxylin and eosin and coverslipped using DPX as a mountant.

Hybridization with sense cRNA probes under the same conditions as above was performed as controls for *in situ* hybridization.

Visualisation of hybridisation

The hybridization signal was quantified by measuring the density in the autoradiographic film under bright field using a computer driven image analysis system (Carl Zeiss, Welwyn Garden City, UK). Semiquantitative analysis by optical

densitometry measurements was carried out blind to genotype. For each lung section, 10 circular area were measured by the image analysis system after an appropriate calibration. Results were calculated as mean number of density per slides after background counted over non-specific areas was subtracted.

2.2.12 Immunohistochemistry

Two methods were used to fix lung specimens: 4% formalin solution and Methyl-Carnoy fixative. For formalin fixation, the lung was inflated with formalin and incubated overnight at room temperature before dehydration and embedding in paraffin. For Methyl-Carnoy fixative, lungs were inflated and immersed in Methyl-Carnoy fixative overnight at 4°C, then embedded in paraffin. For both methods, 5µm thick sections were cut using cryostat (Leica) and floated onto slides. The sections were heated on a slide warmer overnight (37°C). Before staining, sections were deparaffinized by immersion in xylene twice for 5min, and then rehydrated in 100% ethanol for 2min, 100% ethanol 2min, 95% ethanol 1min, 90% ethanol 1min, 80% ethanol 1min. Sections were rinsed in dH_2O before antigen retrieval.

Formalin fixation forms protein cross-links that may mask antigenic sites in tissue sections, thereby giving weak staining for immunohistochemical detection of certain proteins (Puchtler and Meloan 1985). Antigen retrieval can be used to unmask the

antigen in formalin-fixed and paraffin embedded tissue sections, thus enhancing staining intensity of antibodies. Antigen retrieval was carried out in citrate buffer pre-heated to 100°C. Slides were plated in a staining rack and put into 100°C citrate buffer for 30min, then cooled to room temperature for 20min before loading onto sequenza racks for staining.

Slides were washed in PBS containing 0.05% Tween 20 (PBST) 2 times for 3min each. 3 drops of Protein Block (Dako) was added to each slide for 30min to inhibit non-specific binding and then slides were washed 2 times in PBST. Sections were blocked with 3 drops of Vector Avidin Block for 10min at room temperature, then washed in PBST and blocked with 3 drops of Vector Biotin Block for 10min then washed in PBST to block non-specific binding of Avidin/Biotin system reagents, after which they were incubated with primary antibody diluted in Dako antibody diluent overnight at 4°C. After 2 PBST washes, endogenous peroxidase activity was blocked by incubation in 150µl Peroxidase blocking solution for 10min. The slides were subsequently washed in PBST and incubated with biotinylated secondary antibody for 30min. Two PBST washes were performed before adding 150µl Vector ABC reagent 30 min to form avidin and biotinylated horseradish peroxidase complex. After 3 PBST washes, the immune complexes were localized by incubation with 150µl Dako DAB for 5min in a dark room. Upon oxidation, DAB formed a brown end-product at the site of target antigen. Sections were washed in PBST and

counterstained by immersion into Harris' hematoxylin for 15s and Scott's Tap Water Substitute (STWS) for 2min. Finally, sections were mounted in a solution of Mowiol 4-88 Reagent (MERCK) and viewed under a light microscope (Carl Zeiss). A KS300 software (Carl Zeiss), and a JVC camera were used to capture images of sections.

2.2.13 Immunocytochemistry

The procedure of immunocytochemistry is slightly different from immunohistochemistry. First, cytocentrifugation slides were immersed in 0.15% H_2O_2 in methanol for 10min to block endogenous peroxidase activity, before washing in PBST and loading into sequenza racks. Then slides were blocked with 3 drops of Vector Avidin Block for 10min at room temperature, then washed in PBST and blocked with 3 drops of Vector Biotin Block for 10min, then washed in PBST. Slides were incubated with Protein Block (Dako) for 30min, after which they were incubated with 150µl primary antibody diluted in Dako antibody diluent overnight at 4°C. The slides were subsequently washed in PBST and incubated with 150µl biotinylated secondary antibody for 30min. Two PBST washes were performed before incubation in Vector ABC reagent for 30min to form avidin and biotinylated horseradish peroxidase complex. After 3 PBST washes, the immune complexes were visualized with Dako DAB in 5min in a dark room and processed further as described above (section 2.2.12).

2.2.14 Protein assay

Protein concentrations were estimated using the BioRad protein assay, based on the Bradford method. The BioRad protein assay dye reagent concentrate was diluted 1:5 with dH_2O to give a working solution. A standard protein curve was constructed in duplicate by preparing standards containing 0, 0.5, 1, 1.5, 2 and 2.5μg Bovine Serum Albumin (BSA) (made up to 10μl with dH_2O) in a standard 96-well plate. A range of sample concentrations were also prepared in duplicate (adjusted to 10μl with dH_2O), and 200μl BioRad reagent A was added to both controls and samples, then 50μl BioRad reagent B was added into each well before incubation at room temperature for 5min. The plate was then inserted into an OPTI Max microplate reader (Molecular Devices, Sunnyvale, CA) and absorbance at 595nm was measured. A calibration curve was obtained from the standards, against which sample protein concentrations could be calculated.

2.2.15 Antibody purification

HiTrap is designed for purification and isolation of monoclonal and polyclonal IgG from serum. It was used to purify the sheep anti-11β-HSD1 antibody. Protein G is a Type III Fc receptor that binds to the Fc region of IgG by a non-immune mechanism. Protein G has strong affinity with IgG at pH 7.0 and IgG can be eluted at pH 2.7. Fast protein liquid chromatography (FPLC) system was used to sustain the supply of binding buffer or elution buffer. 1ml of sheep anti-11β-HSD1 antiserum was injected

into the Protein G column with syringe and adaptor. The column was washed with binding buffer (20mM sodium phosphate, pH 7.0) at 1ml/min for 20min, then the column was washed with elution buffer (0.1M glycine-HCl, pH 2.7) at 1ml/min for 27min. 47 X 11ml tubes (Sarstedt) were used to collect fractions of 1ml containing IgG. Each tube contained 200μl 1M Tris-HCl pH 9.0 to raise the IgG solution pH to 7.0.

The concentration of each fraction was assayed by protein assay. The highest concentrations were in tube 1 and 2, but these two fractions comprised non-binding protein. The IgG was eluted in fractions 29 to 33, with highest concentration of IgG in fraction 29 (Figure 2.2A). Fractions of highest concentration were dialyzed against PBS containing 50% glycerol in the cold room overnight with gentle stirring. Following dialysis, the concentration of dialyzed IgG was tested and the purified IgG was 0.75 mg/ml. IgG was preserved at 4°C for required use.

To test the specificity of the purified sheep anti-11β-HSD1 antibody, dilutions of antibody (1:500, 1:1000, 1:2000, 1:4000 and unpurified antibody at 1:2000) were tested for ability to recognize 11β-HSD1 in 5μg liver protein by western blotting. The purified antibody only detected 11β-HSD1 in liver protein at 1:500 dilution, but the binding was clear and specific (Figure 2.2B).

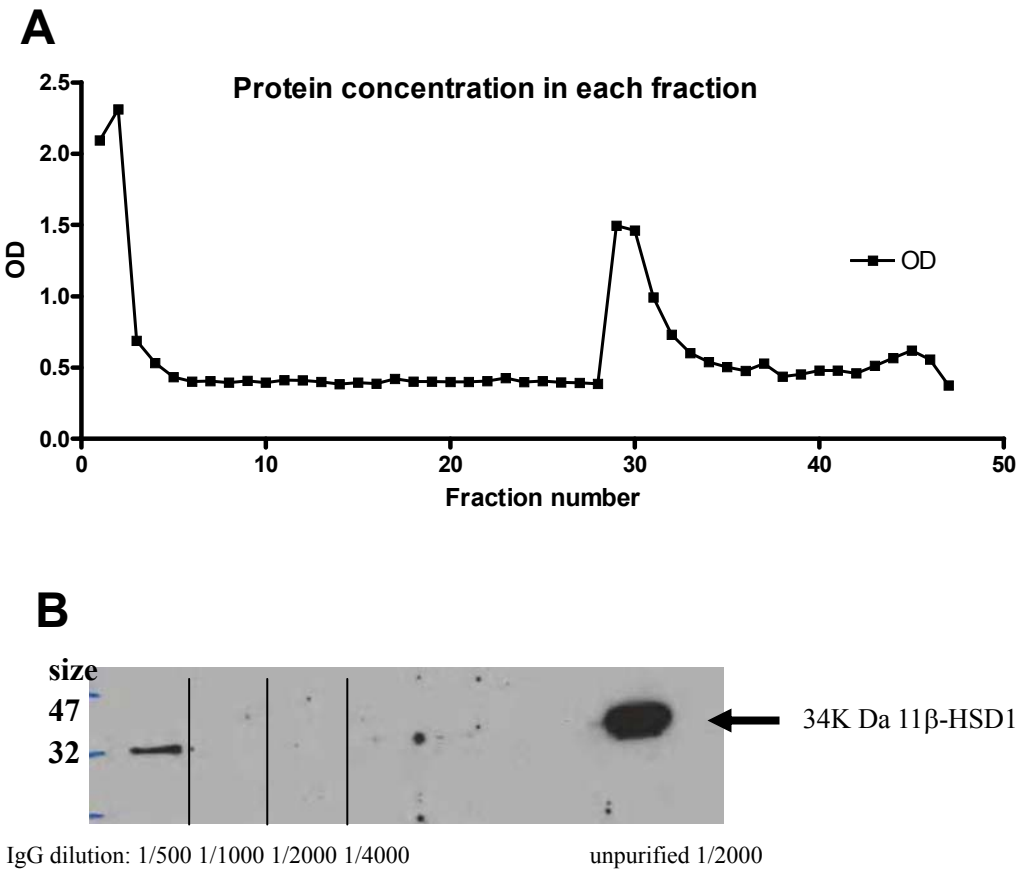

Figure 2.2 Protein concentration in each fraction following elution from protein G column.

(A), the concentration of each fraction was assayed by protein assay, as described in 2.2.14.

(B), western blot technique was used to test the specificity of purified 11β-HSD1 antibody in WT liver protein. 5μg liver protein was loaded per well. 11β-HSD1 protein was apparent at 34k Da.

2.2.16 Tail nick blood collection

For measurement of basal plasma corticosterone levels, peripheral blood was collected under non-stressed conditions via tail nick between 0730h and 0830h. Briefly, one mouse at a time was quickly taken off from its cage and a tiny cut was made at the base of tail with a sterile scalpel. Approximately 25µl of blood was then collected into EDTA coated microvettes (Sarstedt Inc., UK) and placed on ice. Then another 25µl of whole blood was collected by tail nick into a 0.5ml tube and immediately mixed with 25µl of sodium citrate and stored on wet ice for flow cytometry analysis. Samples were centrifuged at 4˚C for 10min at 12,000rpm and plasma stored at -20ºC until further analysis (see section 2.2.21). The procedure was performed with help from Dr Agnes Coutinho. For analysis of blood leukocytes by flow cytometry was described at section 2.2.22

2.2.17 Assessment of lung inflammation and fibrosis

Comparative assessment of inflammation between WT and 11β-HSD1-deficient mice was achieved by measuring total cell number (by Chemometec NucleoCounter) and protein concentration in BALF. Greater infiltration of cells was used to infer greater inflammation. In addition, cells were cytocentrifuged (Section 2.2.22) to confirm cell identification and ratio. Flow cytometry was used to quantify the percentage of apoptotic and necrotic cells as well as cell types (using inflammatory cell markers described in Table 2-5. Histological assessment of lungs was performed

by Dr David Brownstein to identify the degree of tissue damage at various stages of disease. Picrosirius red staining (section 2.2.19) and Masson's trichrome staining and H&E staining (by histology lab) were used to identify fibrosis and Sircol assay (section2.2.20) was used to quantify collagen in lung.

2.2.18 Score of bleomycin induced damage

In order to assess the inflammatory reaction in the lungs and to compare the WT and 11β-HSD1-deficient mice, a scoring system was devised based on the method described in (Fisher, Ahmad et al. 2005). The scoring of peripheral lung inflammation was performed blind to genotype at x200 magnification over 10 random fields in which lungs were completely, but not overly inflated and where the field contained a complete transection of at least one bronchiole less than half a field width in diameter, and a blood vessel as well as an alveolar airway. Large bronchioles were ignored. As the lungs were all perfused and lavaged before fixation, no comment can be made on infiltrate in the alveolar airspaces. The scoring system is presented in Table 2-4.

Table 2-4 Method for scoring peripheral inflammation in bleomycin treated lungs.

Area scored	Score			
	1	2	3	4
(A) Perivascular compartment	<10 cells	10-20 cells	20-50 cells	>50 cells
(B) Peribronchiolar alveolar tissue	<10 cells	10-20 cells	20-50 cells	>50 cells
(C) Alveolar Walls	No infiltration	2-3 cells	4-5 cells	>5 cells

The scoring system was devised based on the method described in (Fisher, Ahmad et al. 2005). The scoring of peripheral lung inflammation was performed at x200 magnification over 10 random fields. Cells were counted in 3 different compartments in each microscope field.
(A), Cells around blood vessel walls
(B), Defined as sub-bronchiolar tissue, beneath basement membrane and smooth muscle, not immediately adjacent to a blood vessel
(C), Scores indicative of focal expansion of alveolar walls by that number of cells

For each section, 10 fields were scored. In each field, the number of inflammatory cells was counted in perivascular compartment, peribronchiolar alveolar tissue and inside alveolar walls. Then according to the number of cells, it converted into a score scale from 1-4 based on Table 2-4. Further, the score for each compartment for the 10 fields were averaged to give the score for the section. Then the averaged scores for each 3 compartment are summated to give an overall score.

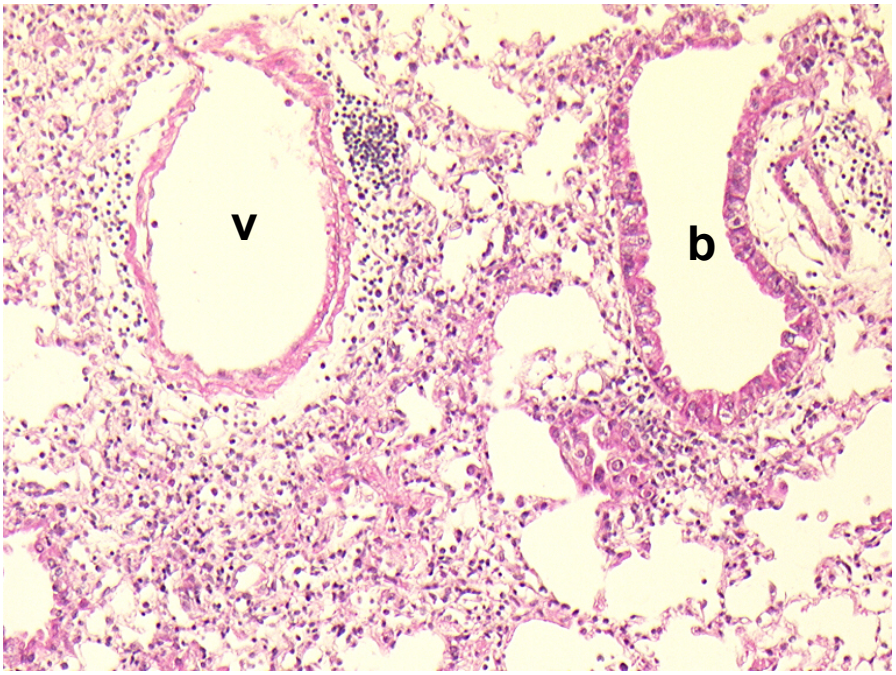

Figure 2.3 H&E stained sections of WT mouse lung 14d after bleomycin.
Typical fields used to score bleomycin induced lung damage. 14d following bleomycin installation, mouse lung was fixed and processed as described in section 2.2.4. Original magnification X100. Scoring was carried out as described in the text from 10 fields per section. The field fulfilled all the requirements: a complete transaction of at least one bronchiole less than half the field width in diameter, a blood vessel, and an alveolar airway. The perivascular compartment, indicated by v, shown above was given a score of "4" in pervascular compartment as there was cellular infiltrate, and more than 50 cells around the blood vessel walls. The peribronchiolar alveolar tissue, indicated by b, was given a score of "3" as there were more than 20 but fewer than 50 cells in this area. Finally, in the alveolar walls there was evidence of focal expansion by 4 to 5 cells, indicating a score of "3". A combined score of "10", calculated by adding all the scores in the field, was then given for that field. This process was repeated over nine additional random fields, and the mean score per field used as the overall score for the animal.

2.2.19 Picrosirius red staining

Picrosirius red staining is commonly used for the assessment of fibrosis as the Sirius Red stain is specific for polymeric and monomeric collagen matrix (Junqueira, Bignolas et al. 1979). Picrosirius red staining for collagen was performed on 5μm methyl carnoy fixed lung sections. The tissue sections were deparaffinised, rehydrated and stained with Picro Sirius red/ fast green stain (equal volume of 0.1% Direct red 80 and 0.1% Fast green were mixed and then 1 in 9 diluted with Aqueous Picric acid solution) for 2h at room temperature in dark room. The sections were then rinsed briefly in running water. The sections were then dehydrated and cleared in Xylene. Then the sections were mounted with DPX and coverslipped.

2.2.20 Sircol assay

Collagen content was estimated using Sircol assay. The Sircol dye reagent (Biocolor Ltd) contains Sirius Red. Sirius Red is anionic dye with sulphonic acid side chain groups. These groups react with the side chain groups of the basic amino acids present in collagen.

The left lobe of lung was removed from mice and placed on dry ice. 3mg/ml pepsin solution was prepared in 0.5M acetic acid. Lungs were wet weighted just prior to sircol assay. Each lung was cut into small cubes with scissors and then placed into a 7ml bijou with 5ml pepsin solution. Samples were placed in a roller at 4˚C for 24h.

After the digestion, 200µl supernatant, containing solubolised collagen, was removed from the centre of the bijou to a 1.5ml tube. The concentration of collagen standard reagent was 1mg/ml. A standard curve of collagen was constructed in duplicate by dilution of a stock reagent (1mg/ml) to give standards containing 0, 12.5, 25, 37.5 and 50µg collagen (made up to 200µl with 0.5M acetic acid) in 1.5ml tubes. 200µl of each sample was also prepared in duplicate and 1ml sircol dye reagent was added to both controls and samples before gentle mixing on a Stuart SB2 rotator at room temperature for 30min. The tubes were then centrifuged at 12,000g for 10min. The collagen with dye was centrifuged to the bottom of tube, the supernatant was removed and the pellet cleaned using cotton buds. Next, 1ml sircol assay alkali (0.5M NaOH) was added into each tube. The tube was vortexted for 15s to dissolve the pellet. 200µl solution was retrieved and placed in a 96 well plate. The plate was then inserted into an OPTI Max microplate reader (Molecular Devices, Sunnyvale, CA) and absorbance at 540nm was measured. A calibration curve was obtained from the standards, against which the sample collagen concentration could be calculated.

2.2.21 Corticosterone radioimmunoassay

Plasma corticosterone levels were measured by radioimmunoassay, in which, unlabeled sample corticosterone and [^{3}H]-corticosterone compete for anti-corticosterone antibody. Plasma samples were diluted 1:10 in borate buffer, heated for 1h at 75˚C then centrifuged for 2min at 13,000rpm at RT. A series of

corticosterone standard (0-500nM) were prepared to produce a standard curve. In a 96 well plate, 20µl standard and sample was added in duplicate to 50µl borate buffer containing [^{3}H]-corticosterone (10,000cpm per sample) and corticosterone antibody. The rabbit-anti-rat corticosterone antiserum (kindly provided by Dr Chris Kenyon) was added at 1:10,000 dilution in borate buffer. This mix was incubated at RT for 2h. Next, 50µl of anti-rabbit scintillation proximity assay (SPA) beads were added to each well and incubated for 16h at dark at RT. Then, the samples were detected by β-scintillation counter. The SPA beads can bind to the rabbit antibody, if that rabbit antibody also binds to [^{3}H]-corticosterone, the radioactive signal is detected by the beads and the scintillation signal was detected by β-scintillation counter. The corticosterone concentration in each sample was determined from a standard curve and calculated using Multicalc software (Wallac, Milton Keynes, UK).

2.2.22 Flow cytometric analysis for phenotyping the Cells:

2.2.22.1 Flow cytometry general information

Flow cytometry have been commonly used for counting and examining cells. The cells are suspended in a stream of fluid and at a point the cells were passed through a light beam. A number of detectors are used to catch the scattered or emitting light (from fluorescent chemicals). It allows simultaneous multiparametric analysis of the physical and chemical characteristics of cells. The data from forward scatter indicate the size of cells. The data from side scatter indicate the granularity and structural

complexity inside the cell. The data from fluorescent detector show the intensity of the staining of antibody on single cell. All experiments were carried out on FACS Calibur flow cytometer (Becton Dickinson, San Jose, CA).

Flow cytometric analysis was performed on blood and digested lung. Prior to flow cytometric analysis, cells in polystyrene tubes were incubated on ice for 10min in PBS with Fc blocker, CD16/CD32 (Fcg III/II Receptor), (BD) (to block non-specific binding). In general, 0.5µl conjugated antibodies were added to the cells (unless otherwise specified by the manufacturer) and incubated on ice for 20min in the dark. Then cells were washed in 2ml PBS and recovered by centrifugation at 300g for 5min then resuspended in 400µl PBS prior to analysis.

2.2.22.2 Phenotyping blood cells

Blood were collected as described at section 2.2.16. 25µl red blood cells were lysed with 500µl FACS Lysis buffer for 8min prior to final wash with PBS. Cells were washed by adding 3ml of PBS, collected by centrifugation at 300g for 5min at 4ºC and fixed with 100µl 10% formalin per sample. Fixed cells were stored (for 24-48h) at 4ºC until analysis.

Prior to flow cytometric analysis, 50µl fluorescent Flow-Check fluorospheres (Beckman Coulter) was added to each sample and specific number of events were

collected in the bead gate (i.e. 5000 events for blood samples and 2500 events for bone marrow samples) enabling accurate calculation of the ratio of cells to beads used to calculate the absolute number of any cell type in the cell suspensions (performed by Dr Tiina Kipari). A combination of antibodies specific for neutrophils, monocytes and lymphocyte was used for blood (Table 2-5) harvested from each mouse. CD11b was marker for neutrophils and monocytes, in CD11b positive cells, neutrophils were identified as Ly6(G) and 7/4 positive cells, 7/4 only positive cells are monocytes.

2.2.22.3 Phenotyping lung cells

Lungs were isolated as described in section 2.2.4. Then lung tissue was minced into small pieces by scissors in a Petri dish. Pieces were incubated and rotated in a 15ml tube with 5ml Collagenase Type IA-S and FBS solution (50mg Collagenase Type IA-S with 11ml FBS in 189ml PBS). After 50min incubation, cells were released from pieces by using a 5ml syringe and a 21G needle to flush the suspension from the syringe against the tube wall. Then all cells were filtered through cell strainer, plated into a FACS tube and centrifuged at 300g for 5min at 4ºC

Table 2-5 Summary of cell markers used to phenotype blood cells.

1) Master mix specific for lymphocytes
● B220, PE, eBioscience ● CD11b, FITC, BioLegend ● CD4, PerCP/Cy5.5, BioLegend ● CD8, APC, eBioscience
2) Master mix specific for neutrophils and monocytes
● 7/4, Alexa 647, AbD Serotec ● CD11b, PerCP/Cy5.5, BioLegend ● Ly6(G), FITC, BioLegend ● CD115, PE, eBioscience

To phenotype recruited inflammatory cells in WT and 11β-HSD1-deficient mice lung 7d following bleomycin instillation, four different master mixes each containing 3 antibodies were prepared, each aimed at identifying specific immune cells, described in Table 2-6. Lung macrophage have very strong autofluorescence (Garn 2006). To exclude the natural autofluorescence of cells, unstained samples were processed in parallel to experimental samples. To confirm the specific binding of each antibody, pooled samples of lung cells obtained following collagenase digestion from all groups were stained with specific isotope controls. Single antibody controls were used to set gates and compensation during collection and subsequent analysis. The data collected from flow cytometry (BD FACArray Bioanalyser) were analysed using WinMDI V2.8 software (Joseph Trotter). Flow cytometry was performed with help from Dr Tiina Kipari and Dr Hongwei Wang.

Table 2-6 Summary of cell markers used to phenotype lung cells.

1) Master mix specific for lymphocytes
● B220, FITC ● CD3, PE ● CD8, APC
2) Master mix specific for neutrophils
● CD11b, PerCP/Cy5.5 ● Ly6(C), FITC ● Ly6(G), PE
3) Master mix specific for Dendritic cells and inflammatory macrophages
● CD11c, APC ● CD11b, PE ● MHCII, FITC
4) Master mix specific for leukocytes and 11β-HSD1
● CD45, PerCP/Cy5.5 ● 11β-HSD1, FITC

2.2.22.4 Phenotyping apoptotic and necrotic cells

Apoptosis is normal physiologic process and the loss of plasma membrane is of one the earliest features. In normal cells, membrance phospholipid phosphatidylserine (PS) is contained in the inner leaflet of cytoplasmic membranes. When cells undergo apoptosis, PS residues flip to the outer leaflet of the membrane and are exposed to the external cellular environment (Vermes, Haanen et al. 1995). Annexin V is a 35-36kDa calcium-dependent phospholipid-binding protein with a high affinity for PS (Vermes, Haanen et al. 1995). Thus, annexin V positive cells indicate early apoptosis. However, the translocation of PS also occurs during necrotic processes. Therefore staining with Annexin V has to be performed in conjunction with a dye exclusion to test the integrity of the cell membrane. 7-Amino-Actinomyxin (7-AAD) is a vital dye which can indicate membrane disruption. Viable cells with intact membrane are both 7-AAD and Annexin V negative, cells in early apoptosis are Annexin V positive and 7-AAD negative and cells that have progressed to post-apoptotic necrosis or have undergone primary necrosis are both Annexin V and 7-AAD positive. Thus apoptosis and necrosis can be detected by labeling cells with Annexin V and 7-AAD and analysis by flow cytometry.

Flow cytometry was used to quantify the percentage of apoptotic and necrotic cells in digested lung cells. Prior to flow cytometric analysis, cells in polystyrene tubes were incubated on ice for 10min in PBS with Fc blocker, CD16/CD32 (Fcg III/II

Receptor), (BD) (to block non-specific binding). After the Fc Block, 10^6 cells were resuspened in 1ml 1X binding buffer, then 100µl cell suspension was transferred to a 5ml polystyrene tube. 2.5µl of PE conjugated Annexin V and 5µl 7-AAD were added to cells. The samples were gently vortexed and incubated for 15 min at RT in the dark. 400µl of 1X binding buffer were added to each tube and the cells were detected within 1h by flow cytometry.

2.2.23 Measurement of 11β-HSD1 activity

2.2.23.1 Synthesis of [3H]-11-Dehydrocorticosterone

[^{3}H]-11-Dehydrocorticosterone was made using homogenized rat placental extract as previously described (Low, Chapman et al. 1994). Rat placenta expresses 11β-HSD2 with very low 11β-HSD1 (Waddell, Benediktsson et al. 1998) so it is efficient at producing 11-dehydrocorticosterone from corticosterone. Briefly, 50µl of [^{3}H]-corticosterone (37Mq/µl) was added to 200µl of 25mM NAD^+ (the 11β-HSD2 specific cofactor), 300µl of rat placental homogenate (gift from Ms Lynne Ramage) and 4.45ml of C buffer, and gently shaken at 37°C for 4h. Then, 4ml of ethyl acetate were added; the solution was vortexed and then centrifuged (Eppendorf 5810R Centrifuge) at 1,700rpm for 5min. The organic (upper) layer containing the steroid was transferred into a borosilicate tube and dried under nitrogen. Dried steroid was reconstituted in 100µl of 100% ethanol and then 1µl of the resuspended steroid was subjected to HPLC to determine the purity of [^{3}H]-A which was routinely >95%.

Specific activity was measured by counting a 1µl aliquot in 1ml scintillation fluid (Pico-fluor 40, Canberra Packard, Berkshire, UK) in a β-counter (Wallac 1450 Microbeta Plus liquid scintillation counter, Milton Keynes, UK). The [^{3}H]-11-dehydrocorticosterone was stored at -20°C for future use.

2.2.23.2 Measurement of 11β-HSD1 activity in homogenised lung

In homogenate, 11β-HSD1 mainly shows dehydrogenase reaction direction thus in homogenised lung, the assays were performed in the 11β-dehydrogenase direction. Lung samples which had been rapidly frozen on dry ice and stored at -80°C were homogenised in 1ml C buffer with an Ultra-Turrax T8 auto-homogenizer (Ika) in 2ml tube and protein concentration of each lung homogenization sample was determined as describes above (section 2.2.14). 11β-dehydrogenase assays contained homogenate (0.5mg/ml protein), 10nM ^{3}H-corticosterone and 400µM NADP. Initial trials were carried out to establish protein concentration and time that gave conversion of 20-40% of subtract within a relatively short time period (less than 20min). For all further experiment, samples were incubated for 10min at 37^{o}C; steroids were extracted by ethyl acetate and quantified by HPLC as described below.

2.2.23.3 Measurement of 11β-HSD1 activity in fibroblast cells

11β-HSD1 activity was measured in intact cells as previously reported (Low,

Chapman et al. 1994). Conversion of [^{3}H]-corticosterone to [^{3}H]-11-dehydrocorticosterone (11β-dehydrogenase activity) or [^{3}H]-11-dehydrocorticosterone to [^{3}H]-corticosterone (11β-reductase activity) was measured in intact primary cells. Normally, 10^6 cells were seeded per well of a 24-well plate in 1ml of medium and incubated at 37ºC for the duration of the experiment (1h to 24h). A trace amount of [^{3}H]-A or B (normally 5nM) was diluted with unlabelled steroid and added to the cell medium to give a final concentration of 200nM steroid. Aliquots of medium (200µl) were collected at various times after addition of [^{3}H]-11-dehydrocorticosterone or [^{3}H]-corticosterone. Steroids were extracted with >4x vol ethyl acetate. The upper layer was removed into 12X75cm borosilicate glass tubes and dried down at 60°C and subjected to analysis by HPLC see below.

2.2.23.4 HPLC

Steroids from 11β-HSD1 activity assays were measured by high-performance liquid chromatography (HPLC), which was carried out by Dr Ruth Andrew. Briefly, dried steroids were resuspended in 600µl of mobile phase, (60% water, 25%methanol and 15% acetonitile). Then the solution was moved into HPLC assay tube and then measured by dual λ absorbance detector (Waters 2487). Each sample was measured for 21min to make sure both peaks of A and B was measured completely.

2.2.24 Western Blot

Frozen lung tissues were homogenized on ice using cold buffer (100g glycerol, 300mg Tris, 186mg EDTA, and 7.7mg DTT made up to 500ml in H_20, pH to 7.5). Total protein concentration was determined as described in section 2.2.14 and 15 µg of total protein was adjusted to 6.5 µl using H_2O and added to 6 µl of a pre-prepared mix of 5 µl NuPAGE® LDS sample buffer (Invitrogen) and 1µl of NuPAGE® Reducing agent (Invitrogen). 10µl of Plus2® pre-stained protein standard (Invitrogen) and all samples were incubated at 80ºC for 10min to denature the protein. According to manufacturer's instructions, samples were loaded into a 15 well 4-12% Bris-Tris Novex® pre-cast gel (Invitrogen) in the Invitrogen XCell II Blot Module. The inner chamber was filled with 200ml of 1X Novex® MOPS running buffer (Invitrogen) and 500µl of NuPAGE® antioxidant (Invitrogen) and the outer chamber filled with 600ml of 1X Novex® MOPS running buffer. Samples were electrophoresed at 200V for ~40min until the bromophenol blue band migrated to the bottom of the gel. The gel was then removed to the plastic cassette and proteins transferred from the gel to a nitrocellulose membrane (Invitrogen) using a wet transfer system which include pad, 3M paper membrane and gel in Invitrogen XCell II Blot Module. Transfer was carried out at 30V for 75min. To reduce non-specific antibody binding, immediately after protein transfer, the membrane was placed in 100ml of blocking solution, consisting of 5% non-fat dry milk in TBST (TBS + 0.1% Tween-20) and incubated with gentle shaking for 1-2h at room temperature. Incubation with primary antibody,

diluted in blocking solution, was performed overnight at 4°C. Following incubation with the primary antibody, the membrane was washed 3 times at room temperature with wash buffer TBST for 15min per wash. The membrane was incubated with the secondary antibody in blocking solution with gentle shaking for 1h at room temperature. Following incubation with the secondary antibody, the membrane was washed 4 times at RT with wash buffer (same as above) for 15min per wash. The membrane was scanned and band intensities were quantified using the Odyssey infrared imaging system (Licor Biosciences; Lincoln, NE).

2.2.25 Statistics

Statistical analysis was performed using GraphPad Prism 4.00 software with $P \leq 0.05$ as the criterion for statistical significance. All data are expressed as mean ± standard error of mean (SEM). Data were analysed by Student's t-tests, Analysis of Variance (ANOVA) or Two-way mixed ANOVA followed by Bonferroni post-tests where appropriate.

3 Chapter Three: Localization of 11β-HSD1 in lung

3.1 Introduction

It is well established that 11β-HSD1 is expressed in lung in humans, rodents and rabbits (Torday, Olson et al. 1976; Monder and Lakshmi 1990; Soldan, Nagel et al. 1999; Speirs, Seckl et al. 2004). Also, 11β-HSD1 has been shown to be expressed in fetal rat lung in late pregnancy (Hundertmark, Ragosch et al. 1994). In addition, 11β-HSD1-deficient mice exhibited delayed fetal lung development (Hundertmark, Dill et al. 2002). Together, these data suggest 11β-HSD1 plays an important role in the physiological function of lung. To look at the role of 11β-HSD1 in lung inflammation, it is important to establish where in lung 11β-HSD1 is expressed. Whilst previous data have demonstrated expression in type 2 alveolar cells (Brereton, van Driel et al. 2001; Suzuki, Tsubochi et al. 2003), it is not clear whether other cell types also express the enzyme. Torday suggested fibroblasts were the only cell in the alveolus that express oxidoreductase activity (Torday, Post et al. 1985). IHC has also localized 11β-HSD1 expression to fibroblasts in rat lung (Brereton, van Driel et al. 2001). However, although 11β-HSD1 is expressed in mouse lung (Speirs, Seckl et al. 2004), the location of 11β-HSD1 expression in mouse lung has not been described. To localize the expression of 11β-HSD1 in mouse lung, *in situ* mRNA hybridization and IHC were used. Lung cell isolation was used to isolate single cell types which allowed confirmation of 11β-HSD1 expression in mouse lung fibroblasts, by RT-PCR. The results in this chapter focus on characterization of 11β-HSD1 in fibroblast cells.

3.2 Results

3.2.1 11β-HSD1 localization in lung

3.2.1.1 *In situ* mRNA hybridization to identify sites of expression of 11β-HSD1 in lung

To localize 11β-HSD1 mRNA within mouse lung, *in situ* mRNA hybridization was carried out on sections of wild-type (WT) mouse lung using an "antisense" [^{35}S]-cRNA probe complementary to mouse 11β-HSD1 mRNA. Whilst fresh frozen tissues are optimal for ISH, paraffin-embedded tissues provide better morphology. Therefore, both paraffin-embedded and fresh-frozen tissues were hybridized. To prepare fresh-frozen lung sections, lungs were injected with OCT prior to freezing to maintain the alveolar structure. Liver highly expresses 11β-HSD1 and was used as a positive control. A "sense" strand cRNA probe (the same as the messenger mRNA) was used as a negative control.

Autoradiography showed hybridization of antisense, but not sense, probe in lung and liver, for both paraffin-embedded and fresh frozen tissue (Figure 3.1A-E). This suggests specific hybridization and both fixing methods show a similar result. Heart, which was also preserved in the sections, showed hybridization to the antisense probe which was similar to the sense probe (Figure 3.1) and was therefore judged to be non-specific. Autoradiography showed that 11β-HSD1 mRNA was expressed throughout the lung and was not specifically confined to any particular part (eg blood vessels or alveoli). Thus, either 11β-HSD1 is expressed in cells which are present

throughout the whole lung, or most of the cells in lung express 11β-HSD1.

For microscopic localization, slides were developed as described in Chapter 2.2.11 and were hematoxylin and eosin stained. Figure 3.1F shows that the density of silver grains on sections hybridized to "antisense" probe was greatest above cells around the alveoli, with much lower density of silver grains above the alveolar spaces (background).

Figure 3.1 Representative autoradiographs showing *in situ* mRNA hybridization of 11β-HSD1 mRNA within WT mouse lung.

(A), Fresh-frozen lung hybridized to an anti-sense [^{35}S]-labelled 11β-HSD1 cRNA probe; (B), Fresh-frozen lung hybridized to a sense [^{35}S]-labelled 11β-HSD1 cRNA probe (negative control); (C), Paraffin-embedded lung hybridized to an anti-sense [^{35}S]-labelled 11β-HSD1 cRNA probe; (D), Paraffin-embedded lung hybridized to a sense [^{35}S]-labelled 11β-HSD1 cRNA probe; arrows indicate lung lobes and white rectangular boxes enclose heart; (E), Paraffin-embedded liver hybridized to an anti-sense [^{35}S]-labelled 11β-HSD1 cRNA probe; (F), Representative image of [^{35}S]-labelled 11β-HSD1 anti-sense cRNA probe hybridized to WT mouse lung. Signal was visualized using photographic emulsion and sections were counterstained with hematoxylin and eosin. Small spots are silver grains hybridized to 11β-HSD1 mRNA and an arrow indicates cells that show strong hybridization (400X magnification).

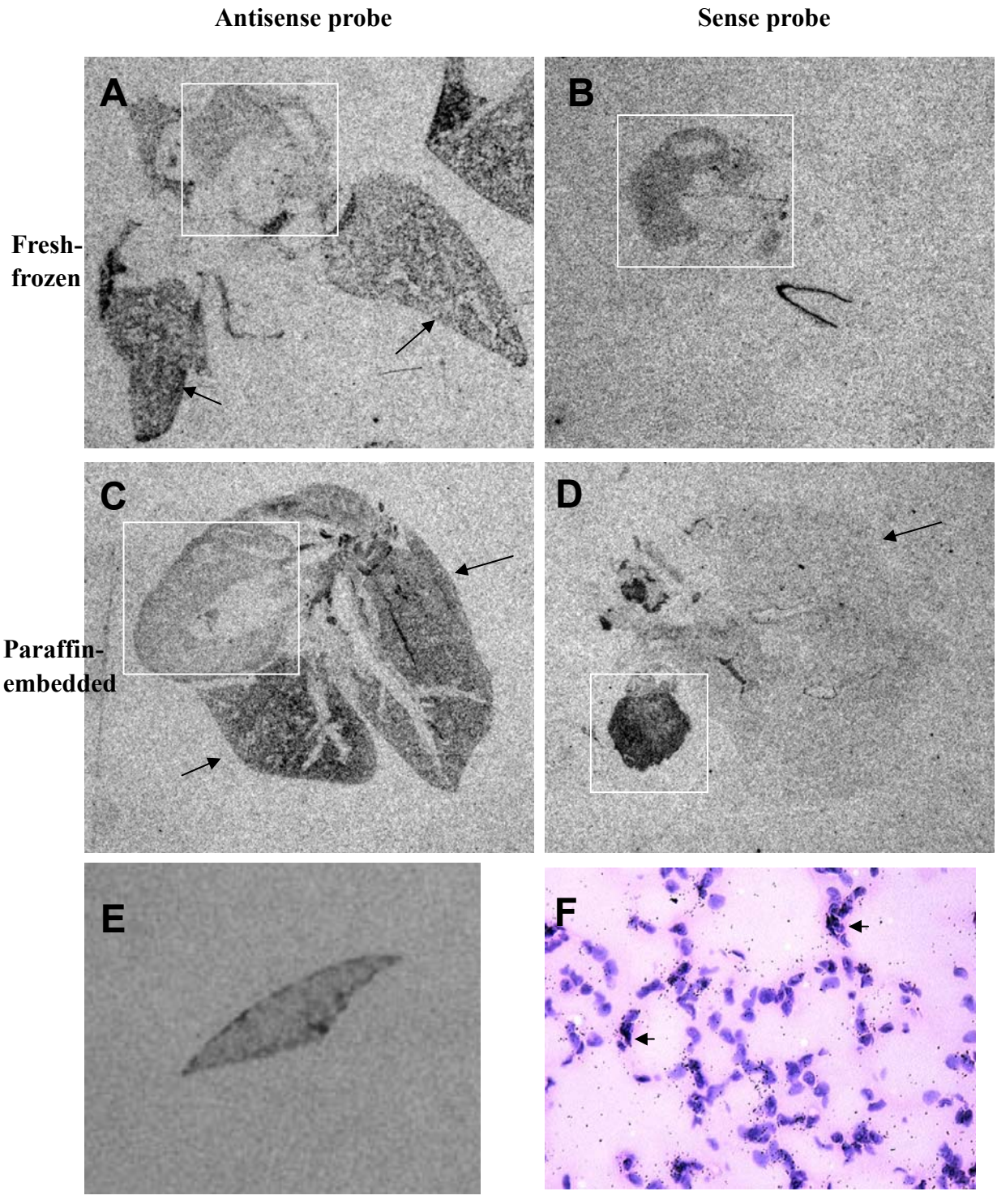
Antisense probe
Sense probe
Fresh-frozen
Paraffin-embedded
A
B
C
D
E
F

3.2.1.2 Immunohistochemical staining of 11β-HSD1 in lung

Cellular localization of 11β-HSD1 mRNA by *in situ* mRNA hybridization was not possible because the radiation of the [^{35}S] probe made the silver grains appear above other cells around hybridized cells rather than restricted to a single cell. Therefore to determine the localization of 11β-HSD1 in lung, immunohistochemistry was carried out using different anti-11β-HSD1 antibodies: a rabbit anti-11β-HSD1 antibody, raised to a peptide corresponding to amino acids 78-92 of human 11β-HSD1, bought from Caymen, and a sheep anti-11β-HSD1 antibody which was raised against purified recombinant mouse 11β-HSD1 protein within the Endocrinology Unit (a gift from Dr Scott Webster). During the course of this work, Dr Agnes Coutinho showed by western analysis that the Caymen anti-11β-HSD1 antibody recognizes 11β-HSD1, but also cross-reacts against a number of other proteins, whilst the sheep antibody appeared more specific for 11β-HSD1 (Coutinho 2009). Therefore, although the Caymen antibody was used during initial experiments (data not shown), it was not used in the experiments described here. Instead, the sheep anti-11β-HSD1 antibody was used. This antibody has also been validated in other experiments within the Endocrinology Unit (De Sousa Peixoto, Turban et al. 2008).

Sheep anti-11β-HSD1 IgG was purified before use and tested as described in Chapter 2.2.15. The specificity of the antibody was determined by staining kidney section (detailed in Appendix I). Paraffin-embedded lung sections from C57BL/6 control

(WT) and 11β-HSD1-deficient mice were stained with purified sheep anti-11β-HSD1 antibody at 1:1000 dilution. Positive staining was seen in some cells in the alveolar wall, which showed morphology typical of type II alveolar cells (Figure 3.2A) and in cells next to the basement membrane of bronchioli and blood vessels (Figure 3.2B and C). No staining was found on bronchiolar epithelial cells (Figure 3.2B). 11β-HSD1-deficient mice show weak staining compared to WT mice, mainly in type II alveolar cells (Figure 3.2D), but there was no staining on cells next to the basement membrane of bronchioli and blood vessels (Figure 3.2E and F).

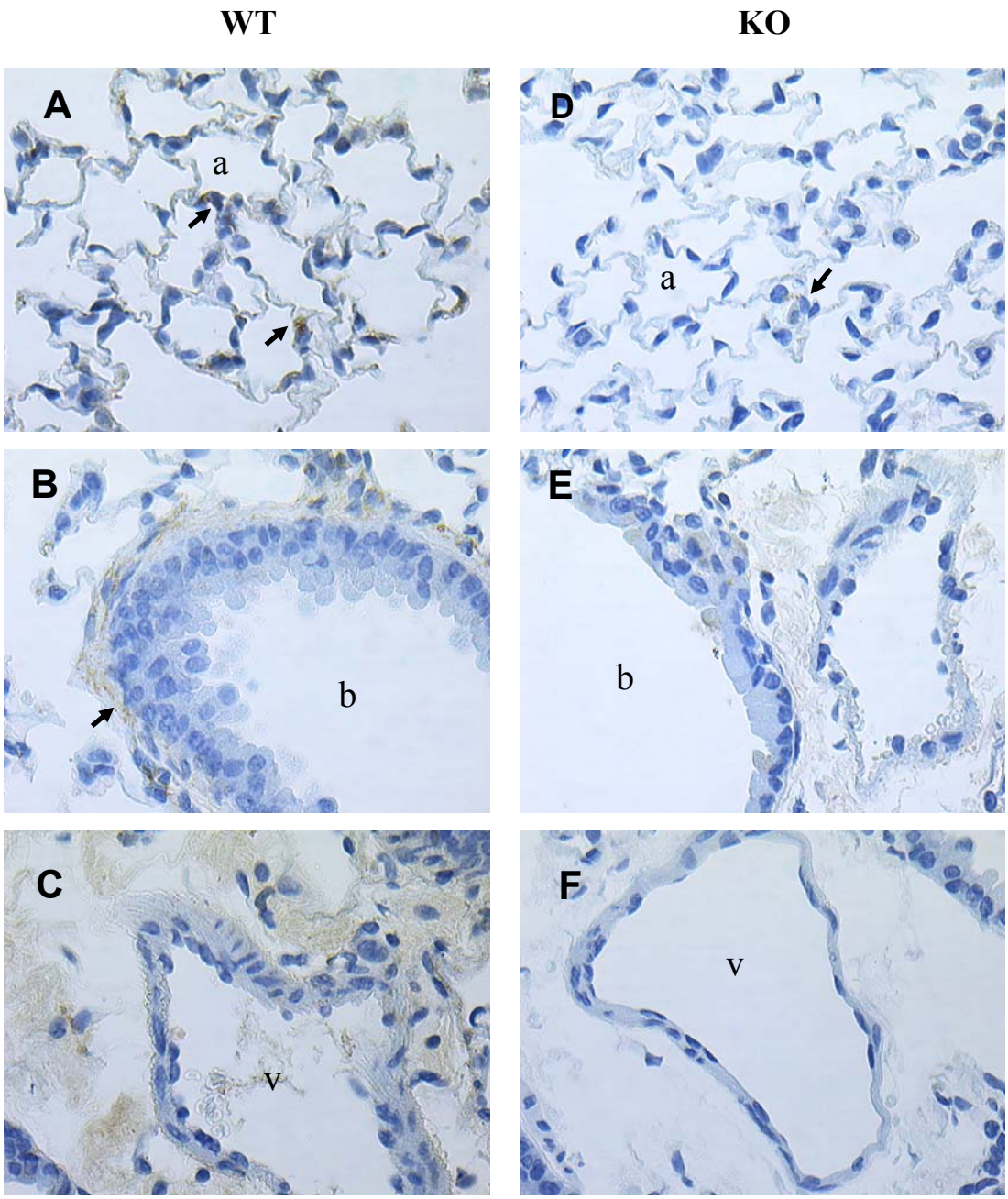

Figure 3.2 Immunohistochemical staining of 11β-HSD1 in mouse lung shows expression in fibroblasts and type2 alveolar cells.

Representative image of Immunohistochemistry carried out on lung sections from WT mice (A-C) or 11β-HSD1-deficient mice (D-F) with purified sheep anti-11β-HSD1 antibody at 1:1000 dilution and biotinylated rabbit-anti-sheep 2nd Ab at 1:400 dilution. Images captured at magnification, X400. A&D show alveolar structure, arrows indicate positive staining on type 2 alveolar cells. B&E show bronchi epithelium, positive staining was seen in connective tissue fibroblasts lying adjacent to epithelium. C&F show blood vessel, positive staining was seen in fibroblasts outside blood vessel in WT but not in 11β-HSD1-deficient mice. "a" indicates alveoli, "b" indicates bronchioles and "v" indicates vessel.

3.2.1.3 Expression and distribution of GR in mouse lung

Expression of 11β-HSD1 occurs primarily in GR-rich tissue (Whorwood, Franklyn et al. 1992; Hardy, Filer et al. 2006). Lung is a major GC target tissue and abundantly expresses GR (Ballard, Baxter et al. 1974; Cole, Blendy et al. 1995; Speirs, Seckl et al. 2004). To determine whether GR is colocalized with 11β-HSD1 in lung, and as a positive control for the IHC, a GR antibody was used in IHC on WT mouse lung sections. No staining was detected without antigen retrieval (data not shown). Following antigen retrieval, some alveolar cells, with morphology typical of type 2 alveolar cells (Figure 3.3A) and endothelial cells (Figure 3.3B) showed a positive signal. Most of the positive staining was in the nuclei of immuno-positive cells (Figure 3.3A), consistent with a nuclear localization of GC-GR complexes. No staining was found in airway epithelial cells (Figure 3.3C). Overall, the GR immuno-staining was quite similar to that of 11β-HSD1 in mouse lung.

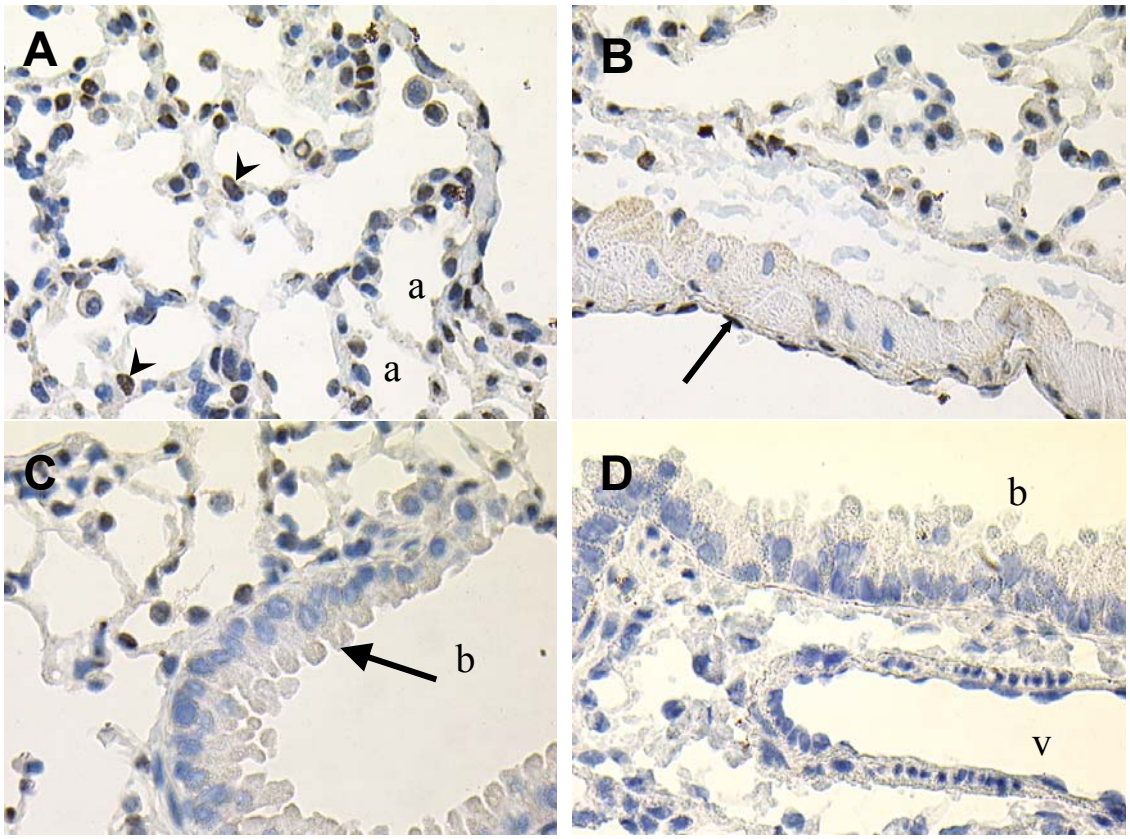

Figure 3.3 Immunohistochemical staining of GR in mouse lung shows expression in type 2 alveolar cells and endothelial cells.
Immunohistochemistry was carried out on paraffin-embedded WT mouse lung. Following antigen retrieval (described in Chapter 2.2.12), sections were incubated with rabbit anti-GR antibody at 1:100 dilution and biotinylated goat-anti-rabbit 2nd Ab at 1:50 dilution. (A), staining in type 2 alveolar cells (arrowheads); (B), GR immuno-staining in endothelial cells (arrow indicates an endothelial cell); (C), no staining in bronchiolar epithelial cells (arrow indicates bronchiolar epithelial cell); (D), Negative control: WT lung with 2nd Ab alone. Images captured at magnification, X400. "a" indicates alveoli, "b" indicates bronchioli and "v" indicates a blood vessel.

3.2.1.4 11β-HSD1-deficient mice have detectable 11β-HSD1 activity in lung

During the course of this work, Dr Agnes Coutinho showed that 11β-HSD1 can be detected by western blotting in 11β-HSD1-deficient mouse lung (Coutinho 2009). Therefore to investigate whether the weak staining in lung of 11β-HSD1-deficient mice was due to cross reactivity with another protein or was due to residual 11β-HSD1 activity in lung of "KO" mice, 11β-HSD1 activity was assayed in homogenate of WT and 11β-HSD1-deficient lung as described in Chapter 2.2.23.2. A selective inhibitor of 11β-HSD1 which does not inhibit the function of 11β-HSD2 (gift from Dr Scott Webster) was used to demonstrate that 11β-HSD activity detected in lung was due to 11β-HSD1. Kidney highly expresses 11β-HSD2 (Krozowski, Albiston et al. 1995) and so was included as a control for the selectivity of the inhibitor.

As expected, 11β-HSD activity in WT lung homogenate was readily detectable ~0.5 pmolproduct/mg/min (Figure 3.4); although lower than in kidney homogenates (Figure 3.4). However, lung from 11β-HSD1-deficient mice showed approximately one third the level of 11β-HSD activity of WT lung homogenate (Figure 3.4). Addition of the selective 11β-HSD1 inhibitor resulted in inhibition of all the 11β-HSD activity in "KO" lung, but kidney was unaffected (Figure 3.4), demonstrating that the 11β-HSD activity detected in "KO" mouse lung was due to residual expression of 11β-HSD1 (kidney highly expresses 11β-HSD2). Therefore

11β-HSD1 immunostaining in KO mouse lung may be due to residual 11β-HSD1 expression. Homogenates of liver from "KO" mice (the tissue that most highly expresses 11β-HSD1 (Speirs, Seckl et al. 2004)) showed no 11β-HSD activity (data not shown).

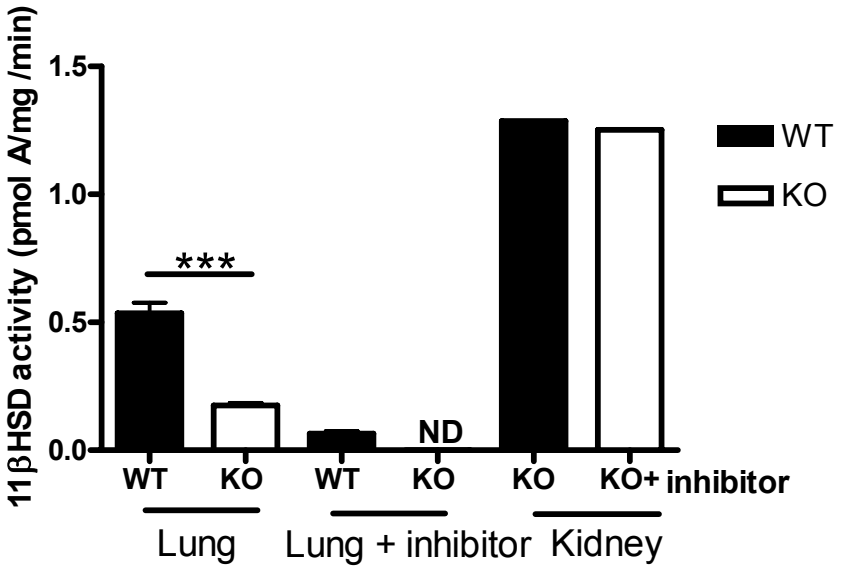

Figure 3.4 Residual 11β-HSD1 enzyme activity in lung of 11β-HSD1 KO mice
11β-HSD activity was measured by conversion of [^{3}H-B] to [^{3}H-A] in a 10 min assay with 0.5mg/ml lung homogenate or kidney homogenate from WT or 11β-HSD1-deficient (KO) mice. 50 μM 11β-HSD1 inhibitor (CC002054) was added to the homogenate before the reaction. Steroids were extracted by ethyl acetate and quantified by HPLC as described in Chapter 2.2.24. 11β-HSD activity is expressed as pmol of corticosterone (B) converted into 11-dehydrocorticosterone (A)/mg protein /min. Values are mean ± SEM of 3 lungs. A single kidney was analysed as control, with assay carried out in duplicate. ND, not detected. There is significant difference between WT and KO mice in lung 11β-HSD activity (***, $p<0.001$) (Student's *t*-test).

3.3 11β-HSD1 expression in isolated alveolar macrophages, lung epithelial cells, and fibroblasts *in vitro*

IHC suggests 11β-HSD1 expression in lung is mainly in fibroblasts and type 2 alveolar cells. To further examine this, individual lung cells were isolated. Alveolar macrophages were isolated by cytocentrifugation of lung lavages and identity confirmed by F4/80 staining (Figure 3.5A). Following lavage, lungs were subject to trypsin digestion as described in Chapter 2.2.5. This enabled epithelial cells (mainly clara cells) to be isolated as clumps of non-adherent or loosely adherent cells (Oreffo, Morgan et al. 1990). Cells which firmly attached to the bottom of the culture dish were largely fibroblasts and interstitial macrophages. Fibroblasts could be removed by mild trypsin digestion and further passaged. In contrast, interstitial macrophages did not proliferate on further passage.

RNA was extracted from isolated lung cells. Semi-quantitative RT-PCR showed that all cells express 11β-HSD1, with similar levels of 11β-HSD1 PCR product from the non-adherent cells (containing epithelial cells) (Figure 3.6, lane 2) and alveolar macrophages (Figure 3.6, lane 3). However, the adherent cells, containing fibroblasts and interstitial macrophages, gave more 11β-HSD1 PCR product (Figure 3.6, lane 4) suggesting a higher level of expression. In further experiments, greater proliferation and characterization of the adherent cells (largely fibroblasts) was achieved (detailed in Chapter 4).

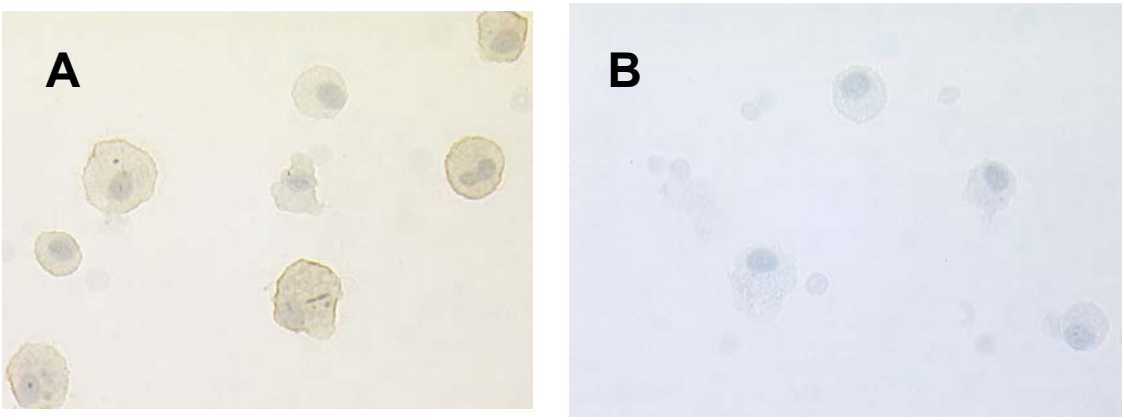

Figure 3.5 F4/80 staining in cytocentrifuged alveolar macrophages
Immunohistochemistry was carried out with rat anti-mouse F4/80 antibody at 1:50 dilution and HRP conjugated rabbit-anti-rat 2nd Ab at 1:200 dilution. Brown indicates positive staining. Both images (A and B) show cytocentrifuged cells from alveolar lavages. (A) cells stained for F4/80; more than 95% cells are positive; (B) negative control (secondary Ab only). Magnification, X400.

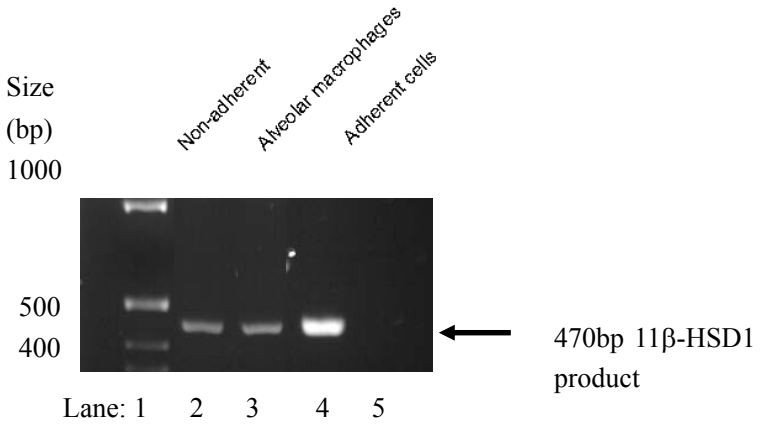

Figure 3.6 11β-HSD1 is expressed in different lung cell populations
RNA was extracted from the indicated lung cells. 1μg of RNA was used in an RT reaction and 4μl RT reaction used in 30 cycles of PCR. Lane 1, 1kb marker. Lane 2, RT-PCR reaction carried out on RNA extracted from non-adherent and loosely adherent cells, which contain epithelial cells. Lane 3, RT-PCR reaction carried out on alveolar macrophage RNA. Lane 4, RT-PCR reaction carried out on RNA isolated from firmly adherent cells. Lane 5, minus RT reaction used as a negative control. An arrow indicates the 470 bp product corresponding to 11β-HSD1 mRNA.

3.4 11β-HSD1 is present in lung fibroblasts

11β-HSD1 expression has been demonstrated in rat lung fibroblasts (Brereton, van Driel et al. 2001). To confirm my IHC findings, 11β-HSD1 expression in mouse lung fibroblasts was investigated. Lung fibroblasts were isolated and cultured according to the method described in Chapter 2.2.6. Fibroblasts were characterized morphologically by a spindle phenotype following inspection under the light microscope (Tarin and Croft 1969). RT-PCR, IHC and activity assay were used to confirm expression of 11β-HSD1.

3.4.1 11β-HSD1 expression in primary lung fibroblasts

Examination of passage 1 fibroblasts showed predominantly spindle shaped cells (Figure 3.7A), typical of the morphology of fibroblasts in culture (Tarin and Croft 1969). Following trypsinization, cells were cultured on cover-slips overnight then subjected to IHC as described in Chapter 2.2.13. Staining with antibody raised against recombinantly expressed 11β-HSD1 showed that the majority of cells were positive for 11β-HSD1 (Figure 3.7B)

.

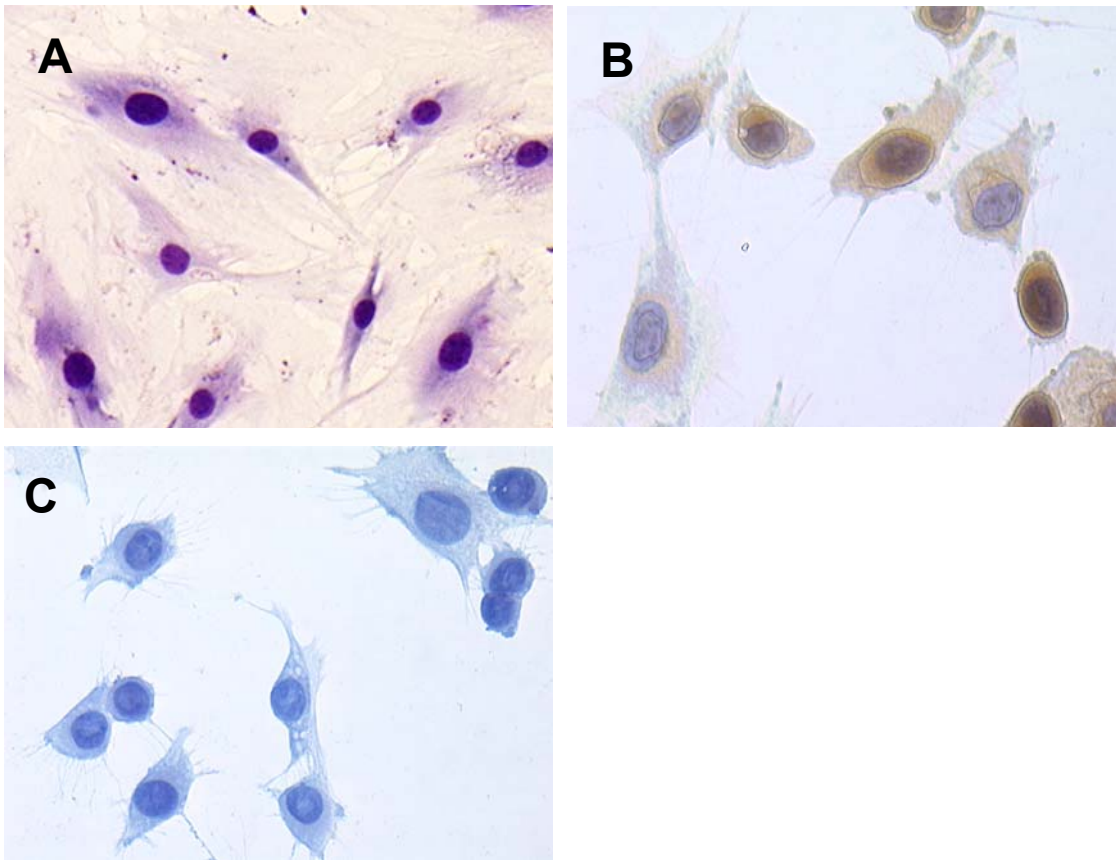

Figure 3.7 Immunohistochemical staining of 11β-HSD1 in primary lung fibroblasts (passage 1)

(A), A confluent monolayer of primary lung fibroblast cells was evident after 7 days of culture and exhibited a characteristic spindle morphology, typical of lung fibroblast (Tarin and Croft 1969). Cells were stained with Diff-Quick red and blue as described in Chapter 2.2.2. These cells were confirmed as fibroblasts on the basis of stellate morphology and ability to propagate in the medium (Hu, Wu et al. 2004). (B), 11β-HSD1 staining with anti-11β-HSD1 Ab at 1:1000 dilution and biotinylated goat-anti-rabbit 2nd Ab at 1:400 dilution; (C), Negative control: biotinylated goat-anti-rabbit 2nd Ab alone. All images captured at X400 magnification.

3.4.2 Mouse lung fibroblasts have 11β-HSD reductase activity

To measure 11β-HSD1 activity in primary fibroblasts, cells from WT mice were assayed for 11β-HSD dehydrogenase and reductase activity. Only 11β-reductase activity was detected, with little dehydrogenase activity, suggesting the presence of 11β-HSD1 and negligible 11β-HSD2 (Figure 3.8).

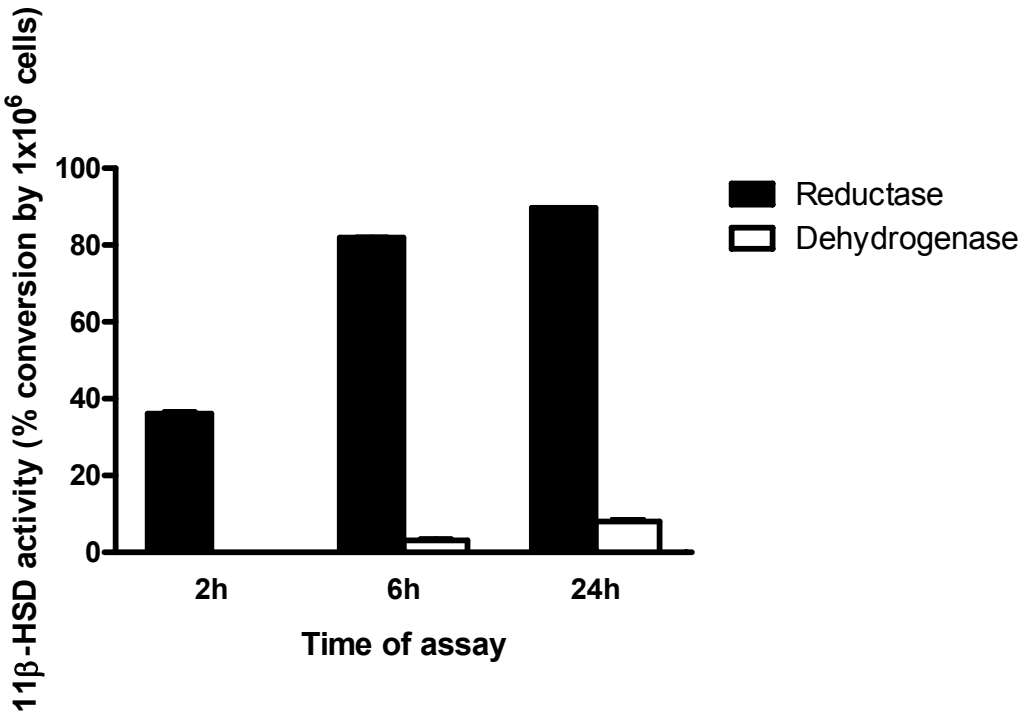

Figure 3.8 11β-HSD1 activity in primary fibroblasts

11β-HSD reductase and dehydrogenase activities in primary fibroblasts were measured by adding [^{3}H]-substrate 11-dehydrocorticosterone or corticosterone, respectively to the medium, removing aliquots at various times up to 24h and calculating conversion of substrate to product (see Chapter 2.2.23.3 for details). Data are expressed as % conversion of 200nM substrate by 1x10^6 cells, over time. Black bars indicate reductase activity (conversion of 11-dehydrocorticosterone to corticosterone) and white bars indicate dehydrogenase activity (conversion of corticosterone to 11-dehydrocorticosterone). Values are mean ± SEM of triplicate assays carried out on pooled primary fibroblasts.

3.5 Discussion

The data contained in this chapter show unequivocally that lung expresses functional 11β-HSD1 in fibroblasts, alverolar macrophages and epithelial cells. In primary fibroblasts, 11β-HSD1 transcripts were obvious by RT-PCR and 11β-HSD activity assay showed exclusively the reductase direction.

In situ hybridization showed strong hybridization to 11β-HSD1 mRNA in lung, with silver grains localized to certain cells rather than all cells in lung. To more specifically identify the cells expressing 11β-HSD1, IHC was used. WT lung showed positive staining on type II alveolar cells and fibroblasts. These results are similar to 11β-HSD1 IHC in rat lung (Brereton, van Driel et al. 2001). However, 11β-HSD1-deficient mice also showed positive staining on lung although to a lesser extent than WT. 11β-HSD activity assay confirmed the presence of low levels of 11β-HSD1 in 11β-HSD1-deficient lung. When lung homogenate was treated with 11β-HSD1-specific inhibitor, the 11β-dehydrogenase activity in WT or 11β-HSD1-deficient lung was abolished, which confirmed that 11β-HSD1-deficient mice express functional 11β-HSD1 in lung. However, no activity was detected in livers (K. Chapman, unpublished result), consistent with previous data at this line of mice (Kotelevtsev, Holmes et al. 1997). Although it was not appreciated at the time this line of mice were generated, it is likely that the homologous recombination event designed to disrupt the 11β-HSD1 gene did not occur exactly as expected (K. Chapman, unpublished data) (Figure 3.9). Instead of replacement of exons 4 and 5

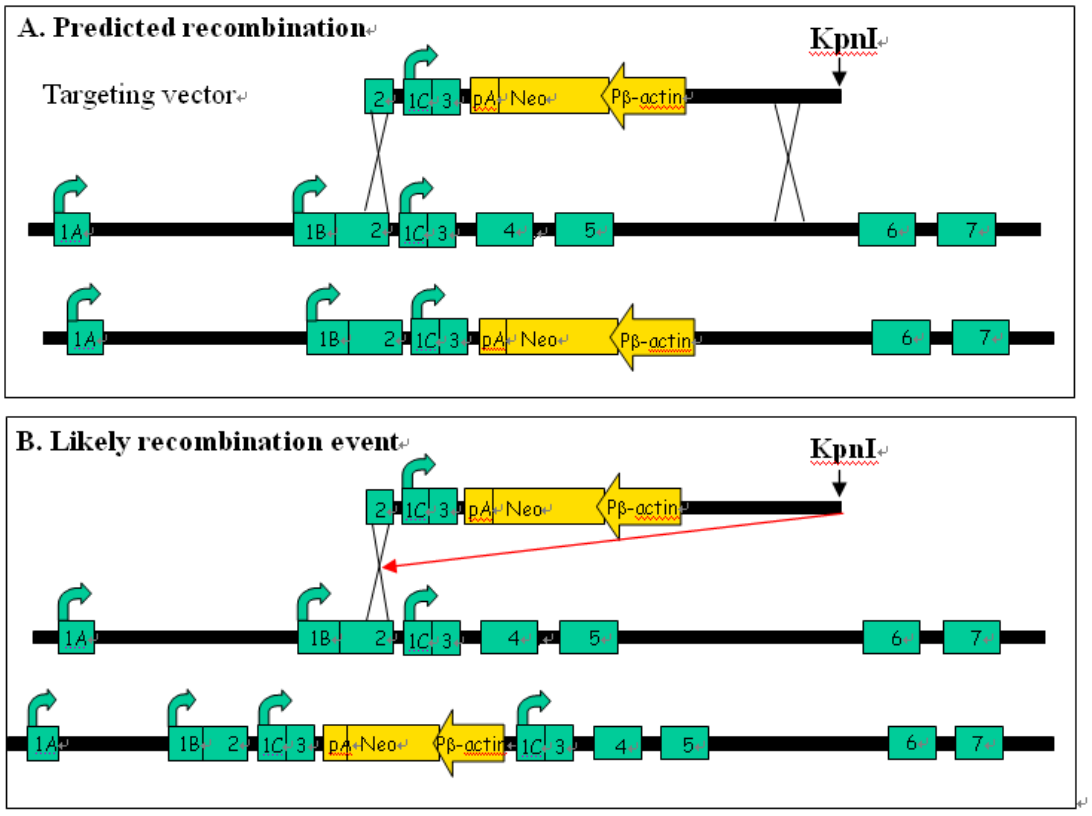

Figure 3.9 Targeted inactivation of the 11β-HSD1 gene

A, predicated recombination event for generating 11β-HSD1 KO mice, showing (top) the targeting vector; (middle), the *Hsd11b1* locus and predicted sites of homologous recombination and (bottom) the predicted targeted allele. The targeting vector was designed to replace exons 4 and 5.

B, likely recombination event. The targeting vector has inserted into the *Hsd11b1* locus rather than replacing exons 4 and 5. Due to the strong β-actin promoter and the disruption to the *Hsd11b1* gene, the 11β-HSD1 transcription from the P2 promoter is abolished, with the P1 promoter less affected because the P1 promoter is >20kb upstream of the targeted sequence.

Transcription starts associated with each promoter are shown by curved arrows. Rectangular boxes indicate exons (numbers in boxes indicate the exon). Neo, neomycin. pA, simian virus 40 polyadenylation signal sequence. pβ-actin, β-actin promoter. KpnI, restriction endonucleases.

(previously designated 3 and 4; Kotelevtsev et al, 97) (Figure 3.9A), all the exons are still present and in the correct order (Figure 3.9B). Therefore, RNA splicing can generate correct 11β-HSD1 transcripts in 11β-HSD1 "KO" mice. Whilst this happens at a very low frequency from transcripts initiated at the P2 promoter (probably because of promoter interference from the strong β-actin promoter present on the neo cassette in the opposite orientation to the 11β-HSD1), because the 11β-HSD1 P1 promoter is >20kb upstream to the neo cassette (see Chapter 1.7.1 for description of the 11β-HSD1 promoters), the interference may be less, allowing some 11β-HSD1 mRNA to be made in tissues such as lung that use the P1 promoter.

Cell separation was used to isolate single cells to further identify the cells expressing 11β-HSD1. Analysis of RNA by RT-PCR was consistent with the IHC finding, with alveolar macrophages and epithelial cells expressing 11β-HSD1 and fibroblasts highly expressing 11β-HSD1. All of those cells contribute to the 11β-HSD activity in lung. Primary cultured fibroblasts showed exclusively 11β-reductase activity, similar to human fibroblasts (Abramovitz, Branchaud et al. 1982). Abramovitz et al incubated human fetal lung at midgestion (at stage when 11β-HSD2 expression is likely to be high and 11β-HSD1 to be low (Stewart, Whorwood et al. 1995)) in monolayer cultures or as explants. Explants mainly converted cortisol to cortisone (dehydrogenase activity). In monolayer cultures consisting almost entirely of fibroblast-like cells, cortisol to cortisone conversion was low, but cortisone to

cortisol conversion steadily increased to 85% and plateaued at confluence (Abramovitz, Branchaud et al. 1982). Thus, cortisone to cortisol conversion only happened in human fetal lung fibroblast-like cells in culture, and apparently not in the *in vivo* (explant) system (Abramovitz, Branchaud et al. 1982). *In vivo* or in explants, 11β-HSD2 is expressed and not 11β-HSD1, as suggested by Stewart et al 1995. However, upon culture and outgrowth of fibroblasts, 11β-HSD1 may be expressed, with its associated reductase activity. This suggests that fibroblast cells express 11β-HSD1 and mainly exhibit 11β-reductase activity.

11β-HSD1 generates ligand for GR. GR staining appears mainly on type 2 alveolar cells which was colocalised with 11β-HSD1 expression. The staining of GR is mainly on nuclear of the cells, it is either because that endogenouse GC occupy the GR or because that the antibody only recognize nuclear GR but not cytoplasmic GR (Sarabdjitsingh, Meijer et al. 2010). However, the antibody I used for the GR IHC could pick up both nuclear and cytoplasmic GR, so the mice may be stressed before the cull.

These data show that lung fibroblasts demonstrate potential for the amplification of GC and therefore such action may contribute to lung inflammation and its reduction.

4 Chapter Four: The regulation of 11β-HSD1 transcription in lung fibroblasts

4.1 Introduction

In lung, 11β-HSD1 mRNA is transcribed from 2 promoters in the *Hsd11b1* gene, P1 and P2, with the majority of the mRNA expressed from the P1 promoter (Bruley, Lyons et al. 2006) (see Chapter 1.7.1). In addition, a further promoter (P3) has been described in rat kidney (Moisan, Edwards et al. 1992), which is also used in mouse and human kidney (Ms V. Kelly, Prof K. Chapman, unpublished results). To test the hypothesis that lung epithelial cells express 11β-HSD1 from the P2 promoter whereas lung fibroblast cells use the P1 promoter, individual lung cell types were tested. Two human lung cell lines, representative of fibroblast and epithelial cells, were first used to test the hypothesis. In addition, cell separation was undertaken to isolate epithelial and fibroblast cells from lung to test the hypothesis in primary cell culture. Recent work has established that bone marrow-derived mast cells exclusively use the P1 promoter (Dr Agnes Coutinho, unpublished data) and lymphocytes ($B220^+$ and $CD4^+$) also predominately use the P1 promoter (Dr Agnes Coutinho, unpublished data), so the promoter usage of other immune cells was also investigated in this Chapter.

4.2 Results

4.2.1 The P1 promoter of *Hsd11b1* predominates in lung

4.2.1.1 Both the P1 and P2 promoters of *Hsd11b1* are used in lung

To validate the PCR assay and confirm that mouse lung mainly uses the P1 promoter to transcribe *Hsd11b1*, RNA was extracted from lung of wild-type mice and subject to RT-PCR, using primers that were specific for each of the 3 promoters; P1, P2 and P3. Figure 4.1 shows that lung uses both the P1 promoter and the P2 promoter with only a very small amount of transcription from the P3 promoter.

4.2.1.2 Validation of real-time PCR assay to measure *Hsd11b1* transcripts initiated at the P1 and P2 promoters

To quantify the promoter usage of the mouse *Hsd11b1* gene, real-time PCR assays for the P1 and P2 promoters were developed by Dr Julie Nixon (Endocrinology Unit, University of Edinburgh). To validate the real-time PCR assay, WT lung and liver cDNA were used to compare the promoter usage in each tissue, as well as in mixtures of cDNA from the 2 tissues, prepared as outlined in Figure 4.2. Real-time PCR results showed that liver mainly uses the P2 promoter and around 90% of lung 11β-HSD1 mRNA was transcribed from the P1 promoter (Figure 4.2).

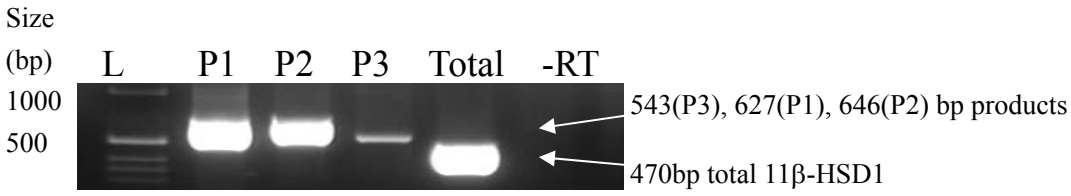

Figure 4.1 11β-HSD1 promoter usage in mouse lung.
RNA was extracted from the lung of WT mice. 1μg of RNA was used in an RT reaction and 4μl RT reaction used in 30 cycles PCR with primers specific for transcripts initiating at each of P1, P2 and P3 promoters as well as primers that detect all 11β-HSD1 transcripts (see Chapter 2.1.7). Lane 1 contains a 1 kb ladder, labeled with L. The positions of the 543bp P3 product, the 627bp P1 product and the 646bp P2 product are indicated, as is the position of the 470bp product derived from total 11β-HSD1 mRNA. A control reaction (-RT) gave no product with primers to amplify total 11β-HSD1.

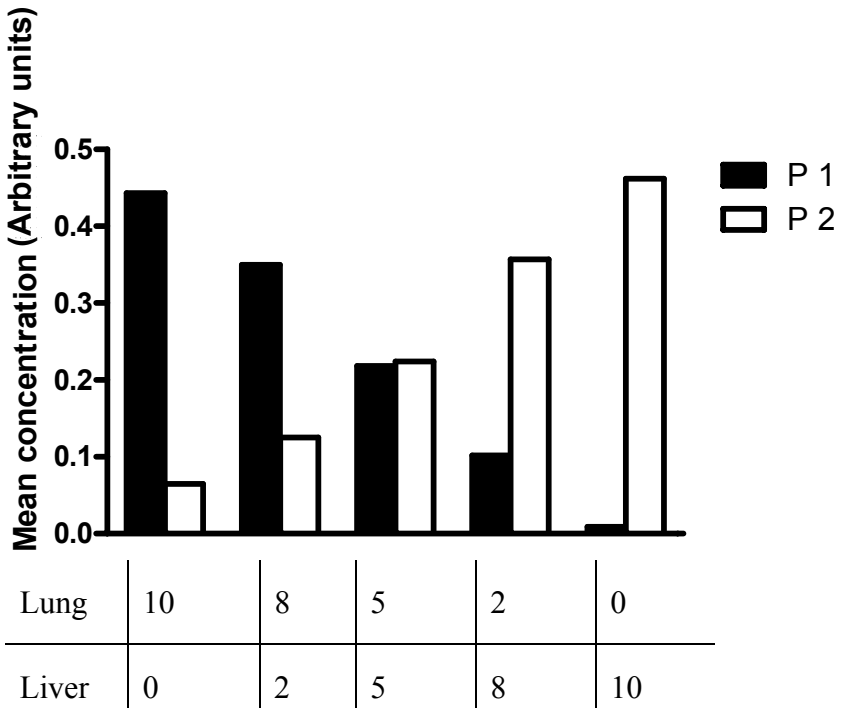

Figure 4.2 Comparison of promoter usage of the *Hsd11b1* gene in lung and liver
Total RNA extracted from lung and liver of WT mice was analysed for P1 and P2 mRNA by real-time PCR. 5 groups of cDNA were prepared by mixing different proportions of lung and liver cDNA as detailed below the graph. The values shown in the graph are mean concentration of each group derived from the standard curve, prepared by mixing equal amounts of liver and lung cDNA.

4.2.2 Human lung cell lines (A549, HFL-1) express endogenous 11β-HSD1 using the P2 promoter

Initially, 2 human lung cell lines were used to test the hypothesis that lung epithelial cells express 11β-HSD1 from the P2 promoter whereas lung fibroblast cells use the P1 promoter. A549 cells were derived from a human lung adenocarcinoma cell line and resemble type 2 alveolar cells (Lieber M, Smith B et al. 1976). HFL-1 cells were derived from human fetal lung fibroblast cells and resemble fibroblast cells (Breul, Bradley et al. 1980), although there is some evidence that they also have myofibroblast characteristics (Kawamoto, Matsunami et al. 1997)

A549 and HFL-1 cells were cultured as described in Chapter 2.2.1. RT-PCR showed that endogenous 11β-HSD1 was expressed in both A549 and HFL-1 cells (Figure 4.3), confirming previous findings in A549 (Sai, Esteves et al. 2008) and more recently in HFL-1 (Yang, Zhu et al. 2009). In both cell lines, *Hsd11b1* was predominately transcribed from the P2 promoter with a lower level of transcription from the P3 promoter (Figure 4.3). Neither cell line used the P1 promoter of *Hsd11b1* (Figure 4.3). A positive control for the P1 promoter was not included due to difficulties in obtaining human tissue, but suitable controls would be lung, kidney or placenta and previous work has established that these P1 primers amplify the correct product from human kidney cDNA (Ms V. Kelly and Prof K.Chapman, unpublished).

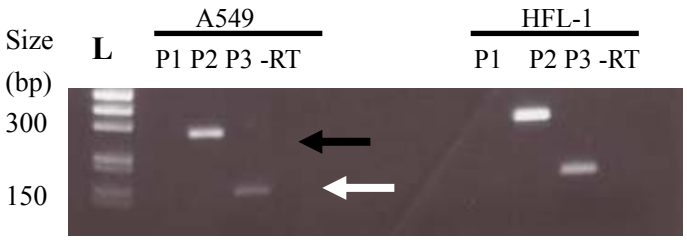

Figure 4.3 11β-HSD1 promoter usage in human A549 and HFL-1 cells.
RNA was extracted from human A549 and HFL-1 cells. 1μg of RNA was used in an RT reaction and 4μl RT reaction used in 35 cycles PCR with primers specific for transcripts initiating at each of P1, P2 and P3 as well as primers that detect all *Hsd11b1* transcripts. Lane 1 contains a 1 kb ladder, labeled with L. A black arrow indicates the position of the 285bp P2 product and a white arrow indicates the 152bp P3 product from human 11β-HSD1 mRNA. A negative control reaction (-RT) gave no product with primers to amplify total 11β-HSD1. The predicted size for the P1 product is 272bp.

4.2.3 Promoter usage of 11β-HSD1 in primary alveolar macrophages, lung epithelial cells, lung fibroblasts and interstitial macrophages

The result from the lung cell lines indicates that the *Hsd11b1* gene is transcribed from the P2 promoter in both epithelial and fibroblast cell lines. Given that lung mainly uses the P1 promoter, this suggests either that another cell type other than fibroblasts or type 2 alveolar cells expresses 11β-HSD1 from the P1 promoter or that the cell lines behave differently in this respect to the primary lung cells. Therefore lung cell isolation was carried out to investigate *Hsd11b1* promoter usage in different primary cell populations in lung. Lung alveolar macrophages, epithelial cells (as clumps of non-adherent or loosely adherent cells), fibroblasts and interstitial macrophages (adherent cells) were isolated as detailed in Chapter 3.3.

RNA was extracted from the indicated lung cell preparations. RT-PCR showed that the non-adherent cells (containing epithelial cells) used both P1 and P2 (Figure 4.4, lanes 2-4). Alveolar macrophages mainly used P2 (Figure 4.4, lanes 5-7) and the adherent cells, containing fibroblasts and interstitial macrophages, predominantly used P1 (Figure 4.4, lanes 8-10). Because the P3 promoter is a very minor promoter in lung (Figure 4.1) and the truncated enzyme encoded by the P3 promoter lacks 11β-HSD1 activity (Mercer, Obeyesekere et al. 1993), only the P1 and P2 promoters were examined further.

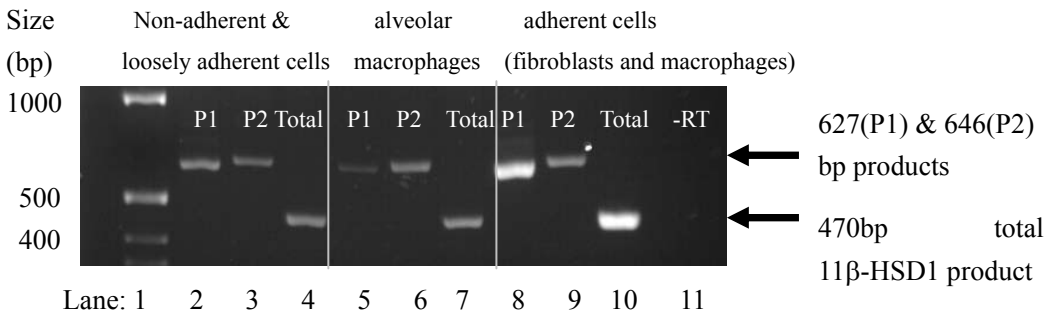

Figure 4.4 *Hsd11b1* promoter usage in different lung cell populations.
RNA was extracted from the indicated primary lung cells. 1μg of RNA was used in an RT reaction and 4μl RT reaction used in 30 cycles PCR with primers specific for transcripts initiating at each of P1 and P2 as well as primers that detect all *Hsd11b1* transcripts. Lane 1, 1kb marker. Lanes 2-4, RT-PCR reactions carried out on RNA extracted from non-adherent and loosely adherent cells, which contain epithelial cells. Lanes 5-7, RT-PCR reactions carried out on alveolar macrophage RNA. Lanes 8-10, RT-PCR reactions carried out on RNA isolated from firmly adherent cells. Lane 11, A control reaction (-RT) on adherent cell RNA gave no product with primers to amplify total 11β-HSD1. Arrows indicate the similar sized products from the P1 (627bp) and P2 promoters (646bp), and the 470 bp product corresponding to total 11β-HSD1 mRNA.

4.2.4 *Hsd11b1* promoter usage in bone marrow-derived myeloid cells

The experiments described above (4.2.3) show alveolar macrophages mainly use the *Hsd11b1* P2 promoter. To investigate *Hsd11b1* promoter usage in a more pure population of macrophages and to explore promoter usage in other innate immune cells present in lung tissue, bone marrow-derived myeloid cells were used. Bone marrow-derived macrophages (BMDM) were differentiated from bone marrow, prepared from femurs of C57BL/6 mice as described in Chapter 2.2.1.2 and used to test whether all macrophages predominately use the P2 promoter. In addition, dendritic cells (DC) were differentiated from bone marrow by culture with Granulocyte Macrophage-Colony Stimulating Factor (GM-CSF). As DC have previously been shown to express 11β-HSD1 (Freeman, Hewison et al. 2005), promoter usage in these cells was also examined.

4.2.4.1 Both P1 and P2 but not P3 are used to transcribe *Hsd11b1* in bone marrow derived macrophages and dendritic cells

RT-PCR on RNA from freshly isolated bone marrow cells from C57BL/6 mice showed that both P1- and P2-initiated 11β-HSD1 mRNAs were present in bone marrow cells, with negligible amounts of P3-initiated transcripts (Figure 4.5).

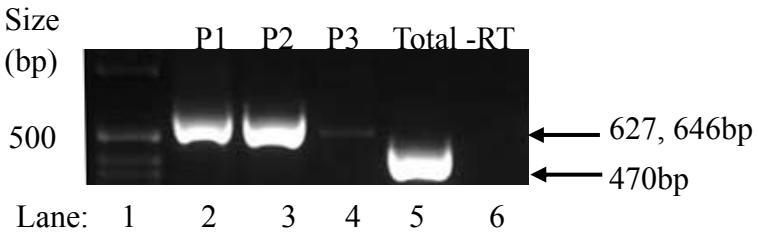

Figure 4.5 Promoter usage of 11β-HSD1 in freshly isolated mouse bone marrow cells.

RNA was extracted from freshly isolated bone marrow cells from C57BL/6 mice. 1μg of RNA was used in an RT reaction and 4μl RT reaction used in 30 cycles PCR with primers specific for transcripts initiating at each of P1, P2 and P3 as well as primers that detect all *Hsd11b1* transcripts. Lane 1, 1kb marker. Lanes 2-4, RT-PCR reactions carried out to detect transcripts initiating from P1 (lane 2, 627bp product), P2 (lane 3, 646bp product) and P3 (lane4, 543bp product). Lane 5 shows the 470bp product from total 11β-HSD1. Lane 6, contains a PCR reaction in which RT was omitted from the RT reaction (-RT). The positions of the 627 bp P1 product and the 646bp P2 product are indicated, as is the position of the 470bp product derived from total 11β-HSD1 mRNA.

4.2.4.2 Bone marrow derived macrophages mainly use the P2 promoter

To confirm macrophage differentiation, immunocytochemical staining for F4/80 was carried out on BMDM as described in Chapter 2.2.13. Generally, more than 90% BMDM cultures were macrophages (Figure 4.6A). Diff-Quick staining was also used to assess morphology (Figure 4.6B). To verify that GR is co-expressed with 11β-HSD1 in BMD macrophages, immunocytochemical staining for GR was also carried out. Intensity of GR staining was variable between BMDM, with most cells showing staining in the nucleus but with some cells appearing negative (Figure 4.6C).

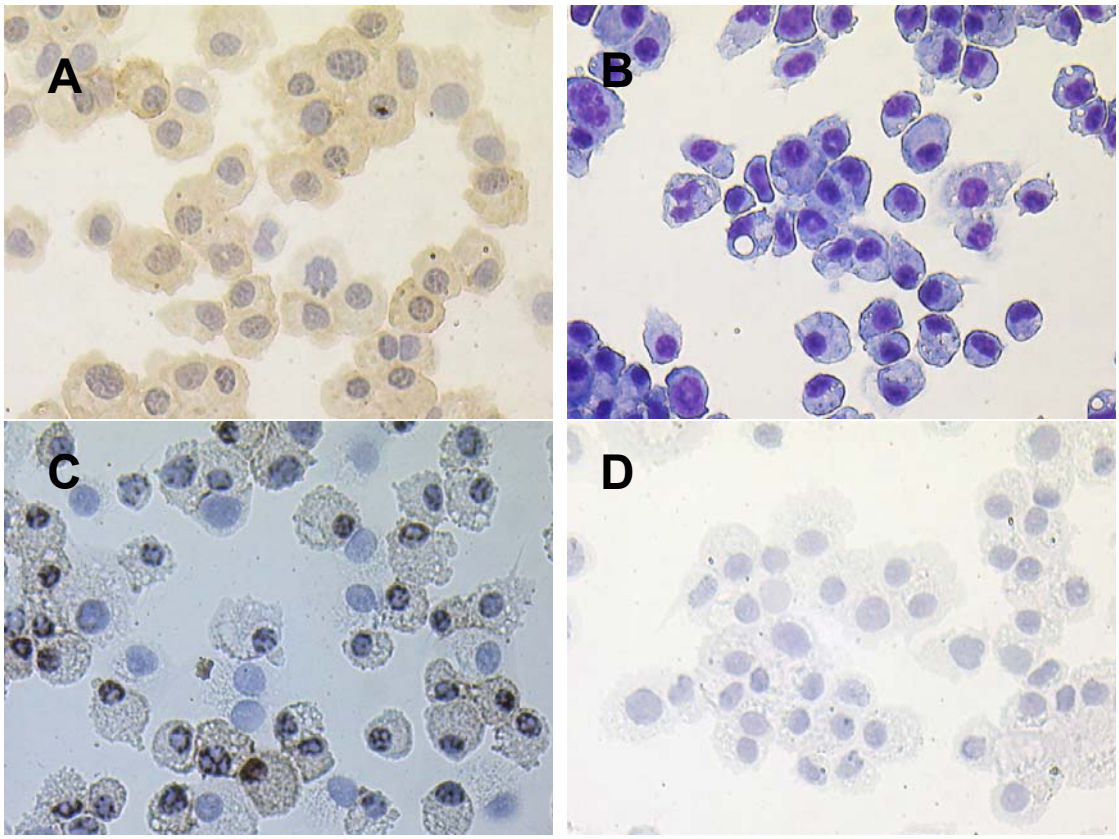

Figure 4.6 Phenotyping of BMDM by F4/80, Diff-Quick and GR staining
Immunohistochemistry was carried out on cytocentrifuged preparations of BMDM cells from WT mice to check maturation. (A), rat anti-mouse F4/80 antibody (1:100 dilution) and biotinylated rabbit-anti-rat 2nd Ab (1:200 dilution); (B), Diff-Quick staining; (C), rabbit anti-GR antibody (1:100 dilution) and biotinylated goat-anti-rabbit 2nd Ab (1:50 dilution); (D), negative control in which primary antibody was omitted with biotinylated goat-anti-rabbit 2nd Ab (1:50 dilution). Images were all captured at magnification X400.

To establish which promoter of *Hsd11b1* was used in BMDM and to test whether activation of macrophage by LPS altered expression levels and/or promoter usage of *Hsd11b1*, BMDM were treated with 100ng/ml LPS for 24h. Previous studies have suggested that macrophage activation by lipopolysaccharide (LPS) may regulate levels of 11β-HSD1 mRNA in a macrophage cell line (Thieringer, Le Grand et al. 2001), although there may be no effect in primary macrophages (Gilmour 2002).

RT-PCR to examine P1 promoter and P2 promoter usage showed that BMDM use the P2 promoter (Figure 4.7), consistent with data in alveolar macrophages (Section 4.2.3). No difference was seen in promoter usage following LPS (Figure 4.7), nor was there an obvious difference in levels of 11β-HSD1 mRNA initiated from the p2 promoter following LPS treatment (Figure 4.7).

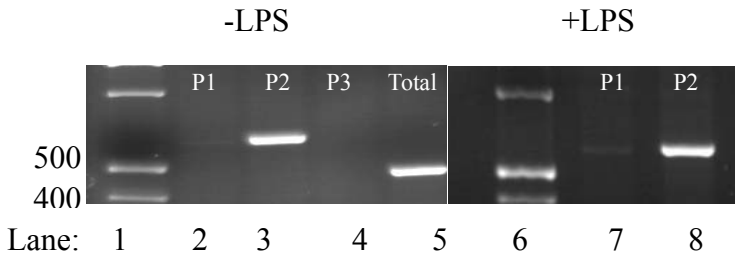

Figure 4.7 BMDM use the 11β-HSD1 P2 promoter and promoter usage is not affected by LPS treatment

BMDM were differentiated and cultured in Teflon pots. 7d after differentiation of BMDM, one pot of BMDM was treated with 100ng/ml LPS for 24h. RNA was extracted from BMDM with or without 24h LPS stimulation. 1μg of RNA was used in an RT reaction and 4μl RT reaction used in 30 cycles PCR with primers specific for transcripts initiating at each of P1, P2 and P3 as well as primers that detect all *Hsd11b1* transcripts. Lane 1, 1kb marker. Lanes 2 to 5, RT-PCR reactions carried out on RNA of BMDM without LPS. Lane 6, 1kb marker. Lanes 7 and 8, RT-PCR reactions carried out on RNA of BMDM with LPS.

4.2.4.3 Bone marrow derived dendritic cells express 11β-HSD1 from the P2 promoter

Previous data has shown that 11β-HSD1 expression is induced in immature human DC then decreases as DC are matured (Freeman, Hewison et al. 2005). To determine which promoter is used in DC cells and whether promoter usage is altered by maturation of DC, DC were differentiated from bone marrow cells as described in Chapter 2.2.1. On d10 of differentiation, DC were resuspended in medium containing GM-CSF to mature. Control cells were left without GM-CSF treatment and considered immature DC. On d11, cells were harvested for RNA extraction. The maturation of DCs was assessed by CD11c staining, which was similar in mature and immature DCs with 65% cells staining positively (Figure 4.8A&B).

IHC showed that expression of 11β-HSD1 decreased with maturation (Figure 4.8C&D). Interestingly, GR immunoreactivity showed the opposite pattern to 11β-HSD1 and was higher in mature DC than in immature DC (Figure 4.8E&F).

RT-PCR showed that both mature and immature DC predominantly used the P2 promoter to express 11β-HSD1 (Figure 4.9), which is similar to BMDM.

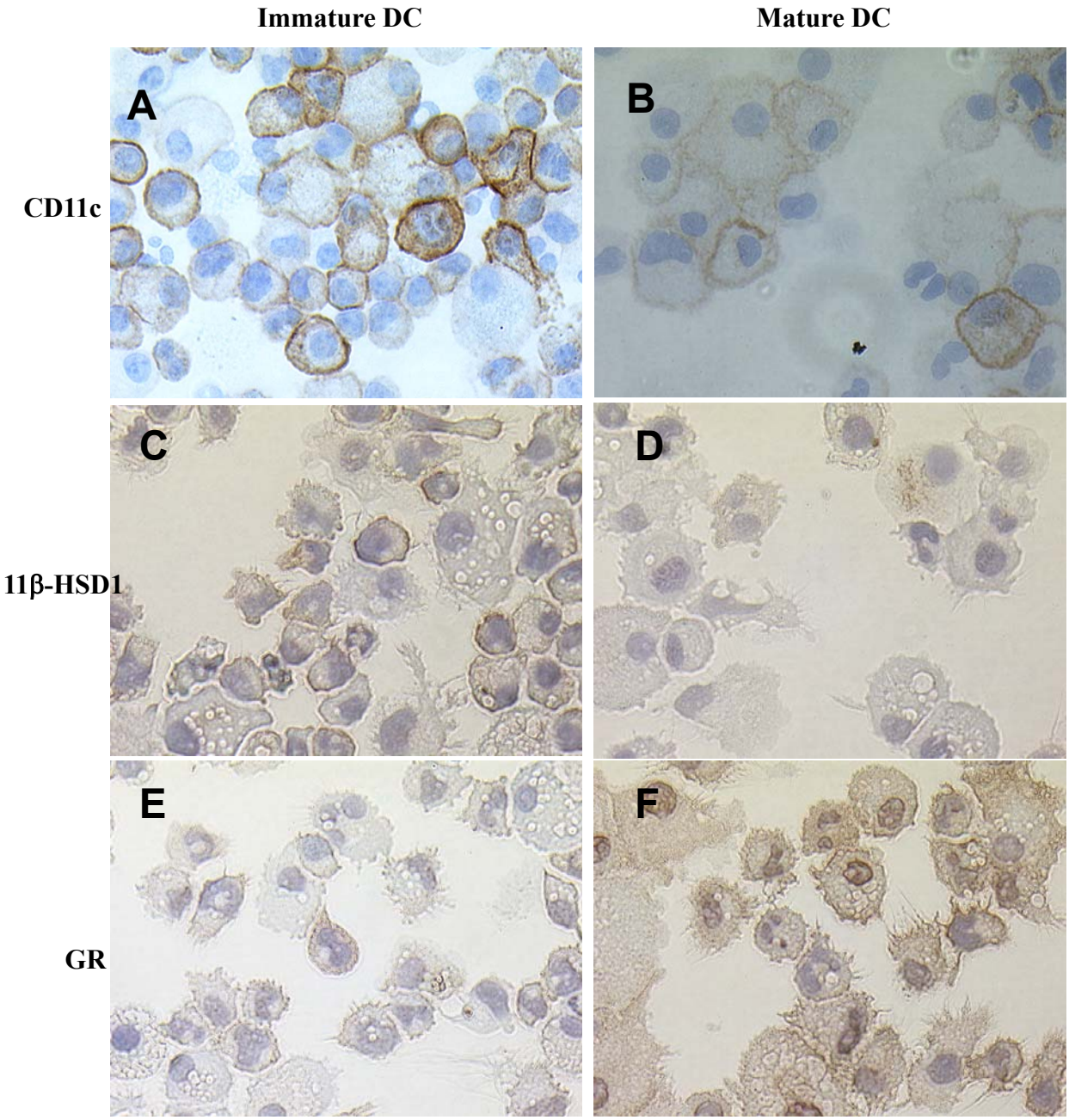

Figure 4.8 Immunohistochemical staining of 11β-HSD1 (rabbit Ab), GR and CD11c on DC

(A-B), DC stained with biotinylated hamster anti-mouse CD11c (1:50 dilution); (A) 11 days immature DC; (B) 11 days mature DC; (C-D), immunohistochemistry was carried out with rabbit anti-11β-HSD1 antibody and biotinylated goat-anti-rabbit 2nd Ab on (C) 11 days immature DC; (D) 11 days mature DC. (E-F), DC stained with rabbit anti-GR antibody (1:100 dilution) and biothylated goat-anti-rabbit 2nd Ab (1:50 dilution); (E) 11 days immature DC; (F) 11 days mature DC; (All, magnification X400)

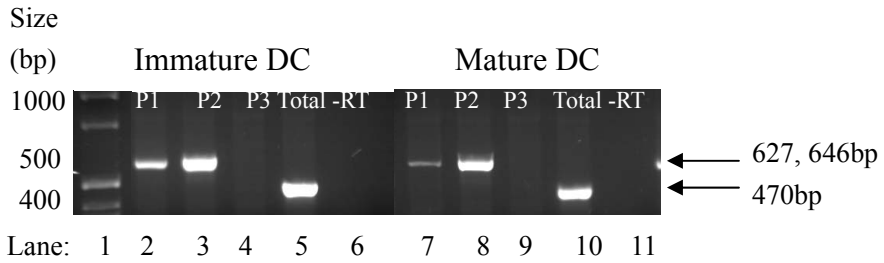

Figure 4.9 Promoter usage of 11β-HSD1 in mature and immature DC.
RNA was extracted from mature and immature DC. 1μg of RNA was used in an RT reaction and 4μl RT reaction used in 30 cycles PCR with primers specific for transcripts initiating at each of P1 and P2 as well as primers that detect all *Hsd11b1* transcripts. Lane 1, 1kb marker. Lane 2-5, RT-PCR reactions carried out on immature DC RNA. Lane 6, minus RT. Lane 7-10, RT-PCR reactions carried out on mature DC RNA. Lane 11, contains a PCR reaction in which RT was omitted from the RT reaction, minus RT. The position of the 627 bp P1 product and the 646bp P2 product is indicated, as is the position of the 470bp product derived from total 11β-HSD1 mRNA.

4.2.5 Further characterization of 11β-HSD1 promoter usage in primary lung fibroblasts

11β-HSD1 expression has been demonstrated in rat lung fibroblasts (Brereton, van Driel et al. 2001) and Chapter 3 shows that 11β-HSD1 is also expressed in mouse primary lung fibroblasts. Moreover, the experiments above suggest that freshly isolated lung fibroblasts mainly use the P1 promoter with the P2 promoter used to a much lesser extent. However, there are still macrophages present in freshly isolated fibroblasts (identified by F4/80 staining), raising the possibility that the small amount of P2 promoter usage in the adherent cells (fibroblasts and macrophages) might be due to macrophage contamination, because macrophages mainly use the P2 promoter (Figure 3.6 and see Chapter 4.2.4.2). As primary macrophages do not proliferate (Stewart, Lin et al. 1975), but fibroblasts proliferate very quickly in culture, further culture was carried out to decrease the possible macrophage contamination, as described in Chapter 2.2.7. However, RT-PCR showed that 11β-HSD1 promoter usage was changed and both the P1 and P2 promoters are used in passage 2 fibroblasts, probably to similar extents (Figure 4.10).

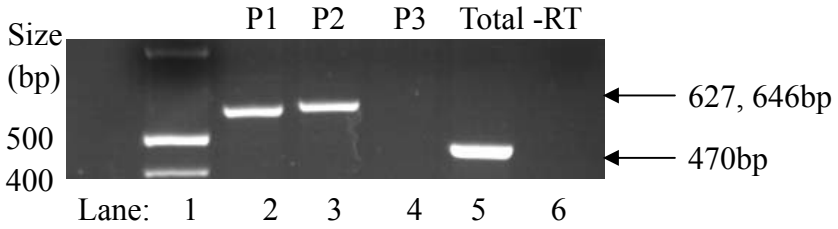

Figure 4.10 Primary lung fibroblasts use similar amount of the P1 and P2 promoter of *Hsd11b1* in passage2

RNA was extracted from lung fibroblasts at passage 2 and subject to PCR with primers specific for *Hsd11b1* transcripts initiating at the P1 promoter (627bp product), the P2 promoter (647bp product) or the P3 promoter (predicted product of 542bp). Total 11β-HSD1 mRNA was amplified to give a product of 470bp (lanes marked total). Control reactions omitted RT (-RT). 1μg of RNA was used in an RT reaction and 4μl RT reaction used in 30 cycles PCR. Lanes 1, 1kb marker. Lanes 2-5, RT-PCR reactions carried out on passage 2 fibroblast RNA. The position of the 627 bp P1 product and the 646bp P2 product is indicated, as is the position of the 470bp product derived from total 11β-HSD1 mRNA.

To determine whether any macrophage contamination cause the increase of the P2 promoter usage, IHC was carried out with anti-F4/80 antibody to identify macrophages in primary lung fibroblasts following 6 passages. As shown in Figure 4.11A very few (<1%) cells stained with F4/80 suggesting there is little macrophage contamination.

As HFL-1 cells are reported to have myofibroblast characteristics and primary fibroblasts may have transformed to myofibroblasts with passage, passage 6 cells were stained with anti-α-SMA antibody to address this possibility. The majority of cells were positive for α-SMA (Figure 4.11C), suggesting that fibroblasts had transformed to myofibroblasts after 6 passages in primary culture. Although the cells were positive for α-SMA, the morphology was still typical of fibroblasts.

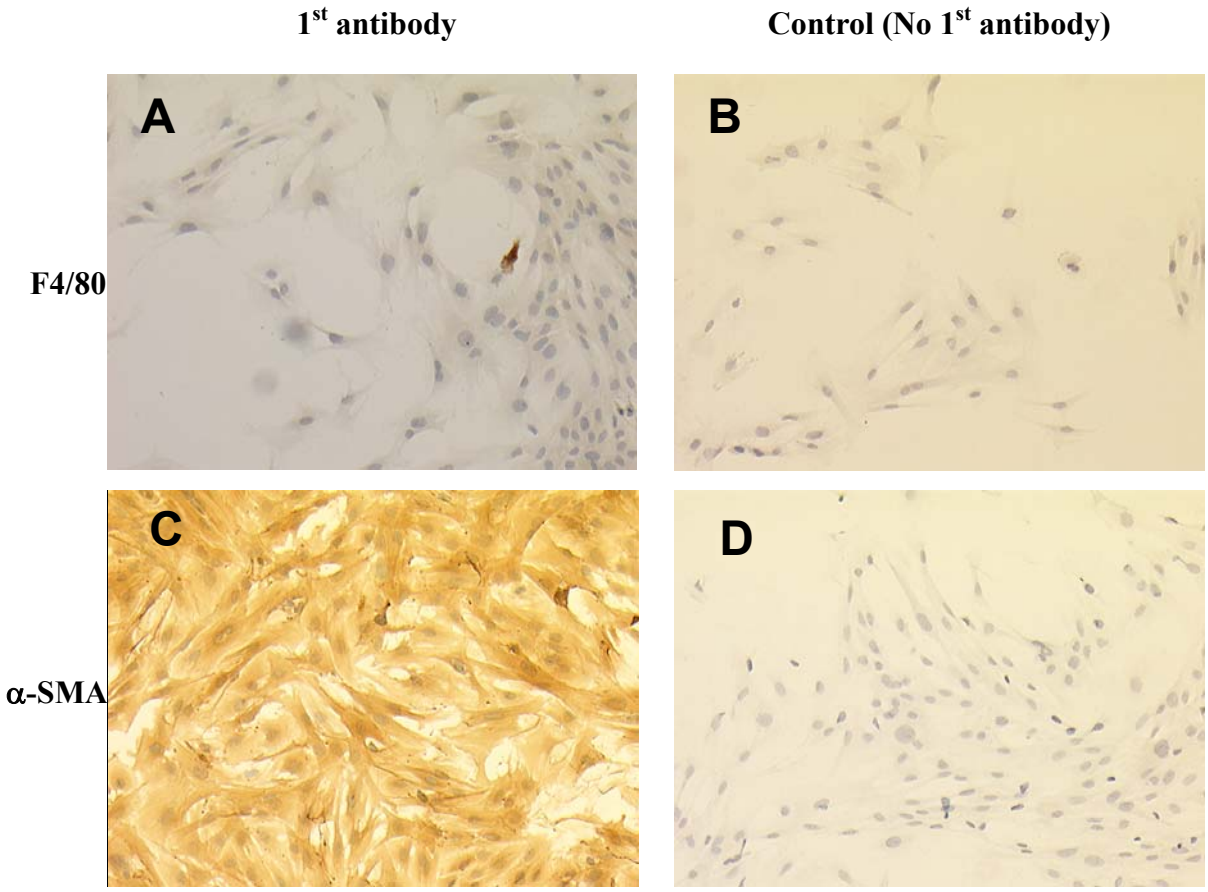

Figure 4.11 Immunocytochemistry on primary cultured lung fibroblasts (passage 6) shows the majority of cells are positive for α-SMA and very few cells are positive for F4/80

Immunocytochemistry showing staining of primary lung fibroblasts (passage 6) (A), F4/80 staining; (B), negative control for F4/80 staining, 2nd Ab only; (C), α-SMA staining; (D), negative control for α-SMA, 2nd Ab only. Immunocytochemistry was carried out with mouse anti-mouse α-SMA antibody at 1:8000 dilution and biotinylated goat-anti-mouse 2nd Ab at 1:400 dilution or rat anti-mouse F4/80 at 1:400 dilution and biotinylated goat-anti-rat 2nd Ab at 1:400 dilution. Brown indicates positive staining. Images were captured at X100 magnification.

4.2.5.1 The promoter usage of *Hsd11b1* changes during culture and passage

The discovery that passaged fibroblasts (which stained positively for α-SMA) and HFL-1 cells use the P2 promoter of *Hsd11b1* whereas freshly isolated fibroblasts appear to mainly use the P1 promoter suggested that promoter usage of *Hsd11b1* may switch with continuous cell culture. To determine whether fibroblast cells switch from the P1 promoter to the P2 promoter after continuous passage, RNA was extracted from fibroblasts after 5 passages and subject to RT-PCR. Control reverse transcription-PCR reactions from lung mRNA served as positive controls for the transcription of 11β-HSD1 from the P1 promoter. Almost no PCR product was obtained with cDNA from the passaged fibroblasts with the primers specific for the P1 promoter (Figure 4.12). At this time, the number of macrophages (identified by F4/80 staining) is very low already (data not shown).

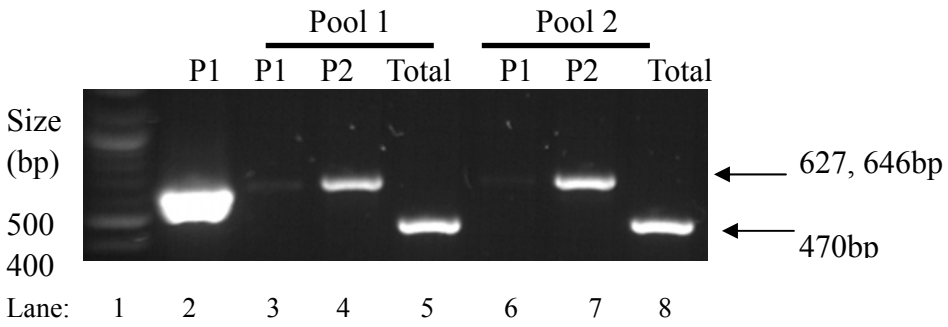

Figure 4.12 Primary lung fibroblasts mainly used the P2 promoter of *Hsd11b1* after 5 passages

RNA was extracted from lung fibroblasts at passage 5 and subject to PCR with primers specific for *Hsd11b1* transcripts initiating at the P1 promoter (627bp product), the P2 promoter (647bp product). Total 11β-HSD1 mRNA was amplified to give a product of 470bp (lanes marked total). Control reactions omitted RT (-RT). 1μg of RNA was used in an RT reaction and 4μl RT reaction used in 30 cycles PCR. Lanes 1, 1kb marker. Lane 2, RT-PCR carried out on RNA from whole lung used as a positive control for the P1 promoter product. Lanes 3-8, RT-PCR reactions carried out on RNA isolated from 2 independent cultures of fibroblasts (passage 5; pool 1 and pool 2). The position of the 627 bp P1 product and the 646bp P2 product is indicated, as is the position of the 470bp product derived from total 11β-HSD1 mRNA.

4.2.5.2 Quantification by real-time PCR of 11β-HSD1 promoter usage in primary lung fibroblasts cultured for 2 weeks, 4 weeks or 22 weeks

To quantify mRNA initiating from the P1 and P2 promoters of 11β-HSD1 in primary lung fibroblasts and to confirm the switch in promoter usage, specially designed primers were used in real-time PCR (validation of assay at 4.2.1.2). Three independent cultures were established, each from a pool of cells from 2 mice. RNA was extracted from fibroblasts at passage 0 (in culture for 2 weeks), passage 3 (in culture for 4 weeks) and passage 12 (in culture for 22 weeks) and subject to real-time PCR.

After 22 weeks of culture (12 passages), only 11β-HSD1 mRNA initiating at the P2 promoter was detected (Figure 4.13). In contrast, after 2 weeks (passage 0) P1 predominated whereas after 4 weeks of culture (passage 3), P1 and P2 were used to a similar extent with P2 possibly predominating (Figure 4.13). These results confirm that at early passages lung fibroblasts mainly use the P1 promoter, but undergo a switch to the P2 promoter following repeated passage.

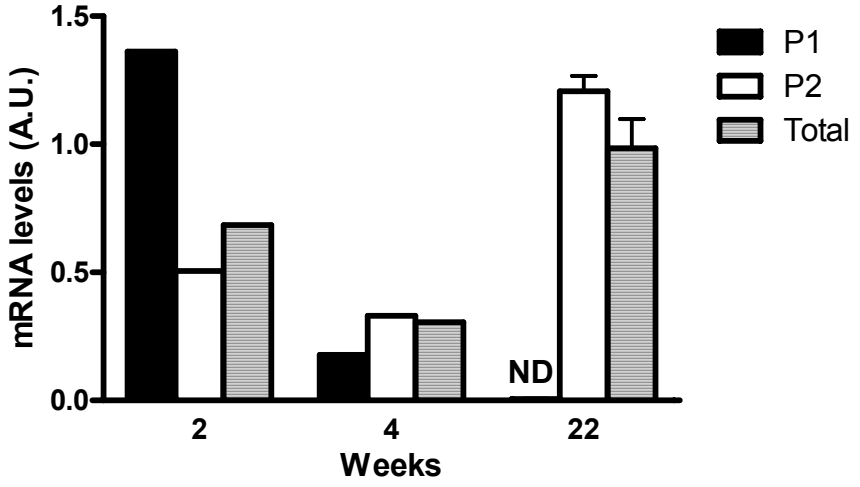

Figure 4.13 The promoter usage of the *Hsd11b1* gene switches from P1 to P2 following extended primary culture.

Total RNA was extracted from 3 independent cultures of primary lung fibroblasts grown for 2 weeks (0 passages), 4 weeks (3 passages), or 22 weeks (12 passages) and analysed for P1-and P2-initiated 11β-HSD1 mRNA as well as total 11β-HSD1 mRNA by real-time PCR. mRNA Levels are expressed relative to the level of TBP mRNA and are in arbitrary units (AU). Data at 2 and 4 weeks are from 2 different cultures. ND, not detectable

4.2.5.3 TGF-β regulates 11β-HSD1 expression during fibroblast to myofibroblasts differentiation

TGF-β plays an important role in inducing fibroblast to myofibroblast differentiation (Hu, Wu et al. 2004). To determine whether TGF-β induces the promoter switch of *Hsd11b1*, primary fibroblasts in passage 1 were treated with 2ng/ml TGF-β or 10μM SB431542 (a TGF-β receptor antagonist) for 72h, as described in Chapter 2.2.7. After removal of the culture medium, cells were washed with PBS, then subject to RNA extraction or IHC. Type 1 collagen and α-SMA expression, two markers of fibroblast activation and myofibroblast differentiation (Liu, Dhanasekaran et al. 2004), were assessed by IHC and the encoding mRNAs measured by real-time PCR to confirm the transformation and to validate the effect of TGF-β.

α-SMA IHC showed that before TGF-β treatment, cells were already positive for α-SMA (Figure 4.14A). TGF-β treatment caused fibroblasts to proliferate and become more spindle-shaped, with cells aligned parallel to one another (Figure 4.14B) and exhibiting increased α-SMA expression (Figure 4.14B), all typical features of myofibroblasts (Hu, Wu et al. 2004). Fibroblasts treated with SB431542 showed similar fibroblast morphology and α-SMA expression to control untreated cells (compare Figure 4.14C with Figure 4.14A). The results confirm that TGF-β increased the fibroblast to myofibroblast transformation, an effect antagonized by SB431542.

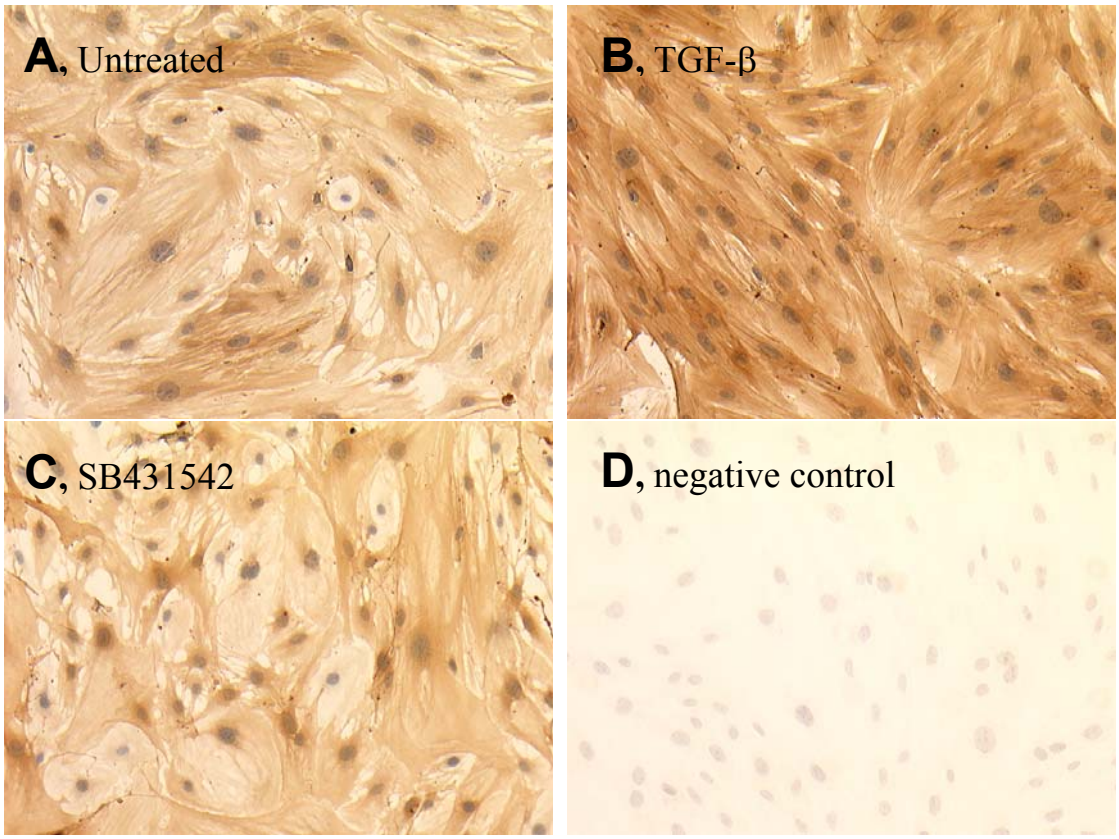

Figure 4.14 α-SMA expression in primary cultured lung fibroblasts confirms a TGF-β–mediated fibroblast to myofibroblast transformation.
Immunohistochemistry was carried out with mouse anti-mouse α-SMA antibody at 1:8000 dilution and biotinylated goat-anti-mouse 2nd Ab at 1:400 dilution. Brown indicates positive staining.
(A), control fibroblasts without treatment (passage 1); (B), fibroblasts treated for 72h with 2ng/ml TGF-β; (C), fibroblasts treated for 72h with 10μM SB431542, a TGF-β receptor antagonist; (D), negative control for α-SMA, mouse IgG only. Images captured at magnification, X100

Real-time PCR showed that type 1 collagen expression was increased with TGF-β treatment and decreased with TGF-β receptor antagonist (Figure 4.15A), consistent with a TGF-β–induced differentiation (from fibroblasts to myofibroblasts). α-SMA mRNA levels showed a similar trend to Type 1 collagen (Figure 4.15B). However, this difference did not reach significance (P=0.15). Nevertheless, these results confirm the effect of TGF-β on the cells and its antagonism by TGF-β receptor antagonist.

Levels of 11β-HSD1 mRNA were markedly decreased by TGF-β whereas 11β-HSD1 mRNA levels were increased by TGF-β receptor antagonist (Figure 4.15C). Levels of P1-initiated 11β-HSD1 transcripts were repressed by TGF-β, to barely detectable levels (Figure 4.15D). Importantly, addition of SB431542 markedly increased levels of P1-initiated mRNA. TGF-β decreased levels of mRNA initiating at the P2 promoter, an effect that was antagonised by SB431542 (Figure 4.15E). However, levels of P2-initiated transcripts were similar in TGF-β receptor antagonist-treated cells and in control cultures (Figure 4.15E).

Because C/EBPβ regulates the P2 promoter (Chapman, Coutinho et al. 2009) and is implicated in the differentiation of fibroblast to myofibroblasts (Hu, Ullenbruch et al. 2007), levels of C/EBPβ mRNA were measured. However, C/EBPβ mRNA levels did not differ between treated and untreated cells (Figure 4.15F).

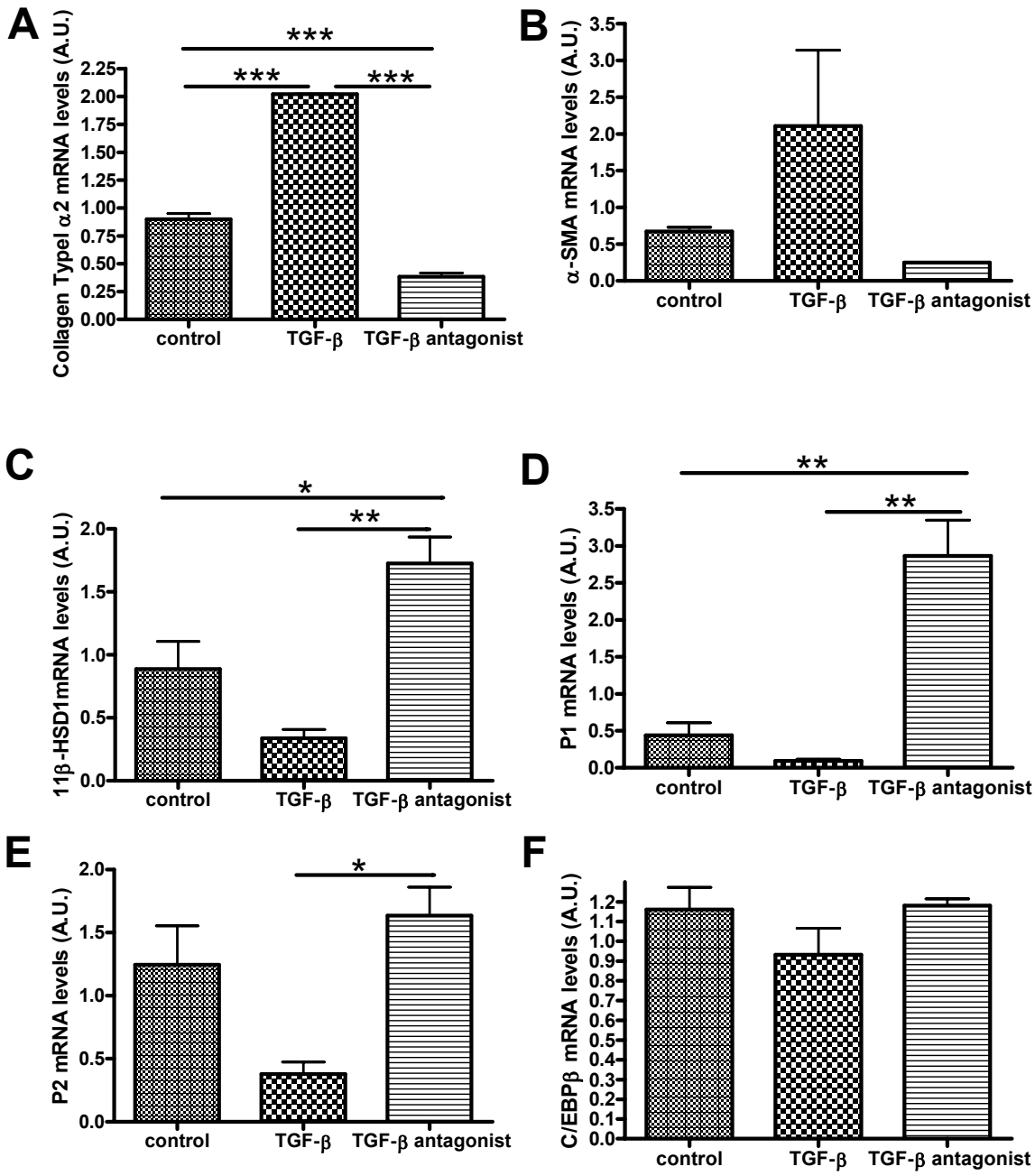

Figure 4.15 TGF-β switches off the P1 promoter of *Hsd11b1*

Total RNA was extracted from passage 1 (9d) fibroblasts following 72h treatment with TGF-β or SB431542 or without treatment (control), reverse transcribed and subject to real-time PCR to measure (A) typeI α2 collagen mRNA levels; (B) α-SMA mRNA levels; (C) total 11β-HSD1 mRNA; (D) mRNA initiating at the P1 or (E) P2 promoter of 11β-HSD1; and (F) C/EBPβ mRNA. Levels are expressed relative to the level of TBP mRNA and are in arbitrary units (AU). Data are mean ± SEM from 3 independent cultures. Data were analysed by ANOVA followed by Tukey's Multiple Comparison Test. *, $p<0.05$; **, $p<0.01$; ***, $p<0.001$.

4.3 Discussion

In the majority of tissues, 11β-HSD1 can be transcribed from 2 promoters although in mouse the P2 promoter predominates (Bruley, Lyons et al. 2006). Data in this chapter confirmed that lung expresses 11β-HSD1 mainly from the P1 promoter and showed that, in contrast to macrophages and dendritic cells which mainly used the P2 promoter, this was likely to be due to expression of *Hsd11b1* from the P1 promoter in lung fibroblasts. A549 cells, an alveolar cell line (Lieber M, Smith B et al. 1976), expressed 11β-HSD1 from the P2 promoter. However, HFL-1, a fibroblast cell line (Breul, Bradley et al. 1980), expressed 11β-HSD1 from the P2 promoter as well. Although primary lung fibroblasts predominantly used the P1 promoter of 11β-HSD1, they completely switched to the P2 promoter after a few passages. Interestingly, total 11β-HSD1 expression was decreased upon initial passage, then was increased thereafter. This might be due to differentiation and/or proliferation of a sub-population of fibroblasts that highly express 11β-HSD1 from the P2 promoter, or may be an adaption to culture shown by all the fibroblasts in the population.

In passage 2 lung fibroblasts, almost all cells were α-SMA positive, which means that fibroblasts had started to transform to myofibroblasts. But compared to TGF-β stimulated myofibroblasts, these passage 2 cells were still like fibroblasts in morphology and had low α-SMA expression. Some groups are using plasma-derived serum to culture fibroblasts, to decrease the transformation to myofibroblast during

culture (Hu, Wu et al. 2004). Fetal Bovine Serum (FBS) has been shown to stimulate lung fibroblast proliferation (Yano, Yoshida et al. 2006) and primary culture with FBS will induce α-SMA expression (personal communication, Dr Sem Phan, University of Michigan, USA). Early passaged fibroblasts were subject to real-time PCR to measure α-SMA mRNA expression, showing that the level of α-SMA was much higher in the first passage, and decreased gradually thereafter (data not shown). It may represent an autocrine regulation mechanism of α-SMA expression. The culture medium and especially serum content may therefore induce the differentiation of fibroblast to myofibroblast.

TGF-β is the key inducer of fibroblast to myofibroblast transformation (Hu, Wu et al. 2003), so early passaged fibroblasts were treated with TGF-β to test whether TGF-β regulates 11β-HSD1 expression and promoter usage. 72h treatment with TGF-β increased expression of collagen type1 α2 and α-SMA, markers of myofibroblast differentiation, and decreased 11β-HSD1 expression, an effect which was not only reversed by SB431542, a TGF-β receptor antagonist, but in fact SB431542 increased 11β-HSD1 expression above control levels. This increase in 11β-HSD1 expression after SB431542 treatment compared to untreated cells, suggests either that the fibroblasts themselves secrete TGF-β or that culture medium containing new born calf serum contains TGF-β; thus antagonism of TGF-β receptors increased 11β-HSD1 mRNA levels relative to untreated cells. Whilst TGF-β reduced levels of

mRNA initiating at the P2 promoter, initiation from the P1 promoter was completely repressed. Treatment with TGF-β receptor antagonist markedly increased levels of P1-initiated 11β-HSD1 mRNA above levels in untreated cells. These data suggest that higher levels of TGF-β are required to decrease the P2 promoter than are present in the culture medium/secreted by the cells and that the P1 promoter may be sensitive to lower dose of TGF-β. A dose response experiment could test this hypothesis. These data suggest that a switch in 11β-HSD1 promoter usage may be regulated by TGF-β during an inflammatory response. TGF-β has been shown to regulate C/EBP-β and C/EBP-δ (Choy and Derynck 2003) and it may regulate 11β-HSD1 expression through those transcription factors.

C/EBP-β regulates 11β-HSD1 expression and is a key regulator of α-SMA expression and myofibroblast differentiation in isolated lung fibroblasts, binding to a C/EBP-β binding element identified in the α-SMA promoter (Hu, Wu et al. 2004; Hu, Ullenbruch et al. 2007). In the experiments reported here, the overall pattern of C/EBP-β expression after TGF-β stimulation was the same as for the 11β-HSD1 P2 promoter, but the treatment effects did not achieve significance. Small changes in transcription factor levels can have large effects on target genes, so perhaps there were changes in C/EBP-β levels that were missed here. Also C/EBP-β is regulated translationally and post-translationally, e.g. by phosphorylation (Park, Qiang et al. 2004) and these were not examined here.

5 Chapter Five: The consequences of 11β-HSD1-deficiency for lung inflammation/ fibrosis

5.1 Introduction and aim

Previous data from our lab have suggested that 11β-HSD1 is important in inflammation, with 11β-HSD1-deficient mice showing earlier and more severe inflammation in three experimental models; peritonitis, pleurisy and arthritis (reviewed in 1.1.6.2). In the peritonitis model, 11β-HSD1-deficient mice showed greater recruitment of inflammatory cells than WT mice, but the inflammation resolved at a similar time in WT and 11β-HSD1-deficient mice (Gilmour 2003). In the pleurisy model, 11β-HSD1-deficient mice similarly showed greater recruitment of inflammatory cells and also hints of early fibrosis, that were not seen in WT control mice, 2d following carrageenan (Coutinho 2009). This suggests that 11β-HSD1 may regulate the inflammatory response in lung by modulating local glucocorticoid action. Because the work described in Chapter 3 showed that in lung 11β-HSD1 is mainly expressed in the fibroblast cells, and Chapter 4 showed lung fibroblast express 11β-HSD1 from the P1 promoter, and TGF-β suppresses 11β-HSD1 expression, these suggested a role in lung fibrosis associated with inflammation.

To delineate the role of 11β-HSD1 in pulmonary inflammation and fibrosis, the bleomycin model was used. Pulmonary fibrosis is the most severe adverse effect associated with clinical use of bleomycin, a cytotoxic chemotherapeutic agent (Sikic, Young et al. 1978), and intratracheal instillation of bleomycin is a commonly used

experimental model of lung inflammation and fibrosis (Borzone, Moreno et al. 2001). Unlike the previous 3 inflammatory models tested, the bleomycin model can investigate both inflammation and fibrosis, which also has features in common with human idiopathic pulmonary fibrosis (IPF) syndrome (Giri, Nakashima et al. 1985). Intratracheal instillation of bleomycin induces inflammatory cell infiltration into interstitial and alveolar lung (Borzone, Moreno et al. 2001). The first 14d following bleomycin installation comprises the acute phase of inflammation, with inflammatory cell recruitment, then the tissue progresses to a fibrotic response which resolves slowly (Borzone, Moreno et al. 2001). The experiments described in this chapter were carried out in collaboration with Dr Rodger Duffin, who performed the intratracheal instillation of bleomycin.

5.2 Experimental plan

Age matched mice were treated with 0.025U bleomycin/mouse, and were killed 2d, 7d, 14d, 28d or 35d after installation of bleomycin. Mice were weighed regularly to assess general response to bleomycin. At each time point, lung tissues were preserved for RNA analysis, histology assessment or collagen measurement.

5.3 Results

5.3.1 WT and 11β-HSD1-deficient mice showed similar weight loss over 28d following bleomycin treatment

Mice were weighed on a regular basis following bleomycin treatment. Repeated-measures ANOVA showed there is no difference in weight between genotypes at any time point. And, there was no effect of bleomycin treatment on body weight of either genotype (Figure 5.1).

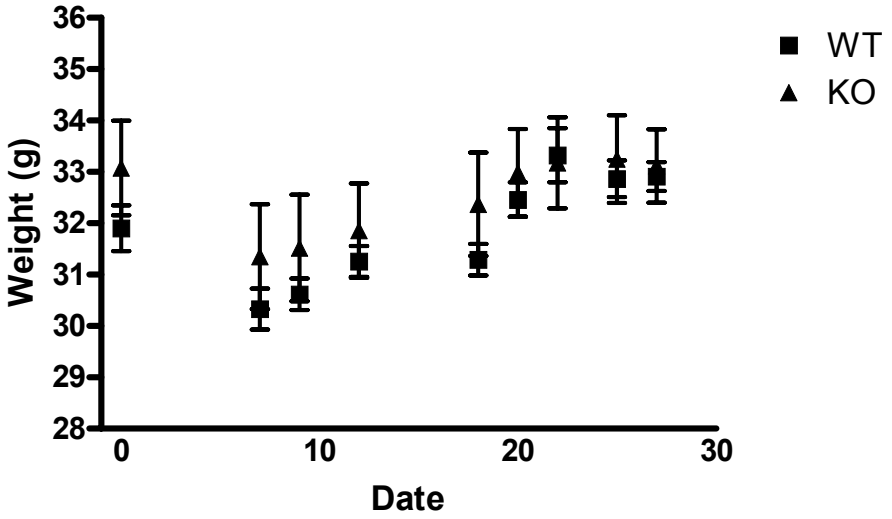

Figure 5.1 Bleomycin treatment for 28d had no effect on body weight of either WT or 11β-HSD1-deficient mice.

Repeated-measures ANOVA showed no difference in body weight between wild-type (WT; squares) and 11β-HSD1-deficient (KO; triangles) mice. Data are mean ± SEM with n = 8.

5.3.2 Characterization of bronchial alveolar cells recovered from bronchial alveolar lavage fluid (BALF)

In order to assess the effects of bleomycin, mice were killed 2d, 7d, 14d, 28d and 35d after treatment and lungs were lavaged to collect cells. Inflammation was assessed by total cell count using a nuclear counter machine and differential cell counts on Diff-Quick stained BALF cells (described in Chapter 2.2.4).

5.3.2.1 Total cell counts were similar between WT and 11β-HSD1-deficient mice after bleomycin treatment

Figure 5.2 compares the total cell count in BALF of bleomycin-treated WT and 11β-HSD1-deficient mice at each of the time points. No significant difference in the total mean cell count was seen between genotypes at any time point. The total cell number gradually increased from d2 through d28 and was significantly higher at d7 and d14 than in untreated mice. After 28d, total cell counts from both groups were reduced and did not significantly differ from basal levels at 35d.

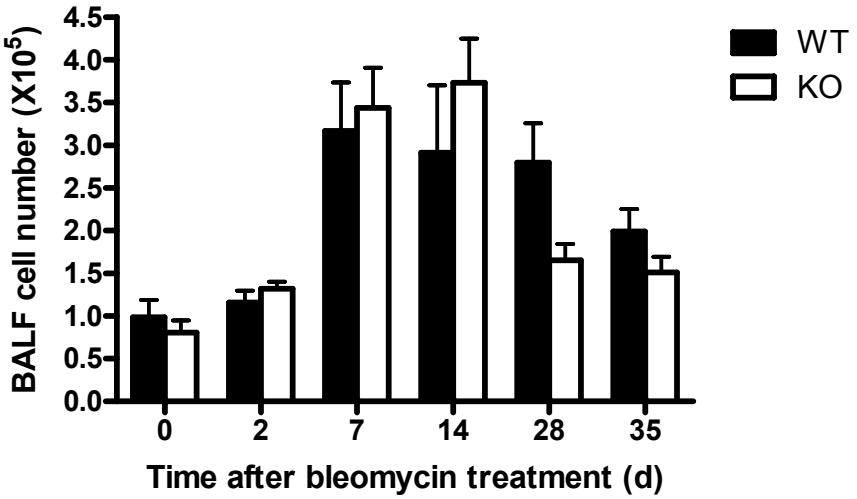

Figure 5.2 Comparison of the total cell number in BALF from WT and 11β-HSD1-deficient mice over the course of bleomycin-induced lung inflammation.

BALF was collected at the time points indicated from both WT and 11β-HSD1-deficient mice, and cells counted. Two-way ANOVA did not reveal any difference in total cell number between wild-type (WT; black bars) and 11β-HSD1-deficient (KO; white bars) mice, but did show a significant effect of time ($p<0.01$). There was not a significant interaction between genotype and time ($p=0.07$). Data are mean ± SEM with n = 5-8.

5.3.2.2 Differential cell counts did not reveal any differences between WT and 11β-HSD1-deficient mice after bleomycin treatment

In order to assess whether the types of inflammatory cells present in the BALF differed between WT and 11β-HSD1-deficient mice, BALF cells were cytocentrifuged and Diff-Quick stained as described in Chapter 2.2.4.

In cytocentrifuge preparations, the typical morphology of macrophages and neutrophils was obvious (Figure 5.3A&B). Similar numbers of macrophages and neutrophils were recovered in BALF from each genotype, 2d after bleomycin instillation (Figure 5.3C). However, almost all the neutrophils were cleared by 7d (Figure 5.3D), after which time the majority of inflammatory cells in BALF were macrophages (Figure 5.3E). The rest of the cell population consisted of either lymphocytes or neutrophils. There were no statistically significant differences between genotypes in the proportion of cell types (neutrophils, macrophages or lymphocytes) at any time point after bleomycin treatment (Figure 5.3C-E).

Total protein levels in BALF are an indication of the severity of lung inflammation (Duffin, Tran et al. 2007). Total protein in BALF recovered 14d after bleomycin installation was measured as described in Chapter 2.2.14. The BALF protein level was similar between the genotypes (Figure 5.4), which is consistent with the similarity found in total cell count at 14d.

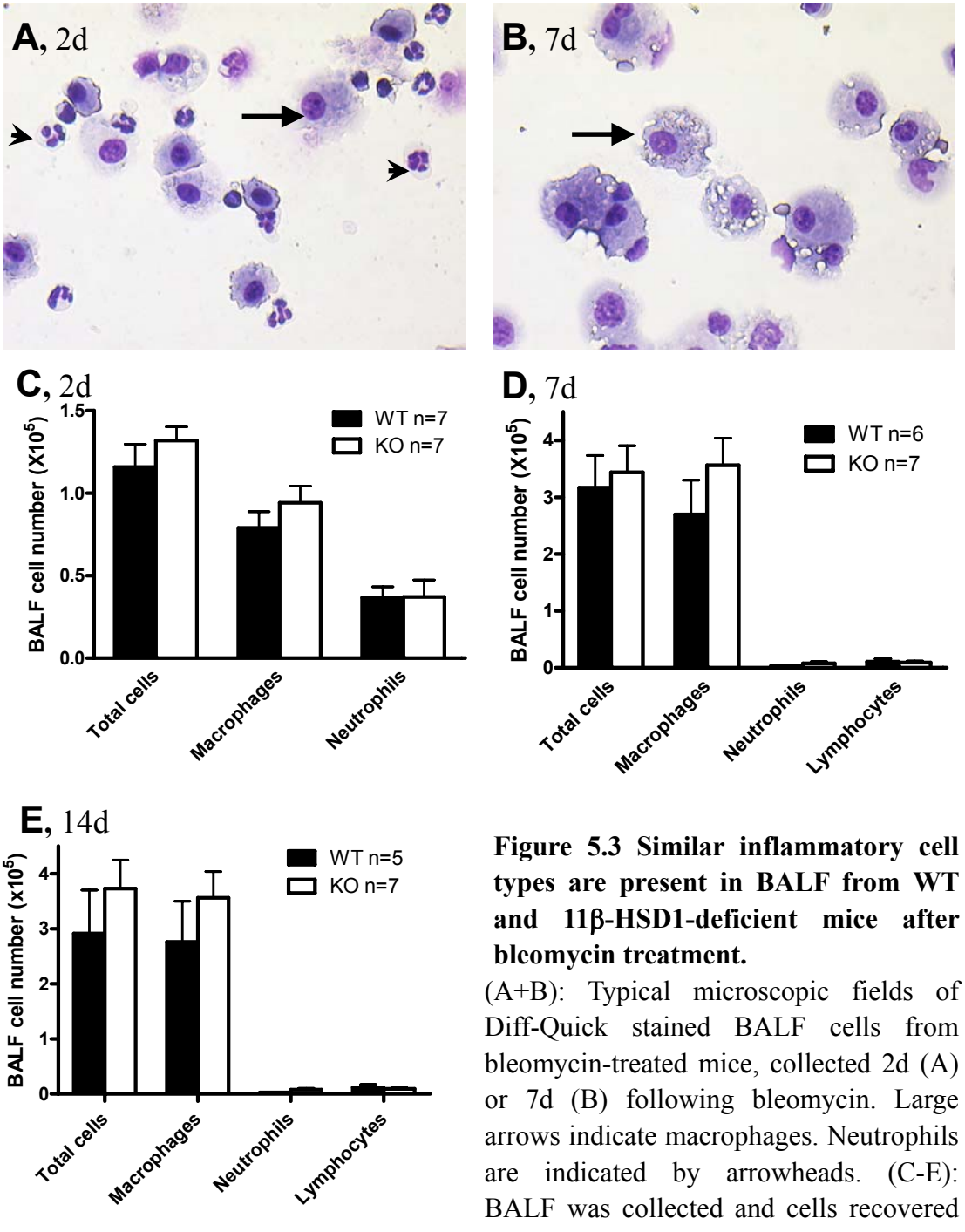

Figure 5.3 Similar inflammatory cell types are present in BALF from WT and 11β-HSD1-deficient mice after bleomycin treatment.

(A+B): Typical microscopic fields of Diff-Quick stained BALF cells from bleomycin-treated mice, collected 2d (A) or 7d (B) following bleomycin. Large arrows indicate macrophages. Neutrophils are indicated by arrowheads. (C-E): BALF was collected and cells recovered 2d (C), 7d (D) or 14d (E) following bleomycin.

Following cytocentrifugation and Diff-Quick staining, relative numbers of cell types were assessed microscopically (blind to genotype). Differential counts were performed by counting 300 cells per slide on random fields at x100 magnification. Data are mean ± SEM, n = 5-8. No significant differences were found between wild type (WT; black bars) and 11β-HSD1-deficient (KO; white bars) mice (Student's *t*-test).

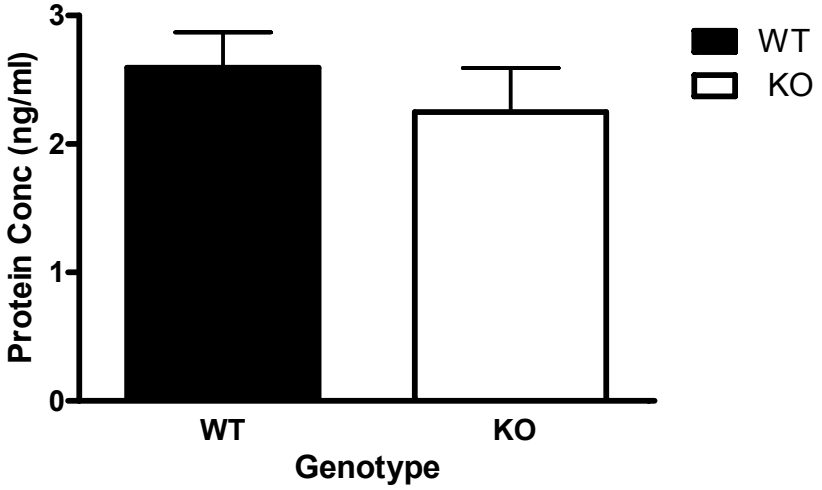

Figure 5.4 The protein concentration of BALF recovered 14d after bleomycin installation was similar between the genotypes.
Measurement of BALF protein from wild type (WT; black bars) and 11β-HSD1-deficient (KO; white bars) mice, 14d after bleomycin instillation. Data are mean ± SEM with n = 5-8. The results were compared by unpaired Student's *t*-test and did not significantly differ between genotypes.

5.3.3 Plasma corticosterone levels did not differ between WT and 11β-HSD1-deficient mice following bleomycin installation

On a C57BL/6 background, 11β-HSD1-deficient mice show normal basal plasma corticosterone levels (Yau, McNair et al. 2007). To investigate if levels differ between genotypes following bleomycin which could indicate differential activation of the HPA axis, nadir (morning) plasma corticosterone levels were measured in tail blood. Morning plasma corticosterone levels did not significantly differ between genotypes at d0 (Figure 5.5). However, morning corticosterone levels above 50-70nM indicate stress (Kotelevtsev, Holmes et al. 1997; Carter, Paterson et al. 2009), suggesting that the levels measured at d0 are elevated due to stress caused by blood collecting. Levels in WT were lower at d10, d14 and d28 than at d0, so that at d10 and d14 they were within the basal range (Figure 5.5), suggesting that at these later collections, the mice were less stressed and that bleomycin treatment did not result in HPA activation d10 later. Although not significant, there was a trend for higher plasma corticosterone levels in 11β-HSD1-deficient mice at d10, d14 and d28, suggesting a possible greater HPA axis response in 11β-HSD1-deficient mice. However, this requires further confirmation.

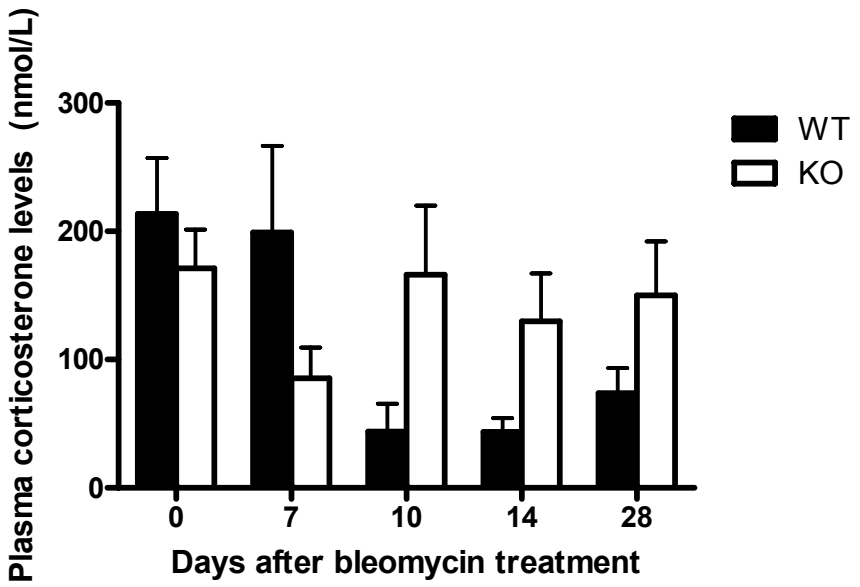

Figure 5.5 Plasma corticosterone levels measured after bleomycin treatment.
Plasma corticosterone levels in WT and 11β-HSD1-deficient mice were measured at different time points following bleomycin installation, as described in Chapter 2.2.21. Two-way ANOVA showed a significant interaction ($P<0.05$), but no genotype ($P=0.34$) or time difference ($P=0.17$) in plasma corticosterone levels between wild type (WT; black bars) and 11β-HSD1-deficient (KO; white bars) mice. Data are mean ± SEM with n = 3-6.

5.3.4 Adrenal gland weights differ between WT and 11β-HSD1-deficient mice

Irrespective of genetic background, 11β-HSD1-deficient mice have larger adrenal glands than WT mice (Kotelevtsev, Holmes et al. 1997; Carter, Paterson et al. 2009). Both adrenal glands (formalin fixed) were weighed for each mouse killed 0d, 7d, 14d or 28d following bleomycin treatment. Two-way ANOVA showed significant genotype differences in the total adrenal gland weight between WT and 11β-HSD1-deficient mice (Figure 5.6). At 0d, 7d and 14d adrenal glands from 11β-HSD1-deficient mice were significantly heavier than those from WT mice (Figure 5.6). However, no significant difference was found at 28d between the genotypes (Figure 5.6). One-way ANOVA showed there was no difference between d0 and other time points in WT mice, although there was a difference between d0 and d28 in 11β-HSD1-deficient mice, which suggests the size of adrenal glands decreased 28d after bleomycin treatment in 11β-HSD1-deficient mice.

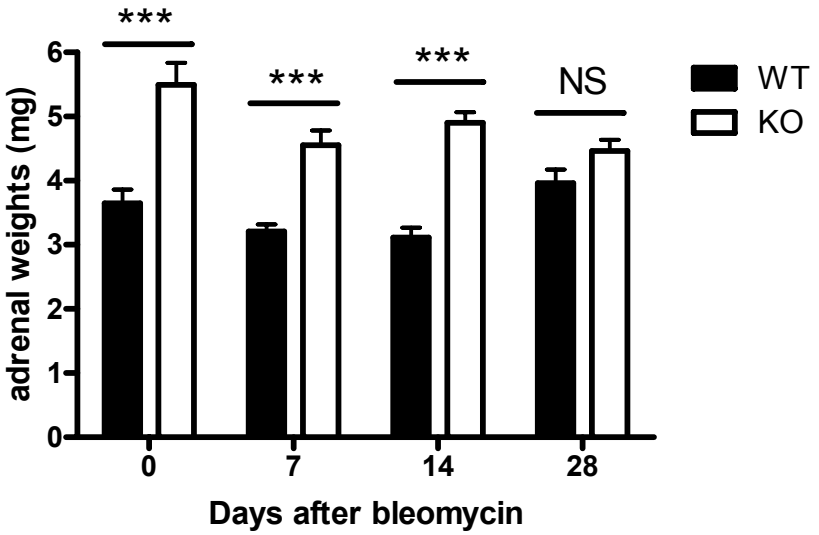

Figure 5.6 Comparison of total adrenal gland weight between WT and 11β-HSD1-deficient mice following bleomycin.

Adrenal glands from either WT or 11β-HSD1-deficient mice at different time points following bleomycin installation were weighed. Weights indicated in graph are the combined weight of both adrenal glands from each animal. Two-way ANOVA showed a significant genotype difference ($P<0.0001$), interaction ($P<0.01$) and time ($P=0.01$) in weight of adrenal glands between wild type (WT; black bars) and 11β-HSD1-deficient (KO; white bars) mice. Data are mean ± SEM with n = 3-8. *** represents a significant difference compared to WT control ($p<0.001$)

5.3.5 Histological assessment indicates more severe inflammation and fibrosis in 11β-HSD1-deficient mice 14d after bleomycin

Lungs (half or whole) were dissected from mice 2d, 7d, 14d or 28d following instillation of bleomycin, fixed in Methyl-Carnoy fixative as described in Chapter 2.2.4, and embedded. Sections (5μm thick) were stained with haematoxylin and eosin (H&E) to assess pathology, and the remaining sections were used for Picrosirius red staining (Chapter 2.2.19) or for immunohistochemistry (IHC) (Chapter 2.2.12). The H&E stained sections were examined by Dr David Brownstein of the CVS Pathology Core Facility. The objective was to determine whether there were differences in inflammation and fibrosis within lung between WT and 11β-HSD1-deficient mice at any stage following instillation of bleomycin.

There was histological variability within groups at every time point. The distribution of inflammation in the lung was patchy, probably due to unequal distribution of bleomycin with the instillation method. Some parts of lung showing normal structure could be found at all time points, but some parts of lung showed the expected inflammatory cell infiltration, thickening of the alveolar walls and deposition of fibrous tissue.

There were no differences in lung histology between untreated WT and 11β-HSD1-deficient mice (data not shown). At 2d following bleomycin treatment

there was noticeable inflammation in both genotypes with similar infiltration of inflammatory cells (Figure 5.7A and B). By 7d, inflammation had worsened in the lungs of both genotypes, but there were no obvious qualitative differences between WT and 11β-HSD1-deficient mice (Figure 5.7C and D).

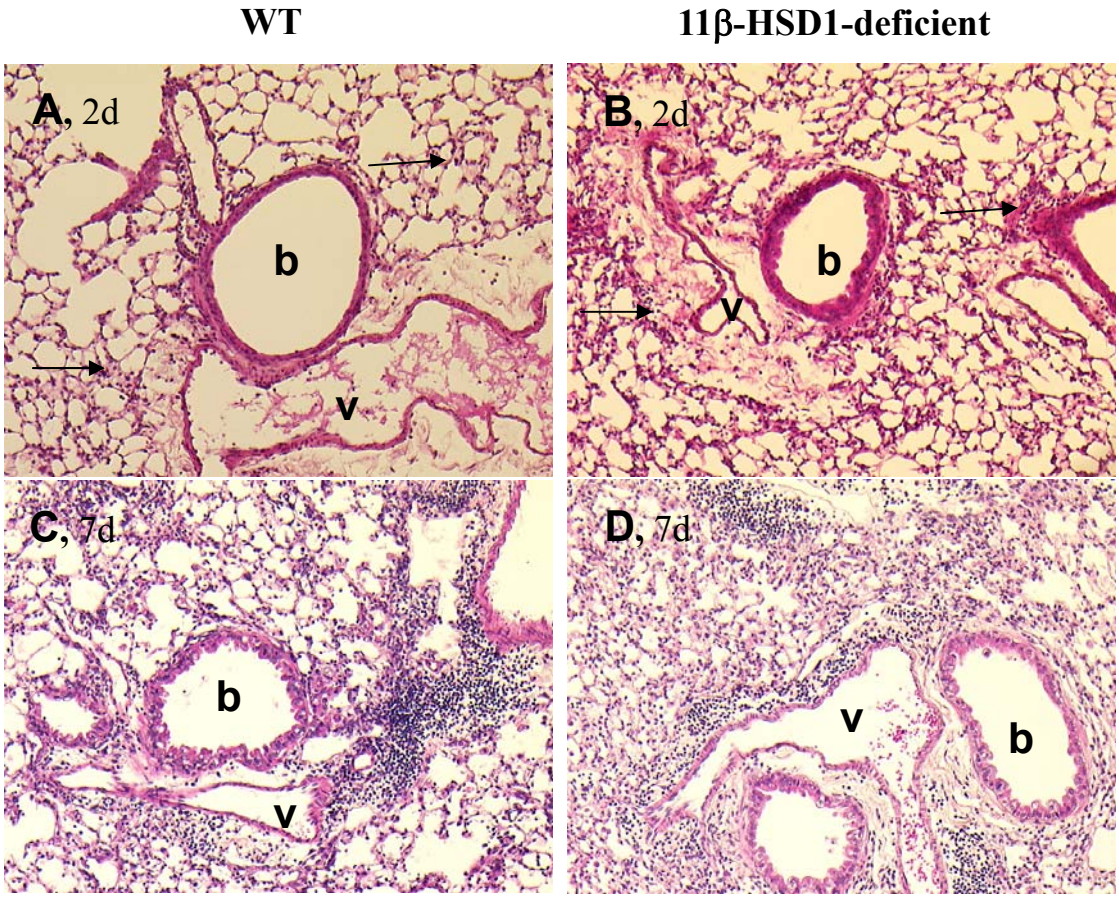

Figure 5.7 2d and 7d following instillation of bleomycin, inflammation is noticeable in both genotypes with inflammatory cell infiltration.
Representative images of H&E stained sections of lung tissue from WT and 11β-HSD1-deficient mice killed 2d or 7d after bleomycin treatment. (A) WT mouse, 2d bleomycin treated; (B) 11β-HSD1-deficient mouse, 2d bleomycin treated. H&E staining shows inflammation within alveolar areas and small areas of thickened alveolar walls (arrows); (C) WT mouse, 7d bleomycin treated; (D) 11β-HSD1-deficient mouse, 7d bleomycin treated. All were photographed at X100 magnification. H&E, hematoxylin and eosin. "b" indicates bronchioli and "v" indicates a blood vessel.

At 14d, many areas of the lung had thickened alveolar walls and some tissues showed loss of architecture. However, whilst WT mice showed relief of inflammation compared to 7d (Figure 5.8A), inflammation was still severe in 11β-HSD1-deficient mice, with more interstitial inflammatory cells (Figure 5.8B). 11β-HSD1-deficient mice showed extensive thickening of alveolar walls, evidence of continued inflammation (Figure 5.8B). Also, 11β-HSD1-deficient mice showed areas of fibrosis with obliteration of alveolar wall architecture and fibrous deposits, adjacent to areas of normal lung tissue (Figure 5.8B).

The final time point examined was 28d after bleomycin. Although the majority of inflammatory cells had cleared in both genotypes, some inflammatory cells were still evident within 11β-HSD1-deficient mouse lungs (Figure 5.8C and D). Both WT and 11β-HSD1-deficient mice showed the expected extensive dense lung fibrosis, characterized by increased interstitial wall thickness and interstitial collagen deposition (Figure 5.8C and D). The fibrotic changes were greater in extent and severity in 11β-HSD1-deficient mice than in WT mice with fibrotic lesions more narrowly confined to central peribronchial and perivascular areas in WT mice compared with 11β-HSD1-deficient mice (Figure 5.8C and D). Thus histopathology suggested that 11β-HSD1 deficiency is associated with increased bleomycin-induced pulmonary fibrosis.

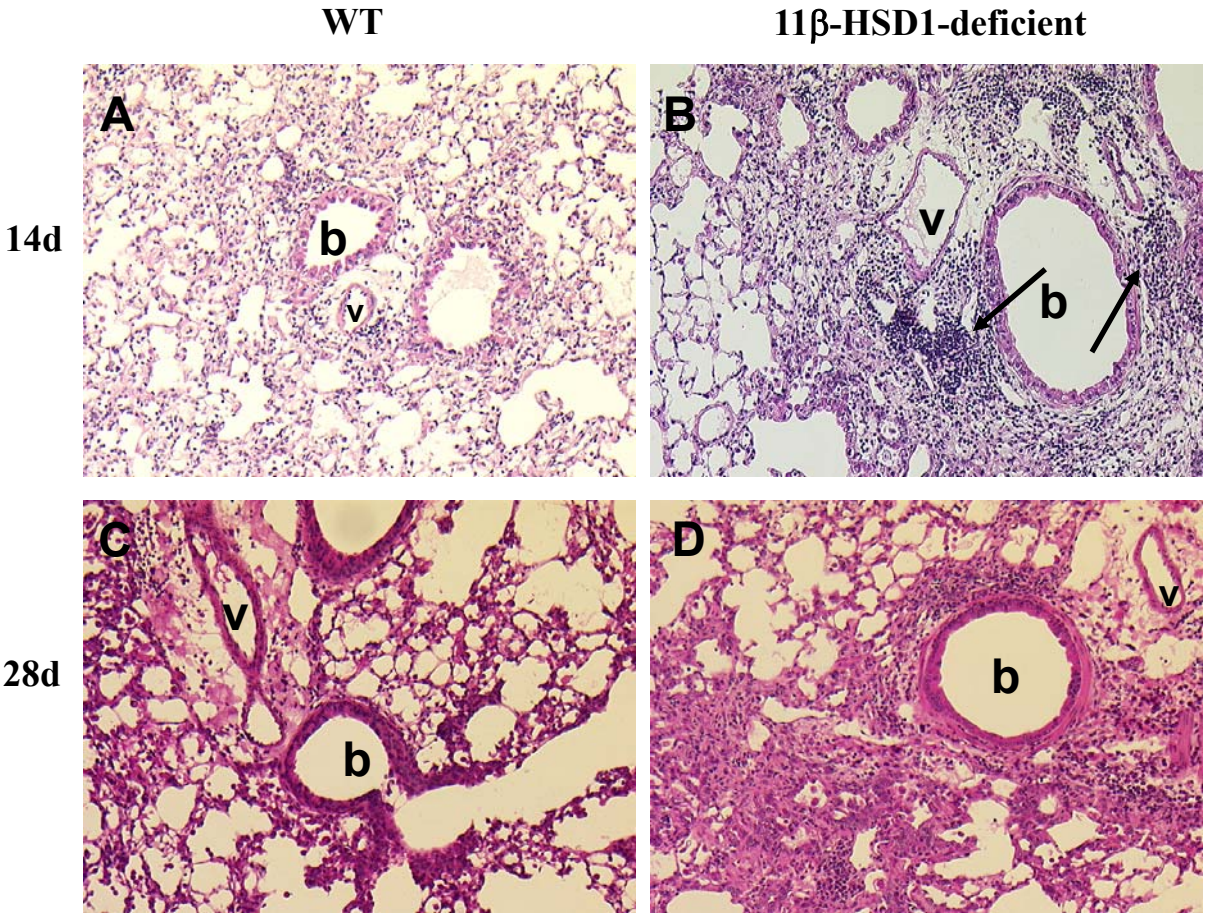

Figure 5.8 Compared to WT mice, 11β-HSD1-deficient mice show a more severe inflammatory response 14d following bleomycin instillation and more fibrosis at 28d

Representative images of H&E stained sections of lung tissue from WT and 11β-HSD1-deficient mice killed 14d or 28d after bleomycin instillation. (A) WT mouse, 14d after bleomycin; (B) 11β-HSD1-deficient mouse, 14d after bleomycin, showing strong inflammation around airways, blood vessels and in the interstitum, indicated by arrows; (C) WT mouse, 28d after bleomycin; (D) 11β-HSD1-deficient mouse, 28d after bleomycin. All images were obtained at X100 magnification. "b" indicates bronchioli and "v" indicates a blood vessel.

In order to semi-quantify the inflammatory reaction in the lungs of WT and 11β-HSD1-deficient mice, lung sections from mice killed 14d and 28d after bleomycin instillation were scored for the severity of inflammation, blind to genotype, as described in Chapter 2.2.18. The scoring system assessed inflammation in the following compartments: perivascular compartment, peribronchiolar alveolar tissue and alveolar walls. At both time points, 11β-HSD1-deficient mice showed a higher score than WT mice (Figure 5.9).

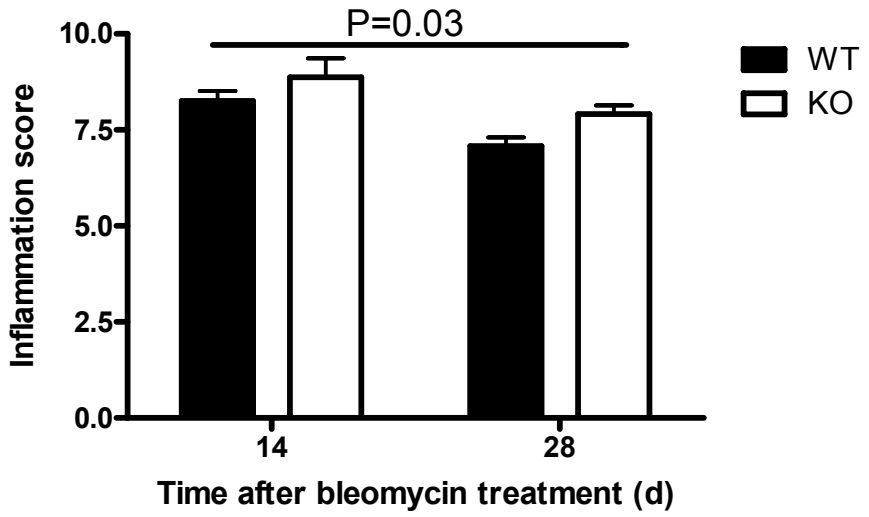

Figure 5.9 Quantification of inflammation in tissue sections shows more severe inflammation in lungs of 11β-HSD1-deficient mice compared to WT, 14d or 28d following bleomycin.

Tissue sections from bleomycin treated lung were scored blind to genotype according to the method described in Chapter 2.2.18. Data are mean ± SEM with n = 5-8. Two-way ANOVA showed a significant genotype (P=0.03) and time (P<0.01) difference but not an interaction (P=0.73) in inflammation score between wild type (WT; black bars) and 11β-HSD1-deficient (KO; white bars) mice.

5.3.6 Lungs of 11β-HSD1-deficient mice show greater collagen accumulation 28d following bleomycin treatment

To investigate whether the greater fibrosis observed in histology was associated with increased collagen deposition in lungs of 11β-HSD1-deficient mice, picrosirius red staining was used to identify collagen (Chapter 2.2.19). The staining showed deposition of collagen in thickened alveolar walls and around vessels or bronchi after bleomycin treatment (Figure 5.10B and D) and further suggested that 11β-HSD1-deficient mice showed more severe fibrosis compared with WT mice (Figure 5.10A and C).

To confirm and quantify the fibrotic changes observed, lung collagen was measured by Sircol assay (described in Chapter 2.2.20) using the left lobe of the lung from naïve mice or mice 14d or 28d after bleomycin treatment. Interestingly, untreated (naïve) 11β-HSD1-deficient mice had significantly lower levels of collagen in lung compared to WT mice (Figure 5.11).

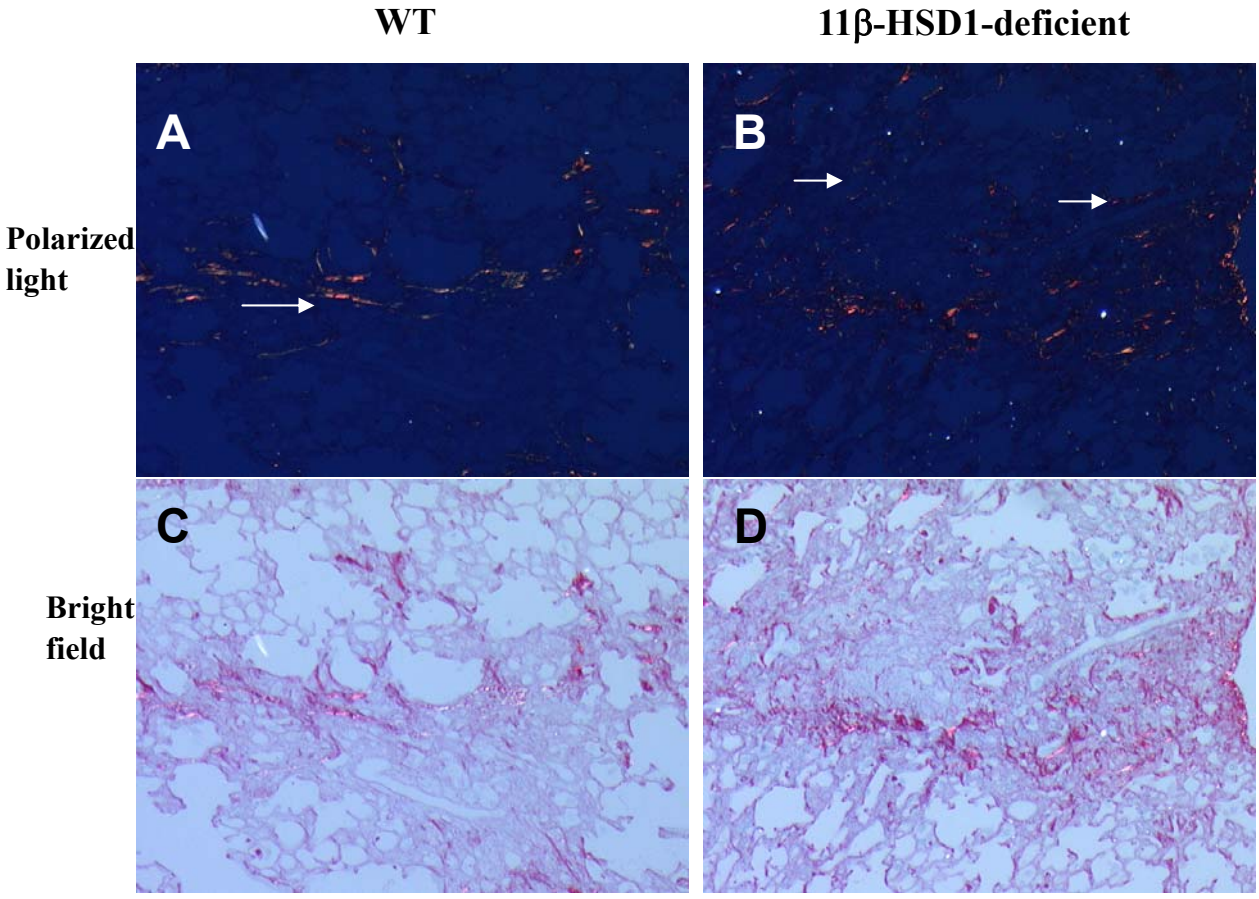

Figure 5.10 Picrosirius red staining showed 11β-HSD1-deficient mice have more severe fibrosis 28d following bleomycin instillation

Representative images of Picrosirius red-stained lung sections from mice, 28d after bleomycin treatment, showing increased collagen deposition in 11β-HSD1-deficient mice. Sections of lung from WT and 11β-HSD1-deficient mice, at 28d following intratracheal instillation of bleomycin, were stained with Picrosirius red and viewed under polarized light (A&B) or bright field (C&D) (X100 magnification). Collagen appears as a yellowish orange color under polarized light and red under bright field. A and C are the same section from a WT mouse, B and D are the same section from an 11β-HSD1-deficient mouse. Arrows indicates the deposition of collagen in lung.

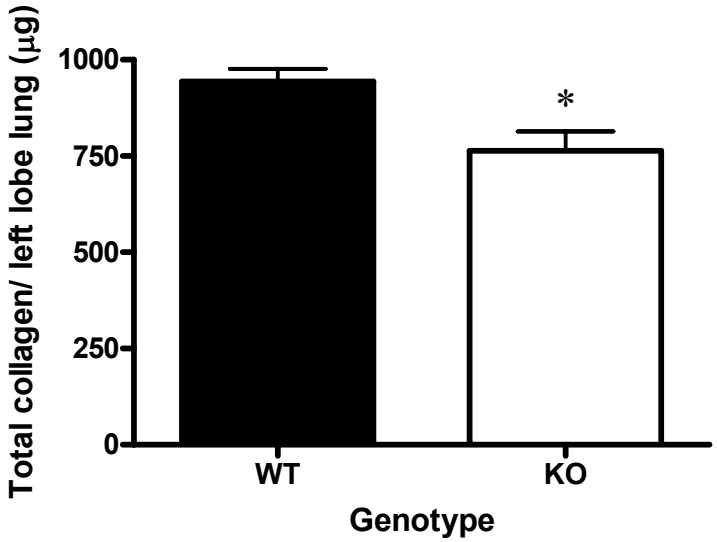

Figure 5.11 Naïve 11β-HSD1-deficient mice have significantly lower levels of lung collagen than WT mice

The left lung lobe was removed from 4 month old male mice, enzyme digested, acid hydrolysed and collagen content measured as described in Chapter 2.2.20. The lungs were not lavaged or perfused prior to digestion. Sircol assay was used to measure the total collagen content of lung. The results are expressed as total collagen per left lobe of lung. The difference between wild type (WT; black bars) and 11β-HSD1-deficient (KO; white bars) mice was statistically significant, compared by unpaired Student's *t*-test（∗, $p<0.05$). Data are mean ± SEM with n = 6 (WT) and 7 (KO).

Because collagen in the bronchial-alveolar space accounts for a significant amount of collagen in lung (Michael Gibbons, personal communication), lungs were lavaged and perfused prior to collagen measurement to exclude those factors. The collagen content of 11β-HSD1-deficient mouse lung remained significantly lower than WT mouse lung following BAL and perfusion (Figure 5.12).

To determine whether collagen levels differed between WT and 11β-HSD1-deficient mice 14d after bleomycin treatment, lungs were lavaged and perfused prior to collagen measurement. Both WT and 11β-HSD1-deficient mice had increased levels of lung collagen after bleomycin, compared to naïve mice. Levels in 11β-HSD1-deficient mice still appeared lower than in WT, although this did not achieve significance (Figure 5.12).

However, by 28d after bleomycin treatment, although both genotypes still expressed significantly higher levels of collagen than naïve mice, the difference between WT and 11β-HSD1-deficient mice in levels of collagen had disappeared (Figure 5.12), suggesting that the increase in collagen content following bleomycin treatment was greater in 11β-HSD1-deficient mice than in WT mice.

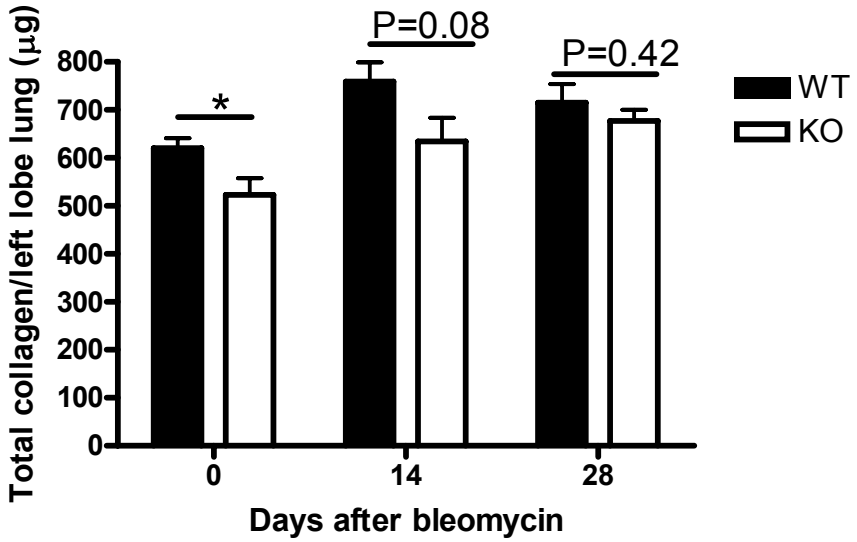

Figure 5.12 Following BAL and perfusion, naïve 11β-HSD1-deficient mice have lower levels of lung collagen than WT mice but not after bleomycin treatment
The left lung lobe was removed, enzyme digested, acid hydrolysed and collagen content measured as described in Chapter 2.2.20. The lungs were lavaged and perfused prior to digestion. Sircol assay was used to measure the total collagen content of lung. The results are expressed as total collagen per left lobe of lung. Data are mean ± SEM with n = 6-8. Wild type (WT; black bars) and 11β-HSD1-deficient (KO; white bars) mice. Within each time point, mice are age-matched. Mice used for d0 were culled at 3 months of age, mice used for 14d bleomycin treatment were culled at 4.5 months and mice used for 28d bleomycin treatment were culled at 5 months of age. Therefore, each time point was analysed separately for significance by t-test. The difference between WT and KO mice at d0 was statistically significant, compared by unpaired Student's *t*-test (*, $p<0.05$).

5.3.7 Quantification of blood leukocytes in WT and 11β-HSD1-deficient mice after bleomycin installation.

Because the histology at 14d suggested more inflammatory cells in lung of 11β-HSD1-deficient mice following installation of bleomycin, blood leukocytes were examined to see if there were differences in number or type of blood leukocytes following treatment. Blood were collected at each time point and cells from blood were subject to flow cytometry to identify different types of blood leukocytes.

5.3.7.1 11β-HSD1-deficient mice have fewer blood monocytes than WT mice, 14d after bleomycin treatment

To monitor monocytes in blood, antibodies to label CD115, CD11b and 7/4 were used in flow cytometry to identify total monocytes ($CD115^+$ $CD11b^+$), the subset of inflammatory monocytes ($CD115^+$ $CD11b^+$ $7/4^{hi}$) and resident monocytes ($CD115^+$ $CD11b^+$ $7/4^{lo}$) as described in Chapter 2. By 2d after bleomycin instillation, the number of monocytes in blood was increased in both genotypes, peaking around 14d (Figure 5.13). Although not statistically significant (2 way ANOVA), there was a trend to fewer monocytes in the blood of 11β-HSD1-deficient mice than in WT mice 14d following bleomycin instillation (Figure 5.13) with reduced numbers of both $7/4^{hi}$ (inflammatory) monocytes and $7/4^{lo}$ (resident) monocytes (Figure 5.13).

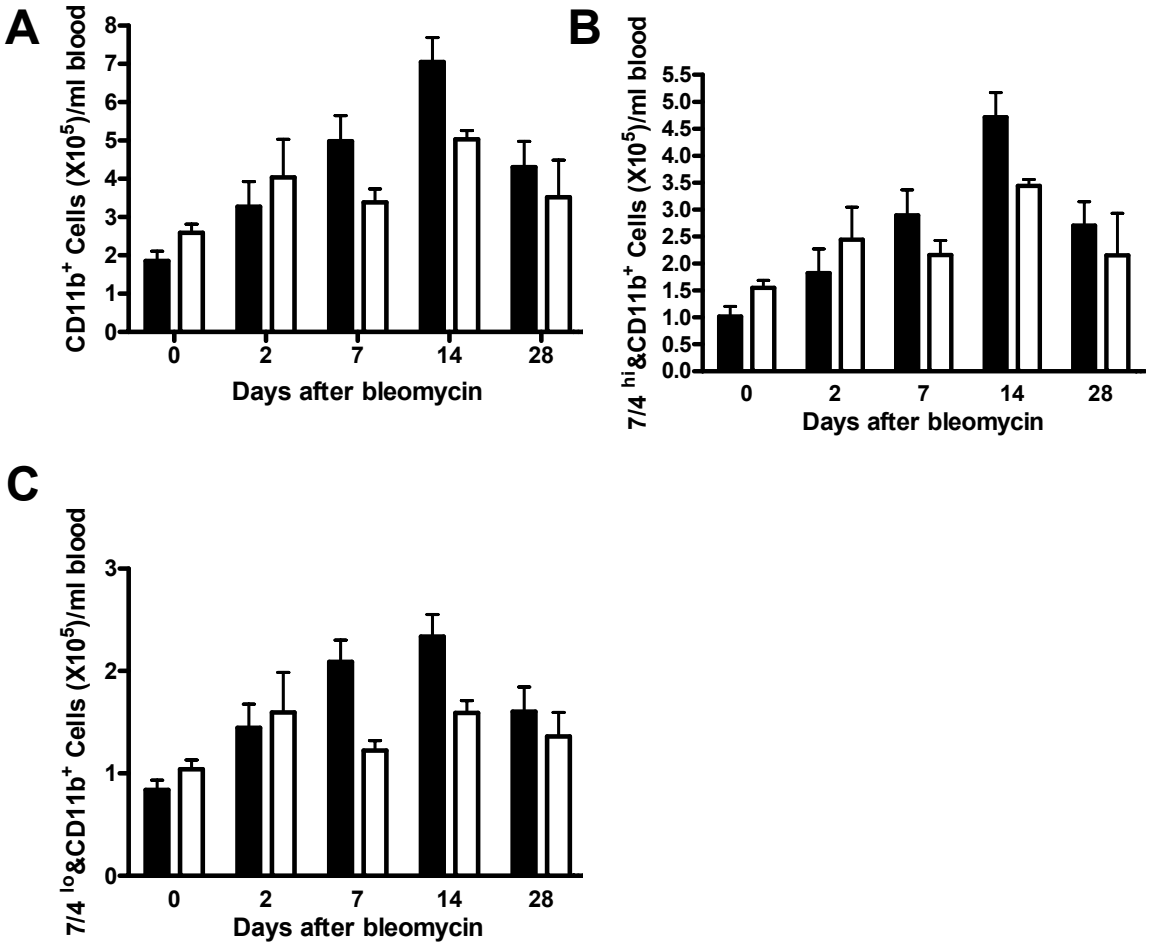

Figure 5.13 Bleomycin treatment have fewer monocytes in blood of 11β-HSD1-deficient mice at 14d compared to WT mice.

Cells collected from blood of either WT or 11β-HSD1-deficient mice at different time points following bleomycin installation were analysed for CD115, CD11b and 7/4 expression by flow cytometry. (A) CD115, $CD11b^+$ monocytes; (B) CD115, $CD11b^+$ and $7/4^{hi}$ monocytes; (C) CD115, $CD11b^+$ and $7/4^{lo}$ monocytes. Levels are expressed as cell number $X10^5$ per ml blood. Two-way ANOVA showed an effect of time ($p<0.001$) and a trend to genotype difference ($p=0.07$) in total monocyte numbers between wild type (WT; black bars) and 11β-HSD1-deficient (KO; white bars) mice. Two-way ANOVA showed an effect of time ($p<0.01$) and a trend to genotype difference ($p=0.06$) in $7/4^{lo}$ monocyte numbers. Two-way ANOVA showed an effect of time ($p=0.0001$) but no effect of genotype or interaction upon $7/4^{hi}$ monocyte numbers between WT and KO mice. Data are mean ± SEM with n = 5-8. Experiment carried out with help from Dr Tiina Kipari.

5.3.7.2 11β-HSD1-deficient mice have similar number of blood neutrophils to WT mice after bleomycin treatment

Neutrophils were gated using CD11b and Ly6(G) markers in cells from the blood, as described in Chapter 2.2.22. No significant differences were observed in the number of $CD11b^{+}$ $Ly6(G)^{+}$ neutrophils in the blood between the two genotypes at any time point (Figure 5.14), although 2d after bleomycin treatment, WT mice had fewer blood neutrophils than untreated mice ($P<0.01$).

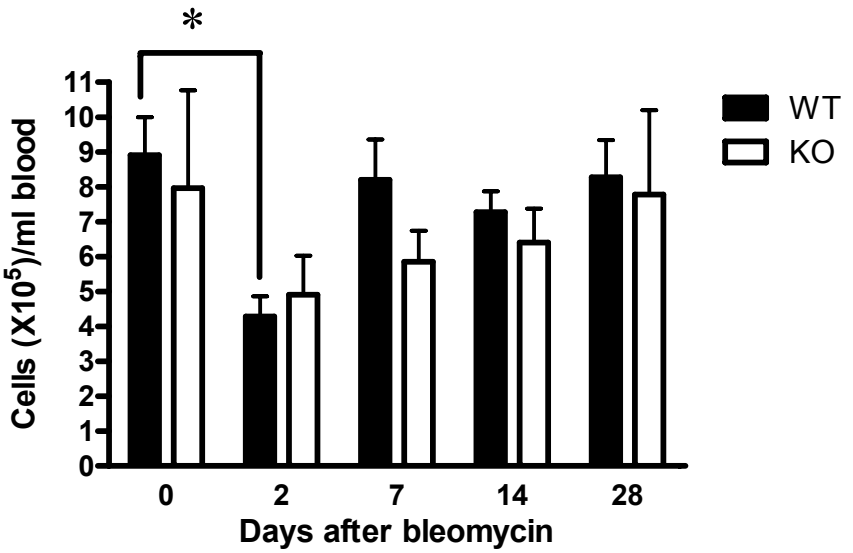

Figure 5.14 Blood neutrophil numbers are similar between genotypes after bleomycin treatment

Cells collected from blood of either WT or 11β-HSD1-deficient at different time points following bleomycin installation were analysed for CD11b and Ly6(G) expression by flow cytometry. Levels are expressed as cell number $X10^5$ per ml blood. Two-way ANOVA showed no genotype difference in $CD11b^+Ly6(G)^+$ number between wild type (WT; black bars) and 11β-HSD1-deficient (KO; white bars) mice, but a significant reduction in the number of neutrophils in blood of WT mice 2d following bleomycin, compared to untreated controls ($p<0.05$; ∗), compared by unpaired Student's *t*-test. Data are mean ± SEM with n = 5-8.

5.3.7.3 Proportion of T cells and B cells in WT vs. 11β-HSD1-deficient mice:

Anti-CD4, anti CD-8 and anti-B-220 antibodies were used to label lymphocytes in blood of WT and 11β-HSD1-deficient mice after bleomycin treatment. Naïve 11β-HSD1-deficient mice had more $CD4^+$ T cells than WT mice (Figure 5.15A), but there were no differences between genotypes in either $CD4^+$ or $CD8^+$ cells following bleomycin treatment (Figure 5.15A&B). Whilst no difference between genotypes was found in $B220^+$ cells after bleomycin treatment, naïve (untreated) 11β-HSD1-deficient mice had significantly more $B220^+$ lymphocytes cells than WT mice (Figure 5.15C). However, levels of these cells declined in blood of 11β-HSD1-deficient mice 2d after bleomycin instillation (Figure 5.15).

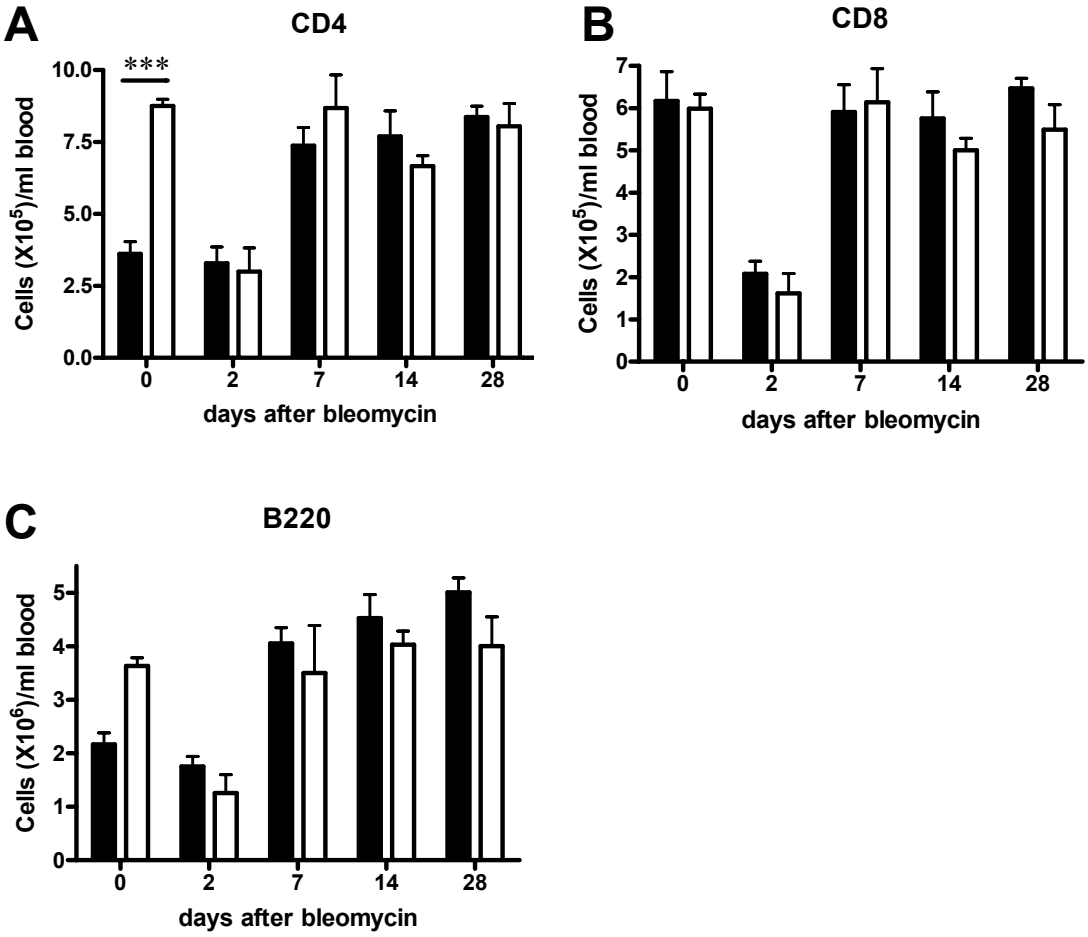

Figure 5.15 Blood $CD4^+$, $CD8^+$ and $B220^+$ cell numbers were similar between genotypes after bleomycin treatment

Cells collected from blood of either WT or 11β-HSD1-deficient at different time points following bleomycin installation were analysed for CD4, CD8 and B220 expression by flow cytometry. Levels are expressed as cell numbers $X10^5$ per ml blood. Two-way ANOVA showed an effect of time ($p<0.0001$) and genotype ($p<0.05$) on $CD4^+$ cell numbers between wild type (WT; black bars) and 11β-HSD1-deficient (KO; white bars) mice. Two-way ANOVA showed no genotype difference in $B220^+$ or $CD8^+$ cell numbers between WT and KO mice. Data are mean ± SEM with n = 5-8. *** represents a significant difference compared to WT control ($p<0.001$)

5.3.8 Proportion of $B220^+$, $CD3^+$ and $CD8^+$ cells in lung of WT and 11β-HSD1-deficient mice 7d following bleomycin instillation

To determine whether inflammatory cells within the lung differed between WT and 11β-HSD1-deficient mice, collagenase digestion was used to release leukocytes prior to flow cytometry, to identify total leukocytes (anti-CD45), T cells (anti-CD3), T-cytotoxic cells (anti-CD8), and B lymphocytes (anti-B220) in lung 7d after bleomycin installation. Whilst no difference between genotypes was found in CD45, CD3 and CD8 populations 7d following bleomycin treatment, 11β-HSD1-deficient mice had a greater proportion of B220 cells, compared to WT mice (Figure 5.16).

Figure 5.16 11β-HSD1-deficient mice have a greater proportion of B cells but similar proportions of $CD3^+$, $CD8^+$ T cells and total CD45 leukocytes in lung, 7d following bleomycin installation.

Following collagenase digestion, flow cytometry was used to estimate the proportion of inflammatory cells in WT and 11β-HSD1-deficient mice 7d after bleomycin installation. (A) Representative dot plots of unstained WT control, to show the gating on CD45 and FSC; (B) WT lung stained with CD45. (C) unstained WT control, to show the gating on CD3 and B220; (D) WT lung stained with CD3 and B220; (E) unstained WT control, to show the gating on CD8; (F) WT lung stained with CD8; Quantification from flow cytometry revealed that wild type (WT; black bars) and 11β-HSD1-deficient (KO; white bars) mice had similar proportions of CD45 positive cells in digested lung cells (G). 11β-HSD1-deficient mice had significantly more B220 positive cells (H) but similar levels of CD3 (I) and CD8 (J) positive cells in lungs from WT and 11β-HSD1-deficient mice 7d after bleomycin instillation. Data are mean ± SEM with n = 6.

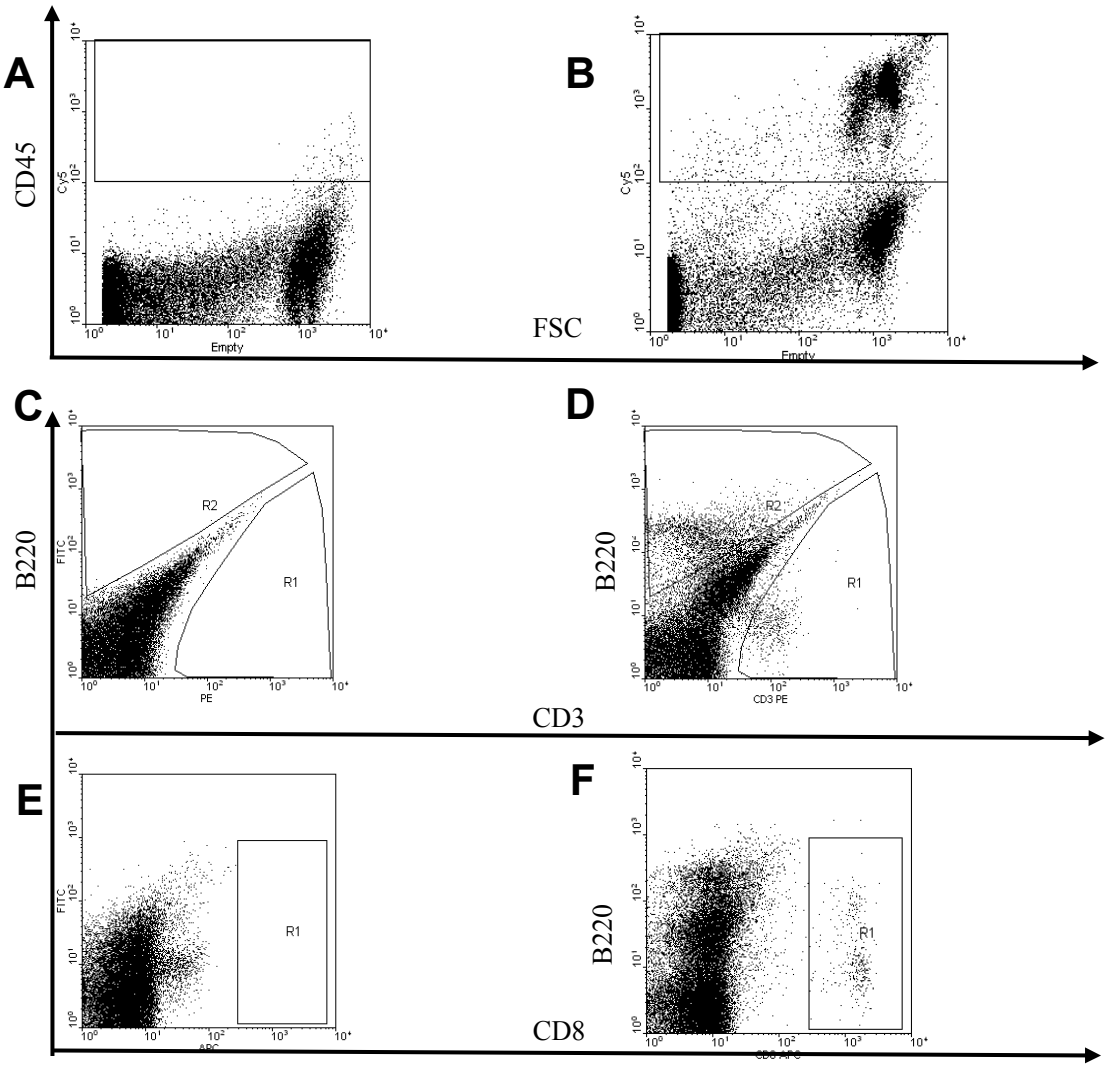
A
CD45
Cy5
Empty
B
FSC
Cy5
Empty
C
B220
FITC
R2
R1
PE
D
B220
R2
R1
CD3 PE
CD3
E
FITC
R1
APC
F
B220
R1
CD8

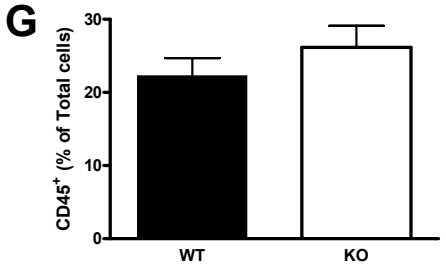
G
CD45+ (% of Total cells)
30
20
10
0
WT
KO

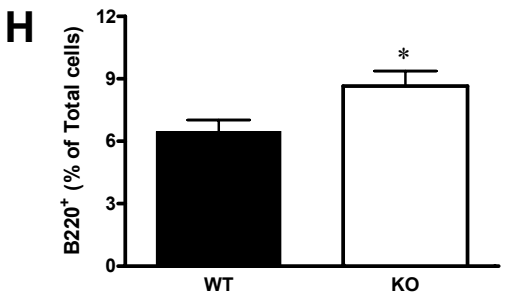
H
B220+ (% of Total cells)
12
9
6
3
0
*
WT
KO

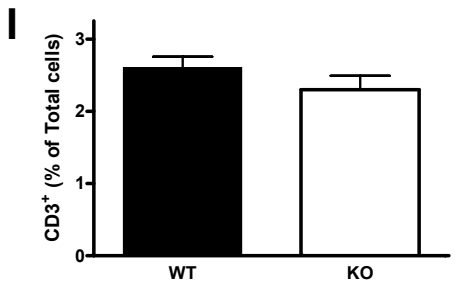
I
CD3+ (% of Total cells)
3
2
1
0
WT
KO

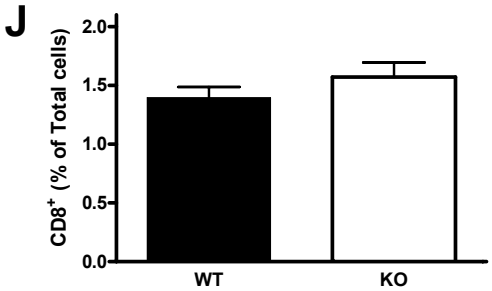
J
CD8+ (% of Total cells)
2.0
1.5
1.0
0.5
0.0
WT
KO

5.3.9 Lung RNA profiles in WT and 11β-HSD1-deficient mice following bleomycin treatment

To investigate changes in gene expression in lung after bleomycin treatment, and to gain insights into the mechanisms underlying the more severe inflammation in 11β-HSD1-deficient mice, real-time PCR was used to measure levels of mRNA encoding proteins important in the inflammatory response, tissue repair and GC action (as described in Chapter 2.2.10).

5.3.9.1 Increased levels of mRNA encoding Heme oxygenase (HO)-1 and inducible nitric oxide synthase (iNOS) in 11β-HSD1-deficient mice 14d after bleomycin installation

HO is the rate-limiting enzyme that catalyses the initial step of heme degradation, producing biliverdin and releasing free ion and carbon monoxide, which may induce lung damage (Atzori, Chua et al. 2004). HO-1 is up-regulated during oxidative stress and is proposed to have a role in the regulation of inflammatory process by acting as a cytoprotective molecule (reviewed in (Morse and Choi 2002). Analysis of lung RNA by real-time PCR showed that bleomycin treatment increased HO-1 mRNA levels in lungs of both genotypes of mice with a peak at 14d and a return to basal levels by 28d (Figure 5.17A). At 14d, lung from 11β-HSD1-deficient mice showed significantly higher levels of HO-1 mRNA relative to WT mice (Figure 5.17A).

Nitric Oxide (NO) is an endogenous short-lived free radical that freely diffuses within the cells (Kalayarasan, Sriram et al. 2008). It has a biological role in modulating physiological and pathological processes. However, during infection and inflammation, *in vivo* formation of NO is increased and can cause damage if unchecked. Activated macrophages highly express inducible NO synthase (iNOS) (Gurujeyalakshmi, Wang et al. 2000). Bleomycin treatment caused a significant increase in iNOS mRNA levels in lungs of mice treated with bleomycin (Figure 5.17B). The pattern of iNOS expression was quite similar to HO-1 gene expression with an increase 2d after bleomycin treatment in both genotypes, peaking at 14d and basal at 28d (Figure 5.17B). At 14d after bleomycin installation, 11β-HSD1-deficient lung showed significantly higher levels of iNOS mRNA relative to WT mice (Figure 5.17B).

IL-6 KO mice show attenuated inflammation and fibrosis compared to WT mice in the bleomycin model (Saito, Tasaka et al. 2008). Release of IL-6 was higher in LPS-stimulated macrophages from 11β-HSD1-deficient mice compared with WT mice (Gilmour, Coutinho et al. 2006; Zhang and Daynes 2007). However, in the bleomycin inflammation model, IL-6 mRNA levels did not differ between genotypes at any time point (Figure 5.17C). In both genotypes, levels of IL-6 mRNA were dramatically increased 2d after bleomycin, and then diminished at 7d and 14d, returning to basal levels on d28 (Figure 5.17C).

Tumor necrosis factor TNF-α is essential for pathogenesis in the bleomycin model of fibrosis (Piguet, Collart et al. 1989), being up-regulated after bleomycin treatment (Zhang, Gharaee-Kermani et al. 1997). To investigate whether TNF-α was expressed differently between WT and 11β-HSD1-deficient mice after bleomycin instillation, levels of mRNA were measured. The increase in TNF-α mRNA in both genotypes was evident from d2 (Figure 5.17D), remaining elevated at d7 and d14, but with similar levels of TNF-α expression in WT and 11β-HSD1-deficient mice. By d28, the level of TNF-α expression had decreased to basal levels (Figure 5.17D). There was no significant difference in TNF-α mRNA levels between genotypes at any time point.

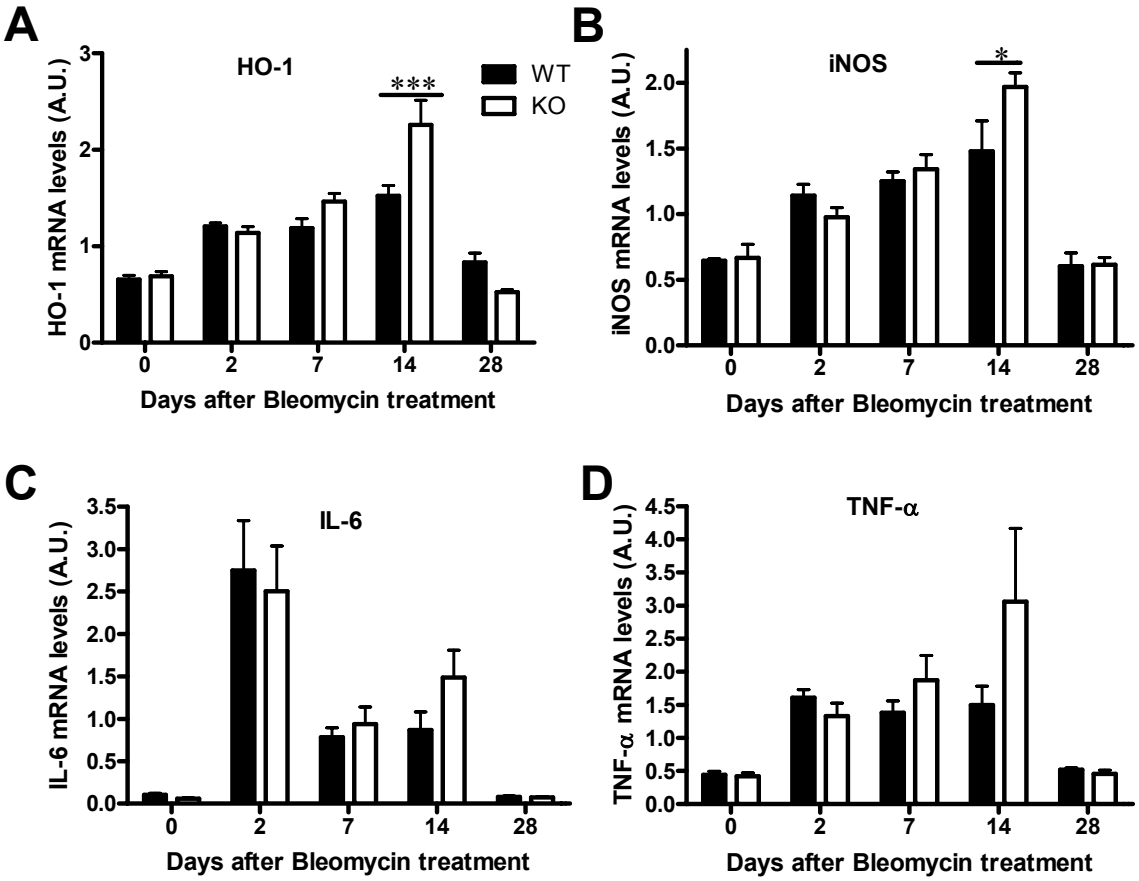

Figure 5.17 Bleomycin treatment induced higher HO-1 and iNOS gene expression in 11β-HSD1-deficient mice at 14d compared to WT mice.

Total RNA extracted from lungs of either WT or 11β-HSD1-deficient mice at different time points following bleomycin installation was analysed for HO-1 (A), iNOS (B), IL-6 (C) and TNF-α (D) mRNA by real-time PCR. Levels are expressed relative to the level of TBP mRNA and are in arbitrary units (AU). Two-way ANOVA showed significant effects of time ($p<0.001$) and interaction ($p=0.001$) upon HO-1 mRNA expression and a trend for genotype difference ($p=0.08$) upon HO-1 expression between wild type (WT; black bars) and 11β-HSD1-deficient (KO; white bars) mice (Post-hoc Bonferroni test showed the difference between WT and KO lung was statistically significant at d14 (***, $p<0.001$). Two-way ANOVA showed a significant effect of time ($p<0.001$) upon all mRNAs measured. There was also a significant interaction ($p=0.05$) (but no genotype effect, $p=0.18$) upon iNOS expression. There was no effect of genotype or interaction with time upon IL-6 or TNF-α expression between WT and 11β-HSD1-deficient mice. Data are mean ± SEM with n = 5-8.

5.3.9.2 11β-HSD1-deficient mice have lower levels of MR and GR mRNA in lung, compared to WT mice

To test whether key parameters of glucocorticoid action differed between WT and 11β-HSD1-deficient mice, real-time PCR was used to quantify levels of GR and MR mRNA. Two-way ANOVA showed a significant difference in GR (Figure 5.18A) but not MR (Figure 5.18B) mRNA levels between genotypes. Following bleomycin, both genotypes showed a significant decrease in GR and MR mRNA levels which were lowest at 7-14d (Figure 5.18). Levels of GR mRNA were lower in 11β-HSD1-deficient mice at all time points examined, including in naïve mice, and were markedly reduced at d7 (Figure 5.18A)

Similarly, in naïve mice and following bleomycin treatment, levels of MR mRNA were consistently slightly lower in 11β-HSD1-deficient mice than WT mice, although this did not achieve significance ($p=0.13$).

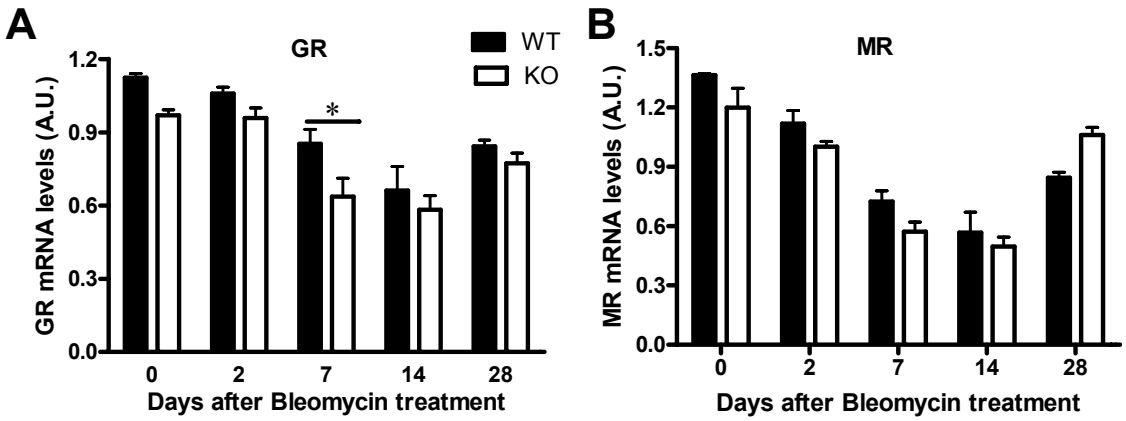

Figure 5.18 11β-HSD1-deficient mice have lower GR and MR mRNA levels in lung compared to WT mice, and levels of GR and MR mRNA are reduced following bleomycin installation.

Total RNA extracted from lungs of either WT or 11β-HSD1-deficient mice at different time points following bleomycin installation was analysed for GR (A) and MR (B) mRNA by real-time PCR. Levels are expressed relative to the level of TBP mRNA and are in arbitrary units (AU). Two-way ANOVA showed an effect of time ($p<0.0001$) and genotype ($p=0.0009$) (but no interaction) upon GR expression in wild type (WT; black bars) and 11β-HSD1-deficient (KO; white bars) mice. (Post-hoc Bonferroni test showed the difference between WT and KO lung at d7 was statistically significant (*, $p<0.05$)). Two-way ANOVA showed an effect of time ($p<0.0001$) and interaction ($p<0.05$) (but no genotype, $p=0.13$) upon MR expression between WT and KO. Data are mean ± SEM with n = 5-8.

5.3.9.3 TGF-β1 and α-SMA mRNA levels increased following bleomycin, but did not differ between the genotypes.

Fibrosis is caused by highly proliferating fibroblasts and myofibroblasts which lay down collagen to repair damaged tissue. To investigate whether the histological difference in fibrosis observed between WT and 11β-HSD1-deficient mice are underpinned by differences in gene expression, a few fibrosis related genes were tested.

Bleomycin treatment increases the transcription of TGF-β mRNA, total cellular TGF-β mRNA, and total cellular type I procollagen mRNAs in rat lung fibroblasts (Cutroneo, Breen et al. 1991) and TGF-β dose-dependently increased collagen synthesis in rat lung fibroblast (Cutroneo, Breen et al. 1991). Bleomycin treatment of rat lung fibroblast cultures increased levels of cellular TGF-β mRNA and increased secretion of TGF-β protein in the medium (Breen, Shull et al. 1992). Because TGF-β1 is one of the most important factors in inducing fibrosis in lung (Shukla, Meisler et al. 1999), levels of its mRNA were measured. In both genotypes, TGF-β1 mRNA levels increased following bleomycin installation, peaking at 7-14d, returning to basal levels at 28d (Figure 5.19A). However, there was no difference in TGF-β1 mRNA levels between genotypes at any time point (Figure 5.19A).

α-SMA is a marker of myofibroblast cells, and it has been found to be highly expressed after bleomycin treatment (Zhang, Rekhter et al. 1994). In both genotypes,

α-SMA mRNA levels were increased in lung following bleomycin and were highest around 7-14d, decreasing to normal levels at 28d (Figure 5.19B). Although there was a trend for α-SMA to be higher in 11β-HSD1-deficient mice at 14d, it did not reach statistical significance (Figure 5.19B).

Collagen levels are increased following bleomycin treatment (Meisler, Chiu et al. 1999). Animal model studies show the myofibroblast to be the primary source of type I collagen gene expression in active fibrotic sites (Phan 2002). Because fibrosis appeared worse in 11β-HSD1-deficient mice, collagen type1 α2 mRNA levels were measured to see whether it was expressed differently between WT and 11β-HSD1-deficient mice after bleomycin instillation. The increase in collagen type1 α2 in both genotypes was evident from d2 (Figure 5.19C). Similar to α-SMA, 14d after bleomycin installation 11β-HSD1-deficient mice tended to have a higher level of collagen type1 α2 mRNA compared with WT mice (Figure 5.19C) but this effect did not reach significance.

Arginase, which hydrolyzes arginine to urea and ornithine, is a precursor for the synthesis of polyamines and proline, the latter being abundant in collagen (Endo, Oyadomari et al. 2003). Levels of mRNA encoding Arginase I (Arg I) were measured in bleomycin-induced fibrosis. Arg1 was highly expressed 2d after bleomycin instillation, increased to 14d in both genotypes, then decreased to basal levels at 28d

(Figure 5.19D). However, at any time point, there was no difference in Arg I mRNA levels between genotypes (Figure 5.19D).

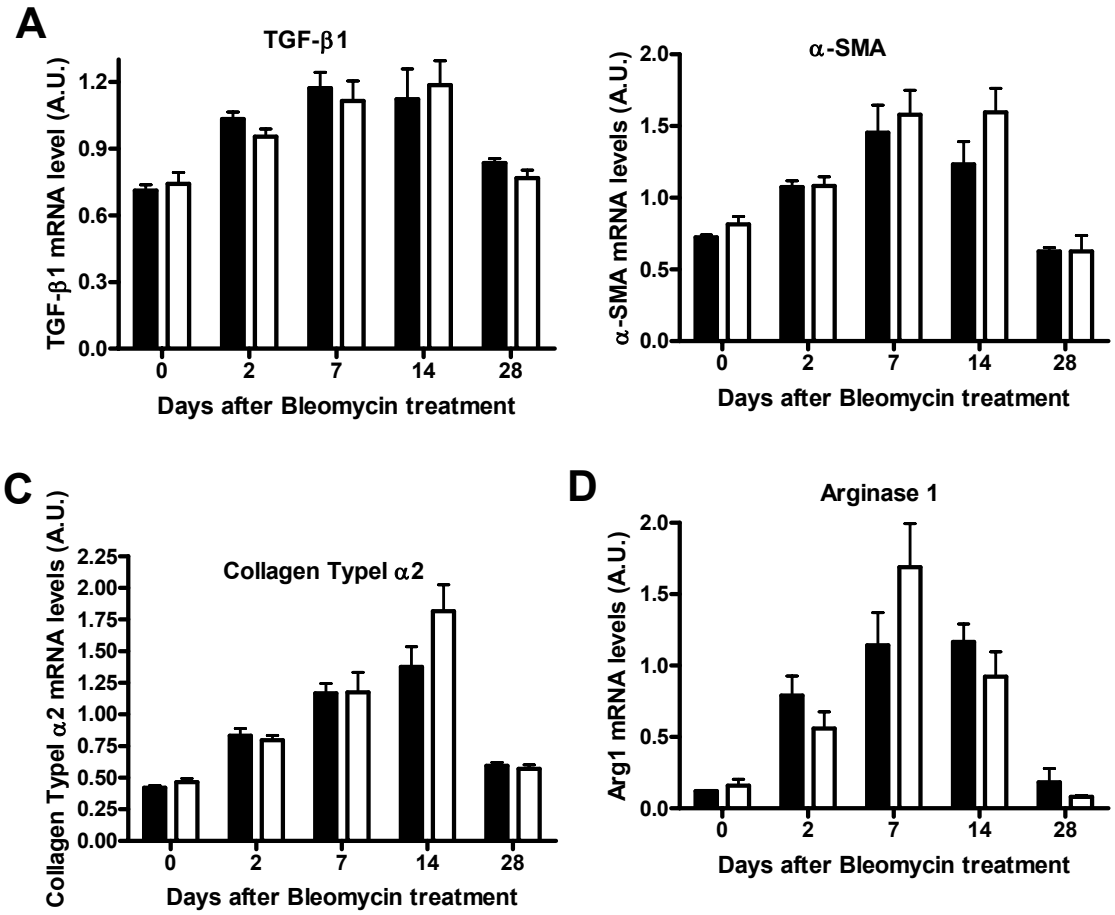

Figure 5.19 Bleomycin treatment induced α-SMA, TGF-β, collagen typeI α2 and Arg I gene expression to a similar extent in both WT and 11β-HSD1-deficient mice

Total RNA extracted from lungs of either WT or 11β-HSD1-deficient mice at different time points following bleomycin installation was analysed for TGF-β1 (A), α-SMA (B), collagen type1 α2 (C) and Arg I (D) mRNA by real-time PCR. Levels are expressed relative to the level of TBP mRNA and are in arbitrary units (AU). Two-way ANOVA showed an effect of time ($p<0.0001$) but no effect of genotype or interaction upon TGF-β1, α-SMA, collagen type1 α2 or Arg 1 expression between wild type (WT; black bars) and 11β-HSD1-deficient (KO; white bars) mice. Data are mean ± SEM with n = 5-8.

5.3.9.4 HIF-1α mRNA levels were upregulated after bleomycin

Lung inflammation is likely to impair function and lead to localized hypoxia. Bleomycin treatment increases hypoxia-inducible factor-1 α (HIF-1α) expression in lungs (Lu, Azad et al. 2009). Consistent with this, HIF-1α mRNA levels were increased 2-fold 2d after bleomycin, remaining elevated at 7d and 14d and returing to basal by 28d (Figure 5.20). However, there was no difference in HIF-1α mRNA expression between WT and 11β-HSD1-deficient mice at any time (Figure 5.20).

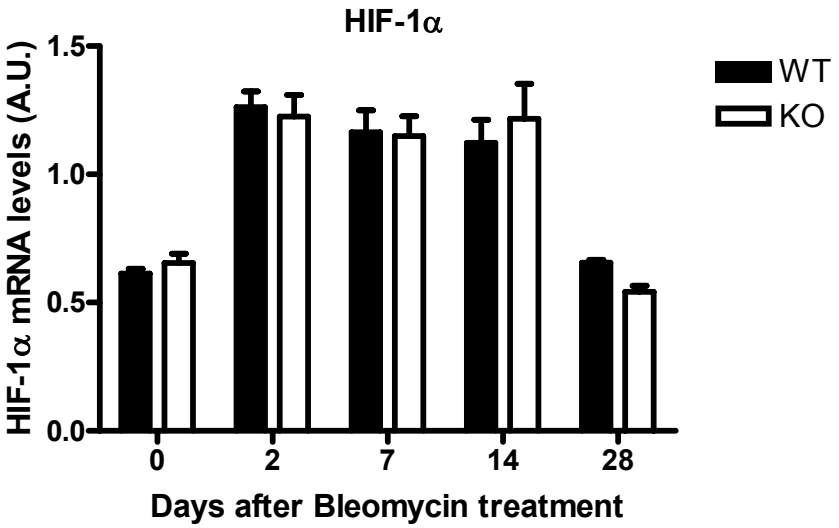

Figure 5.20 Bleomycin treatment induced similar levels of HIF-1α gene expression in both genotypes

Total RNA extracted from lungs of either WT or 11β-HSD1-deficient mice at different time points following bleomycin installation was analysed for HIF-α by real-time PCR. Levels are expressed relative to the level of TBP mRNA and are in arbitrary units (AU). Two-way ANOVA showed an effect of time ($p<0.0001$) but no effect of genotype or interaction upon HIF-1α expression between wild type (WT; black bars) and 11β-HSD1-deficient (KO; white bars) mice. Data are mean ± SEM with n = 5-8.

5.3.9.5 No difference between WT and 11β-HSD1-deficient mice in levels of C/EBP-β and C/EBP-δ following bleomycin

C/EBP-β plays a significant role in the development of pulmonary fibrosis (Hu, Ullenbruch et al. 2007); C/EBP-$\beta^{-/-}$ mice are resistant to bleomycin-induced fibrosis (Hu, Ullenbruch et al. 2007). C/EBP-β is a key regulator of myofibroblast differentiation in isolated lung fibroblasts, and stimulates the expression of α-SMA during myofibroblast differentiation by binding to a C/EBP-β binding element identified in the α-SMA promoter (Hu, Wu et al. 2004). Moreover, C/EBP-β regulates 11β-HSD1 expression (Williams, Lyons et al. 2000; Gout, Tirard et al. 2006; Arai, Masuzaki et al. 2007; Payne, Au et al. 2007; Sai, Esteves et al. 2008). Whilst measurement of C/EBP-β mRNA by real-time PCR showed a significant increase in lungs of mice 2d following treatment with bleomycin, with levels remaining elevated at 14d, levels did not differ between WT and 11β-HSD1-deficient mice at any time point (Figure 5.21A).

C/EBP-δ is also a member of the C/EBP transcription factor family which is highly expressed in lung (Williams, Cantwell et al. 1991) and which has been found to repress 11β-HSD1 expression in transfected HepG2 hepatoma cells (Esteves et al, manuscript submitted). At d0, WT and 11β-HSD1-deficient mice showed similar levels of C/EBP-δ mRNA (Figure 5.21B). By 2d after bleomycin instillation, C/EBP-δ mRNA levels were increased in lungs of both genotypes with expression decreasing gradually thereafter (Figure 5.21B).

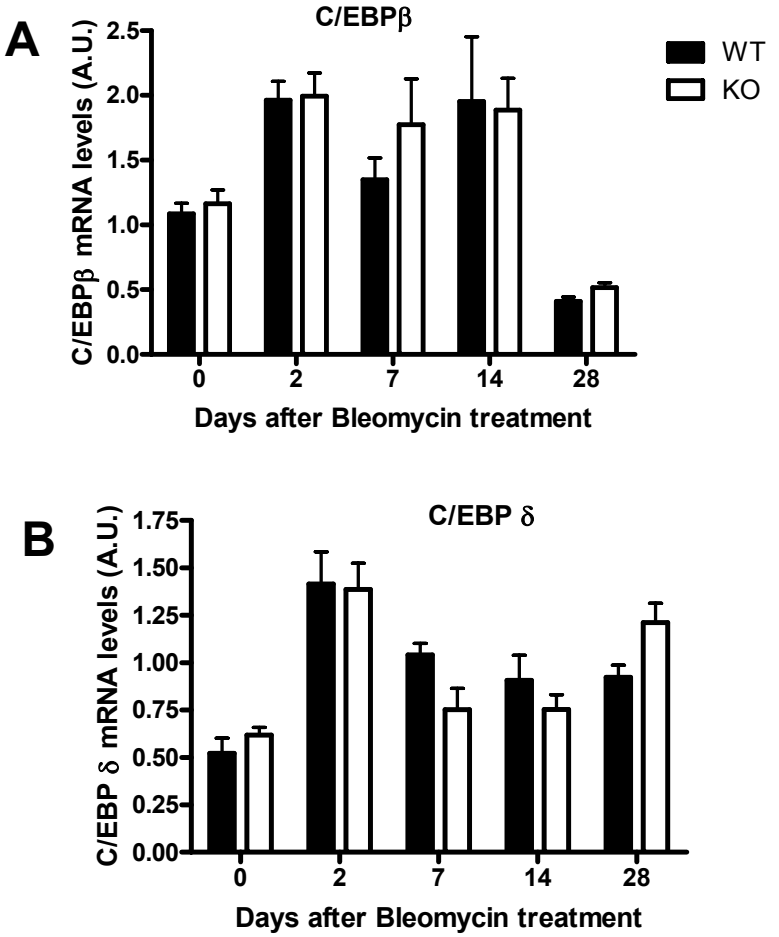

Figure 5.21 Bleomycin treatment induced similar level C/EBP-β and C/EBP-δ gene expression in both genotypes

Total RNA extracted from lungs of either WT or 11β-HSD1-deficient mice at different time points following bleomycin installation was analysed for C/EBP-β (A) and C/EBP-δ (B) mRNA by real-time PCR. Levels are expressed relative to the level of TBP mRNA and are in arbitrary units (AU). Two-way ANOVA showed an effect of time ($p<0.0001$) but no effect of genotype or interaction upon C/EBP-β or C/EBP-δ expression between wild type (WT; black bars) and 11β-HSD1-deficient (KO; white bars) mice. Data are mean ± SEM with n = 5-8.

5.3.10 Regulation of pulmonary 11β-HSD1 expression during bleomycin induced lung inflammation

11β-HSD1 is increased in some tissues during inflammation, but not all (Chapman, Coutinho et al. 2009) (and detailed in Chapter 1.6.3). To see whether 11β-HSD1 expression was affected by bleomycin-induced lung inflammation and fibrosis and whether the promoter of 11β-HSD1 was changed during the progress of fibrosis (as fibroblasts mainly use the P1 promoter), 11β-HSD1 mRNA levels were measured by real-time PCR in C57BL/6J (WT) mice, following bleomycin treatment.

5.3.10.1 Promoter usage of 11β-HSD1 after bleomycin treatment

Total 11β-HSD1 mRNA levels in lung were not significantly changed by bleomycin treatment (Figure 5.22A) ($P=0.15$; ANOVA). However, levels of 11β-HSD1 transcripts initiated at the P1 promoter were significantly changed following bleomycin ($P<0.01$; ANOVA), although they showed a very similar pattern to total 11β-HSD1 mRNA. Thus, levels of P1-initiated mRNA increased between d2 and d14, falling back to basal levels by 28d (Figure 5.22B). P2 promoter-initiated transcripts were significantly decreased after bleomycin treatment (Figure 5.22C) ($P<0.0001$; ANOVA).

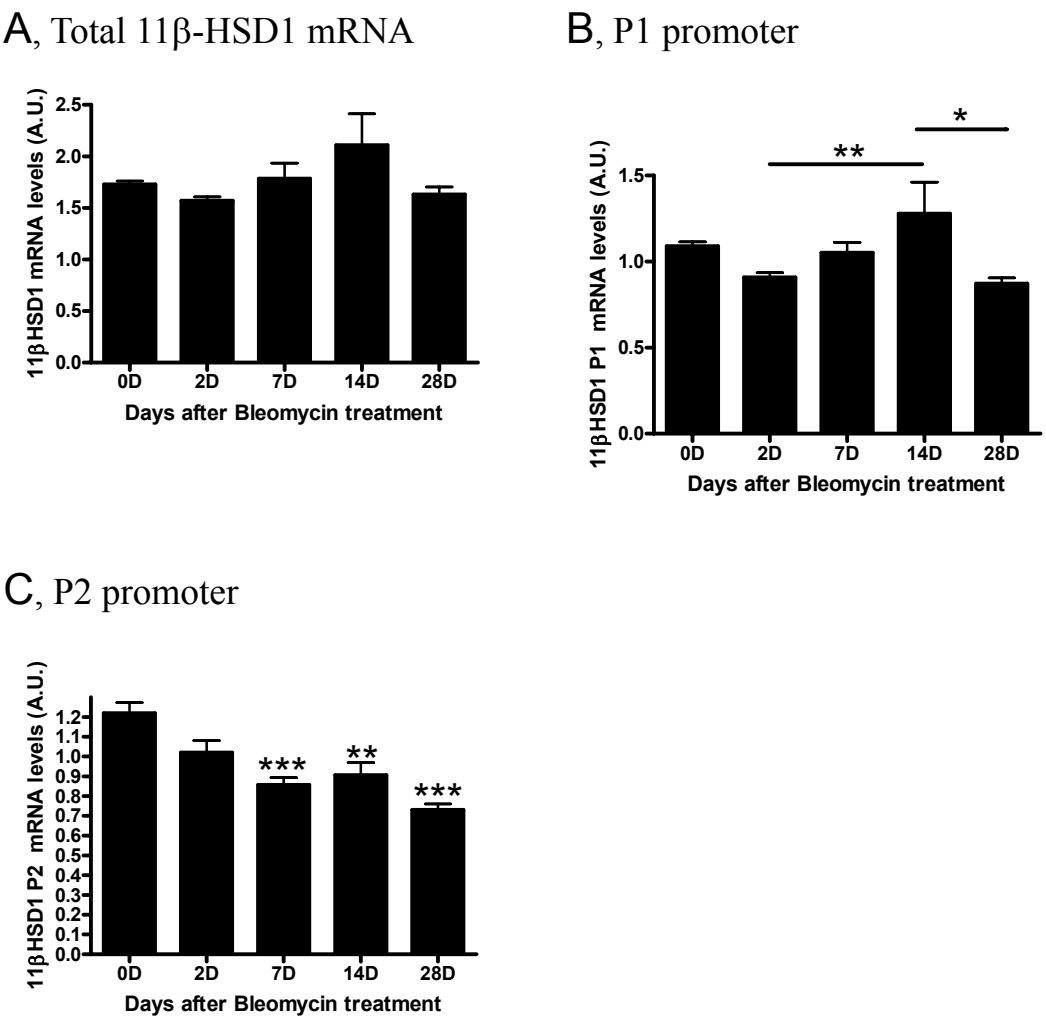

Figure 5.22 Transcripts initiated at P1 promoter and P2 promoter of *Hsd11b1* are differentially regulated following bleomycin treatment of mice

Total RNA was extracted from lungs of WT mice, killed at different time points after bleomycin treatment. Levels of total 11β-HSD1 mRNA (A) and 11β-HSD1 mRNA initiated at the P1 (B) or P2 promoter (C) were measured by real-time PCR. Levels are expressed relative to the level of TBP mRNA and are in arbitrary units (AU). Data are mean ± SEM with n = 5-8. Data were analysed by ANOVA followed by Tukey's Multiple Comparison Test. *, $p<0.05$; **, $p<0.01$; ***, $p<0.001$.

5.3.10.2 IHC staining suggests 11β-HSD1 is upregulated in WT lung 7d and 14d after bleomycin installation

Paraffin-embedded lung sections from WT mouse lung collected 7d or 14d after bleomycin installation were stained with sheep anti-11β-HSD1 antibody at 1:1000 dilution. Compared to untreated mice, 11β-HSD1 immunoreactivity was increased in the alveolar walls with strong staining of interstitial fibroblasts 7d and 14d following intratracheal instillation of bleomycin (Figure 5.23B and C). At 7d, strong staining was also seen in mononuclear cells, a population which was reduced at 14d compared to 7d (Figure 5.23C). Alveolar macrophages showed weak staining of 11β-HSD1.

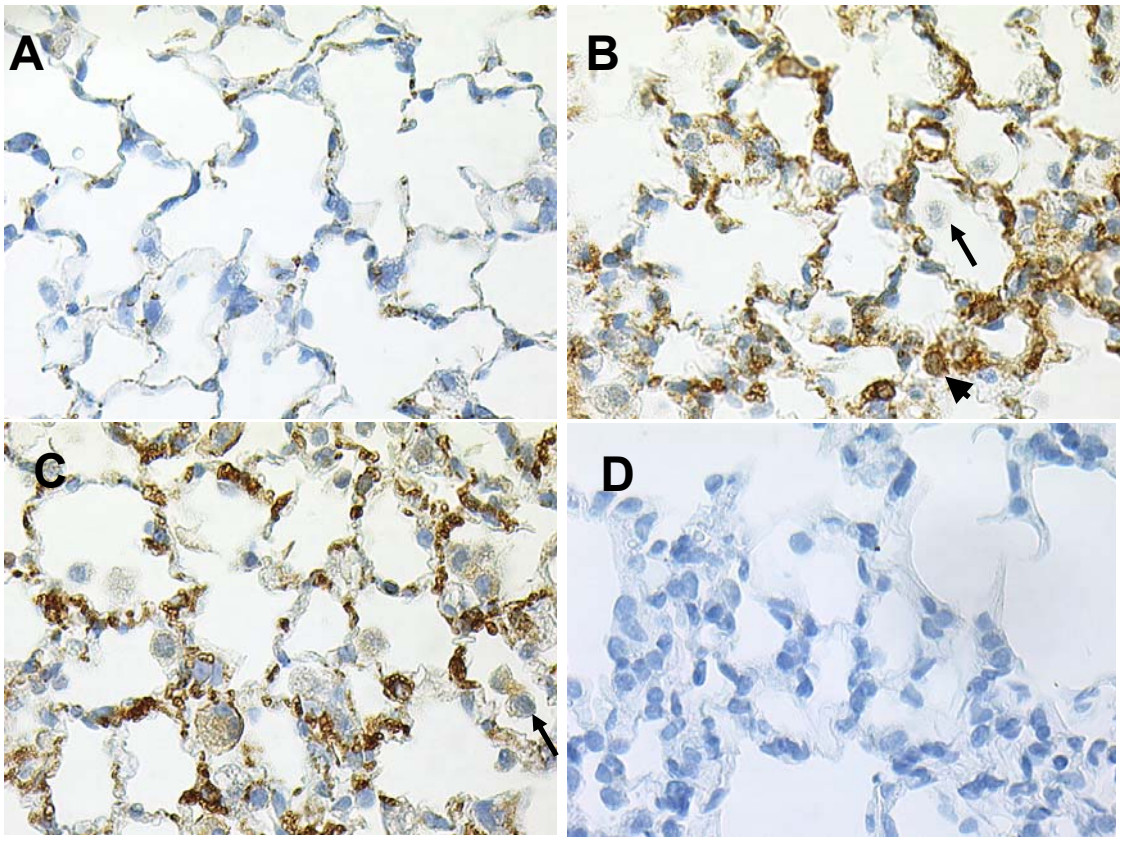

Figure 5.23 11β-HSD1 immunoreactivity is increased in mouse lungs following bleomycin installation.

Immunohistochemistry was carried out on C57BL/6J (WT) mouse lung with purified sheep anti-11β-HSD1 antibody at 1:1000 dilution and biotinylated rabbit-anti-sheep 2nd Ab at 1:400 dilution. (A), untreated lung; (B), 7d after bleomycin treatment; (C), 14d after bleomycin treatment; (D), negative control (WT lung with 2nd Ab alone). All images captured at magnification, X400. Arrows indicate alveolar macrophages and arrow heads indicate mononuclear cells.

5.3.10.3 *In situ* hybridization showed no effect of bleomycin treatement on 11β-HSD1 mRNA levels in WT lung

Because IHC suggested that 11β-HSD1 was upregulated after bleomycin treatment, *in situ* mRNA hybridization was carried out on sections of WT mouse lung harvested 7d or 14d after bleomycin installation, using an "antisense" [^{35}S]-cRNA probe complementary to mouse 11β-HSD1 mRNA, as described in Chapter 2.2.11. Mouse kidney highly expresses 11β-HSD1 (Rajan, Chapman et al. 1995) and was used as a positive control (Figure 5.24E). A "sense" strand cRNA probe (the same as the mRNA) was used as a negative control.

Autoradiography showed hybridization of antisense, but not sense, probe in lung (Figure 5.24A). This suggests specific hybridization. The hybridization signal was quantified as described in Chapter 2.2.11. Figure 5.24F shows that 11β-HSD1 mRNA levels were not changed 7d or 14d after bleomycin treatment, compared with untreated mice.

Figure 5.24 Semi-quantitative analysis of 11β-HSD1 mRNA shows no change following bleomycin treatment.

Representative autoradiographs showing *in situ* hybridization of an anti-sense [^{35}S]-labelled 11β-HSD1 cRNA probe to paraffin-embedded WT lung from (A), untreated mice or mice killed (B), 7d or (C), 14d after bleomycin treatment; (D), representative autoradiograph of paraffin embedded untreated WT lung hybridized to a sense [^{35}S]-labelled 11β-HSD1 cRNA probe (negative control); (E), representative autoradiograph of paraffin embedded untreated WT kidney hybridized to an anti-sense [^{35}S]-labelled 11β-HSD1 cRNA probe (positive control); (F), Semiquantitative analysis of 11β-HSD1 mRNA levels by optical densitometry measurements in whole lung. One-way ANOVA revealed no difference between the 3 different time points. Values are mean ± SEM of 3-8 mice. H indicates heart and L indicates lung.

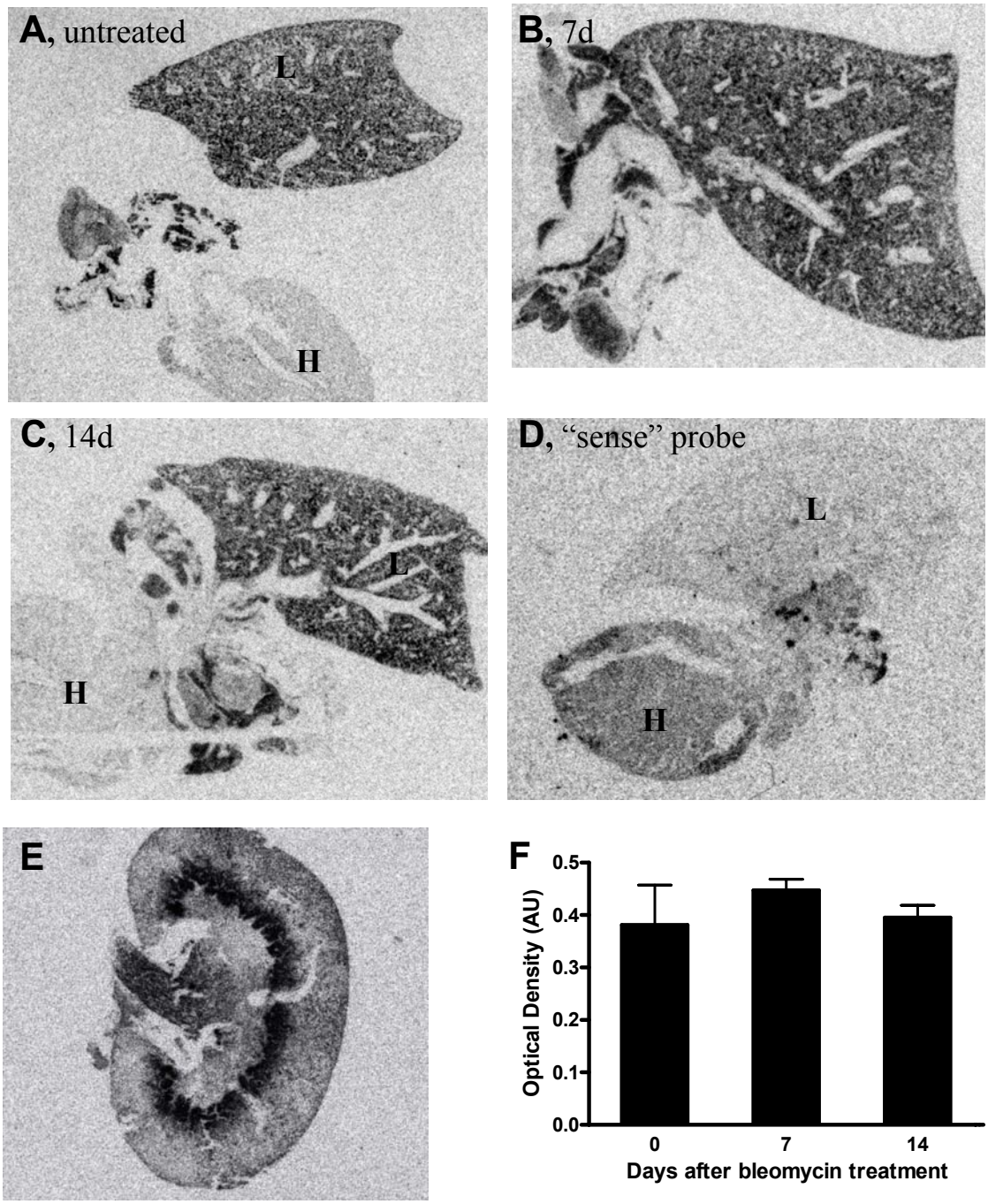
A, untreated
L
H
B, 7d
C, 14d
L
H
D, "sense" probe
L
H
E
F
Optical Density (AU)
0.5
0.4
0.3
0.2
0.1
0.0
0
7
14
Days after bleomycin treatment

5.3.10.4 11β-HSD1 activity assay showed no increase in 11β-HSD1 activity following bleomycin installation

Immunohistochemistry suggested protein levels of 11β-HSD1 may be upregulated, despite no significant increase in total 11β-HSD1 mRNA levels. However, given the problems with the 11β-HSD1 antibody described in Chapter 3.2.1.2, 11β-HSD1 activity assays were carried out to confirm the increase in 11β-HSD1 after bleomycin installation.

Lungs from control mice, or mice culled 7d or 14d after bleomycin treatment were homogenized and assayed for 11β-hydroxysteroid dehydrogenase activity as described in Chapter 2.2.23.2. A selective inhibitor of 11β-HSD1 which does not inhibit 11β-HSD2 (gift from Dr Scott Webster) was used to demonstrate that activity detected in lung homogenate was due to 11β-HSD1. 11β-HSD activity in lung homogenates was similar between untreated mice and following 7d bleomycin treatment and was ~0.8pmol dehydrocorticosterone/mg protein /min (Figure 5.25).

Although there was a trend to decreased 11β-HSD activity at 14d, compared to control untreated mice, this did not achieve significance (Figure 5.26). Addition of 50μM selective 11β-HSD1 inhibitor (CC002054) almost abolished 11β-HSD dehydrogenase activity (Figure 5.26) confirming that activity was due to 11β-HSD1 and not 11β-HSD2.

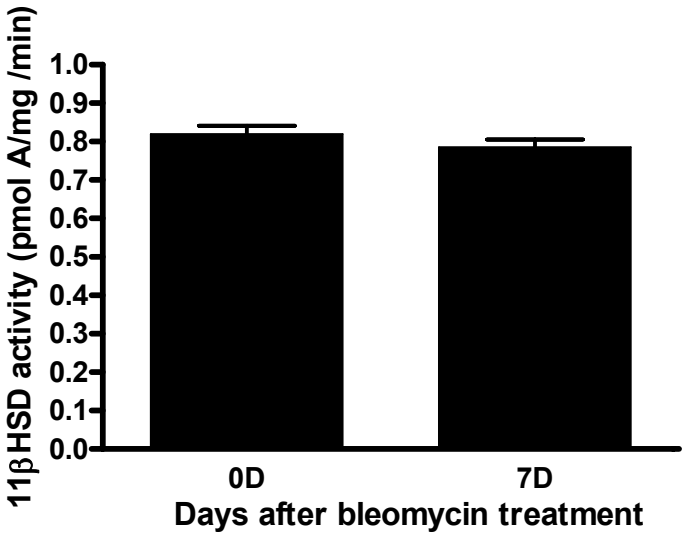

Figure 5.25 11β-HSD1 dehydrogenase activity did not differ in lung homogenates from control untreated mice or mice killed 7d after bleomycin treatment

11β-HSD activity was measured by conversion of [^{3}H]-B to [^{3}H]-A in a 10min assay with 0.5mg/ml lung homogenate. Steroids were extracted by ethyl acetate and quantified by HPLC as described in Chapter 2.2.24. 11β-HSD activity is expressed as pmol of corticosterone (B) converted into 11-dehydrocorticosterone (A)/min/mg protein. Values are mean ± SEM of 8-9 lungs.

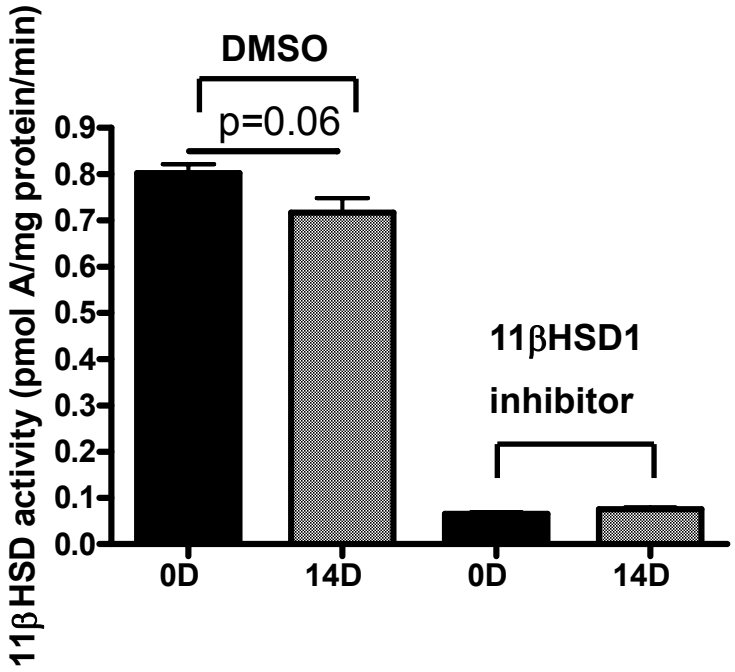

Figure 5.26 11β-HSD activity in mouse lung is largely attributable to 11β-HSD1 and did not differ between control untreated mice and mice killed 14d after bleomycin installation in lung

11β-HSD activity was measured by conversion of [^{3}H]-B to [^{3}H]-A in a 10min assay with 0.5mg/ml lung homogenate. 50μM 11β-HSD1 inhibitor (CC002054) or DMSO (vehicle) was added to the homogenate before the reaction. Steroids were extracted with ethyl acetate and quantified by HPLC as described in Chapter 2.2.24. 11β-HSD activity is expressed as pmol of corticosterone (B) converted into 11-dehydrocorticosterone (A)/min/mg protein. Values are mean ± SEM of 6-8 lungs. A Student's *t*-test showed no activity difference between control untreated mice and mice killed 14d after bleomycin, p=0.06.

5.3.10.5 Immunoblotting shows decreased 11β-HSD1 protein in mouse lung following bleomycin treatment

To further test whether 11β-HSD1 protein levels were unchanged after bleomycin treatment, western blot of whole lung homogenate was performed, as described in Chapter 2.2.24. Immunoblotting with 11β-HSD1 antibody detected a protein of the predicted ~34kDa (Figure 5.27). Quantification of immunoblots showed a reduction in 11β-HSD1 protein levels in lung following bleomycin treatment (Figure 5.27).

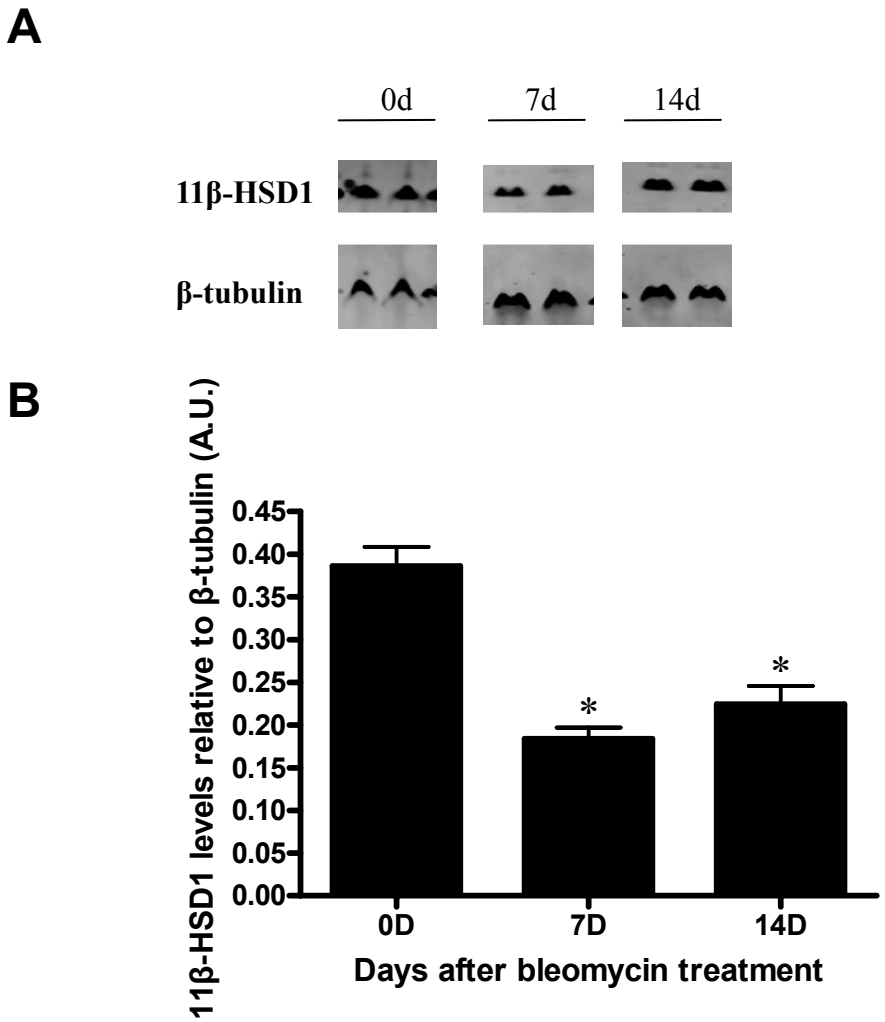

Figure 5.27 Western blotting shows decreased 11β-HSD1 levels following bleomycin installation in lung

Western blot analysis was used to detect 11β-HSD1 protein expression in WT lung tissue following bleomycin treatment, using sheep-anti-mouse 11β-HSD1 antibody (primary antibody used at 1:1000 dilution, Alexa 680 conjugated anti-sheep antibody used at 1:10000 dilution). 15μg of protein was loaded per well. (A) representative image of western blot of protein extracts from lung of mice killed 0d, 7d or 14d after bleomycin. (B) Quantitation of western blots showed decreased 11β-HSD1 levels in lung after bleomycin treatment (arbitrary units). Values are mean ± SEM of 5-8 lungs

5.4 Discussion

The comparative assessment of bleomycin-induced lung inflammation and fibrosis described in this Chapter is consistent with a role for 11β-HSD1 in controlling inflammation. These results suggest that, compared to WT mice, lungs of 11β-HSD1-deficient mice show an exaggerated inflammatory response and fibrosis following bleomycin instillation. Higher levels of iNOS and HO-1 mRNA in 11β-HSD1-deficient mice parallel with greater macrophage infiltration, especially at 14d after bleomycin treatment, which is consistent with the histological inflammatory score finding. The recruitment of more inflammatory cells in 11β-HSD1-deficient mice is indicative of a greater inflammatory response. The collagen assay suggested a bigger gain in collagen in 11β-HSD1-deficient mice than in WT mice during the 28d following bleomycin treatment (although absulote levels in 11β-HSD1-deficient mice were similar to WT at 28d), which is consistent with the Picrosirius staining of lung sections.

Blood inflammatory cell analysis indicated fewer circulating monocytes in 11β-HSD1-deficient mice compared to WT mice, 7d and 14d after bleomycin treatment. At the same time, histological analysis showed 11β-HSD1-deficient mice had more inflammatory cells in lung. This suggests that after bleomycin treatment, more circulating monocytes infiltrated into the lung in 11β-HSD1-deficient mice than in WT mice. After bleomycin treatment, lung starts to express chemokines, such

as CXCL12 and CCL18 to recruit inflammatory cells (Phillips, Burdick et al. 2004; Pochetuhen, Luzina et al. 2007). Overexpression of those chemokines worsens the severity of lung inflammation (Pochetuhen, Luzina et al. 2007). There may be a difference between WT and 11β-HSD1-deficient mice in chemokine expression. In a model of myocardial infarction (MI), more macrophages infiltrated into the infarct zone in 11β-HSD1-deficient mice than in WT mice, 7d post MI (McSweeney, Hadoke et al. 2010). At the same time, monocyte chemoattractant protein-1 (MCP-1) mRNA was higher in 11β-HSD1-deficient mice than in WT mice (McSweeney, Hadoke et al. 2010). Similarly, inhibition of 11β-HSD1 in a mouse model of atherosclerosis (*Apoe*$^{-/-}$ mice) reduced atherosclerosis and also decreased plasma MCP-1 levels (Hermanowski-Vosatka, Balkovec et al. 2005). Thus, the increased inflammation in 11β-HSD1-deficient mice may be due to increased chemokine secretion, including MCP-1. It will be important, in the future, to measure MCP-1 and other chemokines following bleomycin treatment.

Inflammatory gene expression levels are consistent with the histological results. HO-1 has a role in the regulation of inflammatory processes (reviewed in (Morse and Choi 2002). Binding sites for NF-κB and AP-1 have been found in the promoter region of HO-1 (Lavrovsky, Schwartzman et al. 1994), and AP-1 regulates HO-1 gene expression (Hartsfield, Alam et al. 1999). HO-1 has previously been shown to be strongly induced 14d after the instillation of bleomycin (Kaminski, Allard et al.

2000), which is consistent with my result. There may be a threshold effect for cytoprotection by HO-1. Suttner and coworkers observed that although moderate overexpression of HO-1 in lung fibroblasts conferred protection against oxidative injury, higher levels of HO-1 may be detrimental (Suttner, Sridhar et al. 1999). In different models of lung disease, the expression of HO-1 in lung has been localized to alveolar macrophages, bronchoalveolar epithelium, and interstitial and inflammatory cells (Lee, Alam et al. 1996; Nagatomo, Morimoto et al. 2007). Also HO-1 has been observed in various cultured cells including epithelial cells, fibroblasts, macrophages, and smooth muscle cells (Lee, Alam et al. 1996).

After bleomycin treatment, both 11β-HSD1-deficient mice and WT mice showed increased numbers of alveolar macrophages in BALF compared to untreated mice, but there was no difference between genotypes. The histological result suggests there were more macrophages in 11β-HSD1-deficient mice than in WT mice in lung suggesting more interstitial macrophages, and this needs to be confirmed. The greater expression of HO-1 mRNA in 11β-HSD1-deficient mice could be due to the interstitial macrophages and alveolar macrophages in fibrosis lesions. This needs IHC to stain HO-1 in mice lung and find out where is the difference in HO-1 expression between WT and 11β-HSD1-deficient mice 14d after bleomycin treatment. Atzori and colleagues used an HO-1 inhibitor to examine its effects on the development of pulmonary fibrosis in the bleomycin model and they found mice

treated with HO-1 inhibitor showed significantly less fibrosis (Atzori, Chua et al. 2004). TGF-β1 is a ligand for the integrin αυβ6 (Munger, Huang et al. 1999). Integrin $\beta 6^{-/-}$ mice develop inflammation but not fibrosis after bleomycin treatment, microarray data showed that HO-1 gene was dramatically induced by bleomycin in WT mice but was induced to a lesser degree in $\beta 6^{-/-}$ mice (Kaminski, Allard et al. 2000). The greater expression of HO-1 at 14d in 11β-HSD1-deficient mice may account, in fact, for the more severe fibrosis observed at 28d.

Blocking induction of iNOS by taurine and niacin in the bleomycin model caused a significant reduction in lung hydroxyproline content compared with control mice (Gurujeyalakshmi, Wang et al. 2000). Diallylsulfide, an antioxidant and anti-inflammatory agent inhibited the increase in iNOS expression and reduced collagen deposition after bleomycin treatment in rats (Kalayarasan, Sriram et al. 2008). In my experiment, 11β-HSD1-deficient mice showed higher levels of iNOS expression at 14d which is consistent with the greater fibrosis development in the 11β-HSD1-deficient mouse lung. Expression of iNOS is mainly in activated macrophages (Nussler, Billiar et al. 1994), suggesting that there may be more M1 (classically activated) macrophages in 11β-HSD1-deficient mice than in WT mice 14d following bleomycin. Moreover, this is consistent with the histology and inflammation score, which showed more inflammatory cell infiltration in 11β-HSD1-deficient mice than in WT mice, although this needs IHC to identify

M1-polarized macrophages to confirm this finding, such as colocalization of iNOS and F4/80.

The activity of GCs is mediated via GR expression, which is significantly decreased in various inflammatory processes (Kamiyama, Matsuda et al. 2008). In most tissues, GC down-regulate GR (Kalinyak, Dorin et al. 1987). After bleomycin, GR expression was decreased in both genotypes, possibly as a mechanism to protect tissue from over exposure to GC. Interestingly, at all time points, including in naïve mice, 11β-HSD1-deficient mice showed lower GR expression than WT.

Less GR expression in 11β-HSD1-deficient mice could be related to differences in early lung development. GR is essential for lung development (Cole, Blendy et al. 1995; Nemati, Atmodjo et al. 2008). GR knockout mice die within a few hours after birth because of respiratory failure and lung structural immaturity (Cole, Blendy et al. 1995; Nemati, Atmodjo et al. 2008). The differentiation of type I epithelial cells is decreased by about 50% and the mRNA levels of SP-A and SP-C are also reduced by approximately 50% in GR knockout mice at day 18.5 of pregnancy (Cole, Solomon et al. 2004). Although no gross differences was seen in histology in naïve mice (data not shown), there may be subtle differences in cell types present in 11β-HSD1-deficient mice lung, reflected in decreased collagen content and GR mRNA expression. Alternatively, decrease in GR may be a compensatory mechanism

for altered intracellular GC levels in 11β-HSD1-deficient mice, although this has not been reported in other tissues except for the hypothalamus (Carter, Paterson et al. 2009). Hundertmark and colleagues found 11β-HSD1-deficient mice exhibited delayed fetal lung development, with lower surfactant protein-A levels and significant depletion of lung surfactant (Hundertmark, Dill et al. 2002). Chemical inhibition of fetal 11β-HSD1 activity also reduced the gestation-dependent accumulation of SP-A and decreased lamellar body content in alveolar type II cells in lung (Hundertmark, Dill et al. 2002). My results showed lung collagen content was significantly lower in untreated 11β-HSD1-deficient mice, compared with WT mice. Which of the collagens accounted for this difference was not determined, but it is unlikely to be collagen type1 α2 expression, which was similar between naïve mice by real-time PCR measurement. In human fetal lung, GCs increase lung cell proliferation, differentiation of type 2 alveolar epithelial cells and thinning of alveolar walls (reviewed in (Garbrecht, Klein et al. 2006)). Thus there may be differences in the types of lung cells present between fetal 11β-HSD1-deficient mice and WT mice, reflected in decreased collagen content and GR mRNA expression. This needs further investigation in the future. Also, finding out which collagen is different between 11β-HSD1-deficient mice and WT mice may provide a clue to the mechanism.

No significant difference in plasma corticosterone levels was detected between WT

and 11β-HSD1-deficient mice. Although there was variability between mice in each group and naïve mice showed stress level of corticosterone, the corticosterone levels were similar between WT and 11β-HSD1-deficient mice, so we cannot conclude whether bleomycin differentially activates the HPA axis in 11β-HSD1-deficient mice. However, there was a significant interaction of genotype and time, and it appears likely that after bleomycin, corticosterone levels return to basal more rapidly in WT mice than in 11β-HSD1-deficient mice. This would be consistent with worse (or prolonged) inflammation in 11β-HSD1-deficient mice and is similar to findings in an model of experimental arthritis (Coutinho 2009), where corticosterone remained elevated in 11β-HSD1-deficient mice 21d after treatment and at the same time, WT shows reduced corticosterone level. On the same genetic background as used here (C57BL/6J), 11β-HSD1-deficient mice showed similar circadian rhythms of plasma corticosterone to WT, and although they showed a greater plasma corticosterone response to stress, both genotypes returned to the same basal level at the same time (Carter, Paterson et al. 2009). 11β-HSD1-deficient mice show adrenal hypertrophy to compensate for lack of hepatic 11β-HSD1-medicated GC regeneration (Kotelevtsev, Holmes et al. 1997). However, although naïve 11β-HSD1-deficient mice showed heavier adrenal glands than WT mice before and until 14d after bleomycin treatment, they did not differ at 28d. The reason for this is not clear, but might be due to a reduced capacity for adrenal steroidogenesis after prolonged inflammation.

The collagen difference in naïve mice could be due to the lower GR expression and presumed lower intracellular GC levels in 11β-HSD1-deficient mice. It is well established that GCs exert an anti-anabolic effect on collagen metabolism. Dexamethasone treatment of primary fetal chick lung and chick skin fibroblasts resulted in a marked decrease in the steady state levels of procollagen mRNAs (Sterling, Harris et al. 1983). Dexamethasone treatment of chick skin fibroblasts can decrease TGF-β levels, leading to less TGF-β-activated collagen synthesis (Cutroneo 2002). Therefore, the developmental difference in collagen between WT and 11β-HSD1-deficient mice may be due to a combination of reduced GR levels and reduced intracellular GC in 11β-HSD1-deficient mice leading to less collagen synthesis. It would be interesting to measure GR expression in fetal lung of WT and 11β-HSD1-deficient mice to check whether 11β-HSD1-deficient mice express less GR during development, before the massive increase in 11β-HSD1 expression in lung, just prior to birth (Speirs, Seckl et al. 2004).

In 11β-HSD1-deficient mice, biochemical and morphological characteristics of pulmonary fibrosis were observed 14d after bleomycin administration. Picrosirius red staining indicated more collagen deposition in 11β-HSD1-deficient mice. However, the quantification of Picrosirius red staining was not possible due to inter-animal variability in the disease process. The distribution of fibrosis in the lung was patchy, probably due to unequal distribution of bleomycin with the instillation

method. Some parts of lung showing normal structure could be found at all time points, with other some parts of lung showing dense fibrosis. In future, careful matching of specimens may allow a better quantification. Sircol assay confirmed an increase in total collagen content in both genotypes after bleomycin treatment. The difference in lung collagen content between naïve 11β-HSD1-deficient mice and WT mice disappeared after 28d bleomycin treatment suggesting that 11β-HSD1-deficient mice produce more collagen than WT mice.

Increased fibrosis-related gene expression levels (TGF-β and collagen) are consistent with the histological findings in both genotypes. However, the gene expression analysis did not show a difference in fibrosis between genotypes. Previous work has shown that after bleomycin treatment, all of the extracellular matrix components including collagen type1 α2 were induced progressively throughout the 14d period (Kaminski, Allard et al. 2000). My results show that mRNA encoding collagen type1 α2 increased markedly around 14d after bleomycin instillation, but did not differ between genotypes, so the difference between genotypes could be due to other collagen proteins, such as collagen type3 or collagen type1 α1 (Shahzeidi, Mulier et al. 1993; Liu, Dhanasekaran et al. 2004). Also collagen degradation may differ. The turnover of extracellular matrix is partially regulated by proteases such as metalloproteinases (MMPs) and their inhibitors (TIMPs) (Manoury, Nenan et al. 2007). Activity of MMP-2 and MMP-9 peak at 7d after bleomycin installation, but

TIMP-1 and TIMP-2 levels peak at 14d after bleomycin (Oggionni, Morbini et al. 2006), so an altered balance of MMP and TIMP may alter susceptibility to bleomycin-induced pulmonary fibrosis.

Arginase I plays an important role in supplying proline, a key precursor in collagen synthesis and in the process of lung fibrosis (Endo, Oyadomari et al. 2003). In the current studies, arginase I mRNA levels increased 2d after bleomycin, peaked around 7-14d, then returned to basal levels, similar to a previous report (Endo, Oyadomari et al. 2003). Endo and colleagues showed arginase I mRNA was undetectable at d0, was induced 5d after bleomycin treatment reaching a maximum at 7d, then decreased to undetectable levels by 14d (Endo, Oyadomari et al. 2003). They also found arginase I expression was mainly within a subpopulation of macrophages, by immunohistochemical analysis. Activated macrophages can be broadly divided into 2 subpopulations, M1 (classically activated) macrophages and M2 (alternatively activated) macrophages (Gordon 2003). Unlike classically activated M1 macrophages that secrete pro-inflammatory mediators and display phagocytic behaviour, alternatively activated macrophages secrete anti-inflammatory cytokines such as TGF-β and can be identified by their expression of arginase I and by secretion of the chitinase-like molecule YM1 (Raes, Van den Bergh et al. 2005). In the experiments reported here, arginase I mRNA levels were not different between genotypes; however, there may be a difference in protein levels. Following

myocardial infarction, 11β-HSD1-deficient mice showed more accumulation of alternatively activated macrophages, identified by YM1, than WT mice (McSweeney, Hadoke et al. 2010).

C/EBP-β has a potential role *in vivo* in the pathogenesis of pulmonary fibrosis. Mice that lack C/EBP-β are resistant to bleomycin induced lung fibrosis (Hu, Ullenbruch et al. 2007) and there is a two-fold increase in C/EBP-β expression in lung of WT mice 7d after bleomycin treatment (Hu, Ullenbruch et al. 2007). My result shows a similar increase in C/EBP-β mRNA levels after bleomycin treatment, but levels did not differ between genotypes. However, there may be a difference at the protein level. There are two forms of C/EBP-β, liver activating protein (LAP) and liver inhibitory protein (LIP) which may be products of alternative translation (Descombes and Schibler 1991). The LAP protein is a transcriptional activator while LIP acts as a dominant negative inhibitor of LAP even when present at substoichiometric levels (i.e., LAP:LIP ratio of 5:1) (Descombes and Schibler 1991). Levels of LAP/LIP can regulate 11β-HSD1 expression in adipocytes and LAP/LIP ratio is altered in adipose tissue of high fat fed mice without changes in mRNA level (Esteves et al, manuscript submitted). So the ratio of LAP/LIP therefore determines the degree of gene activation.

C/EBP-δ was induced in response to bleomycin (Liu, Dhanasekaran et al. 2004).

Recent data suggest C/EBP-δ may be a negative regulator of 11β-HSD1 expression (Esteves et al, manuscript submitted). My results show that C/EBP-δ is up-regulated after bleomycin. However, there was no difference between genotypes. C/EBP-δ is expressed in lung epithelial cells and regulates surfactant protein A (SP-A) (Lag, Skarpen et al. 2000; Matlapudi, Wang et al. 2002). Due to low expression of 11β-HSD1 in epithelial cells, C/EBP-δ may not play an important role in regulating 11β-HSD1 expression in the bleomycin model.

The fibroblast to myofibroblast differentiation experiments described in Chapter 4 suggest TGF-β regulates 11β-HSD1 expression *in vitro*. *In vivo*, TGF-β may decrease 11β-HSD1 expression to lower intracellular GC levels, which would otherwise restrict collagen deposition and fibrosis development. However, the *in vivo* regulation of 11β-HSD1 may be different from *in vitro*. After bleomycin treatment, TGF-β1 mRNA levels were up-regulated up to 2-fold after bleomycin treatment peaking around 7-14d, but total 11β-HSD1 mRNA was not changed. Moreover, the P1 promoter usage was increased, suggesting increased fibroblast proliferation, but not a promoter switch. Therefore TGF-β may not directly affect 11β-HSD1 expression in the bleomycin model. Zhang and Daynes found increased TGF-β1 protein levels in 11β-HSD1-deficient mice, despite no difference in the encoding mRNA levels (Zhang and Daynes 2007). Accordingly, it is possible that TGF-β1 protein levels may be different between genotypes after bleomycin treatment

and this needs to be examined by western blot or by bioassay in the future. Also, 11β-HSD1 expression is regulated by other transcription factors such as C/EBP-β and C/EBP-δ and increased expression of TGF-β *in vivo* may not be enough to reduce 11β-HSD1 expression.

In other inflammation models, 11β-HSD1 is reported to be upregulated by the inflammatory condition or by inflammatory cytokines (Chapman, Coutinho et al. 2009). After bleomycin treatment, real-time PCR showed that total 11β-HSD1 mRNA levels did not significantly change, although there was a trend to increase between d2 and d14, then fall back to basal levels by 28d. Contrary to expectation, the level of P2 promoter usage was decreased, making less contribution to overall 11β-HSD1 mRNA expression with most 11β-HSD1 transcribed from the P1 promoter, which significantly increased after bleomycin. Perhaps because of the opposite (albeit small) effect of bleomycin treatment on P2-initiated mRNA between d2 and d14, the effect on total 11β-HSD1 mRNA levels did not achieve significance. These data do not support a promoter switch *in vivo*.

The protein results showed no difference in 11β-HSD1 expression after bleomycin. Activity assay, the most quantitative assay, measured no difference in the activity of 11β-HSD1 between d0, d7 and d14 and a trend toward a decrease on d14. Semi-quantitative measurement by western blotting showed a decrease in the protein

levels of 11β-HSD1. In contrast, IHC showed a marked increase in 11β-HSD1 7d and 14d after bleomycin treatment. However, IHC is more subject to artefact from cross-reactivity. Whilst controls appeared supportive, IHC results were not confirmed by western blotting using the same antibody or by activity assay. IHC of 11β-HSD1 in kidney shows similar distribution to previously published ISH result (detailed in appendix 1). Therefore the antibody may have cross-reacted with a protein more highly expressed in WT after bleomycin treatment.

The dissociation between 11β-HSD1 mRNA and protein levels has been described before (De Sousa Peixoto, Turban et al. 2008). The discrepancy in mRNA and protein (activity) may be due to use of different internal standards (TBP mRNA, β-tubulin protein) which may have been differentially affected by bleomycin. The effect of bleomycin on 11β-HSD1 mRNA is subtle and the effect on activity did not achieve significance. Overall, bleomycin may not affect the expression of 11β-HSD1 and further work is needed to confirm this result.

TNF-α and IL-1 are potent inducers of 11β-HSD1 in various cell culture systems including fibroblasts (Escher, Galli et al. 1997; Handoko, Yang et al. 2000; Cai, Wong et al. 2001; Tomlinson, Moore et al. 2001; Yong, Harlow et al. 2002; Sun and Myatt 2003; Hardy, Rabbitt et al. 2008). As TGF-β decreased 11β-HSD1 mainly by repressing the P1 promoter, TNF-α and IL-1 may induce 11β-HSD1 expression by

the P1 promoter as well. After bleomycin treatment, TNF-α was upregulated, but 11β-HSD1 was not changed significantly, so TNF-α may not upregulate 11β-HSD1 in lung fibroblasts *in vivo*. Other evidence supports my findings, TNF-α or IL-1 had no effect on 11β-HSD1 expression *in vivo* (Dover, Hadoke et al. 2007). Most people look at 11β-HSD1 in fibroblasts in culture. Perhaps in other fibroblasts, like lung, there is a P1 to P2 promoter switch. The fibroblasts examined by Hardy et al were skin, bone marrow and synovial (Hardy, Filer et al. 2006). It is important to examine which promoter is used in different types of fibroblast and whether there is a switch, as this will have implications for the regulation of 11β-HSD1 by TNF-α and IL-1.

In summary, 11β-HSD1-deficient mice exhibit an exaggerated response in the bleomycin model of lung inflammation and fibrosis. This chapter corroborates previous findings in carrageenan-induced pleurisy experiments (Coutinho, Mohini Gray et al. 2006), suggesting that 11β-HSD1-deficient mice exhibit an altered course of inflammation and fibrosis. Importantly, the work described here demonstrated that the worse inflammatory response seen in 11β-HSD1-deficient mice is not limited to carrageenan-induced pleurisy. These findings strongly support a role for 11β-HSD1 as an endogenous modulator of inflammation. The findings in the bleomycin model are novel but remain preliminary. However, they provide a basis for further investigation. Future experiments using this model should focus on identifying exactly which inflammatory cells were more abundant in 11β-HSD1-deficient lung

and whether those cells contribute to the more severe fibrosis in 11β-HSD1-deficient mice or whether the difference in fibrosis may be due to differences in the fibroblast and myofibroblast cells.

6 Chapter Six: Summary and Discussion

6.1 Summary

Pharmacologically, GC exert powerful immunosuppressive and anti-inflammatory effects. Physiological GC are also important modulators of inflammation and their levels are regulated "locally" by the 11β-HSDs. The aim of this thesis was to investigate whether amplification of intracellular GC levels by 11β-HSD1 represents an important endogenous mechanism to limit lung inflammation and fibrosis. Recent evidence (reviewed in (Chapman, Coutinho et al. 2009)), including work described in this thesis, suggests that 11β-HSD1 forms part of an endogenous anti-inflammatory mechanism engaged during an inflammatory response that may programme subsequent repair and resolution. The contribution of 11β-HSD1 during an inflammatory response was examined using 11β-HSD1-deficient mice and wild type control mice. Firstly, the expression of 11β-HSD1 was confirmed in lung as well as isolated alveolar macrophages, lung epithelial cells and lung fibroblasts. Lung fibroblasts especially, highly express 11β-HSD1 and show exclusively 11β-HSD reductase activity. Further, bleomycin-induced lung inflammation and fibrosis revealed prolonged inflammation and worse fibrosis in 11β-HSD1-deficient mice compared to WT mice. These data support the original findings, which suggested an anti-inflammatory function for 11β-HSD1 in models of peritonitis, pleurisy and self-resolving experimental arthritis (Coutinho, Mohini Gray et al. 2006; Gilmour, Coutinho et al. 2006; Coutinho 2009) and importantly, emphasize a role for 11β-HSD1 in restraining inflammation. Furthermore, in contrast to the other organs

which express 11β-HSD1 from the P2 promoter, lung expresses 11β-HSD1 from the P1 promoter. Freshly isolated lung fibroblasts express 11β-HSD1 from the P1 promoter but switch to the P2 promoter after culture. TGF-β decreased 11β-HSD1 expression in fibroblasts; an effect which was not only reversed by SB431542, a TGF-β receptor antagonist, but SB431542 increased 11β-HSD1 expression above levels in untreated cells. Also, TGF-β reduced levels of mRNA initiating at the P2 promoter whilst initiation from the P1 promoter was completely repressed. Treatment with TGF-β receptor antagonist markedly increased levels of P1-initiated 11β-HSD1 mRNA above levels in untreated cells. This finding provides a mechanistic insight into how 11β-HSD1 may be regulated during inflammatory conditions and also how other cytokines may regulate 11β-HSD1, such as IL-1 and TNF-α. The studies presented in this thesis suggest more fibrosis development in the bleomycin lung inflammation model, in 11β-HSD1-deficient mice. This may be due to 11β-HSD1-deficiency in fibroblasts, which may lead to changes in chemokine expression or collagen synthesis. Further *in vitro* investigation of 11β-HSD1-deficient fibroblasts is needed.

6.2 Discussion

The locus of the anti-inflammatory effect of 11β-HSD1 remains a central question. 11β-HSD1 has been identified in immune cells (reviewed in (Chapman, Gilmour et al. 2006)). It is also expressed in lung epithelial cells (Brereton, van Driel et al. 2001)

and, as shown in the current work, in lung fibroblasts. Although lung fibroblasts are critical in lung inflammation, highly express 11β-HSD1 and show different transcriptional regulation of the 11β-HSD1 gene to other cells, it remains unclear whether it is the 11β-HSD1-deficiency in fibroblasts, in other lung cell populations or in the resident immune or recruited inflammatory cells that is responsible for the worsened inflammatory response and fibrosis in 11β-HSD1-deficient mice after bleomycin treatment or a combination of more than one of these factors. It will be important to clearly identify which of these cells are involved in the mechanism responsible for the anti-inflammatory effects of 11β-HSD1.

During the course of my PhD research, 11β-HSD1-deficient mice were found to be "leaky". My work confirmed these mice have 11β-HSD activity in lung. Moreover, recent work in the laboratory identified a "sub-line" of 11β-HSD1-deficient mice which showed 11β-HSD activity in liver and brain (J, Noble, personal communication), in contrast to the original line (Kotelevtsev, Holmes et al. 1997). This may have been due to a secondary mutation in the transgene cassette which allowed more P2 promoter activity. Nevertheless, the 11β-HSD1-deficient mice had lower levels of 11β-HSD1 in lung than WT mice and allowed the investigation of the effects of 11β-HSD1 deficiency to be investigated. With hindsight, a lung inflammation model may not have been the best choice given the level of 11β-HSD activity in 11β-HSD1-deficient mouse lung. However, this might model effects of

inhibitors of 11β-HSD1, which rarely give 100% enzyme inhibition. A new line of mice with a germline disruption of *Hsd11b1* (created from a new line of "floxed" mice) and which lack 11β-HSD1 activity in all tissues is now available in the lab and it will be important to use these new mice to repeat the bleomycin experiments to investigate the anti-inflammatory mechanisms of 11β-HSD1.

"Floxed" 11β-HSD1 mice are now available in the lab and a LysMcre myeloid-specific knockout of 11β-HSD1 has recently been generated, so these mice could be used to test whether 11β-HSD1-deficiency in myeloid cells causes more severe inflammation. A fibroblast specific-Cre mice has been reported, in which the fibroblast specific protein promoter drives Cre expression (Bhowmick, Chytil et al. 2004), which could be used to examine the effect of 11β-HSD1-deficiency in fibroblasts. Also bone marrow transplantation can investigate the contribution of the host (non-immune or resident immune cells) in worsening inflammation.

Additionally, in parallel to the investigations suggested above, it will be important to establish the mechanisms responsible for the greater number of inflammatory cells in lung in 11β-HSD1-deficient mice after bleomycin. Two possible mechanisms responsible for the greater recruitment of inflammatory cells are; first, greater cytokine and chemokine regulation of the inflammatory response involving the resident immune cell and/or incoming inflammatory cells, and second, the

immuno-regulatory function of resident fibroblasts and differentiated myofibroblasts. Future experiments using this model should focus on identifying exactly which inflammatory cells were more abundant in 11β-HSD1-deficient lung and whether those cells contribute to the more severe fibrosis in 11β-HSD1-deficient mice or whether the difference in fibrosis may be due to 11β-HSD1 function in the fibroblast and myofibroblast cells.

In preliminary experiments in which flow cytometry was used to analyse collagenase-digested lung following bleomycin treatment both genotypes showed a similar percentage of apoptosis and necrotic cells. A "cocktail" of antibodies to Ly6C, CD11c, CD11b and MHC-II was used to identify monocytes, macrophages and DC in lung. However, the results were unclear and could not identify distinct cell populations (data not shown). Future experiments should focus on refining this technique to identify and phenotype the inflammatory cells in lung following bleomycin treatment, particularly the M1 and M2 macrophages. Classically activated M1 macrophages secrete pro-inflammatory mediators and display phagocytic behaviour; alternatively activated M2 macrophages secrete anti-inflammatory cytokines such as TGF-β and act to repair the damaged tissue by stimulating collagen deposition (Raes, Van den Bergh et al. 2005). Therefore an altered balance between M1 and M2 macrophages would affect the inflammatory and fibrosis condition. Such an altered balance has recently been suggested following myocardial infarction in

11β-HSD1-deficient mice where more M2 macrophages accumulated in the infarct zone of 11β-HSD1-deficient mice compared to WT (McSweeney, Hadoke et al. 2010).

The inflammation and fibrosis resulting from bleomycin treatment may reflect different mechanisms. TGF-β1 is a ligand for the integrin αυβ6 (Munger, Huang et al. 1999). Integrin $\beta 6^{-/-}$ mice are protected against bleomycin-induced pulmonary fibrosis but show a greater inflammatory response (Munger, Huang et al. 1999), which suggests the protection from bleomycin-induced pulmonary fibrosis is not due to inhibition of the inflammatory response to bleomycin. To separate the processes of inflammation and fibrosis, it may also be possible to use silicon to induce fibrosis in lung without inducing strong inflammation.

The focus of Chapter 4 was to further investigate 11β-HSD1 expression in fibroblasts from WT mice, since 11β-HSD1 had not been characterized in mouse lung fibroblasts before. Lung fibroblasts appear to be the main cell type in lung expressing 11β-HSD1. TGF-β reduced 11β-HSD1 expression in primary cultures of lung fibroblasts; however, the mechanism of regulation is not clear. Real-time PCR showed no difference in mRNA encoding C/EBP-β, which has been shown to regulate 11β-HSD1 (Chapman, Coutinho et al. 2009), so it is important to measure C/EBP-β protein levels including the LAP/LIP ratio and also to measure

C/EBP-δ levels. During the differentiation of fibroblasts to myofibroblasts induced by TGF-β, dex treatment augmented TGF-β-induced α-SMA expression (Gu, Zhu et al. 2004). Based on this GC effect, it is possible that GC-regeneration by 11β-HSD1 would increase fibroblast to myofibroblast differentiation. It will be important to test whether 11β-HSD1-deficient fibroblasts are more resistant to TGF-β induced differentiation.

It is important to phenotype lung fibroblasts from 11β-HSD1-deficient mice. After GR^{dim} mice (see Chapter 1.4) were wounded, they showed markedly enlarged granulation tissue with a high fibroblast density (Grose, Werner et al. 2002). This was attributed to increased migration and proliferation of GR^{dim} fibroblasts together with increased expression of soluble factors, such as TGF-β and IL-1β. Lung fibroblasts from 11β-HSD1-deficient mice may show similar increased migratory and proliferative capacity to GR^{dim} mice, as this phenotype reflects the function of endogenous glucocorticoids. It is possible that 11β-HSD1-deficient fibroblasts show a higher level of expression and secretion of cytokines and/or chemokines to recruit inflammatory cells which might lead to the more severe inflammation in 11β-HSD1-deficient mice. These possibilities could be tested in fibroblasts isolated using flow cytometry or MACS bead separation by $CD90^{+}$ to analyze mRNA or cytokine secretion.

These findings raise intriguing questions about the importance of local modulation of GC by 11β-HSD1 in lung, particular in fibroblasts, and provide a basis for further investigation (Figure 6.1). Besides lung, kidney is the other main tissue expressing 11β-HSD1 from the P1 promoter (V. Kelly et al, unpublished). Like lung, kidney is also susceptible to fibrosis. Understanding the role and regulation of 11β-HSD1 in lung fibrosis may shed light into research on kidney fibrosis. The efficacy of high dose, long-term, GC-based therapeutic regimes are compromised by side effects, it may therefore be desirable to target the beneficial effects of GC to fibroblasts in certain conditions where activated fibroblasts contribute to disease.

In conclusion, the experiments described in this thesis support an anti-inflammatory and anti-fibrotic role for 11β-HSD1 during bleomycin-induced lung inflammation and fibrosis and begin to address the underlying mechanisms for the altered inflammatory phenotype of 11β-HSD1-deficient mice. These studies have provided a basis for future experiments to tease apart the role and regulation of 11β-HSD1 in inflammation. Thus, further investigations are warranted and better understanding of the immune-regulated role of 11β-HSD1 in inflammation may lead to improved and even targeted steroid therapies on fibroblasts.

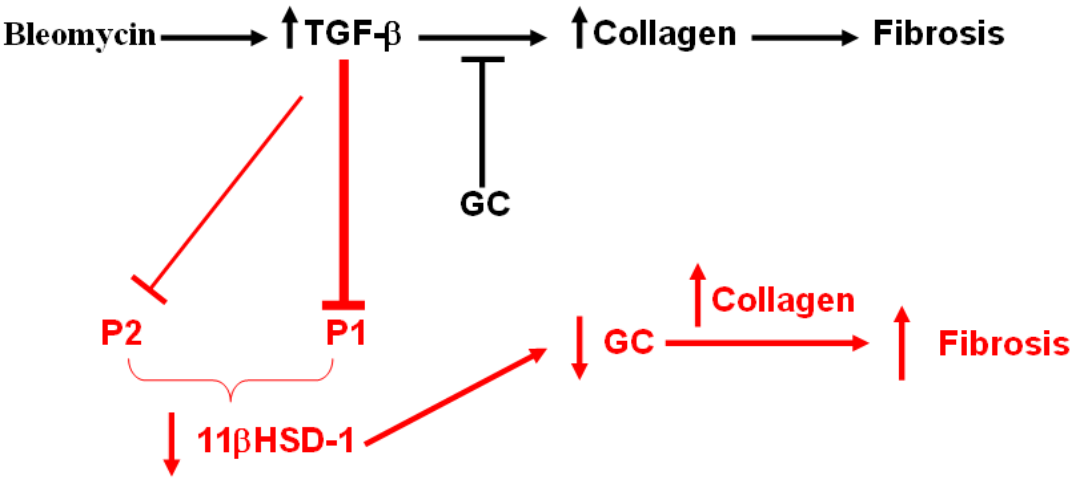

Figure 6.1 Models of the inter-relationship between TGF-β, 11β-HSD1 P1 and P2 promoter, GC and fibrosis.

Bleomycin treatment induces strong fibrosis in part by increasing TGF-β action which stimulates collagen synthesis. GC inhibit collagen production. TGF-β strongly reduced the P1 promoter of 11β-HSD1 and reduced the P2 promoter of 11β-HSD1 to a lesser extent. Less 11β-HSD1 will result in lower intracellular GC levels, which is predicted to lead to more collagen production and severe fibrosis. As 11β-HSD1 -deficient mice only have 30% of 11β-HSD activity compared to WT mice. It generates much less intracellular GC, which lead to more severe fibrosis, compared to WT mice.

Reference

Abraham, S. M., T. Lawrence, et al. (2006). "Antiinflammatory effects of dexamethasone are partly dependent on induction of dual specificity phosphatase 1." J Exp Med **203**(8): 1883-9.

Abramovitz, M., C. L. Branchaud, et al. (1982). "Cortisol-cortisone interconversion in human fetal lung: contrasting results using explant and monolayer cultures suggest that 11 beta-hydroxysteroid dehydrogenase (EC 1.1.1.146) comprises two enzymes." J Clin Endocrinol Metab **54**(3): 563-8.

Adams, M., O. C. Meijer, et al. (2003). "Homodimerization of the glucocorticoid receptor is not essential for response element binding: activation of the phenylethanolamine N-methyltransferase gene by dimerization-defective mutants." Mol Endocrinol **17**(12): 2583-92.

Agarwal, A. K. and R. J. Auchus (2005). "Minireview: cellular redox state regulates hydroxysteroid dehydrogenase activity and intracellular hormone potency." Endocrinology **146**(6): 2531-8.

Agarwal, A. K., C. Monder, et al. (1989). "Cloning and expression of rat cDNA encoding corticosteroid 11 beta-dehydrogenase." J Biol Chem **264**(32): 18939-43.

Alberts, P., L. Engblom, et al. (2002). "Selective inhibition of 11beta-hydroxysteroid dehydrogenase type 1 decreases blood glucose concentrations in hyperglycaemic mice." Diabetologia **45**(11): 1528-32.

Albiston, A. L., V. R. Obeyesekere, et al. (1994). "Cloning and tissue distribution of the human 11ß-hydroxysteroid dehydrogenase type 2 enzyme." Mol Cell Endocrinol **105**(2): R11-R17.

Andrews, R. C., O. Rooyackers, et al. (2003). "Effects of the 11 beta-hydroxysteroid dehydrogenase inhibitor carbenoxolone on insulin sensitivity in men with type 2 diabetes." J Clin Endocrinol Metab **88**(1): 285-91.

Arai, N., H. Masuzaki, et al. (2007). "Ceramide and adenosine 5'-monophosphate-activated protein kinase are two novel regulators of 11beta-hydroxysteroid dehydrogenase type 1 expression and activity in cultured preadipocytes." Endocrinology **148**(11): 5268-77.

Atanasov, A. G., L. G. Nashev, et al. (2004). "Hexose-6-phosphate dehydrogenase determines the reaction direction of 11®-hydroxysteroid dehydrogenase type 1 as an oxoreductase." FEBS Lett **571**(1-3): 129-133.

Atzori, L., F. Chua, et al. (2004). "Attenuation of bleomycin induced pulmonary fibrosis in mice using the heme oxygenase inhibitor Zn-deuteroporphyrin IX-2,4-bisethylene glycol." Thorax **59**(3): 217-23.

Axelrod, J. and T. D. Reisine (1984). "Stress hormones: their interaction and regulation." Science **224**(4648): 452-9.

Baker, M. E. (1994). "Licorice and Enzymes Other Than 11-Beta-Hydroxysteroid Dehydrogenase - an Evolutionary Perspective." Steroids **59**(2): 136-141.

Ballard, P. L., J. D. Baxter, et al. (1974). "General presence of glucocorticoid receptors in mammalian tissues." Endocrinology **94**(4): 998-1002.

Barf, T., J. Vallgarda, et al. (2002). "Arylsulfonamidothiazoles as a new class of potential antidiabetic drugs. Discovery of potent and selective inhibitors of the 11beta-hydroxysteroid dehydrogenase type 1." J Med Chem **45**(18): 3813-5.

Bartram, U. and C. P. Speer (2004). "The role of transforming growth factor beta in lung development

and disease." Chest **125**(2): 754-65.

Basset, F., V. J. Ferrans, et al. (1986). "Intraluminal fibrosis in interstitial lung disorders." Am J Pathol **122**(3): 443-61.

Beato, M. (1989). "Gene regulation by steroid hormones." Cell **56**(3): 335-44.

Berg, T., L. Didon, et al. (2005). "Glucocorticoids increase C/EBPbeta activity in the lung epithelium via phosphorylation." Biochem Biophys Res Commun **334**(2): 638-45.

Bertini, R., M. Bianchi, et al. (1988). "Adrenalectomy sensitizes mice to the lethal effects of interleukin 1 and tumor necrosis factor." J Exp Med **167**(5): 1708-12.

Bhowmick, N. A., A. Chytil, et al. (2004). "TGF-beta signaling in fibroblasts modulates the oncogenic potential of adjacent epithelia." Science **303**(5659): 848-51.

Blum, R. H., S. K. Carter, et al. (1973). "A clinical review of bleomycin--a new antineoplastic agent." Cancer **31**(4): 903-14.

Borish, L. C. and J. W. Steinke (2003). "2. Cytokines and chemokines." J Allergy Clin Immunol **111**(2 Suppl): S460-75.

Borzone, G., R. Moreno, et al. (2001). "Bleomycin-induced chronic lung damage does not resemble human idiopathic pulmonary fibrosis." Am J Respir Crit Care Med **163**(7): 1648-53.

Bowden, D. H. (1984). "Unraveling pulmonary fibrosis: the bleomycin model." Lab Invest **50**(5): 487-8.

Boyle, C. D. and T. J. Kowalski (2009). "11beta-hydroxysteroid dehydrogenase type 1 inhibitors: a review of recent patents." Expert Opin Ther Pat **19**(6): 801-25.

Breen, E., S. Shull, et al. (1992). "Bleomycin regulation of transforming growth factor-beta mRNA in rat lung fibroblasts." Am J Respir Cell Mol Biol **6**(2): 146-52.

Brereton, P. S., R. R. van Driel, et al. (2001). "Light and electron microscopy localization of the 11β-hydroxysteroid dehydrogenase type I enzyme in the rat." Endocrinology **142**(4): 1644-1651.

Breul, S. D., K. H. Bradley, et al. (1980). "Control of collagen production by human diploid lung fibroblasts." J. Biol. Chem. **255**(11): 5250-5260.

Brody, A. R. (1998). "Whither goes the alveolar macrophage? Another small chapter is written on the localized response of this crucial cell." J Lab Clin Med **131**(5): 391-2.

Brown, R. W., K. E. Chapman, et al. (1996). "Cloning and production of antisera to human placental 11 beta-hydroxysteroid dehydrogenase type 2." Biochem J **313 (Pt 3)**: 1007-17.

Bruley, C., V. Lyons, et al. (2006). "A novel promoter for the 11beta-hydroxysteroid dehydrogenase type 1 gene is active in lung and is C/EBPalpha independent." Endocrinology **147**(6): 2879-2885.

Bujalska, I., M. Shimojo, et al. (1997). "Human 11®-hydroxysteroid dehydrogenase: studies on the stably transfected isoforms and localization of the type 2 isozyme within renal tissue." Steroids **62**(1): 77-82.

Cai, T., B. Wong, et al. (2001). "Induction of 11®-hydroxysteroid dehydrogenase type 1 but not -2 in human aortic smooth muscle cells by inflammatory stimuli." J Steroid Biochem Mol Biol **77**(2-3): 117-122.

Carter, R. N., J. M. Paterson, et al. (2009). "Hypothalamic-pituitary-adrenal axis abnormalities in response to deletion of 11beta-HSD1 is strain-dependent." J Neuroendocrinol **21**(11): 879-87.

Chapman, K. E., A. E. Coutinho, et al. (2009). "The role and regulation of 11beta-hydroxysteroid

dehydrogenase type 1 in the inflammatory response." Mol Cell Endocrinol **301**(1-2): 123-31.

Chapman, K. E., J. S. Gilmour, et al. (2006). "11Beta-hydroxysteroid dehydrogenase type 1- a role in inflammation?" Mol Cell Endocrinol **248**(1-2): 3-8.

Choy, L. and R. Derynck (2003). "Transforming growth factor-beta inhibits adipocyte differentiation by Smad3 interacting with CCAAT/enhancer-binding protein (C/EBP) and repressing C/EBP transactivation function." J Biol Chem **278**(11): 9609-19.

Christy, C., P. W. Hadoke, et al. (2003). "11beta-hydroxysteroid dehydrogenase type 2 in mouse aorta: localization and influence on response to glucocorticoids." Hypertension **42**(4): 580-7.

Chrousos, G. P. (2004). "Is 11beta-hydroxysteroid dehydrogenase type 1 a good therapeutic target for blockade of glucocorticoid actions?" Proc Natl Acad Sci U S A **101**(17): 6329-30.

Clark, A. R. (2007). "Anti-inflammatory functions of glucocorticoid-induced genes." Mol Cell Endocrinol **275**(1-2): 79-97.

Cohen, J. J., M. Fschbach, et al. (1970). "Hydrocortisne resistance of graft vs host activity in mouse thymus, spleen and bone marrow." J Immunol **105**(5): 1146-50.

Coker, R. K., G. J. Laurent, et al. (1997). "Transforming growth factors-beta 1, -beta 2, and -beta 3 stimulate fibroblast procollagen production in vitro but are differentially expressed during bleomycin-induced lung fibrosis." Am J Pathol **150**(3): 981-91.

Cole, T., J. A. Blendy, et al. (1995). "Targeted disruption of the glucocorticoid receptor blocks adrenergic chromaffin cell development and severely retards lung maturation." Genes Dev **9**: 1608-1621.

Cole, T. J., N. M. Solomon, et al. (2004). "Altered epithelial cell proportions in the fetal lung of glucocorticoid receptor null mice." Am J Respir Cell Mol Biol **30**(5): 613-9.

Cooper, J. A., Jr., R. J. Zitnik, et al. (1988). "Mechanisms of drug-induced pulmonary disease." Annu Rev Med **39**: 395-404.

Cooper, M. S. and P. M. Stewart (2009). "11Beta-hydroxysteroid dehydrogenase type 1 and its role in the hypothalamus-pituitary-adrenal axis, metabolic syndrome, and inflammation." J Clin Endocrinol Metab **94**(12): 4645-54.

Coutinho, A. E. (2009). "Consequences of 11b-Hydroxysteroid Dehydrogenases deficiency during inflammatory response." PhD thesis University of Edinburgh.

Coutinho, A. E., Mohini Gray, et al. (2006). "Deficiency in 11?-Hydroxysteroid Dehydrogenase Type 1 Results in a More Rapid

and Severe Inflammation." Abstracts of the Endocrine Society, 88th annual meeting.

Cumberbatch, M., R. J. Dearman, et al. (1999). "Inhibition by dexamethasone of Langerhans cell migration: influence of epidermal cytokine signals." Immunopharmacology **41**(3): 235-43.

Cupps, T. R., T. L. Gerrard, et al. (1985). "Effects of in vitro corticosteroids on B cell activation, proliferation, and differentiation." J Clin Invest **75**(2): 754-61.

Cutroneo, K., E. Breen, et al. (1991). "Bleomycin regulation of transforming growth factor-beta mRNA in rat lung fibroblasts and subpopulations." Chest **99**(3 Suppl): 65S.

Cutroneo, K. R. (2002). "Relationship between glucocorticoid-mediated early decrease of protein synthesis and the steady state decreases of glucocorticoid receptor and TGF-[beta] activator protein." The International Journal of Biochemistry & Cell Biology **34**(2): 194-203.

Cutroneo, K. R. and D. F. Counts (1975). "Anti-inflammatory steroids and collagen metabolism: glucocorticoid-mediated alterations of prolyl hydroxylase activity and collagen synthesis."

Mol Pharmacol **11**(5): 632-9.

Dahlman-Wright, K., A. Wright, et al. (1991). "Interaction of the glucocorticoid receptor DNA-binding domain with DNA as a dimer is mediated by a short segment of five amino acids." J Biol Chem **266**(5): 3107-12.

De Kloet, E. R., P. Rosenfeld, et al. (1988). "Stress, glucocorticoids and development." Prog Brain Res **73**: 101-20.

De Sousa Peixoto, R. A., S. Turban, et al. (2008). "Preadipocyte 11beta-hydroxysteroid dehydrogenase type 1 is a keto-reductase and contributes to diet-induced visceral obesity in vivo." Endocrinology **149**(4): 1861-8.

Dean, J. L., G. Sully, et al. (2004). "The involvement of AU-rich element-binding proteins in p38 mitogen-activated protein kinase pathway-mediated mRNA stabilisation." Cell Signal **16**(10): 1113-21.

Descombes, P. and U. Schibler (1991). "A liver-enriched transcriptional activator protein, LAP, and a transcriptional inhibitory protein, LIP, are translated from the same mRNA." Cell **67**(3): 569-79.

Desmouliere, A., M. Redard, et al. (1995). "Apoptosis mediates the decrease in cellularity during the transition between granulation tissue and scar." Am J Pathol **146**(1): 56-66.

Dorn, L. D., E. S. Burgess, et al. (1995). "Psychopathology in patients with endogenous Cushing's syndrome: 'atypical' or melancholic features." Clin Endocrinol (Oxf) **43**(4): 433-42.

Dover, A. R., P. W. F. Hadoke, et al. (2007). "Intravascular Glucocorticoid Metabolism during Inflammation and Injury in Mice." Endocrinology **148**(1): 166-172.

Draper, N., E. A. Walker, et al. (2003). "Mutations in the genes encoding 11beta-hydroxysteroid dehydrogenase type 1 and hexose-6-phosphate dehydrogenase interact to cause cortisone reductase deficiency." Nat Genet **34**(4): 434-9.

Duffin, R., L. Tran, et al. (2007). "Proinflammogenic effects of low-toxicity and metal nanoparticles in vivo and in vitro: highlighting the role of particle surface area and surface reactivity." Inhal Toxicol **19**(10): 849-56.

Dulkerian, S. J., L. W. Gonzales, et al. (1996). "Regulation of surfactant protein D in human fetal lung." Am J Respir Cell Mol Biol **15**(6): 781-6.

Dunn, J. F., B. C. Nisula, et al. (1981). "Transport of steroid hormones: binding of 21 endogenous steroids to both testosterone-binding globulin and corticosteroid-binding globulin in human plasma." J Clin Endocrinol Metab **53**(1): 58-68.

Edwards, C. R., P. M. Stewart, et al. (1988). "Localisation of 11 beta-hydroxysteroid dehydrogenase--tissue specific protector of the mineralocorticoid receptor." Lancet **2**(8618): 986-9.

Edwards, C. R., B. R. Walker, et al. (1993). "Congenital and acquired syndromes of apparent mineralocorticoid excess." J Steroid Biochem Mol Biol **45**(1-3): 1-5.

Ehrchen, J., L. Steinmuller, et al. (2007). "Glucocorticoids induce differentiation of a specifically activated, anti-inflammatory subtype of human monocytes." Blood **109**(3): 1265-74.

Endo, M., S. Oyadomari, et al. (2003). "Induction of arginase I and II in bleomycin-induced fibrosis of mouse lung." Am J Physiol Lung Cell Mol Physiol **285**(2): L313-321.

Ergang, P., P. Leden, et al. (2010). "Local metabolism of glucocorticoids and its role in rat adjuvant arthritis." Mol Cell Endocrinol.

Escher, G., I. Galli, et al. (1997). "Tumor necrosis factor a and interleukin 1b enhance the cortisone/cortisol shuttle." J Exp Med **186**: 189-198.

Fine, A. and R. H. Goldstein (1987). "The effect of transforming growth factor-beta on cell proliferation and collagen formation by lung fibroblasts." J Biol Chem **262**(8): 3897-902.

Fisher, C. E., S. A. Ahmad, et al. (2005). "FITC-induced murine pulmonary inflammation: CC10 up-regulation and concurrent Shh expression." Cell Biol Int **29**(10): 868-76.

Fitch, P. M. (2005). "SHH signalling in acute pulmonary cell injury and chronic fibrosis " PhD thesis University of Edinburgh.

Floros, J., M. Post, et al. (1985). "Glucocorticoids affect the synthesis of pulmonary fibroblast-pneumonocyte factor at a pretranslational level." J Biol Chem **260**(4): 2265-7.

Fowden, A. L., J. Li, et al. (1998). "Glucocorticoids and the preparation for life after birth: are there long-term consequences of the life insurance?" Proc Nutr Soc **57**(1): 113-22.

Frank, M. G., Z. D. Miguel, et al. (2010). "Prior exposure to glucocorticoids sensitizes the neuroinflammatory and peripheral inflammatory responses to E. coli lipopolysaccharide." Brain Behav Immun **24**(1): 19-30.

Franke, W. W., E. Schmid, et al. (1978). "Different intermediate-sized filaments distinguished by immunofluorescence microscopy." Proc Natl Acad Sci U S A **75**(10): 5034-8.

Freeman, L., M. Hewison, et al. (2005). "Expression of 11β-hydroxysteroid dehydrogenase type 1 permits regulation of glucocorticoid bioavailability by human dendritic cells." Blood **106**: 2042-2049.

Funder, J. W., P. T. Pearce, et al. (1988). "Mineralocorticoid action: target tissue specificity is enzyme, not receptor, mediated." Science **242**: 583-585.

Gabbiani, G., B. J. Hirschel, et al. (1972). "Granulation tissue as a contractile organ. A study of structure and function." J Exp Med **135**(4): 719-34.

Gagnon, S., W. Atmodjo, et al. (2006). "Transgenic glucocorticoid receptor expression driven by the SP-C promoter reduces neonatal lung cellularity and midkine expression in GRhypo mice." Biol Neonate **90**(1): 46-57.

Gaillard, D., M. Wabitsch, et al. (1991). "Control of terminal differentiation of adipose precursor cells by glucocorticoids." J Lipid Res **32**(4): 569-79.

Garbrecht, M. R., J. M. Klein, et al. (2006). "Glucocorticoid metabolism in the human fetal lung: implications for lung development and the pulmonary surfactant system." Biol Neonate **89**(2): 109-19.

Garn, H. (2006). "Specific aspects of flow cytometric analysis of cells from the lung." Exp Toxicol Pathol **57 Suppl 2**: 21-4.

Giles, K. M., K. Ross, et al. (2001). "Glucocorticoid augmentation of macrophage capacity for phagocytosis of apoptotic cells is associated with reduced p130Cas expression, loss of paxillin/pyk2 phosphorylation, and high levels of active Rac." J Immunol **167**(2): 976-86.

Gilmour, J. S. (2002). "Glucocorticoids, 11b-Hydroxysteroid Dehydrogenases and Macrophage Function." PhD thesis University of Edinburgh.

Gilmour, J. S. (2003). Glucocorticoids, 11®-hydroxysteroid dehydrogenases and macrophage function., PhD thesis, University of Edinburgh. **PhD thesis**.

Gilmour, J. S., A. E. Coutinho, et al. (2006). "Local amplification of glucocorticoids by 11beta-hydroxysteroid dehydrogenase type 1 promotes macrophage phagocytosis of

apoptotic leukocytes." J Immunol **176**(12): 7605-11.

Giri, S. N., J. M. Nakashima, et al. (1985). "Effects of intratracheal administration of bleomycin or saline in pair-fed and control-fed hamsters on daily food intake and on plasma levels of glucose, cortisol, and insulin, and lung levels of calmodulin, calcium, and collagen." Exp Mol Pathol **42**(2): 206-19.

Gomperts, B. N. and R. M. Strieter (2007). "Fibrocytes in lung disease." J Leukoc Biol **82**(3): 449-56.

Gordon, S. (2003). "Alternative activation of macrophages." Nat Rev Immunol **3**(1): 23-35.

Gout, J., J. Tirard, et al. (2006). "CCAAT/enhancer-binding proteins (C/EBPs) regulate the basal and cAMP-induced transcription of the human 11beta-hydroxysteroid dehydrogenase encoding gene in adipose cells." Biochimie **88**(9): 1115-24.

Grad, I. and D. Picard (2007). "The glucocorticoid responses are shaped by molecular chaperones." Mol Cell Endocrinol **275**(1-2): 2-12.

Greenberg, S. and S. Grinstein (2002). "Phagocytosis and innate immunity." Curr Opin Immunol **14**(1): 136-45.

Grose, R., S. Werner, et al. (2002). "A role for endogenous glucocorticoids in wound repair." EMBO Rep **3**(6): 575-82.

Gu, L., Y. J. Zhu, et al. (2004). "Effect of IFN-gamma and dexamethasone on TGF-beta1-induced human fetal lung fibroblast-myofibroblast differentiation." Acta Pharmacol Sin **25**(11): 1479-88.

Gurujeyalakshmi, G., Y. Wang, et al. (2000). "Suppression of bleomycin-induced nitric oxide production in mice by taurine and niacin." Nitric Oxide **4**(4): 399-411.

Hamamichi, N., A. Natrajan, et al. (1992). "On the role of individual bleomycin thiazoles in oxygen activation and DNA cleavage." Journal of the American Chemical Society **114**(16): 6278-6291.

Hammami, M. M. and P. K. Siiteri (1991). "Regulation of 11 beta-hydroxysteroid dehydrogenase activity in human skin fibroblasts: enzymatic modulation of glucocorticoid action." J Clin Endocrinol Metab **73**(2): 326-34.

Hammer, M., J. Mages, et al. (2006). "Dual specificity phosphatase 1 (DUSP1) regulates a subset of LPS-induced genes and protects mice from lethal endotoxin shock." J Exp Med **203**(1): 15-20.

Handoko, K., K. Yang, et al. (2000). "Insulin attenuates the stimulatory effects of tumor necrosis factor alpha on 11beta-hydroxysteroid dehydrogenase 1 in human adipose stromal cells." J Steroid Biochem Mol Biol **72**(3-4): 163-8.

Hardy, R., E. H. Rabbitt, et al. (2008). "Local and systemic glucocorticoid metabolism in inflammatory arthritis." Ann Rheum Dis **67**(9): 1204-10.

Hardy, R. S., A. Filer, et al. (2006). "Differential expression, function and response to inflammatory stimuli of 11beta-hydroxysteroid dehydrogenase type 1 in human fibroblasts: a mechanism for tissue-specific regulation of inflammation." Arthritis Res Ther **8**(4): R108.

Harris, H. J., Y. Kotelevtsev, et al. (2001). "Intracellular regeneration of glucocorticoids by 11β-hydroxysteroid dehydrogenase (11β-HSD)-1 plays a key role in regulation of the hypothalamic-pituitary-adrenal axis: analysis of 11β-HSD-1 deficient mice." Endocrinology **142**: 114-120.

Hartsfield, C. L., J. Alam, et al. (1999). "Differential signaling pathways of HO-1 gene expression in

pulmonary and systemic vascular cells." Am J Physiol **277**(6 Pt 1): L1133-41.

Haslett, C., A. Lee, et al. (1991). "Apoptosis (programmed cell death) and functional changes in aging neutrophils. Modulation by inflammatory mediators." Chest **99**(3 Suppl): 6S.

Haslett, C., J. S. Savill, et al. (1994). "Granulocyte apoptosis and the control of inflammation." Philos Trans R Soc Lond B Biol Sci **345**(1313): 327-33.

Heasman, S. J., K. M. Giles, et al. (2003). "Glucocorticoid-mediated regulation of granulocyte apoptosis and macrophage phagocytosis of apoptotic cells: implications for the resolution of inflammation." J Endocrinol **178**(1): 29-36.

Hecht, S. M. (2000). "Bleomycin: new perspectives on the mechanism of action." J Nat Prod **63**(1): 158-68.

Hench, P. S., C. H. Slocumb, et al. (1949). "The effects of the adrenal cortical hormone 17-hydroxy-11-dehydrocorticosterone (Compound E) on the acute phase of rheumatic fever; preliminary report." Mayo Clin Proc **24**(11): 277-97.

Hermanowski-Vosatka, A., J. M. Balkovec, et al. (2005). "11®-HSD1 inhibition ameliorates metabolic syndrome and prevents progression of atherosclerosis in mice." J Exp Med **202**(4): 517-527.

Hollenberg, S. M., C. Weinberger, et al. (1985). "Primary structure and expression of a functional human glucocorticoid receptor cDNA." Nature **318**(6047): 635-41.

Hu, B., J. Sonstein, et al. (2000). "Deficient in vitro and in vivo phagocytosis of apoptotic T cells by resident murine alveolar macrophages." J Immunol **165**(4): 2124-33.

Hu, B., M. R. Ullenbruch, et al. (2007). "An essential role for CCAAT/enhancer binding protein beta in bleomycin-induced pulmonary fibrosis." J Pathol **211**(4): 455-62.

Hu, B., Z. Wu, et al. (2004). "CCAAT/enhancer-binding protein beta isoforms and the regulation of alpha-smooth muscle actin gene expression by IL-1 beta." J Immunol **173**(7): 4661-8.

Hu, B., Z. Wu, et al. (2003). "Smad3 mediates transforming growth factor-beta-induced alpha-smooth muscle actin expression." Am J Respir Cell Mol Biol **29**(3 Pt 1): 397-404.

Hundertmark, S., A. Dill, et al. (2002). "11beta-hydroxysteroid dehydrogenase type 1: a new regulator of fetal lung maturation." Horm Metab Res **34**(10): 537-44.

Hundertmark, S., A. Dill, et al. (2002). "Foetal lung maturation in 11®-hydroxysteroid dehydrogenase type 1 knockout mice." Horm Metab Res **34**(10): 545-549.

Hundertmark, S., V. Ragosch, et al. (1994). "Gestational age dependence of 11 beta-hydroxysteroid dehydrogenase and its relationship to the enzymes of phosphatidylcholine synthesis in lung and liver of fetal rat." Biochim Biophys Acta **1210**(3): 348-54.

Ignatova, I. D., R. M. Kostadinova, et al. (2009). "Tumor necrosis factor-alpha upregulates 11beta-hydroxysteroid dehydrogenase type 1 expression by CCAAT/enhancer binding protein-beta in HepG2 cells." Am J Physiol Endocrinol Metab **296**(2): E367-77.

Ignotz, R. A. and J. Massague (1986). "Transforming growth factor-beta stimulates the expression of fibronectin and collagen and their incorporation into the extracellular matrix." J Biol Chem **261**(9): 4337-45.

Iwasaki, H., S.-i. Mizuno, et al. (2006). "The order of expression of transcription factors directs hierarchical specification of hematopoietic lineages." Genes Dev. **20**(21): 3010-3021.

Jaffe, H. L. (1924). "The influence of the suprarenal gland on the thymus." J. Exp. Med. **XL**: 325-343.

Jamieson, P. M., K. E. Chapman, et al. (1995). "11 beta-hydroxysteroid dehydrogenase is an exclusive

11 beta- reductase in primary cultures of rat hepatocytes: effect of physicochemical and hormonal manipulations." Endocrinology **136**(11): 4754-61.

Jamieson, P. M., B. R. Walker, et al. (2000). "11 beta-hydroxysteroid dehydrogenase type 1 is a predominant 11 beta-reductase in the intact perfused rat liver." J Endocrinol **165**(3): 685-92.

Junqueira, L. C., G. Bignolas, et al. (1979). "Picrosirius staining plus polarization microscopy, a specific method for collagen detection in tissue sections." Histochem J **11**(4): 447-55.

Justesen, J., L. Mosekilde, et al. (2004). "Mice deficient in 11®-hydroxysteroid dehydrogenase type 1 lack bone marrow adipocytes, but maintain normal bone formation." Endocrinology **145**(4): 1916-1925.

Kalayarasan, S., N. Sriram, et al. (2008). "Diallyl sulfide attenuates bleomycin-induced pulmonary fibrosis: critical role of iNOS, NF-kappaB, TNF-alpha and IL-1beta." Life Sci **82**(23-24): 1142-53.

Kalinyak, J. E., R. I. Dorin, et al. (1987). "Tissue-specific regulation of glucocorticoid receptor mRNA by dexamethasone." J Biol Chem **262**(22): 10441-10444.

Kalluri, R. and M. Zeisberg (2006). "Fibroblasts in cancer." Nat Rev Cancer **6**(5): 392-401.

Kaminski, N., J. D. Allard, et al. (2000). "Global analysis of gene expression in pulmonary fibrosis reveals distinct programs regulating lung inflammation and fibrosis." Proc Natl Acad Sci U S A **97**(4): 1778-83.

Kamiyama, K., N. Matsuda, et al. (2008). "Modulation of glucocorticoid receptor expression, inflammation, and cell apoptosis in septic guinea pig lungs using methylprednisolone." Am J Physiol Lung Cell Mol Physiol **295**(6): L998-L1006.

Kane, S. A., A. Natrajan, et al. (1994). "On the role of the bithiazole moiety in sequence-selective DNA cleavage by Fe.bleomycin." J Biol Chem **269**(14): 10899-904.

Kardon, T., S. Senesi, et al. (2008). "Maintenance of luminal NADPH in the endoplasmic reticulum promotes the survival of human neutrophil granulocytes." FEBS Lett **582**(13): 1809-15.

Karin, M. (1998). "New twists in gene regulation by glucocorticoid receptor: is DNA binding dispensable?" Cell **93**(4): 487-90.

Kawamoto, M., T. Matsunami, et al. (1997). "Selective migration of alpha-smooth muscle actin-positive myofibroblasts toward fibronectin in the Boyden's blindwell chamber." Clin Sci (Lond) **93**(4): 355-62.

Keller, S. E., J. M. Weiss, et al. (1981). "Suppression of immunity by stress: effect of a graded series of stressors on lymphocyte stimulation in the rat." Science **213**(4514): 1397-400.

Kolaczkowska, E., S. Shahzidi, et al. (2002). "Early vascular permeability in murine experimental peritonitis is co-mediated by resident peritoneal macrophages and mast cells: crucial involvement of macrophage-derived cysteinyl-leukotrienes." Inflammation **26**(2): 61-71.

Kotelevtsev, Y., M. C. Holmes, et al. (1997). "11β-hydroxysteroid dehydrogenase type 1 knockout mice show attenuated glucocorticoid inducible responses and resist hyperglycaemia on obesity or stress." Proc Natl Acad Sci USA **94**: 14924-14929.

Krozowski, Z., A. L. Albiston, et al. (1995). "The human 11 beta-hydroxysteroid dehydrogenase type II enzyme: comparisons with other species and localization to the distal nephron." J Steroid Biochem Mol Biol **55**(5-6): 457-64.

Kuhn, C., 3rd, J. Boldt, et al. (1989). "An immunohistochemical study of architectural remodeling and connective tissue synthesis in pulmonary fibrosis." Am Rev Respir Dis **140**(6): 1693-703.

Kuhn, C. and J. A. McDonald (1991). "The roles of the myofibroblast in idiopathic pulmonary fibrosis. Ultrastructural and immunohistochemical features of sites of active extracellular matrix synthesis." Am J Pathol **138**(5): 1257-65.

Lag, M., E. Skarpen, et al. (2000). "Cell-specific expression of CCAAT/enhancer-binding protein delta (C/EBP delta) in epithelial lung cells." Exp Lung Res **26**(5): 383-99.

Lakshmi, V. and C. Monder (1988). "Purification and characterization of the corticosteroid 11 beta-dehydrogenase component of the rat liver 11 beta-hydroxysteroid dehydrogenase complex." Endocrinology **123**(5): 2390-8.

Laurent, G. J. (1987). "Dynamic state of collagen: pathways of collagen degradation in vivo and their possible role in regulation of collagen mass." Am J Physiol **252**(1 Pt 1): C1-9.

Lavery, G. G., E. A. Walker, et al. (2006). "Hexose-6-phosphate dehydrogenase knock-out mice lack 11 beta-hydroxysteroid dehydrogenase type 1-mediated glucocorticoid generation." J Biol Chem **281**(10): 6546-51.

Lavery, G. G., E. A. Walker, et al. (2008). "Steroid biomarkers and genetic studies reveal inactivating mutations in hexose-6-phosphate dehydrogenase in patients with cortisone reductase deficiency." J Clin Endocrinol Metab **93**(10): 3827-32.

Lavrovsky, Y., M. L. Schwartzman, et al. (1994). "Identification of binding sites for transcription factors NF-kappa B and AP-2 in the promoter region of the human heme oxygenase 1 gene." Proc Natl Acad Sci U S A **91**(13): 5987-91.

Lee, P. J., J. Alam, et al. (1996). "Regulation of heme oxygenase-1 expression in vivo and in vitro in hyperoxic lung injury." Am J Respir Cell Mol Biol **14**(6): 556-68.

Lekstrom-Himes, J. and K. G. Xanthopoulos (1998). "Biological role of the CCAAT/enhancer-binding protein family of transcription factors." J Biol Chem **273**(44): 28545-8.

Li, K. X. Z., R. E. Smith, et al. (1996). "Rat 11 beta-hydroxysteroid dehydrogenase type 2 enzyme is expressed at low levels in the placenta and is modulated by adrenal steroids in the kidney." Molecular and Cellular Endocrinology **120**(1): 67-75.

Liberman, A. C., J. Druker, et al. (2007). "Glucocorticoids in the regulation of transcription factors that control cytokine synthesis." Cytokine Growth Factor Rev **18**(1-2): 45-56.

Lieber M, Smith B, et al. (1976). "A continuous tumor-cell line from a human lung carcinoma with properties of type II alveolar epithelial cells." Int J Cancer **15**(1): 62-70.

Liggins, G. C. and R. N. Howie (1972). "A controlled trial of antepartum glucocorticoid treatment for prevention of the respiratory distress syndrome in premature infants." Pediatrics **50**(4): 515-25.

Liley, H. G., R. T. White, et al. (1989). "Regulation of messenger RNAs for the hydrophobic surfactant proteins in human lung." J Clin Invest **83**(4): 1191-7.

Lim, H. Y., N. Muller, et al. (2007). "Glucocorticoids exert opposing effects on macrophage function dependent on their concentration." Immunology **122**(1): 47-53.

Liu, T., S. M. Dhanasekaran, et al. (2004). "FIZZ1 stimulation of myofibroblast differentiation." Am J Pathol **164**(4): 1315-26.

Liu, Y. Q., J. M. Cousin, et al. (1999). "Glucocorticoids promote nonphlogistic phagocytosis of apoptotic leukocytes." J Immunol **162**: 3639-3646.

Low, S. C., K. E. Chapman, et al. (1994). "'Liver-type' 11 beta-hydroxysteroid dehydrogenase cDNA encodes reductase but not dehydrogenase activity in intact mammalian COS-7 cells." J Mol

Endocrinol **13**(2): 167-174.

Low, S. C., K. E. Chapman, et al. (1994). "'Liver-type' 11β-hydroxysteroid dehydrogenase cDNA encodes reductase not dehydrogenase activity in intact mammalian COS-7 cells." J Mol Endocrinol **13**: 167-174.

Lu, Y., N. Azad, et al. (2009). "Phosphatidylinositol-3-Kinase/Akt Regulates Bleomycin-Induced Fibroblast Proliferation and Collagen Production." Am J Respir Cell Mol Biol.

Luther, C., E. Adamopoulou, et al. (2009). "Prednisolone treatment induces tolerogenic dendritic cells and a regulatory milieu in myasthenia gravis patients." J Immunol **183**(2): 841-8.

Lutz, M. B., N. Kukutsch, et al. (1999). "An advanced culture method for generating large quantities of highly pure dendritic cells from mouse bone marrow." J Immunol Methods **223**(1): 77-92.

MacFadyen, J. R., O. Haworth, et al. (2005). "Endosialin (TEM1, CD248) is a marker of stromal fibroblasts and is not selectively expressed on tumour endothelium." FEBS Lett **579**(12): 2569-75.

Mahnke, K., E. Schmitt, et al. (2002). "Immature, but not inactive: the tolerogenic function of immature dendritic cells." Immunol Cell Biol **80**(5): 477-83.

Manoury, B., S. Nenan, et al. (2007). "Influence of early neutrophil depletion on MMPs/TIMP-1 balance in bleomycin-induced lung fibrosis." Int Immunopharmacol **7**(7): 900-11.

Manwani, N., S. Gagnon, et al. (2009). "Reduced Viability of Mice with Lung Epithelial-Specific Knockout of Glucocorticoid Receptor." Am J Respir Cell Mol Biol.

Martinet, Y., O. Menard, et al. (1996). "Cytokines in human lung fibrosis." Arch Toxicol Suppl **18**: 127-39.

Mason, P. J., D. Stevens, et al. (1999). "Human hexose-6-phosphate dehydrogenase (glucose 1-dehydrogenase) encoded at 1p36: coding sequence and expression." Blood Cells Mol Dis **25**(1): 30-7.

Mason, R. J. (2006). "Biology of alveolar type II cells." Respirology **11 Suppl**: S12-5.

Matlapudi, A., M. Wang, et al. (2002). "A role for C/EBP delta in human surfactant protein A (SP-A) gene expression." Biochim Biophys Acta **1575**(1-3): 91-8.

Matyszak, M. K., S. Citterio, et al. (2000). "Differential effects of corticosteroids during different stages of dendritic cell maturation." Eur J Immunol **30**(4): 1233-42.

Mays, P. K., R. J. McAnulty, et al. (1989). "Age-related changes in lung collagen metabolism. A role for degradation in regulating lung collagen production." Am Rev Respir Dis **140**(2): 410-6.

McColl, A., S. Bournazos, et al. (2009). "Glucocorticoids induce protein S-dependent phagocytosis of apoptotic neutrophils by human macrophages." J Immunol **183**(3): 2167-75.

McEwen, B. S., C. A. Biron, et al. (1997). "The role of adrenocorticoids as modulators of immune function in health and disease: neural, endocrine and immune interactions." Brain Res Brain Res Rev **23**(1-2): 79-133.

McKay, L. I. and J. A. Cidlowski (1999). "Molecular control of immune/inflammatory responses: interactions between nuclear factor-kappa B and steroid receptor-signaling pathways." Endocr Rev **20**(4): 435-59.

McKnight, S. L. (2001). "McBindall--a better name for CCAAT/enhancer binding proteins?" Cell **107**(3): 259-61.

McKnight, S. L., M. D. Lane, et al. (1989). "Is CCAAT/enhancer-binding protein a central regulator of energy metabolism?" Genes Dev **3**: 2021-2024.

McSweeney, S. J., P. W. Hadoke, et al. (2010). "Improved heart function follows enhanced inflammatory cell recruitment and angiogenesis in 11{beta}HSD1-deficient mice post-MI." Cardiovasc Res.

Meagher, L. C., J. M. Cousin, et al. (1996). "Opposing effects of glucocorticoids on the rate of apoptosis in neutrophilic and eosinophilic granulocytes." J Immunol **156**(11): 4422-8.

Meijsing, S. H., M. A. Pufall, et al. (2009). "DNA binding site sequence directs glucocorticoid receptor structure and activity." Science **324**(5925): 407-10.

Meisler, N., S. Shull, et al. (1995). "Glucocorticoids coordinately regulate type I collagen pro alpha 1 promoter activity through both the glucocorticoid and transforming growth factor beta response elements: a novel mechanism of glucocorticoid regulation of eukaryotic genes." J Cell Biochem **59**(3): 376-88.

Meisler, N. T., J. F. Chiu, et al. (1999). "Promoter competitors as novel antifibrotics that inhibit transforming growth factor-beta induction of collagen and noncollagen protein synthesis in fibroblasts." J Cell Biochem **75**(2): 196-205.

Mercer, W., V. Obeyesekere, et al. (1993). "Characterization of 11β-HSD1B gene expression and enzymatic activity." Mol Cell Endocrinol **92**(2): 247-251.

Moisan, M. P., C. R. Edwards, et al. (1992). "Differential promoter usage by the rat 11 beta-hydroxysteroid dehydrogenase gene." Mol Endocrinol **6**(7): 1082-7.

Moisan, M. P., C. R. Edwards, et al. (1992). "Ontogeny of 11 beta-hydroxysteroid dehydrogenase in rat brain and kidney." Endocrinology **130**(1): 400-4.

Moisan, M. P., J. R. Seckl, et al. (1990). "11Beta-Hydroxysteroid Dehydrogenase Messenger Ribonucleic Acid Expression, Bioactivity and Immunoreactivity in Rat Cerebellum." J Neuroendocrinol **2**(6): 853-8.

Monder, C. and V. Lakshmi (1990). "Corticosteroid 11 beta-dehydrogenase of rat tissues: immunological studies." Endocrinology **126**(5): 2435-2443.

Morse, D. and A. M. K. Choi (2002). "Heme Oxygenase-1 . The "Emerging Molecule" Has Arrived." Am. J. Respir. Cell Mol. Biol. **27**(1): 8-16.

Morton, N. M., M. C. Holmes, et al. (2001). "Improved lipid and lipoprotein profile, hepatic insulin sensitivity, and glucose tolerance in 11®-hydroxysteroid dehydrogenase type 1 null mice." J Biol Chem **276**: 41293-41300.

Morton, N. M., J. M. Paterson, et al. (2004). "Novel adipose tissue-mediated resistance to diet-induced visceral obesity in 11®-hydroxysteroid dehydrogenase type 1-deficient mice." Diabetes **53**(4): 931-938.

Munck, A., P. M. Guyre, et al. (1984). "Physiological functions of glucocorticoids in stress and their relation to pharmacological actions." Endocr Rev **5**(1): 25-44.

Munck, A. and A. Naray-Fejes-Toth (1992). "The ups and downs of glucocorticoid physiology. Permissive and suppressive effects revisited." Mol Cell Endocrinol **90**(1): C1-4.

Munger, J. S., X. Huang, et al. (1999). "The integrin alpha v beta 6 binds and activates latent TGF beta 1: a mechanism for regulating pulmonary inflammation and fibrosis." Cell **96**(3): 319-28.

Mziaut, H., G. Korza, et al. (1999). "Targeting proteins to the lumen of endoplasmic reticulum using N-terminal domains of 11beta-hydroxysteroid dehydrogenase and the 50-kDa esterase." J Biol Chem **274**(20): 14122-9.

Nagatomo, H., Y. Morimoto, et al. (2007). "Change of heme oxygenase-1 expression in lung injury

induced by chrysotile asbestos in vivo and in vitro." Inhal Toxicol **19**(4): 317-23.

Nakagawa, M., T. Terashima, et al. (1998). "Glucocorticoid-induced granulocytosis: contribution of marrow release and demargination of intravascular granulocytes." Circulation **98**(21): 2307-13.

Nemati, B., W. Atmodjo, et al. (2008). "Glucocorticoid receptor disruption delays structural maturation in the lungs of newborn mice." Pediatr Pulmonol **43**(2): 125-33.

Nicholas, T. E. and M. A. Lugg (1982). "The physiological significance of 11 beta-hydroxysteroid dehydrogenase in the rat lung." J Steroid Biochem **17**(1): 113-8.

Nussler, A. K., T. R. Billiar, et al. (1994). "Coinduction of nitric oxide synthase and argininosuccinate synthetase in a murine macrophage cell line. Implications for regulation of nitric oxide production." J Biol Chem **269**(2): 1257-61.

O'Riordan JLH, M. P., Gould RP (1982). "Essentials of Endocrinology." Blackwell Scientific Publications: 83.

Odermatt, A., P. Arnold, et al. (1999). "The N-terminal anchor sequences of 11beta-hydroxysteroid dehydrogenases determine their orientation in the endoplasmic reticulum membrane." J Biol Chem **274**(40): 28762-70.

Odermatt, A., A. G. Atanasov, et al. (2006). "Why is 11beta-hydroxysteroid dehydrogenase type 1 facing the endoplasmic reticulum lumen? Physiological relevance of the membrane topology of 11beta-HSD1." Mol Cell Endocrinol **248**(1-2): 15-23.

Ogawa, M., A. C. LaRue, et al. (2006). "Hematopoietic origin of fibroblasts/myofibroblasts: Its pathophysiologic implications." Blood **108**(9): 2893-6.

Oggionni, T., P. Morbini, et al. (2006). "Time course of matrix metalloproteases and tissue inhibitors in bleomycin-induced pulmonary fibrosis." Eur J Histochem **50**(4): 317-25.

Oreffo, V. I., A. Morgan, et al. (1990). "Isolation of Clara cells from the mouse lung." Environ Health Perspect **85**: 51-64.

Ozols, J. (1998). "Determination of lumenal orientation of microsomal 50-kDa esterase/N-deacetylase." Biochemistry **37**(28): 10336-44.

Park, B. H., L. Qiang, et al. (2004). "Phosphorylation of C/EBPbeta at a consensus extracellular signal-regulated kinase/glycogen synthase kinase 3 site is required for the induction of adiponectin gene expression during the differentiation of mouse fibroblasts into adipocytes." Mol Cell Biol **24**(19): 8671-80.

Parrelli, J. M., N. Meisler, et al. (1998). "Identification of a glucocorticoid response element in the human transforming growth factor beta 1 gene promoter." Int J Biochem Cell Biol **30**(5): 623-7.

Parsonage, G., F. Falciani, et al. (2003). "Global gene expression profiles in fibroblasts from synovial, skin and lymphoid tissue reveals distinct cytokine and chemokine expression patterns." Thromb Haemost **90**(4): 688-97.

Parsonage, G., A. D. Filer, et al. (2005). "A stromal address code defined by fibroblasts." Trends Immunol **26**(3): 150-6.

Paterson, J. M., M. C. Holmes, et al. (2007). "Liver-selective transgene rescue of hypothalamic-pituitary-adrenal axis dysfunction in 11beta-hydroxysteroid dehydrogenase type 1-deficient mice." Endocrinology **148**(3): 961-6.

Payne, V. A., W. S. Au, et al. (2007). "Sequential regulation of diacylglycerol acyltransferase 2

expression by CAAT/enhancer-binding protein beta (C/EBPbeta) and C/EBPalpha during adipogenesis." J Biol Chem **282**(29): 21005-14.

Phan, S. H. (2002). "The myofibroblast in pulmonary fibrosis." Chest **122**(6 Suppl): 286S-289S.

Phillips, R. J., M. D. Burdick, et al. (2004). "Circulating fibrocytes traffic to the lungs in response to CXCL12 and mediate fibrosis." J Clin Invest **114**(3): 438-46.

Picard, D. and K. R. Yamamoto (1987). "Two signals mediate hormone-dependent nuclear localization of the glucocorticoid receptor." Embo J **6**(11): 3333-40.

Piemonti, L., P. Monti, et al. (1999). "Glucocorticoids affect human dendritic cell differentiation and maturation." J Immunol **162**(11): 6473-81.

Piguet, P. F., M. A. Collart, et al. (1989). "Tumor necrosis factor/cachectin plays a key role in bleomycin-induced pneumopathy and fibrosis." J Exp Med **170**(3): 655-63.

Pochetuhen, K., I. G. Luzina, et al. (2007). "Complex regulation of pulmonary inflammation and fibrosis by CCL18." Am J Pathol **171**(2): 428-37.

Poli, V. (1998). "The role of C/EBP isoforms in the control of inflammatory and native immunity functions." J Biol Chem **273**(45): 29279-82.

Pratt, W. B., M. D. Galigniana, et al. (2004). "Role of hsp90 and the hsp90-binding immunophilins in signalling protein movement." Cell Signal **16**(8): 857-72.

Puchtler, H. and S. N. Meloan (1985). "On the chemistry of formaldehyde fixation and its effects on immunohistochemical reactions." Histochemistry **82**(3): 201-4.

Raes, G., R. Van den Bergh, et al. (2005). "Arginase-1 and Ym1 are markers for murine, but not human, alternatively activated myeloid cells." J Immunol **174**(11): 6561; author reply 6561-2.

Rajan, V., K. E. Chapman, et al. (1995). "Cloning, sequencing and tissue-distribution of mouse 11 beta-hydroxysteroid dehydrogenase-1 cDNA." J Steroid Biochem Mol Biol **52**(2): 141-7.

Reichardt, H. M., K. H. Kaestner, et al. (1998). "DNA binding of the glucocorticoid receptor is not essential for survival." Cell **93**(4): 531-41.

Reichardt, H. M. and G. Schutz (1998). "Glucocorticoid signalling--multiple variations of a common theme." Mol Cell Endocrinol **146**(1-2): 1-6.

Reichardt, H. M., J. P. Tuckermann, et al. (2001). "Repression of inflammatory responses in the absence of DNA binding by the glucocorticoid receptor." Embo J **20**(24): 7168-73.

Rettig, W. J., P. Garin-Chesa, et al. (1993). "Regulation and heteromeric structure of the fibroblast activation protein in normal and transformed cells of mesenchymal and neuroectodermal origin." Cancer Res **53**(14): 3327-35.

Rhen, T. and J. A. Cidlowski (2005). "Antiinflammatory action of glucocorticoids--new mechanisms for old drugs." N Engl J Med **353**(16): 1711-23.

Richard, E. M., J. C. Helbling, et al. (2010). "Plasma transcortin influences endocrine and behavioral stress responses in mice." Endocrinology **151**(2): 649-59.

Ricketts, M. L., J. M. Verhaeg, et al. (1998). "Immunohistochemical localization of type 1 11beta-hydroxysteroid dehydrogenase in human tissues." J Clin Endocrinol Metab **83**(4): 1325-35.

Rousseau, G. G., J. D. Baxter, et al. (1972). "Glucocorticoid receptors: relations between steroid binding and biological effects." J Mol Biol **67**(1): 99-115.

Sai, S., C. L. Esteves, et al. (2008). "Glucocorticoid regulation of the promoter of

11beta-hydroxysteroid dehydrogenase type 1 is indirect and requires CCAAT/enhancer-binding protein-beta." Mol Endocrinol **22**(9): 2049-60.

Saito, F., S. Tasaka, et al. (2008). "Role of interleukin-6 in bleomycin-induced lung inflammatory changes in mice." Am J Respir Cell Mol Biol **38**(5): 566-71.

Sandeep, T. C., J. L. Yau, et al. (2004). "11Beta-hydroxysteroid dehydrogenase inhibition improves cognitive function in healthy elderly men and type 2 diabetics." Proc Natl Acad Sci U S A **101**(17): 6734-9.

Sapolsky, R. M., L. M. Romero, et al. (2000). "How do glucocorticoids influence stress responses? Integrating permissive, suppressive, stimulatory, and preparative actions." Endocr Rev **21**(1): 55-89.

Sarabdjitsingh, R. A., O. C. Meijer, et al. (2010). "Specificity of glucocorticoid receptor primary antibodies for analysis of receptor localization patterns in cultured cells and rat hippocampus." Brain Res **1331**: 1-11.

Savill, J., I. Dransfield, et al. (2002). "A blast from the past: clearance of apoptotic cells regulates immune responses." Nat Rev Immunol **2**: 965-975.

Schmidt, M., C. Weidler, et al. (2005). "Reduced capacity for the reactivation of glucocorticoids in rheumatoid arthritis synovial cells: possible role of the sympathetic nervous system?" Arthritis Rheum **52**(6): 1711-20.

Schneider, J., W. Bruckmann, et al. (1997). "Extravasation of leukocytes assessed by intravital microscopy: effect of thalidomide." Inflamm Res **46**(10): 392-7.

Seckl, J. R. (2004). "11beta-hydroxysteroid dehydrogenases: changing glucocorticoid action." Curr Opin Pharmacol **4**(6): 597-602.

Seckl, J. R., N. M. Morton, et al. (2004). "Glucocorticoids and 11beta-Hydroxysteroid Dehydrogenase in Adipose Tissue." Recent Prog Horm Res **59**(1): 359-393.

Selman, M. and A. Pardo (2002). "Idiopathic pulmonary fibrosis: an epithelial/fibroblastic cross-talk disorder." Respir Res **3**: 3.

Serhan, C. and J. Savill (2005). "Resolution of inflammation: the beginning programs the end." Nature Immunology **6(12)**: 1191-7.

Shahzeidi, S., B. Mulier, et al. (1993). "Enhanced type III collagen gene expression during bleomycin induced lung fibrosis." Thorax **48**(6): 622-8.

Shukla, A., N. Meisler, et al. (1999). "Transforming growth factor-β: crossroad of glucocorticoid and bleomycin regulation of collagen synthesis in lung fibroblasts." Wound Repair and Regeneration **7**(3): 133-140.

Shull, S., N. Meisler, et al. (1995). "Glucocorticoid-induced down regulation of transforming growth factor-beta 1 in adult rat lung fibroblasts." Lung **173**(2): 71-8.

Sikic, B. I., D. M. Young, et al. (1978). "Quantification of bleomycin pulmonary toxicity in mice by changes in lung hydroxyproline content and morphometric histopathology." Cancer Res **38**(3): 787-92.

Small, G. R., P. W. Hadoke, et al. (2005). "Preventing local regeneration of glucocorticoids by 11beta-hydroxysteroid dehydrogenase type 1 enhances angiogenesis." Proc Natl Acad Sci U S A **102**(34): 12165-70.

Soldan, M., G. Nagel, et al. (1999). "Interindividual variability in the expression and NNK carbonyl reductase activity of 11beta-hydroxysteroid dehydrogenase 1 in human lung." Cancer Lett

145(1-2): 49-56.

Souverein, P. C., A. Berard, et al. (2004). "Use of oral glucocorticoids and risk of cardiovascular and cerebrovascular disease in a population based case-control study." Heart **90**(8): 859-65.

Speirs, H. J., J. R. Seckl, et al. (2004). "Ontogeny of glucocorticoid receptor and 11®-hydroxysteroid dehydrogenase type-1 gene expression identifies potential critical periods of glucocorticoid susceptibility during development." J Endocrinol **181**(1): 105-116.

Sterling, K. M., Jr., T. DiPetrillo, et al. (1982). "Inhibition of collagen accumulation by glucocorticoids in rat lung after intratracheal bleomycin instillation." Cancer Res **42**(2): 405-8.

Sterling, K. M., Jr., M. J. Harris, et al. (1983). "Dexamethasone decreases the amounts of type I procollagen mRNAs in vivo and in fibroblast cell cultures." J Biol Chem **258**(12): 7644-7.

Stewart, C. C., H. S. Lin, et al. (1975). "Proliferation and colony-forming ability of peritoneal exudate cells in liquid culture." J Exp Med **141**(5): 1114-32.

Stewart, P. M. and Z. S. Krozowski (1999). "11 beta-Hydroxysteroid dehydrogenase." Vitam Horm **57**: 249-324.

Stewart, P. M., C. B. Whorwood, et al. (1995). "Type 2 11 beta-hydroxysteroid dehydrogenase in foetal and adult life." J Steroid Biochem Mol Biol **55**(5-6): 465-71.

Strickland, D., U. R. Kees, et al. (1996). "Regulation of T-cell activation in the lung: alveolar macrophages induce reversible T-cell anergy in vitro associated with inhibition of interleukin-2 receptor signal transduction." Immunology **87**(2): 250-8.

Strutz, F., H. Okada, et al. (1995). "Identification and characterization of a fibroblast marker: FSP1." J Cell Biol **130**(2): 393-405.

Sun, K. and L. Myatt (2003). "Enhancement of glucocorticoid-induced 11beta-hydroxysteroid dehydrogenase type 1 expression by proinflammatory cytokines in cultured human amnion fibroblasts." Endocrinology **144**(12): 5568-77.

Suttner, D. M., K. Sridhar, et al. (1999). "Protective effects of transient HO-1 overexpression on susceptibility to oxygen toxicity in lung cells." Am J Physiol **276**(3 Pt 1): L443-51.

Suzuki, S., H. Tsubochi, et al. (2003). "Expression of 11 beta-hydroxysteroid dehydrogenase type 1 in alveolar epithelial cells in rats." Endocr J **50**(4): 445-51.

Swaisgood, C. M., E. L. French, et al. (2000). "The development of bleomycin-induced pulmonary fibrosis in mice deficient for components of the fibrinolytic system." Am J Pathol **157**(1): 177-87.

Tannin, G. M., A. K. Agarwal, et al. (1991). "The human gene for 11 beta-hydroxysteroid dehydrogenase. Structure, tissue distribution, and chromosomal localization." J Biol Chem **266**(25): 16653-8.

Tarin, D. and C. B. Croft (1969). "Ultrastructural features of wound healing in mouse skin." J Anat **105**(Pt 1): 189-90.

Tchen, C. R., J. R. Martins, et al. (2010). "Glucocorticoid regulation of mouse and human dual specificity phosphatase 1 (DUSP1) genes: unusual cis-acting elements and unexpected evolutionary divergence." J Biol Chem **285**(4): 2642-52.

Thieringer, R., C. B. Le Grand, et al. (2001). "11β-Hydroxysteroid dehydrogenase type 1 is induced in human monocytes upon differentiation to macrophages." J Immunol **167**: 30-35.

Tiwari, A. (2010). "INCB-13739, an 11beta-hydroxysteroid dehydrogenase type 1 inhibitor for the

treatment of type 2 diabetes." IDrugs **13**(4): 266-75.

Tomlinson, J. W., J. Moore, et al. (2001). "Regulation of expression of 11beta-hydroxysteroid dehydrogenase type 1 in adipose tissue: tissue-specific induction by cytokines." Endocrinology **142**(5): 1982-9.

Topley, N., R. Mackenzie, et al. (1993). "Cytokine networks in continuous ambulatory peritoneal dialysis: interactions of resident cells during inflammation in the peritoneal cavity." Perit Dial Int **13 Suppl 2**: S282-5.

Torday, J. S. and S. Kourembanas (1990). "Fetal rat lung fibroblasts produce a TGF beta homolog that blocks alveolar type II cell maturation." Dev Biol **139**(1): 35-41.

Torday, J. S., E. B. Olson, Jr., et al. (1976). "Production of cortisol from cortisone by the isolated, perfused fetal rabbit lung." Steroids **27**(6): 869-80.

Torday, J. S., M. Post, et al. (1985). "Compartmentalization of 11-oxidoreductase within fetal lung alveolus." Am J Physiol Cell Physiol **249**(1): C173-176.

Tronche, F., C. Kellendonk, et al. (1998). "Genetic dissection of glucocorticoid receptor function in mice." Curr Opin Genet Dev **8**(5): 532-538.

Vagnerova, K., M. Kverka, et al. (2006). "Intestinal inflammation modulates expression of 11beta-hydroxysteroid dehydrogenase in murine gut." J Endocrinol **191**(2): 497-503.

Varga, G., J. Ehrchen, et al. (2008). "Glucocorticoids induce an activated, anti-inflammatory monocyte subset in mice that resembles myeloid-derived suppressor cells." J Leukoc Biol **84**(3): 644-50.

Vermes, I., C. Haanen, et al. (1995). "A novel assay for apoptosis. Flow cytometric detection of phosphatidylserine expression on early apoptotic cells using fluorescein labelled Annexin V." J Immunol Methods **184**(1): 39-51.

Waddell, B. J., R. Benediktsson, et al. (1998). "Tissue-specific messenger ribonucleic acid expression of 11beta-hydroxysteroid dehydrogenase types 1 and 2 and the glucocorticoid receptor within rat placenta suggests exquisite local control of glucocorticoid action." Endocrinology **139**(4): 1517-23.

Walker, G. A., I. A. Guerrero, et al. (2001). "Myofibroblasts: molecular crossdressers." Curr Top Dev Biol **51**: 91-107.

Webster, J. I. and E. M. Sternberg (2004). "Role of the hypothalamic-pituitary-adrenal axis, glucocorticoids and glucocorticoid receptors in toxic sequelae of exposure to bacterial and viral products." J Endocrinol **181**(2): 207-21.

White, E. S., M. H. Lazar, et al. (2003). "Pathogenetic mechanisms in usual interstitial pneumonia/idiopathic pulmonary fibrosis." Journal of Pathology **201**: 343–354.

Whorwood, C. B., J. A. Franklyn, et al. (1992). "Tissue localization of 11 beta-hydroxysteroid dehydrogenase and its relationship to the glucocorticoid receptor." J Steroid Biochem Mol Biol **41**(1): 21-8.

Williams, L. J. S., V. Lyons, et al. (2000). "C/EBP regulates hepatic transcription of 11β-hydroxysteroid dehydrogenase type 1; a novel mechanism for cross talk between the C/EBP and glucocorticoid signalling pathways." J Biol Chem **275**: 30232-30239.

Williams, S. C., C. A. Cantwell, et al. (1991). "A family of C/EBP-related proteins capable of forming covalently linked leucine zipper dimers in vitro." Genes Dev **5**(9): 1553-67.

Willis, B. C. and Z. Borok (2007). "TGF-beta-induced EMT: mechanisms and implications for fibrotic

lung disease." Am J Physiol Lung Cell Mol Physiol **293**(3): L525-34.

Wrange, O., P. Eriksson, et al. (1989). "The purified activated glucocorticoid receptor is a homodimer." J Biol Chem **264**(9): 5253-9.

Yamamoto, K. R. (1985). "Steroid receptor regulated transcription of specific genes and gene networks." Annu Rev Genet **19**: 209-52.

Yang, H., J. Mammen, et al. (2005). "Expression and activity of C/EBPbeta and delta are upregulated by dexamethasone in skeletal muscle." J Cell Physiol **204**(1): 219-26.

Yang, Z., X. Zhu, et al. (2009). "Stimulation of 11beta-HSD1 expression by IL-1beta via a C/EBP binding site in human fetal lung fibroblasts." Endocrine.

Yano, Y., M. Yoshida, et al. (2006). "Anti-fibrotic effects of theophylline on lung fibroblasts." Biochem Biophys Res Commun **341**(3): 684-90.

Yau, J. L., K. M. McNair, et al. (2007). "Enhanced hippocampal long-term potentiation and spatial learning in aged 11beta-hydroxysteroid dehydrogenase type 1 knock-out mice." J Neurosci **27**(39): 10487-96.

Yau, J. L., J. Noble, et al. (2001). "Lack of tissue glucocorticoid reactivation in 11beta -hydroxysteroid dehydrogenase type 1 knockout mice ameliorates age-related learning impairments." Proc Natl Acad Sci U S A **98**(8): 4716-21.

Yau, J. L., A. D. Van Haarst, et al. (1991). "11 beta-Hydroxysteroid dehydrogenase mRNA expression in rat kidney." Am J Physiol **260**(5 Pt 2): F764-7.

Yeager, M. P., P. M. Guyre, et al. (2004). "Glucocorticoid regulation of the inflammatory response to injury." Acta Anaesthesiol Scand **48**(7): 799-813.

Yong, P. Y., C. Harlow, et al. (2002). "Regulation of 11β-hydroxysteroid dehydrogenase type 1 gene expression in human ovarian surface epithelial cells by interleukin-1." Hum Reprod **17**(9): 2300-2306.

Zbankova, S., J. Bryndova, et al. (2007). "11beta-hydroxysteroid dehydrogenase 1 and 2 expression in colon from patients with ulcerative colitis." J Gastroenterol Hepatol **22**(7): 1019-23.

Zhang, H. Y. and S. H. Phan (1999). "Inhibition of myofibroblast apoptosis by transforming growth factor beta(1)." Am J Respir Cell Mol Biol **21**(6): 658-65.

Zhang, K., K. C. Flanders, et al. (1995). "Cellular localization of transforming growth factor-beta expression in bleomycin-induced pulmonary fibrosis." Am J Pathol **147**(2): 352-61.

Zhang, K., M. Gharaee-Kermani, et al. (1997). "TNF-alpha-mediated lung cytokine networking and eosinophil recruitment in pulmonary fibrosis." J Immunol **158**(2): 954-9.

Zhang, K., M. D. Rekhter, et al. (1994). "Myofibroblasts and their role in lung collagen gene expression during pulmonary fibrosis. A combined immunohistochemical and in situ hybridization study." Am J Pathol **145**(1): 114-25.

Zhang, T. Y. and R. A. Daynes (2007). "Macrophages from 11beta-hydroxysteroid dehydrogenase type 1-deficient mice exhibit an increased sensitivity to lipopolysaccharide stimulation due to TGF-beta-mediated up-regulation of SHIP1 expression." J Immunol **179**(9): 6325-35.

Zhang, T. Y., X. Ding, et al. (2005). "The expression of 11®-hydroxysteroid dehydrogenase type I by lymphocytes provides a novel means for intracrine regulation of glucocorticoid activities." J Immunol **174**(2): 879-889.

Zhang, X., E. Moilanen, et al. (2001). "Beclomethasone, budesonide and fluticasone propionate inhibit human neutrophil apoptosis." Eur J Pharmacol **431**(3): 365-71.

Appendix I: Comparison of *in situ* hybridization and IHC using sheep anti-11β-HSD1 antibody on kidney section

The specificity of the purified sheep anti-11β-HSD1 antibody was determined by staining kidney section. In kidney 11β-HSD1 is expressed in all renal tubular epithelia but is not detected in medullary interstitial cells (Yau, Van Haarst et al. 1991) (Figure 1.1A and B). Paraffin-embedded kidney sections from C57BL/6 control (WT) mice were stained with purified sheep anti-11β-HSD1 antibody at 1:1000 dilution. Positive staining was seen in proximal and distal tubular epithelia and glomeruli did not show 11β-HSD1 expression (Figure 1.1C).

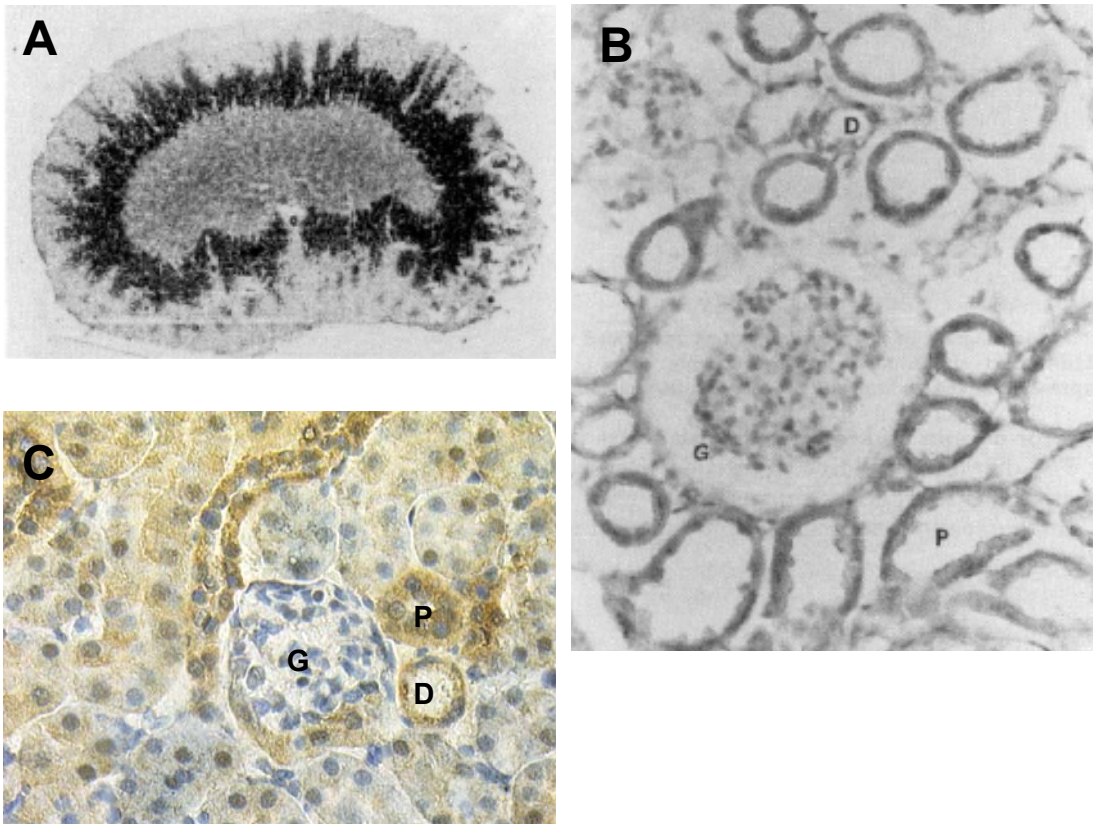

Figure 1.1 Immunohistochemical staining of 11β-HSD1 in mouse kidney shows expression in renal tubular epithelial cells.

(A and B) previously published *in situ* hybridization result showing 11β-HSD1 expression in (A), juxtamedullary cortex/outer medulla; (B), renal tubular epithelial cells of proximal (P) and distal (D) convoluted tubules. Interstitial cells and glomerular (G) epithelium are negative (Yau, Van Haarst et al. 1991). (C) Representative image of Immunohistochemistry carried out on kidney sections from WT mice with purified sheep anti-11β-HSD1 antibody at 1:1000 dilution and biotinylated rabbit-anti-sheep 2nd Ab at 1:400 dilution. Image was captured at magnification, X400.

Appendix II: Awards, Presentations and Publications

Awards:

Oct 2009	Scottish Stem Cell Network Travel Grant
June 2009	The Endocrine Society Travel Grant
May 2009	The British Pharmacology Travel Grant
Mar 2009	The Endocrine Society Travel Grant
2006-2009	College of Medicine and Veterinary Medicine PhD Scholarship, University of Edinburgh

Abstracts:

Fu Yang, Rodger Duffin, David G. Brownstein, Agnes Coutinho, Adriano G. Rossi, John S Savill, Jonathan R. Seckl and Karen E. Chapman. 11β-hydroxysteroid dehydrogenase type 1 activity limits inflammation following bleomycin lung injury by augmenting active glucocorticoids. *The Endocrine Society 91st Meeting* (June 2009, Washington DC, USA) **Poster presentation**

Fu Yang, Rodger Duffin, David G. Brownstein, Agnes Coutinho, Adriano G. Rossi, John S Savill, Jonathan R. Seckl and Karen E. Chapman. 11β-hydroxysteroid dehydrogenase type 1 activity limits fibrosis following bleomycin lung injury by augmenting active glucocorticoids. *British Endocrine Society Meeting* (March 2009, Harrogate, UK) **Oral Presentation**

Fu Yang, Rodger Duffin, David G. Brownstein, Agnes Coutinho, Adriano G. Rossi, John S Savill, Jonathan R. Seckl and Karen E. Chapman. Glucocorticoid amplification by 11β-hydroxysteroid dehydrogenase type 1 limits fibrosis following bleomycin lung injury. *Scottish Society for Experimental Medicine Meeting* (November 2008, Edinburgh, Scotland, UK) **Oral Presentation**